Heimdal

A Powerful Instrument for Novel Material Science

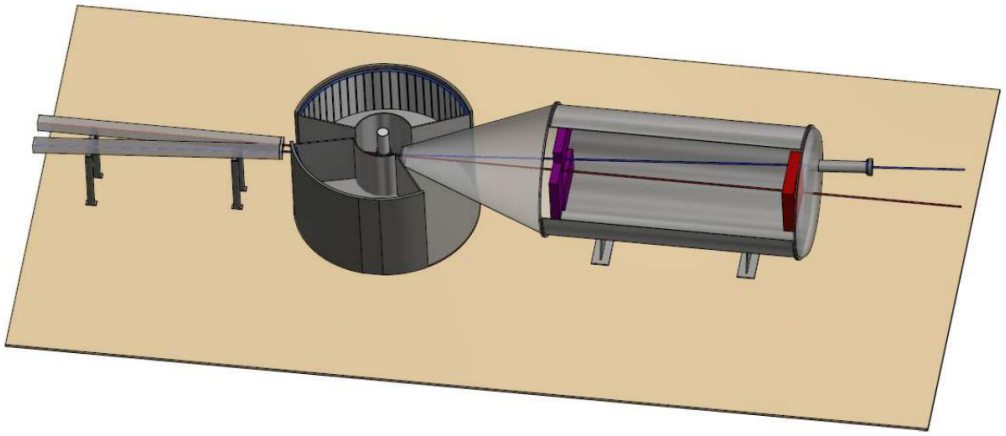

Master Thesis

March 4, 2014

Sonja Lindahl Holm

Nano-Science Center
Niels Bohr Institute
University of Copenhagen

Supervisor:
Prof. Dr. Kim Lefmann

External collaborators:
Dr. Paul Henry, European Spallation Source
Dr. Mogens Christensen, University of Aarhus

Contents

List of Figures

Preface

This master thesis by Sonja Lindahl Holm was written as part of a 4+4 Ph.D. at the Niels Bohr Institute. The European Spallation Source (ESS) has co-financed a third of the Ph.D. though the Danish in-kind contribution and a part of the work is hence about instrument design for ESS. This is what I have chosen to deal with in this M.Sc. thesis.

My supervisor, Kim Lefmann, has a close collaboration with the staff at ESS, and he is also involved in the Danish contribution to ESS. This has been a great advantage in this project since this work done with Paul Henry, instrument responsible for powder diffraction at ESS, and Mogens Christensen, work paged leader of the Danish-Swiss project concerning powder diffraction, has been constructive and fruitful.

In January 2010 I was employed as a student assistant to help out with computer simulations of a generic instrument suite for ESS. This was done in order to investigate the impact of the source time structure (frequency and pulse length) on the instrument performance. The results of this study can be found in appendix A.1 where the performance of the full instrument suite is presented. My contribution to the results concerning the powder diffraction instruments can be found in appendix A.2.

During the work on the generic instrument suite for ESS a concern regarding feasibility of long guides (150 m or more) was raised. As this was an unresolved issue a lot of thought and effort was put into this question in our group. One of the things that came out of this was the idea of feeding several instruments from the same beam port by splitting the neutron guide. This idea of mine is presented in chapter 5 and will hopefully be published soon. A draft of this can be found in appendix A.3.

The simulation work done as a student assistant has been the stepping stone for me in the simulation and design work of a thermal powder diffractometer for ESS. These simulations then led to the work concerning a multi purpose machine, Heimdal, including a thermal powder diffractometer, an imaging station and a small angle neutron scattering set-up.

The aim of the project was to support the preproposal of the multi purpose machine Heimdal designed under the Danish-Swiss work package number four (WP4). In chapter 6 the instrument design considerations and simulations are presented, and in appendix A.4 the final preproposal can be found.

The work on the Heimdal instrument has also been used by Paul Henry to describe the thermal powder diffractometer in the reference suite for the Technical Design Report for ESS (see appendix A.5).

Acknowledgment

First of all I would like to thank my supervisor, Kim Lefmann, whom I have been working with for nearly four years. Kim's optimism and joy for science is very contagious and the atmosphere in his group is friendly and cheerful. I'm very happy and feel privileged to be working in this group at the Niels Bohr Institute.

I would like to thank Paul Henry and Mogens Christensen for fruitful discussions and for sharing of their knowledge and expertise in the field of powder diffraction. This project would not have been possible without them.

Peter Wilendrup and Mads Bertelsen have been very helpful with solving McStas problems. Especially Mads has also helped out with simulations and optimizations of the guide system for Heimdal.

My thanks also go to Henrik Jacobsen and Nina Holm for proofreading my thesis.

Finally I would like to thank my family, friends, and colleagues for support and motivation.

Resumé

Neutronspredning er en enestående teknik til at studere atom- og molekylestrukturer samt deres dynamik. De resultater neutronspredning giver inden for materialeforskning er vigtige, så selv om det er dyrt at producere neutroner, bliver det gjort verden over. En af fordelene ved neutronspredning er, at neutroner interagerer svagt med materiale, hvilket betyder, at man kan lave forsøg ind gennem prøveomgivelser som f.eks. kryostater eller trykceller, hvilket ikke kan gøres med f.eks. lys eller elektroner. Neutroner har en bølgelængde og en energi i samme størrelsesorden som afstanden mellem atomerne og de fundamentale eksitationer i faste stoffer. Desuden varierer spredningstværsnittet for neutronen på en tilsyneladende tilfældig måde for grundstofferne op gennem det periodiske system. Dette betyder, at neutronspredning giver en enestående mulighed for at undersøge, hvor lette grundstoffer befinder sig i materialer.

Monte Carlo metoden bliver brugt i en bred vifte af numeriske simuleringer. Algoritmen benytter gentaget tilfældig sampling for at opnå præcise numeriske resultater. I Monte Carlo ray tracing programmet, McStas, bliver neutronpakker sendt gennem en række komponenter, der indeholder en matematisk beskrivelse af fysiske processer som foregår i hver enkelt del af et instrument.

The European Spallation Source (ESS) er i øjeblikket i den bygningsforberedende fase og bliver den første langpulsede neutronkilde i verden. Med den lange pulslængde bliver instrumenterne også lange og der skal udvikles nye neutronguides. Jeg har designet og simuleret et nyt guidekoncept, som gør det muligt at sende neutroner til mange prøvepositioner fra samme beamport uden et mærktbart tab af neutronintensitet på prøvepositionerne. Jeg har testet tre versioner af guide-split-idéen i McStas for tre forskellige versioner; for to, fire og otte sekundære instrumenter, alle med en samlet længde på 150 m. Under simuleringerne opdagede jeg, at parameterrummet indeholdt flere områder hvor brilliansoverførslen var høj (over 90%), hvilket er meget højere end for traditionelle beam-guides. Jeg fandt endvidere et sæt parametre for beam-guiden, der giver en uniform divergensfordeling i et sådant højintensitetsområde.

Et vigtigt område inden for neutronsperdning er pulverdiffraktion, hvor materialestrukturen bliver undersøgt. De små enkeltrystaller i prøven er tilfældigt orienteret i prøveholderen, og når man sender et monokromatisk beam ind på prøven, vil kegler af spredte neutroner blive udsendt fra denne. Fra keglevinklerne og information om beamets bølgelængde er det muligt at at udregne prøvens struktur. To andre neutronteknikker er imaging, hvor prøvens absorption omdannes til et billede, og neutron-småvinkelspredning (SANS), som kan måle størrelser, former og orden af systemer med karekteristiske længder på 1-1000 nm.

Heimdal instrumentet, som er et projektforslag til ESS, kommer til at kombinere et

termisk pulverdiffraktometer med et SANS instrument og en imagingstation. Heimdals hovedformål vil være at undersøge 'functional materials in action'. Jeg har lavet analytiske udregninger og computersimuleringer i McStas for at designe pulverdiffraktometerdelen af Heimdal. Dette instrument har en instrumentopløsningschopper, med en åbningstid på 123 μs placeret 6,5 meter fra kilden. Alle pulser fra kilden bliver brugt, så for at udfylde tidsrammen og undgå overlap mellem pulserne, er instrumentet nødt til at være 168,8 meter langt og bølgelængdebåndet skal holdes inden for 1,74 Å. Middelbølgelængden er valgt til at være 1,5 Å, hvilket giver et interval fra 0,63 Å til 2,37 Å. Detektorens udformning er holdt simpel, fordi detektorteknologien i øjeblikket er under hurtig udvikling. Den er derfor cylinderformet med en radius på 1,5 m og har en pixelopløsning på of 3×3 mm^2. Dette giver en naturlig instrumentopløsning på $\frac{\sigma_d}{d} = 0.0707\%$, når de forskellige bidrag til opløsningen holdes lige store. Mine computersimulationer og analytiske udregninger stemmer overens, og med data fra simulationerne har det vist sig, at det er nødvendigt skrive nyt software, der kan analysere 2D data. Et endeligt guidedesign er ikke blevet valgt, da de fysiske rammer bliver revideret og opdateret samtidig med det løbende arbejde udført af de forskellige arbejdsgrupper på ESS. Med dette speciale har jeg vist, at et termisk pulverdiffraktometer er en mulighed på ESS og instrumentforslaget for Heimdal baserer sig på mit arbejde.

Abstract

Neutrons are a unique probe for studying the atomic and molecular structure and dynamics of materials. Even though neutrons are very expensive to produce the advantages neutrons provide overshadow the price, as neutrons interact weakly with materials compared to many other probes, e.g. electrons or photons, it is possible to make a neutron scattering experiment through sample environment devices like cryostats or pressure cells. Another advantage of neutron experiments is that the wavelength and energy of the neutron match the inter-atomic distances and basic excitations of solid materials. The scattering cross section varies through the periodic table in a seemingly random fashion. Neutron scattering offers thus a unique possibility to study light elements.

The Monte Carlo method is used in a broad variety of numerical simulations. The algorithms rely on a repeated random sampling to obtain accurate numerical results. In the Monte Carlo ray tracing program McStas, neutron rays are propagated through components that contain a mathematical description of the physical processes of each particular device of an instrument.

The European Spallation Source (ESS) is currently in the pre-construction phase and is going to be the first long pulsed spallation source. The long source pulse calls for long instruments, and hence new guide designs are being developed. I have developed and simulated a guide-split concept that makes it possible to feed several cold neutron instruments with low divergence on the sample, from the same beam port without compromising the neutron flux notably at any of the sample positions. Three guide split set-ups have been tested via computer simulations in McStas; with two, four, or eight secondary guides with a total length of 150 m. During the optimization, the parameter space was found to have several plateaus with high brilliance transfer (>90%). A smooth divergence distribution at the sample position can be obtained by choosing parameters that further this.

One important use of neutrons is powder diffraction where the structure of materials is studied. The small single crystals are randomly oriented in the sample container, and when shining a monochromatic beam onto the sample, cones of scattered neutrons are emitted. From the angles of the cones together with information on the incoming wavelength, the crystal structure of the sample can be derived. Other neutron techniques are neutron imaging that measures the absorption of the sample to make an image, and the small angle neutron scattering (SANS) technique which is used to probe the size, shape, and order of systems that have a characteristic length scale of 1-1000 nm.

The multipurpose machine, Heimdal proposed for ESS, will combine thermal neutron powder diffraction, SANS, and neutron imaging in one single instrumental set-up at ESS, and the task of the instrument will be to study advanced functional materials in action. Analytical calculations, as well as simulations in McStas have been made in order to

design the Heimdal powder diffractometer instrument. The instrument has a resolution chopper with a full time opening of 123 μs at 6.5 m from the source. Every pulse is used, so in order to fill the time frame and avoid frame overlap the instrument is 168.8 m long. The wavelength band is from 0.63 Å to 2.37 Å. The detector is kept simple, as the detector technologies presently are undergoing transformative developments, and it therefore has a cylindrical shape with a radius of 1.5 m and a pixel resolution of 3×3 mm^2. This gives a natural instrument resolution of $\frac{\sigma_d}{d} = 0.0707\%$, when resolution matching is desired. Simulations and calculations are in agreement. From the data produced in the simulations it has become clear that new software is needed in order to analyze these 2D data sets. A final guide design has not yet been chosen as the physical requirements for an optimization are revised and updated with the ongoing work from the different divisions of ESS. With this work a feasible design for a thermal powder diffractometer at ESS has been presented. The instrument preproposal for the Heimdal diffractometer is based on this work.

Chapter 1

Introduction

Neutrons are a unique probe for studying the atomic and molecular structure and dynamics of materials. One important reason is that their energy scale and wavelength match the basic excitations and inter-atomic distances of solid materials. As the neutron has no electrical charge, it interacts weakly with materials making it a gentle and non-destructive probe. However, neutrons are hard to produce in the quantities necessary for performing neutron scattering experiments and scientists have to travel to large-scale facilities in order to perform their experiments. There are more than 20 facilities around the world with user programs open to the science community.

The European Spallation Source (ESS) is currently in the pre-construction phase and is going to be the first long pulsed spallation source and is scheduled to deliver its first neutrons in 2019 and have its full complement of 22 public instruments by 2025 at a total cost of € $1.8 \cdot 10^9$. ESS is going to be the most powerful neutron source in the world, at least 5 times brighter than any source today.

With the opportunities presented by a long pulse spallation source, there is a drive towards elaborating and optimizing instrument concepts across the whole range of neutron instruments. However, the long pulse also calls for long instruments. Therefore new neutron guide design ideas are necessary. In the recent years the so-called "ballistic" guides and full elliptical geometries have been investigated with the aim of reducing transport losses in guide systems. This I describe in chapter 5.

In chapter 5 of this thesis a new guide concept is also presented enabling an increase the instrument capacity of a neutron source. The idea is to have two elliptical guides in series, where the second guide is slightly rotated around a point near to their closely spaced focal points. In turn, this rotation gives the possibility of placing several secondary elliptical guides at one beamport.

Many of the instrument concepts at ESS are new and untested. In the pre-construction phase of ESS it is vital to know how different instrument designs perform. In chapter 6 the calculations and computer simulations of a thermal powder diffractometer per-

formed within the Danish-Swiss work package is presented. Finding an optimal design of a high-resolution powder diffraction instrument is a most difficult task, because the high-resolution required is in clear contrast to the time uncertainty given by the long pulse.

The work on the thermal neutron powder diffractometer presented in this thesis will be used to make an instrument proposal for ESS. It will hopefully be chosen as one of the instruments that are going to be built and will, if all goes well, be ready for user operation in 2019.

Throughout the thesis it is assumed that the reader has a basic knowledge about solid state physics and crystallography, e.g. the reciprocal space.

Chapter 2

Neutron scattering

In the early days of the neutron techniques (1940'ies) it was only used in chemical crystallography and solid state physics. Over the years many other science communities have come to use the neutron scattering techniques as part of their scientific work. Today fuel cells, drug delivery systems, molecular magnets, composite materials, protein dynamics, high temperature superconductors, and paleoclimatology are being discovered, investigated, and developed with neutrons.

This chapter accounts for the basic properties of the neutron starting with a historical overview.

2.1 The first neutron experiments

In 1911 Ernest Rutherford proposed an atomic model with a charged cloud surrounding a small core with a opposite sign of charge [1]. In 1917 he split the atom and three years later in a proceeding article of the Royal Society on "Nuclear Constitution of Atom" he wrote:

> *"On present views, the neutral hydrogen atom is regarded as a nucleus of unit charge with an electron attached at a distance, and the spectrum of hydrogen is ascribed to the movements of this distant electron. Under some conditions, however, it may be possible for an electron to combine much more closely with the H nucleus, forming a kind of neutral doublet. Such an atom would have very novel properties."*

This was the first hypothesis describing the nucleon that later turned out to be the neutron.

James Chadwick graduated in 1912 from Victoria University of Manchester where Rutherford was head of the physics department. Chadwick moved to Berlin to work with

Hans Geiger. At the end of World War I he returned to Rutherford's laboratory from Germany and started working on experiments that could lead to proof of the existence of the neutron. In 1932 he succeeded [2, 3].

The first neutron diffraction experiments were carried out by two different groups both in 1936 but with the aim of demonstrating the wave-particle duality of the particle and not to study materials [4]. After the Manhattan Project was launched in 1942, a new powerful source for neutrons was at the scientists' disposal. In 1944 the first neutron scattering experiments probing solids were done at the graphite-moderated X-10 pile and heavy-water reactor CP-3 at the Oak Ridge National Laboratory [5] (see figure 2.1).

Neutron scattering was established as an effective probe for solid state materials. This was done by observations of an antiferromagnetic Bragg peak from a manganese oxide powder sample in 1949 by Shull and Smart [6] and the by spectroscopy measurements by Brockhouse in 1958 [7] on a germanium single crystal. These experiments opened up a new field of research:

> *The Nobel Prize in Physics 1994 was awarded "for pioneering contributions to the development of neutron scattering techniques for studies of condensed matter" jointly with one half to Bertram N. Brockhouse "for the development of neutron spectroscopy" and with one half to Clifford G. Shull "for the development of the neutron diffraction technique".*
>
> - the Nobel Prize homepage [8].

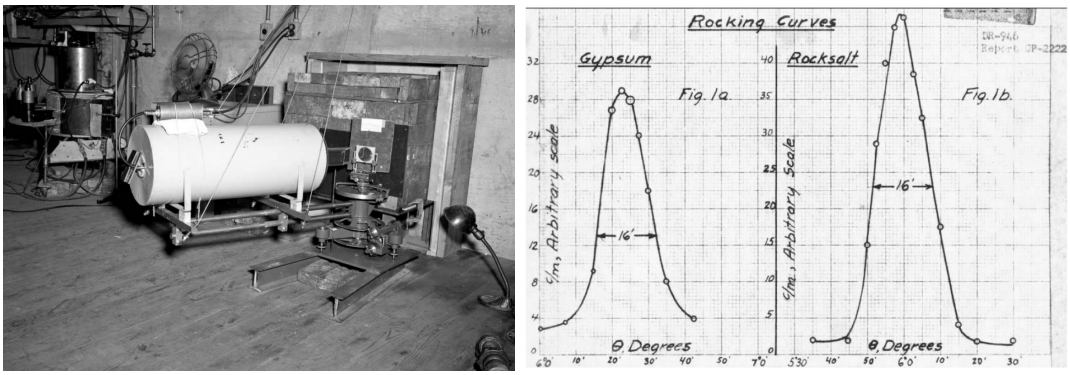

Figure 2.1: Left: A picture from 1946 of one of the first single crystal spectrometers in the world built by Wollan at the graphite reactor in Oak Ridge. The instrument is placed right next to the reactor with the neutrons coming out of a hole in the main wall. Note the alarmingly small amount of shielding used at that time. **Right:** Rocking curves of Bragg peaks from two single crystals ($CaSO_4 \cdot 2H_2O$ and NaCl) obtained by Wollan and Borst (two great physicists also working at the Manhattan Project) in December 1944 at the X-10 pile. Figures taken from [4].

2.2 Simple properties of the neutron

The mass of the neutron is roughly the same as the proton namely $m_n = 1.675 \cdot 10^{-27}$ kg = 1.009 u and has a life time of $\tau_n = 886$ s = 14.8 minutes[1]. It has no charge but a magnetic moment of

$$\mu = \gamma \mu_N, \qquad \gamma = -1.913 \tag{2.1}$$

where $\mu_N = \frac{e\hbar}{2m_p} = 5.051 \cdot 10^{-27}$ J/T is the nuclear magneton. The neutron is a spin half particle ($s = \frac{1}{2}$). As the neutron can be viewed both as a wave and a particle (cf. de Broglie) the wavelength of the neutron is

$$\lambda = \frac{2\pi\hbar}{m_n v} \tag{2.2}$$

which, when doing neutron scattering experiments, is of the order of Ångström. The neutron can described as a plane wave

$$\psi_i(\boldsymbol{r}) = \frac{1}{\sqrt{Y}} \exp(i\boldsymbol{k}_i \cdot \boldsymbol{r}) \tag{2.3}$$

where Y is a normalization constant. The ***wave vector*** of the neutron is

$$\boldsymbol{k} = \frac{m_n \boldsymbol{v}}{\hbar} \qquad k = \frac{2\pi}{\lambda} \tag{2.4}$$

and the energy of a free neutron is

$$E = \frac{\hbar^2 |\boldsymbol{k}|^2}{2m_n} \tag{2.5}$$

2.3 The neutron as a probe

Neutron experiments are laborious and very expensive. It is therefore advisable, if possible, to get the answer to a scientific question by using another technique. So why do we bother with neutrons? Even though neutrons are very expensive to produce it is a unique probe for material science. In this section some of the main advantages neutrons provide are presented, but first we need to go through some definitions and equations.

2.3.1 Basic scattering theory

The neutron ***flux***, Ψ, is defined as the number of neutrons hitting a surface per second normalized by the surface area perpendicular to the neutron beam direction. The flux in a point $\boldsymbol{r}_j$ from an incoming neutron wave, ψ_i, is

$$\Psi_i = v_i |\psi_i(\boldsymbol{r}_j)|^2 = \frac{1}{Y} \frac{\hbar k_i}{m_n}. \tag{2.6}$$

[1] In sections 2.2 and 2.3 numbers and equations are from the neutron scattering course notes by Kim Lefmann [9].

Flux is traditionally measured in n/cm^2/s [9].

The neutron ***scattering cross section***, σ, is defined as the fraction of an incoming neutron beam that is scattered from an area perpendicular to the beam multiplied by that area or

$$\sigma = \frac{\text{number of neutrons scattered per second}}{\Psi_i}. \tag{2.7}$$

The scattering cross section has the unit of m^2. If you place an atom in a neutron beam, σ can be viewed as the effective area of the nucleus seen by the neutrons [9]. The ***differential scattering cross section*** describes the angular dependence of the scattered neutrons

$$\frac{d\sigma}{d\Omega} = \frac{\text{number of neutrons scattered per second into a solid angle } d\Omega}{\Psi_i d\Omega}. \tag{2.8}$$

A measure of how strong a particular nucleus scatters a neutron is the ***scattering length***, b. The scattering length of a single atom, b_j, is found in the following equation describing elastic scattering of a neutron on a nuclei.

$$\psi_f(\boldsymbol{r}) = -b_j \frac{\psi_i(\boldsymbol{r}_j)}{|\boldsymbol{r} - \boldsymbol{r}_j|} \exp(ik_f|\boldsymbol{r} - \boldsymbol{r}_j|) \tag{2.9}$$

where ψ_f is the wave function of the neutron after the collision. Note that ψ_f is spherical. ψ_i is the initial wave function of the neutron (see eq. (2.3)), $\boldsymbol{r}_j$ is the position of the atom j, $\boldsymbol{r}$ is a point in space, and k_f is the magnitude of the outgoing wave vector. b_j can be both positive and negative depending on the nucleus.

If we have more that one nucleus, the outgoing spherical waves will interfere with each other. For a two atom system (j and j') the final wave is

$$\psi_f(\boldsymbol{r}) = -b_j \frac{\psi_i(\boldsymbol{r}_j)}{|\boldsymbol{r} - \boldsymbol{r}_j|} \exp(ik_f|\boldsymbol{r} - \boldsymbol{r}_j|) - b_{j'} \frac{\psi_i(\boldsymbol{r}_{j'})}{|\boldsymbol{r} - \boldsymbol{r}_{j'}|} \exp(ik_f|\boldsymbol{r} - \boldsymbol{r}_{j'}|) \tag{2.10}$$

which, under the assumption that the two atoms are close together compared to the distance of the observation point, can be rewritten as (a thorough explanation of how this is done can be found in [9])

$$\psi_f(\boldsymbol{r}) = \frac{1}{\sqrt{Y}} \frac{1}{r} \exp(i\boldsymbol{k}_f \cdot \boldsymbol{r}) \Big(- b_j \exp(i(\boldsymbol{k}_i - \boldsymbol{k}_f) \cdot \boldsymbol{r}_j) - b_{j'} \exp(i(\boldsymbol{k}_i - \boldsymbol{k}_f) \cdot \boldsymbol{r}_{j'}) \Big). \tag{2.11}$$

We define the ***scattering vector*** as

$$\boldsymbol{q} = \boldsymbol{k}_i - \boldsymbol{k}_f \tag{2.12}$$

which is a central definitions in neutron scattering. Generalizing eq. (2.11) to many nuclei, the outgoing wave is

$$\psi_f(\boldsymbol{r}) = \frac{1}{\sqrt{Y}} \frac{1}{r} \exp(i\boldsymbol{k}_f \cdot \boldsymbol{r}) \sum_j -b_j \exp(i\boldsymbol{q} \cdot \boldsymbol{r}_j). \tag{2.13}$$

The number of neutrons scattered per second into a solid angle, $d\Omega$, can be calculated as the flux of the outgoing neutron wave through a small area, dA. We can hence write eq. (2.8) as

$$\frac{d\sigma}{d\Omega} = \frac{v_f |\psi_f|^2 dA}{v_i |\psi_i|^2 d\Omega}. \tag{2.14}$$

Since $dA = r^2 d\Omega$ we can divide the solid angles out and insert the expressions for ψ_i and ψ_f and get

$$\frac{d\sigma}{d\Omega} = \frac{v_i}{v_f} \frac{\left| \frac{1}{\sqrt{V}} \frac{1}{r} \exp(i\boldsymbol{k}_f \cdot \boldsymbol{r}) \sum_j -b_j \exp(i\boldsymbol{q} \cdot \boldsymbol{r}_j) \right|^2 r^2}{\left| \frac{1}{\sqrt{V}} \exp(i\boldsymbol{k}_i \cdot \boldsymbol{v}) \right|^2}. \tag{2.15}$$

If we let the scattering from the nuclei be elastic ($k_i = k_f$), the final equation for nuclear elastic scattering is

$$\left. \frac{d\sigma}{d\Omega} \right|_{nucl.el.} = \left| \sum_j b_j \exp(i\boldsymbol{q} \cdot \boldsymbol{r}_j) \right|^2. \tag{2.16}$$

More on this will follow in section 3.4.

2.3.2 Scattering cross section

The cross section varies through the periodic table in a seemingly random fashion. This gives neutron scattering a unique possibility to study light elements. This is unlike x-rays where hydrogen is nearly invisible since the scattering cross section for x-rays is proportional to the atomic number squared (because they scatter from the electrons). In figure 2.2 proportions of the coherent x-ray and neutron scattering cross sections are shown for a small selection of atoms.

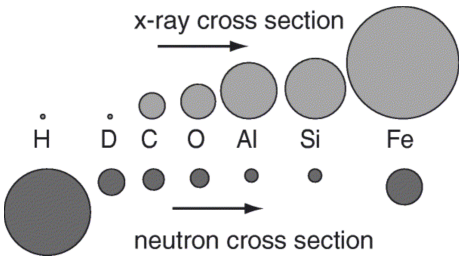

Figure 2.2: The total scattering cross section for neutrons and x-rays for different isotopes compared [10]. Note the large difference between hydrogen and deuterium for neutrons.

2.3.3 Isotope contrast

Deuteration of samples, in which hydrogen is exchanged with deuterium in order to change the contrast of the sample, is widely used in neutron science. A simple example of contrast manipulation is shown in figure 2.3 where a liposome is placed in solutions with different water to heavy water ratios, so that the scattering length of the solution either matches the hydrophilic heads or hydrophobic tails of the lipids. This is possible because the scattering length of hydrogen is negative ($b_H = -3.741 \cdot 10^{-15}$ m) and positive for deuterium ($b_D = 6.674 \cdot 10^{-15}$ m) [9].

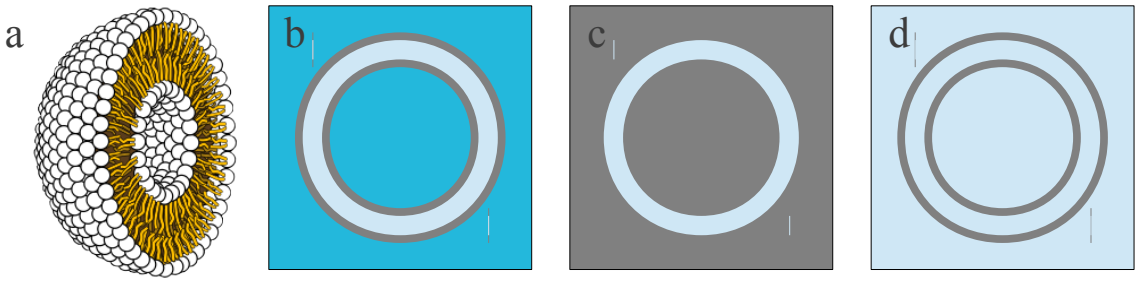

Figure 2.3: Neutron scattering from liposomes. a) is a sketch drawing of half a liposome taken from quickwiki.com [11]. b-d) are three different contrast conditions for enhancing different parts of the liposome. b) shows a liposome in normal water seen by a neutron. If one measures a scattering pattern and then from that reconstructs the image, a scattering pattern with all the information on top of each other might not be analyzable. Hence conditions like in c) are produced where only the hydrophobic tail layer is visible to the neutrons. In d) the neutrons see the hydrophilic heads. This is done by mixing normal and deuterated water in different ratios. Combining all the information from b-d can give a much more precise picture of the structure and content of the sample.

2.3.4 Transparency

As neutrons interact weakly with materials compared to many other probes e.g. electrons or photons, it is possible to make a neutron scattering experiment through sample environment devices like cryostats or pressure cells.

This transparency also has the effect that the entire bulk sample is probed as opposed to most other techniques that only probe the surface of a sample.

With neutrons the higher order effects (e.g. many interactions inside the sample) of scattering are small due to this weak interaction with matter. This makes it possible to make theoretical models that can describe the measured experimental data with high accuracy.

2.3.5 Energy and wavelength

When you do a neutron experiment the wavelength is typically of the order Å and the corresponding energy is of the order meV. The conversion between the two is

$$E = \frac{(2\pi\hbar)^2}{2m_n\lambda^2} = [9.0446 \text{ meV Å}^2] \frac{1}{\lambda^2}. \tag{2.17}$$

An inter-atomic distance in a solid is typically 3 Å. When neutrons scatter on a lattice with the same characteristic length as its wavelength, a very strong interference effect known as ***Bragg scattering*** (see section 3.4) may occur.

The low lying dispersion curves of phonons (fundamental excitations in a crystal) are typically in the meV regime, and as Brockhouse shows neutrons are very sensitive to these phonons [7]. The process where a neutron creates or absorbs a phonon is known as ***inelastic scattering***.

2.3.6 Magnetism

The neutron has a magnetic moment. So in a magnetically ordered sample, the neutrons will scatter coherently from the magnetic structure. Solving magnetic structures and study magnetic excitations are hard tasks not many other techniques can do.

2.4 Neutron sources

In this section it is described how neutrons for scattering experiments are produced. Furthermore a short presentation of the European Spallation Source (ESS) is given.

2.4.1 Neutron production

There are two main ways of producing neutrons: either fission or spallation. With both techniques it is possible to let the source have either a pulsed or a continuous neutron flux emitted from them.

Fission and spallation

In nuclear reactors more neutrons are produced in the fission process than needed in order to maintain the chain reaction. Hence, a nuclear reactor can be used as a neutron source. This technique was the first one to used for neutron production and is still widely used today.

The other main neutron production technique is spallation. Here protons are accelerated into the GeV regime and stopped by a target made of a material containing heavy nuclei. This violent collision spalls off bits of the heavy nuclei and creates free neutrons

among the reaction products. The first neutron spallation source, IPNS Argonne USA, was opened in 1982 [12].

Schematic drawings of single events of these two neutron production techniques are displayed in figure 2.4.

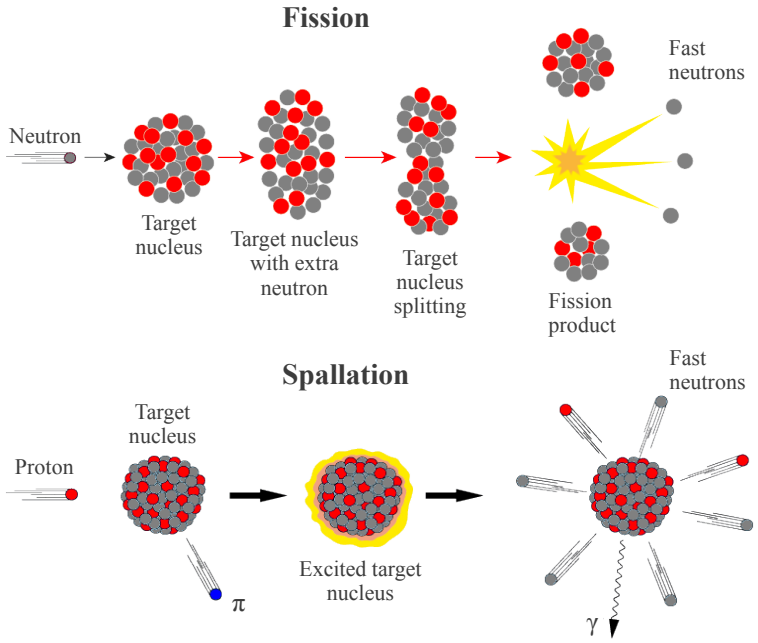

Figure 2.4: Nuclear reactions that produce neutrons. **Top:** One event in the chain reaction that takes place in a fission reactor. The target nucleus is typically uranium and the fission products are typically krypton and barium. **Bottom:** In a spallation process the proton is accelerated to the GeV regime and into the target nucleus which is typically a heavy element like lead or tungsten. The nuclear processes taking place in the two types of neutron production are not within the scope of this thesis but can be found in textbooks like [13]. The drawings are inspired by pictures found on the PSI (spallation) and HZB (fission) web pages [14, 15].

Continuous or pulsed sources

When making neutron experiments, two main categories of instruments are used; ***time of flight*** (ToF) and ***monochromator instruments***. They both have the same objective, namely to determine and control the wavelength of the neutrons before and/or after the sample.

When using ToF one needs to know when the neutrons leave the source and when they arrive at the sample in order to calculate their speed and hence their wavelength. This is done by sending the neutrons out in short bursts. It can be done by either having a pulsed source or by chopping the continuous neutron stream right after the source by blocking

the beam with a suitable frequency. A typical pulse length is of the order of hundreds of microseconds.

The ***time of flight equation*** is used when making ToF experiments.

$$t = \alpha \lambda L \tag{2.18}$$

where t is the flight time, $\alpha = m_n/h = 0.2528 \frac{\text{ms}}{\text{Åm}}$, L is the flight path, and λ is the wavelength.

With a monochromator instrument a single crystal is used to scatter the beam in a specific direction and hence pick out a specific wavelength by utilizing ***Braggs law***;

$$n\lambda = 2d \sin(\theta) \tag{2.19}$$

where n is a real number, d is a lattice spacing in the material, and θ is half the scattering angle.

Around the world different design decisions and solutions of neutron sources have been implemented. In table 2.1 the main neutron sources of the world are listed. There are still by far more reactor sources in the world but spallation sources are getting more popular and with the construction of the European Spallation Source a new landmark for neutron production will be set.

2.4.2 Moderation of neutrons

After the neutrons are produced it is necessary to slow them down from energies of MeV to an energy and wavelength scale of a solid material namely meV and Å. This is done with a moderator which is essentially a tank of water, heavy water, or liquid nitrogen. The idea is to let the neutrons pass through a material where they will deposit their energy by colliding with the nuclei and in the end reach thermal equilibrium with the surroundings. A typical wavelength distribution for a ***cold moderator*** operating at 30 K and a ***thermal moderator*** operating at 300 K is displayed in figure 2.5. The two spectra are used by different types of instrument that investigate samples with different characteristic lengths or energies. Neutron moderator design is out of the scope of this project, but more introduction to this subject can be found in [16].

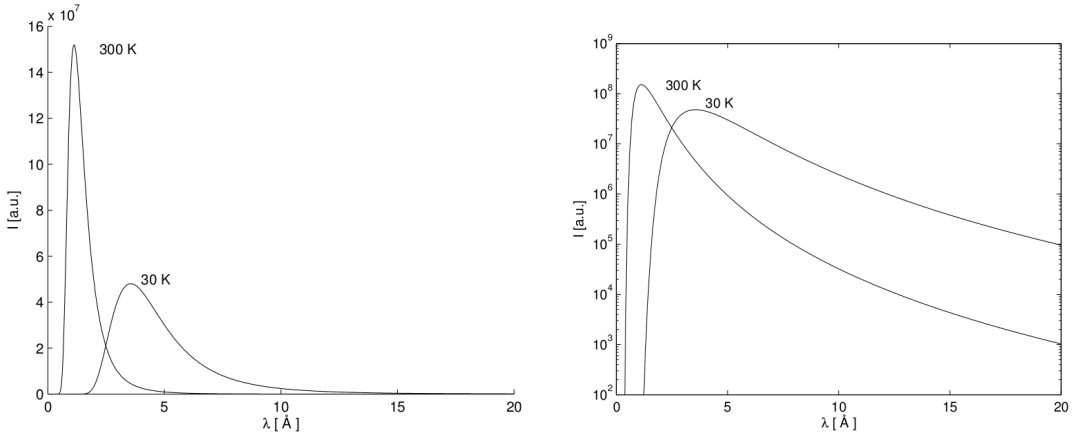

Figure 2.5: Source spectra emitted from a moderator surface. A Maxwellian wavelength distribution is typical for both cold (30 K) and thermal (300 K) moderators. The figure is from [9].

	Continous	**Pulsed**
Reactor	BARC, Mumbai, India CARR and CIAE, China FRM2, Munich, Germany HANARO, Daejeon, South Korea HFIR, Oak Ridge, USA HZB, Berlin, Germany ILL, Grenoble, France IRI, Delft, Netherlands JAERI, Tokai, Japan KAMINI, Kalpakkam, India KFKI, Budapest, Hungary LLB, Paris, France NIST, Washington D.C., USA NRC, Chalk River, Canada OPAL, Sydney, Australia	IBR-2, Dubna, Russia
Spallation	PSI, Villigen, Swizerland	ISIS, Oxford, England J-PARC, Tokai, Japan LANSCE, Los Alamos, USA SNS, Oak Ridge, USA

Table 2.1: List of large neutron research facilities world wide.

2.5 The European Spallation Source

ESS is a neutron spallation source that will be built in Lund in Sweden. Seventeen European countries are working together to fulfill their common goal of having this, the world's brightest source, on-line in 2019 [17].

ESS will be the first long pulsed source with a pulse length above 1 ms (τ=2.86 ms). This is a ten times longer pulse than found at conventional spallation sources (e.g. ISIS, SNS, and J-PARC). In figure 2.6 the expected pulse shape of ESS is compared to three other spallation sources and the reactor source ILL. With the construction of ESS, the field of neutron scattering is on the verge of entering a new era with short measurement times and vast amounts of data. With modern computers it is possible to record an experiment in ***event mode*** which means that every neutron detected in an experiment will get a time stamp and a position. This is of great advantage for ToF experiments, and it is easy to make a spallation source pulsed which is needed in ToF.

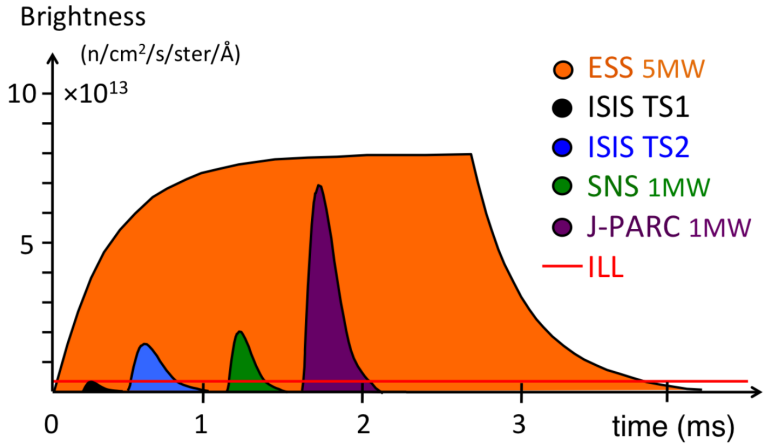

Figure 2.6: ESS pulse shape compared to three other spallation sources and the reactor source ILL. From appendix A.5.

2.5.1 New ToF instrument designs

As ESS is a pulsed source most instruments at ESS will use the ToF technique. But since the pulse is long the flight path of the neutrons also needs to be long in order to obtain a high time resolution ($\Delta t/t \sim$ 0.1-1 %). If one designs an instrument that uses the full pulse and has a resolution of $\Delta t/t = 0.1$ % instrument length needs to be (from eq. (2.18))

$$L = \frac{\tau}{0.1\%\ \alpha\ \lambda} = \frac{2.86\text{ ms}}{0.1\%\ 0.2528\ \frac{\text{ms}}{\text{Å m}}\ 4\text{Å}} \approx 3000\text{ m} \tag{2.20}$$

if the operation wavelength is 4 Å. It is neither affordable nor feasible to build instruments that are 3 km long. So clever schemes where the only parts of the pulse are used, are being

implemented.

The simplest way is to have a ***chopper*** (a device that opens and closes the neutron beam path) close to the source. It should then be tuned so that it is open in the time interval that is needed in order to get the desired time resolution for the instrument.

A picture of one type of chopper, a disc chopper, is displayed in figure 2.7. This chopper is designed to be light and is made of carbon-fiber-reinforced boron-containing plastic and can therefore drive at 350 Hz. Boron is a strong neutron absorber.

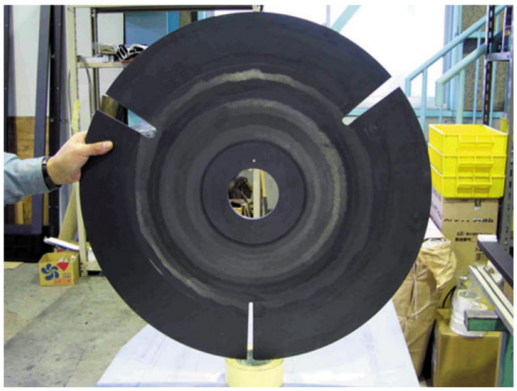

Figure 2.7: A picture of a high speed disc chopper made of carbon fiber reinforced boron containing plastic from the J-PARC spallation source in Japan.

Also more elaborate chopper systems can be used. F. Mezei describes how this can be done in [18]. The two schemes he describes are ***wavelength frame multiplication*** (WFM) and ***repetition rate multiplication*** (RRM).

RRM is a scheme where the neutron pulse is chopped just before the sample into many short and almost monochromatic pulses. From one main pulse all the sub-pulses will arrive at different times with the short wavelength sub-pulse arriving first and longer wavelength later. In this way short pulses with a well defined wavelength in each pulse arrive at the sample with a steady frequency. A ToF diagram showing this is displayed in figure 2.8.

In WFM scheme it is utilized that the pulse is long and that all wavelengths are emitted through the entire pulse. The slow neutrons emitted in the beginning of the pulse are let through the chopper system, and the fast neutrons from the end of the pulse are likewise let through. This means that N pulses with high resolution hit the sample at different times and the instrument only needs to be 1/N as long for the time frame (source period) to be filled out.

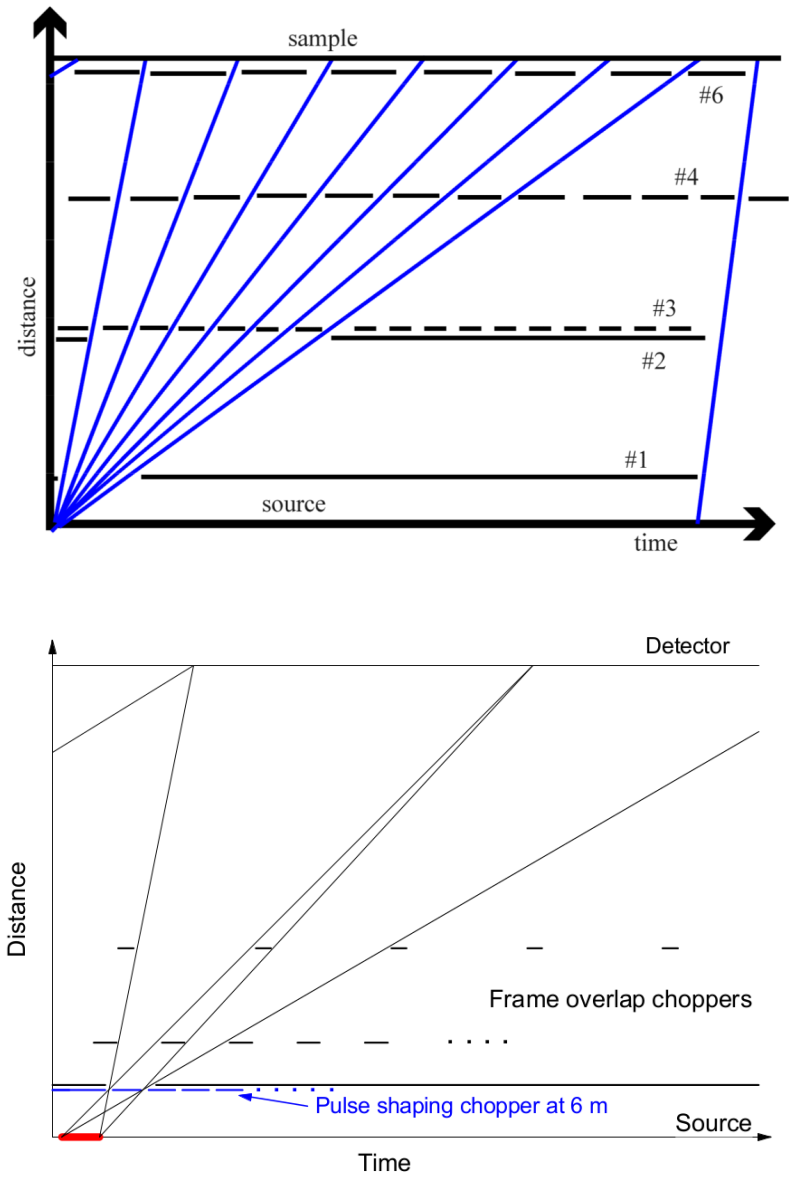

Figure 2.8: ToF diagrams of RRM (top) and WFM (bottom). The black horizontal dotted lines mark where the chopper is closed. The steeper the slope of the neutron flight path, the faster the neutron. Both plots are from [18].

Chapter 3

Neutron scattering techniques

There are five main technique categories that all use neutrons to investigate materials. These techniques utilize the different interactions a neutron can have with a material, i.e. absorption, elastic processes, inelastic processes, and reflection.

3.1 Imaging

The imaging technique is perhaps the most commonly known of the five main techniques, as most people (in the first world) have had an x-ray picture taken at some point in their lives. Neutron imaging, however, is less known.

Both x-ray and neutron imaging exploit the fact that different materials have different absorption coefficients, e.g. x-rays pass through the soft tissue made from oxygen, hydrogen, and carbon but not through the hard bone containing calcium.

The remarkable thing about neutrons is that the absorption for the elements does not follow the atomic number in a systematic fashion, unlike x-rays where the absorption is proportional to the atomic number hyper-cubed (Z^4).

As seen in figure 3.1, aluminum is almost transparent whereas water has a large absorption so that one can study how an Italian coffee maker works in action. Many more scientific questions can be answered using the imaging techniques.

The basic idea in imaging is to have a beam with a large cross section shining onto a two dimensional detector. The beam is then attenuated by the object of interest and record the image. Of course modern imaging stations utilize a variety of different clever modifications to this set-up in order to enhance the image resolution. E.g. one can shine a highly divergent[1] beam through a small pinhole so that the projected image of the object on the detector is many times larger than the object itself as shown in figure 3.1.

[1] A measure of how straight the neutrons fly or in a more formal wording; the spread of the neutron velocity directions. See section 5.1 for further explanation.

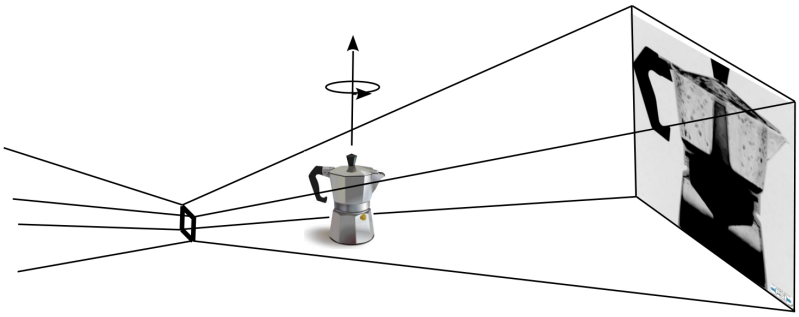

Figure 3.1: Schematic drawing of the neutron imaging technique. The sample is rotated and images are taken at different angles when making neutron tomography. The image used in the drawing was taken by Anders Kaestner at PSI and can be found on `Youtube` a very nice video of how an Italian coffee maker works [19]

3.1.1 Tomography

The word tomography is derived from the Greek tomos ("part" or "section") or tome ("cut") and is a technique where 3D computer generated objects are constructed from many 2D absorption images taken at different angles of the object. It is a widely used technique, especially at hospitals where it is known as CT-scanning (computed tomographic scan).

On the computer, doctors (both medical and scientific) can pull out slices of the 3D object for examination enabling them to look into things or people without cutting them open. At the Niels Bohr Institute it is possible to take images of small objects (2cm×2cm×2cm) and I had the pleasure of trying the equipment as part of the exercises in the x-ray scattering course. Our results from these exercises are displayed in figure 3.2 and shows a 3D reconstruction of an elderberry bud.

3.2 Small angle scattering

The small angle neutron scattering (SANS) technique is used to probe the size, shape, and order of systems that have a characteristic length scales of 1-1000 nm.

Since small differences in angles are measured when doing SANS, it is important to have a well defined measure for both the incoming and outgoing angles in the experiment. This is achieved by having the incoming neutrons pass through a set of pinholes before the sample and placing the detector far away from the sample so that you can calculate the scattering angle with high precision. Since the neutrons scatter on air, a SANS machine typically has the detector in a long vacuum tank so that the neutrons can move freely from the sample to the detector. A schematic drawing of a SANS set-up can be found in figure 3.3.

Typical samples that are measured with a SANS set-up are biological systems in solu-

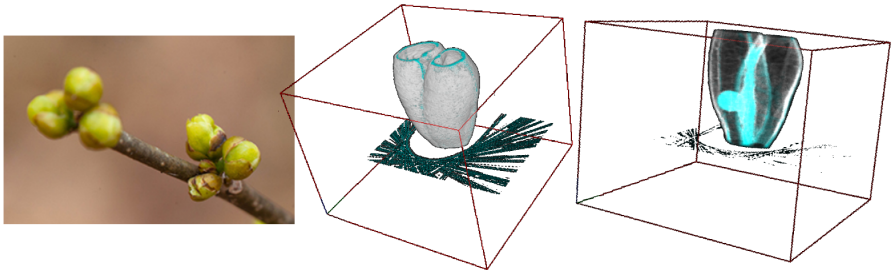

Figure 3.2: X-ray tomograms of a developing elderberry bud taken in the lab at the Niels Bohr Institute as part of the x-ray scattering course. **Left:** Photo of the a developing elderberry bud from `overtonpark.org` [20]. **Center and right:** The computed 3D object generated from 180 2D images (195×195 pixels). The two constructed images are shown with two different thresholds for the absorption, highlighting different parts of the elderberry bud. The plane made from stripes, clearly visible in the center picture, is an artifact from the reconstruction.

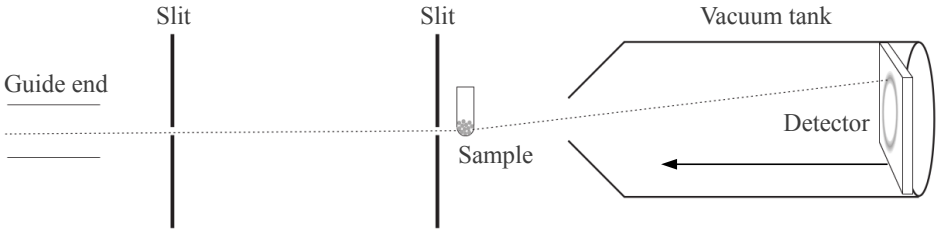

Figure 3.3: Schematic drawing of a SANS instrument from [9]. The detector can move back and forth in the vacuum tank so that the resolution and angle coverage can be tuned to fit the experimental needs.

tion like membranes and proteins. Also many magnetic structures have a typical length scale that are well suited to be studied using SANS. An example of this, from work I have participated in, is presented below.

3.2.1 SANS measurements on haematite exsolution lamellae

The sample with haematite exsolution lamellae oriented parallel in an ilmenite host is a natural rock sample found in Norway. A SANS image of this is shown in figure 3.4. This was measured at D22 at ILL and the data has not yet been fully analyzed. However, it is clear that the lamellae structure (long in one direction and short in the other) is visible in the data as the intense spot in the middle is elongated. In figure 3.4 the radially integrated intensity curves are plotted on double logarithmic scale. This is how SANS data is typically displayed. The sections of integration are chosen so that the information in the data is not lost. This is symmetry and sample dependent.

Analyzing SANS data is an art. The model for a SANS system is typically complicated as the samples are complicated This gives many free parameters. But too many free parameters may result in good fits to the data, and one can therefore not be sure that the results are valid. Hence it takes a lot of training to make a model that describes the system in an efficient way so that the fitting results can be trusted.

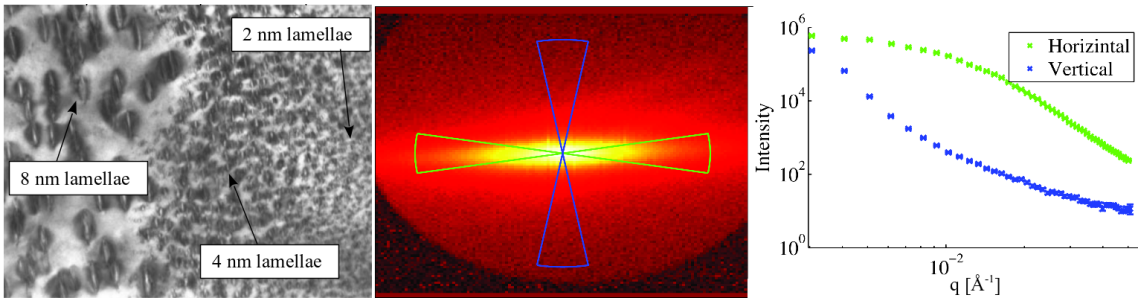

Figure 3.4: SANS image of lamellar haematite-ilmenite. **Left:** Transmission electron microscope image of haematite exsolution lamellae parallel to (001) in an ilmenite host [21]. **Center:** Colour plot of the detected neutron intensity on the detector. **Right:** Radially integrated intensity curves of the SANS data on double logarithmic scale. The position on the detector is calculated into q.

3.3 Reflectometry

In reflectometry surfaces and thin samples are investigated. Types of materials that are often studied include biological membranes, magnetic multilayers, and polymer films.

Reflectometry and SANS have many similarities as neutrons are scattered from the sample with small angles. The data is presented in the same way with intensity as a function of q on a double logarithmic scale but the instrumental set-ups differ from each other. The models used to analyze reflectivity data are strongly sample dependent like in SANS.

Apart from being used to address a large variety of interesting science, reflectivity is also used in neutron optics. Neutron supermirrors have played a major role in the advances made in guide systems for neutron instruments over the last two decades.

3.3.1 Neutron optics

Snell's law is probably the most fundamental equation in optics and has been known in the Arabic world for over a thousand years [22] but is named after the Dutch astronomer Willebrord Snellius (1580-1626). It describes the relationship between the angle of incidence and the refraction of a wave when going from one medium to another with the refractive indices n_1 and n_2. A drawing of this can be found in figure 3.5.

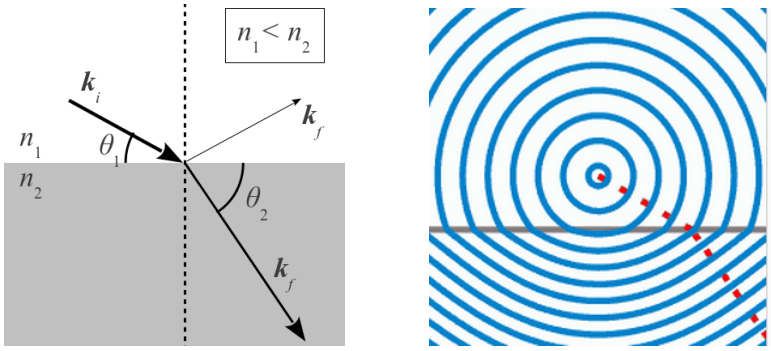

Figure 3.5: Two illustrations of Snell's law. In the left picture the angles θ_n are the ones usually used in neutron optics. The incoming wave ($\boldsymbol{k}_i$) can be refracted and goes into material 2 or be reflected and proceed back up into material 1 depending on incident angle θ_1. The illustration on the right is from [23] and shows a spherical wave being refracted.

Since the incident angles in neutron optics are small, the convention is to use θ and not α which is $\pi/2-\theta$ and is used in light optics. Snell's law using the neutron convention is

$$\frac{\cos(\theta_1)}{\cos(\theta_2)} = \frac{n_2}{n_1}. \tag{3.1}$$

When θ_1 gets sufficiently small ($\cos(\theta_1) \to 1$) there is no way the equation can be satisfied if $n_2/n_1 < 1$ as $\cos(\theta_2)$ can never be larger than one and therefore the wave cannot be refracted and is hence mostly reflected. It is called total reflection. The angle at which this happens is called the critical angle, θ_c, and is typically on the order of $0.1°$. θ_c increases linearly with the wavelength. If the critical angle is expressed in terms of q, the critical scattering vector, q_c which is independent of λ, will be

$$q_c = 2k\sin(\theta_c(\lambda)) \approx 4\pi\frac{\theta_c(\lambda)}{\lambda}. \tag{3.2}$$

3.3.2 Neutron guide materials

Nickel is the standard material for guide mirrors and has $q_{c,\mathrm{Ni}} = 0.0219\text{Å}^{-1}$. This gives a critical angle of $1°$ for 10 Å and $0.1°$ for 1 Å neutrons meaning that guides have a hard time transporting thermal neutrons.

With supermirrors it is possible to boost q_c and hence θ_c. The idea behind supermirrors is to make many layers of two materials with different coherent scattering cross sections and low absorption on top of each other. The neutrons will then make Bragg scattering, if the incident angle of the neutron and layer thickness satisfy the Bragg condition. One may vary the thickness of the layers up through the layers so that many lattice spacings are optained and hence many Bragg angles. An illustration of this principle can be found

in figure 3.6. Supermirrors are given a value, m, relative to the critical angle of nickel

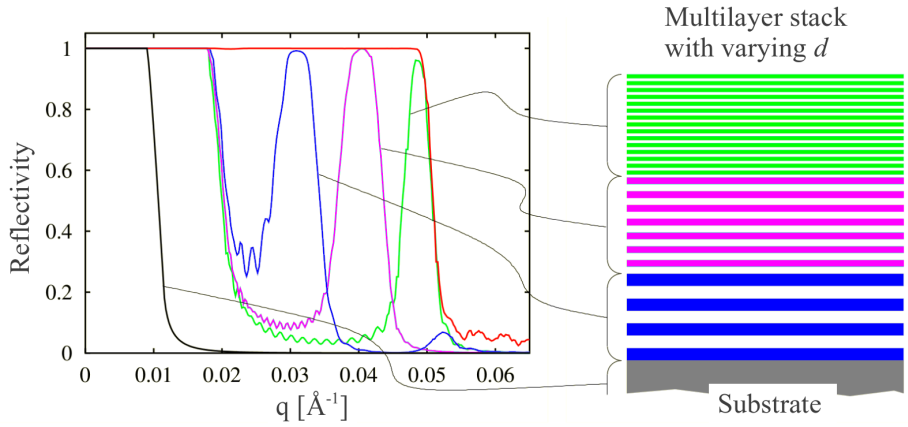

Figure 3.6: Reflectivity curves of supermirror layers of different thicknesses. As more layer thicknesses are added on top of each other a higher m value of the supermirror is obtained. The red line is the reflectivity curve for a perfect supermirror. The graph is from [24].

defined as $q_c = m\ q_{c,\mathrm{Ni}}$. In figure 3.7 reflectivity curves for supermirrors made by Swiss Neutronics [25] are displayed. From the graph it can be seen that when the m value is pushed up the reflectivity goes down. Mirrors with $m = 7$ are currently the state of the art but the reflectivity is down to 0.5 close to q_c.

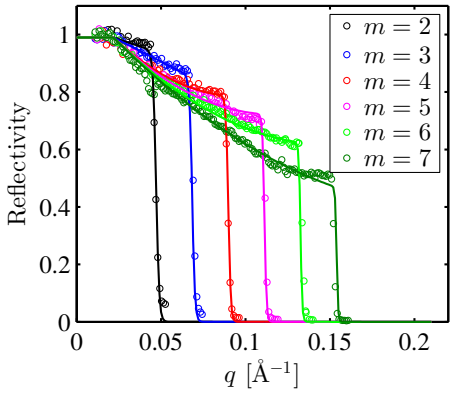

Figure 3.7: Measured reflectivity curves for different m values of supermirrors made by Swiss Neutronics. The figure is from [26].

3.4 Diffraction

The structure of materials is studied with diffraction. In chemistry neutron diffraction is used to find out where light elements like hydrogen are placed in the unit cells of

materials as this cannot be done with a normal x-ray lab source. Specialized biologists use macromolecular crystallography to study biological molecules such as proteins, viruses and nucleic acids (RNA and DNA). As neutron scattering is a unique probe for studying magnetism, physicists use diffraction to solve magnetic structures.

Neutron diffraction is mainly done on crystalline materials either as powder diffraction or as single crystal diffraction.

3.4.1 Simple diffraction theory

The equation of elastic nuclear scattering found in section 2.3.1 states that

$$\left.\frac{d\sigma}{d\Omega}\right|_{nucl.el.} = \left|\sum_j b_j \exp(i\boldsymbol{q}\cdot\boldsymbol{r}_j)\right|^2 \tag{3.3}$$

where j runs over all atoms. For most values of $\boldsymbol{q}$ the sum of complex exponentials will average to zero, but if $\boldsymbol{q}\cdot\boldsymbol{r}_j = 2\pi n$ interference occurs. If the sample is a crystalline material it, has a periodic lattice structure with the reciprocal lattice vector $\boldsymbol{\tau}$ (for a simple cubic system $\tau = 2\pi/a$). As the atom sites ($\boldsymbol{r}_j$) are ordered with the distance a between them (simple cubic) interference occurs when $\boldsymbol{q} = \boldsymbol{\tau}$.

The sum in eq. (3.3) can be divided into a sum over the unit cells and a sum over the atoms inside the unit cells in the following way

$$\left.\frac{d\sigma}{d\Omega}\right|_{nucl.el.} = \left|\sum_{i,j} b_i \exp(i\boldsymbol{q}\cdot(\boldsymbol{\mathcal{R}}_j + \boldsymbol{R}_i))\right|^2 = \left|\sum_j \exp(i\boldsymbol{q}\cdot\boldsymbol{\mathcal{R}}_j)\right|^2 \left|\sum_i b_i \exp(i\boldsymbol{q}\cdot\boldsymbol{R}_i)\right|^2 \tag{3.4}$$

where i counts the atoms inside the cell and j counts the cells. Using that the structure is periodic and that you only get scattering when the scattering vector is a multiplum of the period, the differential scattering cross section can be written as

$$\left.\frac{d\sigma}{d\Omega}\right|_{nucl.el.} = N\sum_j \delta(\boldsymbol{q}-\boldsymbol{\tau}_j)\left|\sum_{\text{cell}} b_i \exp(i\boldsymbol{q}\cdot\boldsymbol{R}_i)\right|^2. \tag{3.5}$$

The sum over the cell is usually called the ***form factor***, F_N. The intensity measured on a detector covering the solid angle $d\Omega$ is

$$I \propto \sum_j \delta(\boldsymbol{q}-\boldsymbol{\tau}_j)|F_N|^2. \tag{3.6}$$

The prefactors left out in eq. (3.6) are the incoming intensity on the sample, the sample volume, and a term from the vibration of the nuclei.

The condition $\boldsymbol{q} = \boldsymbol{\tau}$ is the ***Laue condition*** . From figure 3.8 it is clear that

$$q = 2k\sin(\theta) \Rightarrow \tau = 2k\sin(\theta) \Rightarrow \frac{2\pi}{d} = 2\frac{2\pi}{\lambda}\sin(\theta) \Rightarrow \lambda = 2d\sin(\theta). \tag{3.7}$$

The relation $dq = k\lambda = 2\pi$ should be kept in mind.

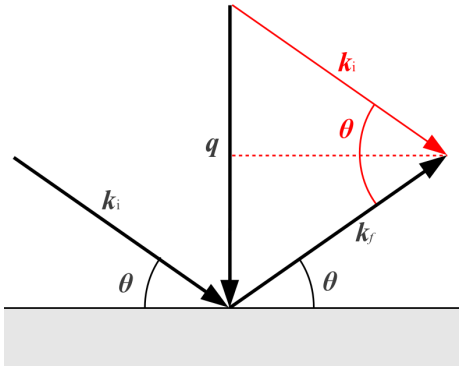

Figure 3.8: An illustration of the scattering process when doing Bragg scattering ($\boldsymbol{q} = \boldsymbol{k}_i - \boldsymbol{k}_f$ and $|\boldsymbol{k}_i| = |\boldsymbol{k}_f|$). When looking at the triangles created by the red part of the drawing, it is clear that $q = 2k\sin(\theta)$.

3.4.2 Diffraction experiments

Powders are small single crystals with a typical grain size of μm. The grains are randomly oriented in the sample container so when shining a monochromatic beam onto the sample, cones of scattered neutrons are emitted from the sample as illustrated in figure 3.9. They are called ***Debye-Scherrer cones*** and will be emitted where the Bragg condition (eq. (3.7)) is satisfied with an angle corresponding to a d-spacing between the lattice planes in the grains. When making a diffraction experiment you will typically get tens to hundreds of reflections.

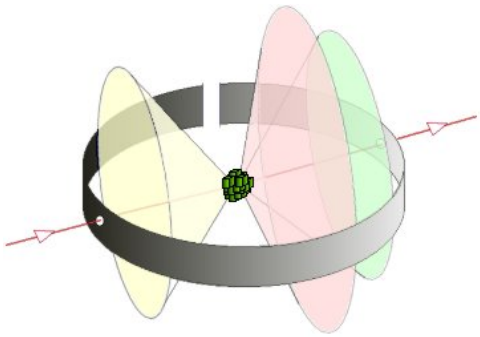

Figure 3.9: Debye-Scherrer cones scattered from a powder sample. The red line is the monochromatic neutron beam hitting the sample. The gray cylinder represents a typical powder diffraction instrument detector. The signal from the cones on the detector will appear as slightly curved vertical lines. The figure is from [27].

An example of a powder diffraction data set is shown in figure 3.10. It is data from a virtual experiment performed with the instrument described in chapter 6. The sample used in the simulation is $Na_2Ca_3Al_2F_{14}$ (NaCaLF) which is a compound commonly used for

calibrating powder diffractometers as the q positions of the Bragg peaks are well separated and the space group (P-43n (218)) is one with low symmetry giving rise to many reflections.

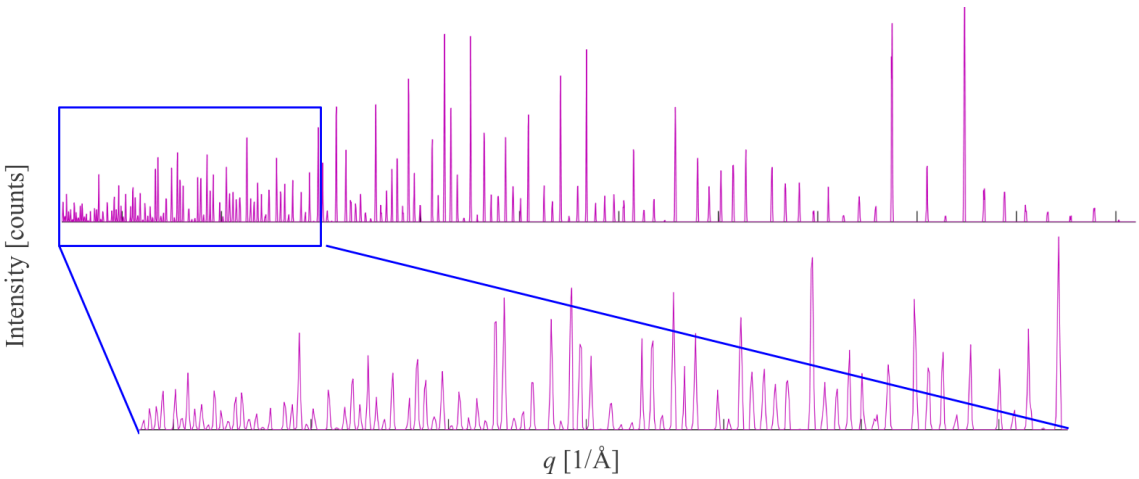

Figure 3.10: Virtual powder diffraction data of a NaCaLF sample. The data is from the backscattering bank ($165° < 2\theta < 175°$) integrated over the scattering angle of the full 2D data set displayed in figure 6.9. The q range displayed is between 2.5 $Å^{-1}$ and 12.5 $Å^{-1}$, which is the range of the backscattering bank.

There is a broad variety of software tools and data refinement methods to make data analysis of powder diffraction data. Two of the methods are ***Rietveld refinement*** and the ***pair distribution function*** (PDF) analysis. The Rietveld method uses a least squares approach to refine a theoretical line profile until it matches the measured profile with respect to the intensity, width, and position of the Bragg reflections. Rietveld refinement only works when the atoms are in a crystal structure due to the fact that the atoms in the model are moved around inside the unit cell in order to change the line shape of the fit. PDF determines the inter-atomic distances between pairs of particles and can hence also be used to analyze disordered systems like liquids or gases as the model does not contain structural information.

In single crystal diffraction the scattering from a lattice plane only goes in one single direction (and not in a cone like powder diffraction). One way to measure this is with the ***Laue diffraction*** technique where a white beam (a spectrum of wavelengths) is shined onto a single crystal sample and the Bragg reflections are recorded by a detector. For every lattice plane with a reachable d, there will be a wavelength in the beam such that Bragg's law is fulfilled. A picture of such a set-up is shown in figure 3.11. Laue diffraction is often used to align single crystal samples for other types of experiments (e.g. spectroscopy experiments explained in section 3.5).

When making single crystal experiments for refinement purposes, it is desirable to

cover a full 4π for the solid angle from the sample with the detector to catch as many reflections as possible. When using a monochromatic beam, all angles can be covered by moving a single detector around to measure the desired reflections if the sample is turned around to match the detector positions. With ToF large detector arrays are used and the sample is turned 180° around in small steps and all the recorded data sets are patched together before the data refinement is made.

Figure 3.11: Laue diffraction. **Left:** The Laue diffractometer OrientExpress at ILL. The white dot in the center of the detector plate is where the neutrons hitting the sample are coming from. The neutrons hit the sample and get scattered back onto the detector where the pattern is recorded. To the right of the sample is a normal camera with a live feed to the control computer so that the sample alignment and orientation can be viewed at all times. **Center and right:** Two plots of Laue diffraction pattens from a superconducting $(La,Sr)_2CuO_4$ single crystal taken at the OrientExpress (center) and at a x-ray lab source at RISØ DTU (right). This was done in order to check the sample alignment before a spectroscopy experiment.

3.5 Inelastic scattering

Inelastic neutron scattering or spectroscopy is used to study excitations in materials. These quasiparticles living inside the crystal, described by their momentum, q', and energy, $\hbar\omega_{q'}$, can be measured because the neutrons can interact with both phonons (lattice vibrations) and magnons (magnetic excitations). By using conservation of energy it possible to measure the excitations by knowing the energy of the neutrons both before and after the sample. The energy transfer of the neutron to the quasiparticle is

$$\hbar\omega = E_i - E_f \tag{3.8}$$

where ω is the angular frequency of the excitation, E_i is the energy of the neutron before the sample, and E_f is the energy after the sample.

There are many experimental ways of determining the energy of the neutron. The most commonly used technique is triple-axis spectroscopy where the beam before and after the sample is Bragg scattered with crystals that are part of the set-up. As the lattice of the two crystals (called monochromator and analysator) are well known, one wavelength is picked out by a chosen angle of scattering. The name of this technique refers to the three rotation axes of the monochromator, sample, and analyser.

3.5.1 Neutron spectroscopy measurements on $YMnO_3$

An example of a sample that I measured with triple-axis spectrosopy is $YMnO_3$ a geometrically frustrated antiferromagnet with multiferroic properties. $YMnO_3$ has a magnetic phase transition at T_N =72 K, so when making one measurement above and one below the Néel temperature and comparing the two spectra, one can get information on how both the structural and magnetic excitations behave. In this way the coupling between magnons and phonons in the material is explored. It may explain an anomaly in the heat conductivity measured in the sample (see figure 3.12).

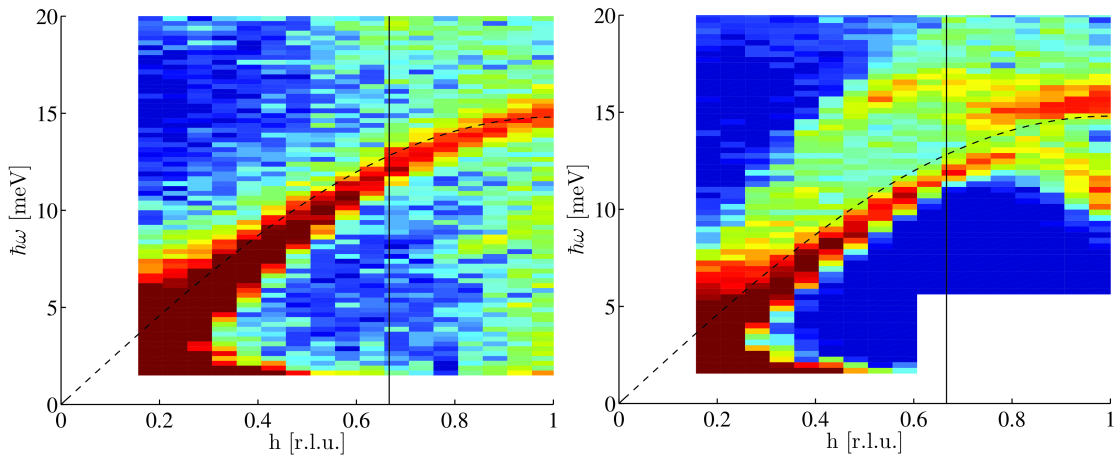

Figure 3.12: Inelastic neutron data measured around q = (030) at the thermal triple-axis instrument EIGER at PSI. The maps of inelastic scattering is taken at 100 K (left) and 40 K (right). The vertical line shows the zone boundary of this hexagonal unit cell. The 100 K data shows a single phonon branch, illustrated by a dashed line. The 40 K data shows the same phonon branch out to $h = 0.7$, where a discontinuity appears, seeming like a gap. In addition, a magnon branch appear, but is also irregular around $h = 0.7$. This could be the signature of magnon-phonon hybridization.

Chapter 4

Computer simulations of neutron instruments

In this chapter the method behind computer simulations of neutron instruments is described. We shall have a look at the underlying computational technique, the Monte Carlo (MC) method, and how to set this up in order to perform neutron ray tracing simulations that at the end can provide a full virtual experiment.

4.1 The Monte Carlo method

The MC method is used in a broad variety of numerical simulation. The algorithms rely on a repeated random sampling to obtain accurate numerical results. It can e.g. be used to solve differential equations, integrals, simulate experiments, and find optimal strategies in game theory.

4.1.1 The invention of the Monte Carlo method

The MC method was invented in 1946 by the Polish-American mathematician Stanislaw Marcin Ulam and developed in collaboration with John von Neumann. Ulam was taken ill, and during his illness he played solitaire. He tried to calculate the chance of success in a game of Canfield solitaire laid out with 52 cards, but after fruitless calculations he instead decided to play the game over and over to gather statistics. In that way he would get an estimate of the chance of success with a higher and higher prediction as the games went by [28].

Ulam was working at the Los Alamos Scientific Laboratory as part of the Manhattan Project, and when he returned to work after his illness he discussed his newly invented way of calculating probabilities with von Neumann. Ulam wanted to calculate neutron diffusion in materials (not game theory) with his new technique. However, von Neumann,

who founded game theory in 1928 with his minimax theorem [29], gave this new computing technique the name Monte Carlo after a casino in Monaco [28].

4.1.2 Random numbers

Random numbers are the backbone in MC simulations. One problem is that it is very hard to generate truly random numbers on a computer. In a MC simulation you typically use billions of random numbers and if there is a systematic trend in your pool of random numbers, your results will also carry that trend and hence may be misleading.

One of the most used ways of of generating random numbers is called the ***multiplicative linear congruential algorithm*** where you start with an integer, n_1, called the ***seed***. From the seed new integers are generated by calculating the modulo in the following way:

$$n_{i+1} = (an_i) \bmod m \tag{4.1}$$

where a and m are integers. This will give you a sequence of numbers in the interval $n_i \in [1; m-1]$ that can be transformed into the interval $r_i \in (0; 1)$ by calculating a new series of random numbers $r_i = n_i/m$. The values of $m = 2,147,483,399$ and $a = 40,692$ have been shown to have a period of $m - 1 \approx 2 \cdot 10^9$ in 1988 by [30]. Today we have more complicated algorithms that produce sequences of random numbers with periods larger than 10^{43}.

Of course all these computer algorithms do not generate truly random numbers as the numbers are calculated. Truly random numbers can be generated by making a physical experiment like tossing a coin or measuring the spin of a particle, but this is a cumbersome and inconvenient way of generating billions of numbers. For most applications the computer generated numbers are sufficiently random and are called ***pseudo random numbers***.

4.2 Ray tracing simulations

In the MC ray tracing program McStas [31] the neutron rays are propagated from component to component in the simulation. A neutron ray in McStas has ten variables assigned to them. Nine of them are physical, a position (x,y,z), a velocity (v_x,v_y,v_z), and a spin (s_x,s_y,s_z), and one variable is used in the ray tracing, the ***weight factor***, p, which contains information on how probable the specific neutron path is. Every time a simulation is run, the number of rays, N, need to be specified. If you have a simple source with a uniform distribution of neutrons emitted from the surface in all directions with a uniform wavelength distribution, the weight factors will all be $p = I/N$ where I is the ***intensity*** of the source measured in neutrons per second. For more complicated source spectra and

emission distributions the intensity is

$$I = \sum_{i=1}^{N} p_i \tag{4.2}$$

where i is the ray index. The intensity is valid through all components of the simulation and is mostly used in detector components. It is important to note that N has no physical meaning and one should always use the intensity when evaluating the performance of an instrument. If the ray for some reason does not hit a component, the ray will be killed and the number of rays will therefore decrease.

There are three types of components in McStas;

Source components are components that create the N rays in the simulation run. In order to increase the efficiency of the simulation the input values for a source component often include a wavelength band, a solid angle in which neutrons are emitted, and a time window that the rays are created to be within. The weight factor is then corrected correspondingly e.g. a solid angle is divided by 4π and multiplied onto the weight factor.

An **analytical component** is a component that contains a function which takes in a ray and gives back out the ray but with changed parameters e.g. a simple mirror that only changes the direction of the ray. The probability of being reflected, and not absorbed or refracted, will be multiplied onto the weight factor and all other processes are ignored as they are not important for the instrument simulation.

Monte Carlo choice components contain a list of stochastic processes that may occur and their corresponding probabilities. The component will then take a MC choice between the processes and after that the corresponding probability is multiplied onto the weight factor of the ray. This could for example be an advanced mirror where the neutrons transmitted through the mirror also are of interest in the simulation (e.g. a bi-spectral switch [26]). Here you have two processes of interest, reflection and transmission. The neutron ray can only do one of the processes and a MC choice is hence needed. The most straightforward way would be to weigh the choice of the processes with the probability of their occurrence. So if there is a 20% chance of reflection this will then occur one in five times a ray is sent through the component. Most MC components work that way. But even if one process is much more probable than the other, one may still choose to have a, say, fifty fifty chance between the two if they are equally important for the simulation as long as the weight factors are lowered correctly.

When you have a component with a MC choice near the end of the instrument (e.g. a sample with thousands of reflections), one can use the SPLIT command that from one ray hitting the component generates multiple rays, with an accordingly lower weight factor. This splitting is performed before the MC choice. In this way better statistics may be obtained on the detector with fewer calculations.

This method employing weight factors used in the McStas code is one of many ***variance reduction techniques***. Further reading on this subject can be found in reference [32].

4.3 Building a virtual instrument in McStas

When building a virtual instrument components are placed geometrically after each other via McStas, which in fact is a "meta language" written on top of the programming language C [33]. The components cover all parts of a neutron instrument (e.g. sources, mirrors, monochromators, beam stops, choppers, polarizers, filters, samples, and detectors) and if the McStas library does not contain a component that describes some equipment that is needed for a simulation, it is possible for expert users to write a new component and add it to the library. The core of McStas that translates the McStas code into C should not be modified by users.

In general you start a simulation by defining an origin at (0,0,0). The source is typically placed there and all other components are placed relative to the source or relative to other previous components. In McStas the convention is to have the instrument and ray direction along z, and use x for left and right, leaving y to be up and down. All components need to be placed in order along the beam direction and it is not possible to have normal components inside each other (note that the guide should be cut into segments in order to fit in another component. That could for instance be a chopper).

4.3.1 An instrument example

I here present an example of a simple powder diffractometer placed at the ESS source. It is followed by an elliptical guide interrupted by a chopper placed 6 m from the source. The sample is placed at the end of the guide in the middle of a cylindrical detector. The instrument layout is displayed in figure 4.1.

It is easy to get out information in McStas that one would normally not have access to in a real life experiment. This is one of the reasons why simulations are such a powerful tool. If one want to get information on how the real data from an instrument would look like it is necessary to write a component that only uses information available in a real experiment. I have therefore written a detector that calculates q from Bragg's law where the angle is measured on the detector taking into account the shape of the Debye-Scherrer cones in the out of plane scattering. The wavelength is calculated via ToF using the instrument length and the information about the delay of the resolution chopper and distance from the source. Data from this detector is displayed in figure 5.11.

Running a simulation with a hundred million rays ($N = 10^8$) using one core (Intel Core i7-3520M Processor, 3.6 GHz) on a laptop takes about 12 minutes for the instrument described in section 5.3.6. But the run time is strongly dependent on how many and which components you use. To get data in a quality that can be displayed in a thesis one should

probably should spend 3-4 hours on a simulation or use the ESS Data Management Center cluster [34].

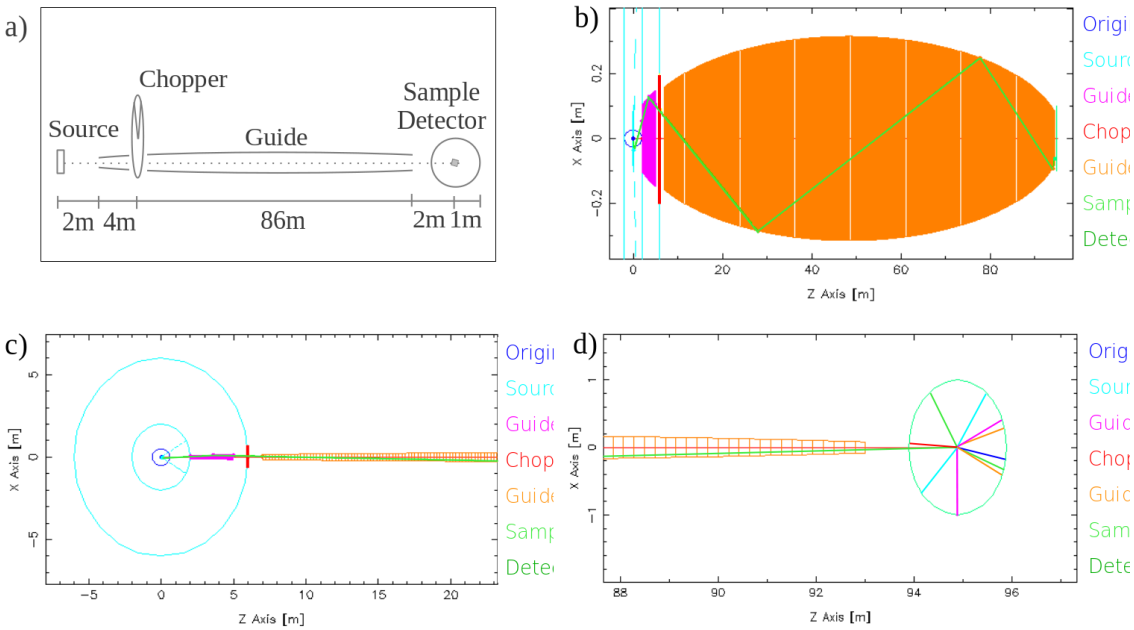

Figure 4.1: Layout of a simple powder diffractometer instrument example for McStas. **a)** shows a schematic drawing of the instrument. **b-d)** are output plots that McStas can generate. **b)** shows a top view of the full instrument. The green zigzag line shows a ray path thought the instrument. The circles representing the source (turquoise) and the detector (green) are flattened due to the stretched axis. **c)** is a zoom in of the first part of the instrument. The blue circle is the origin in the simulation and is defined as (x,y,z)=(0,0,0). The two concentric circles in turquoise represent target monolith and is part of the source component. The first part of the guide (magenta) is inside the shielding and a chopper (red) is placed right outside the monolith at 6 m. The front end of the second part of the guide (orange) is also displayed. **d)** is a zoom in of the end of the second guide piece (orange), the sample (lime green) and the cylinder-shaped detector (green). The multiple lines going from the sample are ten rays generated from the one ray hitting the sample. This is done using the SPLIT command.

Chapter 5

Neutron guides

The design of neutron guides has gone through many transformations since the first straight guides of the sixties [35, 36]. The realization that a removal of the sample from line of sight to the source leads to a significant reduction of the background noise from fast neutrons and gamma radiation, gave rise to a slightly curved version of the straight guide which is still the standard guide design at many neutron facilities [35, 36].

With the addition of the super-mirror coating in the seventies [37, 38], another vital step in the improvement of neutron guides was taken. In the recent years ballistic guides with straight tapering [39, 40], parabolic tapering [10] and full elliptical [41, 42, 43] geometries have been investigated with the aim of reducing transport losses in guide systems.

In this chapter we shall go through some aspects of neutron guides and optics. A new guide bundle concept of mine will be presented and is the core part of this chapter. But first we need to define a measure with which we can compare neutron transport performances of different types of guides.

5.1 Brilliance transfer and the Liouville Theorem

When describing neutron transport from the moderator to the sample, it is convenient to view the neutrons in a semi-classical way. When the neutrons are emitted from the moderator surface they have a position and a velocity. In order for the neutrons to hit the sample they need to be guided as most of the neutrons are not going straight towards the sample.

The ***Liouville Theorem*** describes the time evolution of the phase space distribution function. Consider a Hamiltonian dynamical system of n particles where q_i are the canonical coordinates, p_i are the conjugate momenta, and $\rho(p,q)$ is the phase space distribution. This distribution determines the probability $\rho(p,q)d^nqd^np$ that the system will be found in the infinitesimal phase space volume d^nqd^np. The equation that Liouville proved in 1938 [44] states that the time evolution of the phase space density is described by

$$\frac{d\rho}{dt} = \frac{\partial\rho}{\partial t} + \sum_i^n \left(\frac{\partial\rho}{\partial q_i}\dot{q}_i + \frac{\partial\rho}{\partial p_i}\dot{p}_i \right) = 0 \tag{5.1}$$

and can be found in textbooks about classical mechanics, e.g. [45]. This leads to the Liouville Theorem stating that *"the distribution function is constant along any trajectory in phase space"* [28].

Since neutrons do not interact, we need only to consider one particle at the time which reduces the phase space from $6N$ dimensions to 6. For a neutron beam it is convenient to express the 6D phase space as x, y, z, λ, η_x, and η_y where η_i is the horizontal and vertical divergences respectively. ***Divergence*** is the spread of the neutron velocity directions passing through an area. This gives a measure of how straight the neutrons fly.

Since reflections are an elastic process, λ is unchanged. Furthermore, we are only interested in the brilliance at the moderator ($z = 0$) and at the sample position ($z = L$). So the variables we are usually concerned with are x, y, η_x, and η_y.

For our purpose, neutron transport, it is convenient to have a measure for guide performance. One of them is ***brilliance transfer***. It is defined as the transmission of the four dimensional (2D position, 2D divergence) phase space through the guide system to the samples [46] within a certain wavelength band. From the Liouville Theorem it follows that the brilliance transfer cannot exceed unity and we can hence compare guide performances by a simple number between 0 and 1.

With guides one can manipulate phase space but you can not condense it (eq. (5.1)). The best solution is to transport everything within a defined volume of phase space, e.g. 1 cm^2, maximum 0.5° horizontal and vertical divergence and a wavelength band of 2-5 Å.

If the angular uncertainty of the beam is too high (large divergence) in order to perform an experiment with a desired resolution, one can ***collimate*** the neutron beam. This means to throw away neutrons that have a too large divergence. It can be done with a collimator, a device with channels made from a neutron absorbing material that absorbs the neutrons not going straight. Or one can use ***collimation by distance*** that exploits the fact that the further away you are from a source the smaller it appears in size (see figure 5.1).

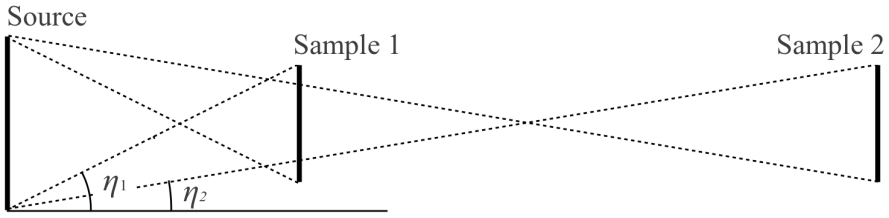

Figure 5.1: Collimation by distance. As the sample is moved further away from the source the maximal divergence that can hit the sample from the source becomes smaller.

5.2 Guide geometries

For every reflection in the guide there is a probability that the neutron is absorbed. With ***ballistic*** guides (see figure 5.2) one can lower the divergence by increasing the area of the volume of the desired phase space. In this way one will have fewer reflections in the guide. The smaller incident angles to the guide walls also increases the probability of reflection of the neutron. There are different ways to expand the guide but the most efficient ones are the ballistic guide with parabolic tapering (ends) or a fully elliptical shape. These guides can transport more than 90% of a desired brilliance for most neutron experiments [43].

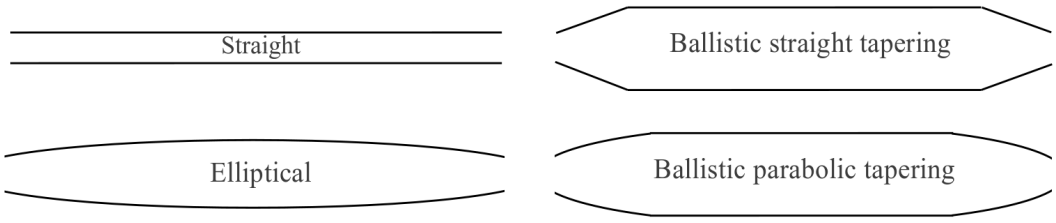

Figure 5.2: Schematic drawings of four different guide geometries.

5.3 Guide-split

Since the number of beam ports at neutron facilities are limited due to the source geometries, the concept of having several instruments on the same beam port is well known using straight or curved guides of constant cross section. These ***guide bundles*** are e.g. found at ILL [47] and enable a sharing of the neutron flux amongst the instruments placed on a beam port. However, this reduces the flux. The new ***guide-split*** concept presented in this section makes it possible to feed several cold neutron instruments with low divergence on the sample, from the same beam port without compromising the neutron flux notably at any of the sample positions.

The guide-split could become a great advantage as it will be possible to increase the instrument capacity at neutron facilities without compromising the instrument performances.

Examples of instruments that could be placed at a guide-split, with particular emphasis on instruments for ESS, are presented at the end of the section, along with a full virtual experiment performed on a magnetism diffractometer proposed for ESS.

The guide-split concept will be published soon and the draft of the article can be found in appendix A.3.

5.3.1 The concept of split elliptical guides

Elliptical guides are capable of transporting an almost completely filled phase space within a large divergence ($\pm 2^\circ$), for cold neutrons [43]. The end of a primary guide can therefore be used as a virtual source point. Consequently, it is possible to place several secondary guides side by side oriented along slightly different directions, and hence exploit different parts of the transported phase space. An illustration of this arrangement is shown in figure 5.3.

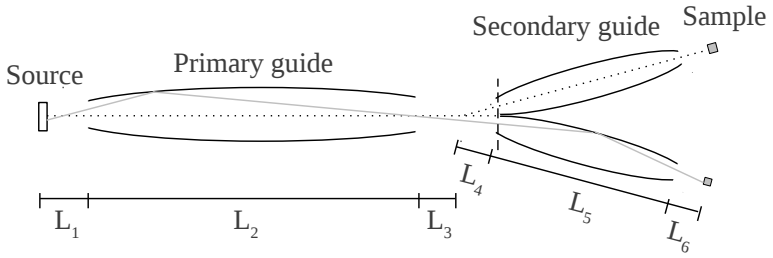

Figure 5.3: Layout of the guide-split set-up with two secondary guides. The dotted line represents the primary axis through one instrument, the gray line is an example of a neutron path through the guide system, and the dashed line marks the junction of the secondary guides. The cross section of the junction area is shown in figure 5.5. Each of the sibling instruments on the secondary guides exploits different parts of the phase space transported by the primary guide, and thus retains a high brilliance transfer ($\sim 90\%$) for each sibling instrument. L_i represents the naming of the lengths in the set-ups.

The guide-split can be realized in numerous variations with many different shapes of the primary and secondary guides in different combinations, e.g. elliptic, parabolic or ballistic with different taperings. However, only the double ellipse case is investigated here.

5.3.2 The guide-split set-up and simulations

Three guide-split set-ups where the guide junction supports two, four, or eight secondary guides have been investigated each with a total length (distance from moderator to sample) of 150 m. The cross section of the guide junctions are illustrated in figure 5.5. In this study the primary guides are chosen to be elliptical and 98 m long and the secondary guide lengths were optimized. Other guide length ratios are also feasible (e.g. 75 m long primary guide).

The guide parameters of the set-up are restricted by the requirement that the secondary guides cannot overlap. An illustration used in the geometrical considerations of a two-split set-up is shown in figure 5.4.

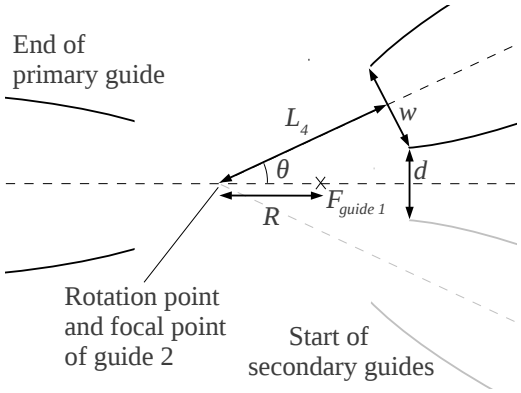

Figure 5.4: Top view of the guide junction of the two-split set-up. θ is the rotation angle of the secondary guide, R is the rotation displacement length, F_{guide1} is the focal point of the primary guide, L_4 is the length from the rotation point to the secondary guide entrance, w is the width of the secondary guide entrance, and d is the distance between the secondary guides. The focal point of the primary guide and the rotation point is not necessarily the same (for detailed information see table 5.1).

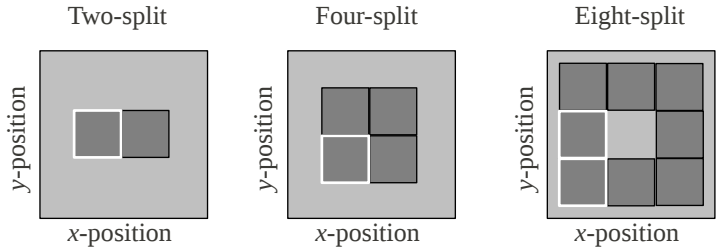

Figure 5.5: Sketch of the cross sections of the secondary guide junction for the two-, four- and eight-split variations of the set-up. The position of this cross section is marked as L_4 in figure 5.3. The guide positions marked with white outlines are simulated and the results presented in this article. The two positions in the eight split option are referred to as the side and the corner positions.

The relation between the distance from the focal point to the start of the secondary guides (L_4 shown in figure 5.3) and the rotation angle (θ) of the secondary guides is

$$\theta = \operatorname{atan}\left(\frac{w}{2L_4}\right) + \operatorname{asin}\left(\frac{d}{2\sqrt{\frac{1}{4}w^2 + L_4^2}}\right) \approx \frac{w+d}{2L_4} \tag{5.2}$$

where w is the width and height of the secondary guides and d is the distance between the secondary guides at their starting points.

For the two- and four-split set-up it is chosen to let the secondary guide openings be joined at the primary axis (ignoring the substrate thickness, $d = 0$ is used, see figure 5.5) and in the eight-split option d is fixed to be equal to w in order to reduce the number of free parameters. This parameter reduction furthers small kink angles which has been shown to give good results in the optimizations. Another parameter reduction was done by locking the focal point of the second ellipses to the rotation point (see figure 5.4). The rotation angles are small ($\sim 0.4°$, for detailed information see table 5.1) in all three test cases. Due to the symmetric nature of the set-up only selected simulated data is presented: the guide rotated to the left in the two-split version, the lower left corner of the four-split, and the middle and lower left guides in the eight-split set-up as highlighted in figure 5.5. The effect of gravity, which breaks the symmetry in the vertical dimension, is minor and will not be discussed in this work. No guide is placed in the middle of the eight-split variation, due to the line-of-sight considerations. It is most likely, however, that a curved guide will perform adequately in this position.

The optimizations were performed using McStas (see chapter 4) and run at the computer cluster of the ESS Data Management and Software Center cluster [48].

The optimized phase space was chosen to have a divergence within $\pm 0.5°$ a cold wavelength band (4.25-5.75 Å) and a sample size of 1×1 cm^2. These parameters were chosen to match the requirements of the cold powder diffractometer described in the technical design report for ESS (appendix A.5).

The elliptical guide component used in the simulation has a perfect elliptical shape in the x- and y-direction and a quadratic cross section [49]. For simplicity the m-value is set to be the high but expensive value $m = 6$ for all guides. When making a specific case study of an instrument, coating should be cost optimized [49]. The moderator used has a surface of 12×12 cm^2. The wavelength distribution is described by the McStas ESS long-pulsed cold source from 2000 [50].

During the optimization the parameter space (lengths, focal points, angles) was found to have several plateaus with high brilliance transfer (>90%) and hence the final parameters were chosen such that a smooth divergence distribution at the sample position was obtained. The hereby obtained parameters of the guides are listed in table 5.1.

Layout option	**Two- and Four-split**	**Eight-split**
Parameters of the primary guide		
L_1, distance from moderator to guide entrance	2.0 m	2.0 m
L_2, length of the primary guide	92.0 m	96.0 m
L_3, distance from exit to rotation point	0.897 m	2.780 m
Width and height at guide entrance	0.105 m	0.105 m
Entrance focal length	2.5 m	1.3 m
Exit focal length	1.7 m	3.0 m
Parameters of the secondary guide		
R, rotation point displacement	-0.8 m	-0.2 m
θ, angular rotation of secondary guides	0.39 °	0.41 °
L_4, distance from rotation point to entrance	2.7 m	4.9 m
L_5, length of the secondary guide	51.3 m	46.1 m
L_6, distance from guide exit to sample	1.4 m	1.0 m
Width and height at guide entrance	0.037 m	0.035 m
Entrance focal length	2.7 m	5.3 m
Exit focal length	2.33 m	2.89 m

Table 5.1: The optimized parameters for the different variations of the set-up. The parameters for the two- and four-split variations are identical, whereas the parameters for the eight-split differ. See figure 5.3 for a graphical explanation of the lengths.

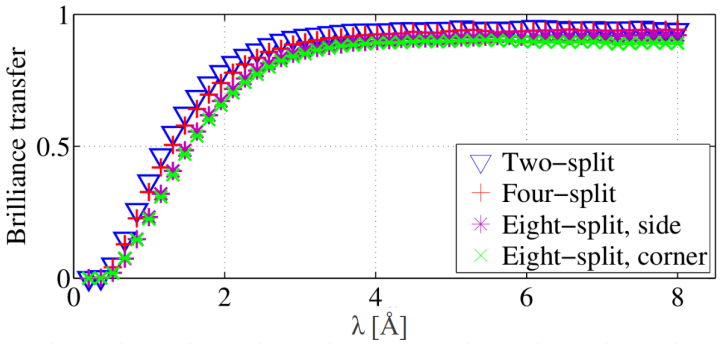

Figure 5.6: The brilliance transfer at the sample position for the two-, four-, and eight-split options as a function of wavelength.

5.3.3 Results for the guide-split simulations

The main result in this study is how the brilliance transfer depends on the wavelength for the four optimized guide systems. These data are shown in figure 5.6. It is clear that the guide-split concept shows excellent performance for cold neutrons ($\lambda > 3$ Å). The brilliance transfers obtained (for the chosen phase phase $\pm 0.5°$, 4.25-5.75 Å, 1×1 cm^2) in the optimizations are 94% for the two-split, 93% for the four-split, and 89%, 90% for the two eight-split options, respectively. At $\lambda = 1.47$ Å the brilliance transfer is 62% for the two-split, 58% for the four-split, and 48%, 47% for the two eight-split options.

It is desirable to have a homogeneously filled four dimensional phase space at the sample position within the optimized wavelength band. The brilliance transfer as a function of each of the four parameters is displayed in figure 5.7. The optimizations obtain a flat divergence distribution in the desired divergence range ($\pm 0.5°$) in all four test cases (figure 5.7). In the eight-split cases there are small features on the sides of the central peak, at $\pm 0.9°$. This can also be seen in figure 5.8. These features can be removed by tighter collimators, pinhole collimation, or distance collimation.

The results are simulated for neutrons within the wavelength interval for which the set-ups have been optimized (4.25-5.75 Å). In the figure the performance of the four guide-split set-ups are shown with regard to sample illumination, divergence distribution, and their correlations. The two zoom-ins on the right side display the neutrons within our phase space restrictions only. On the left side the illumination and divergence distribution is shown for larger intervals, making the phase space outside the boundaries visible. The two bottom plots show the horizontal and vertical position versus divergence correlations, also known as ***acceptance diagrams***. It is observed that for all four guide set-ups and all correlations monitored, the neutron phase space is quite uniformly filled within the set requirements.

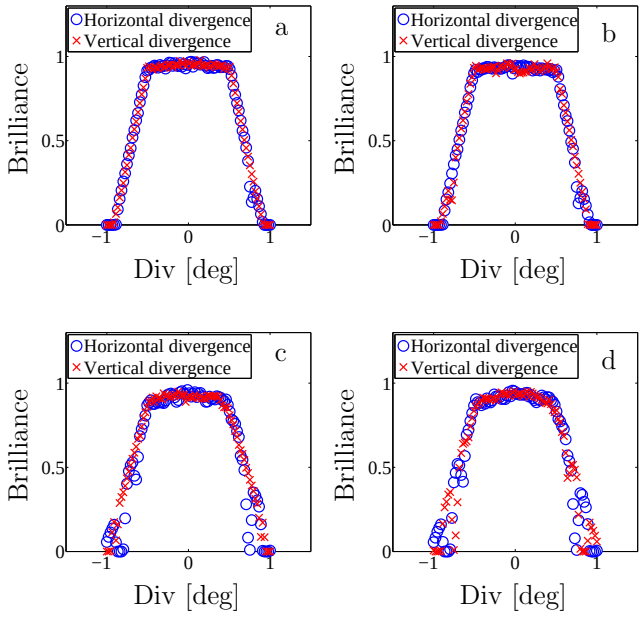

Figure 5.7: Horizontal and vertical divergence distributions summed from -0.5° to 0.5° perpendicular to the displayed direction at the sample position for neutrons with wavelengths within 4.25-5.75 Å. **a:** Two split. **b:** Four-split. **c:** Eight-split side. **d:** Eight-split corner.

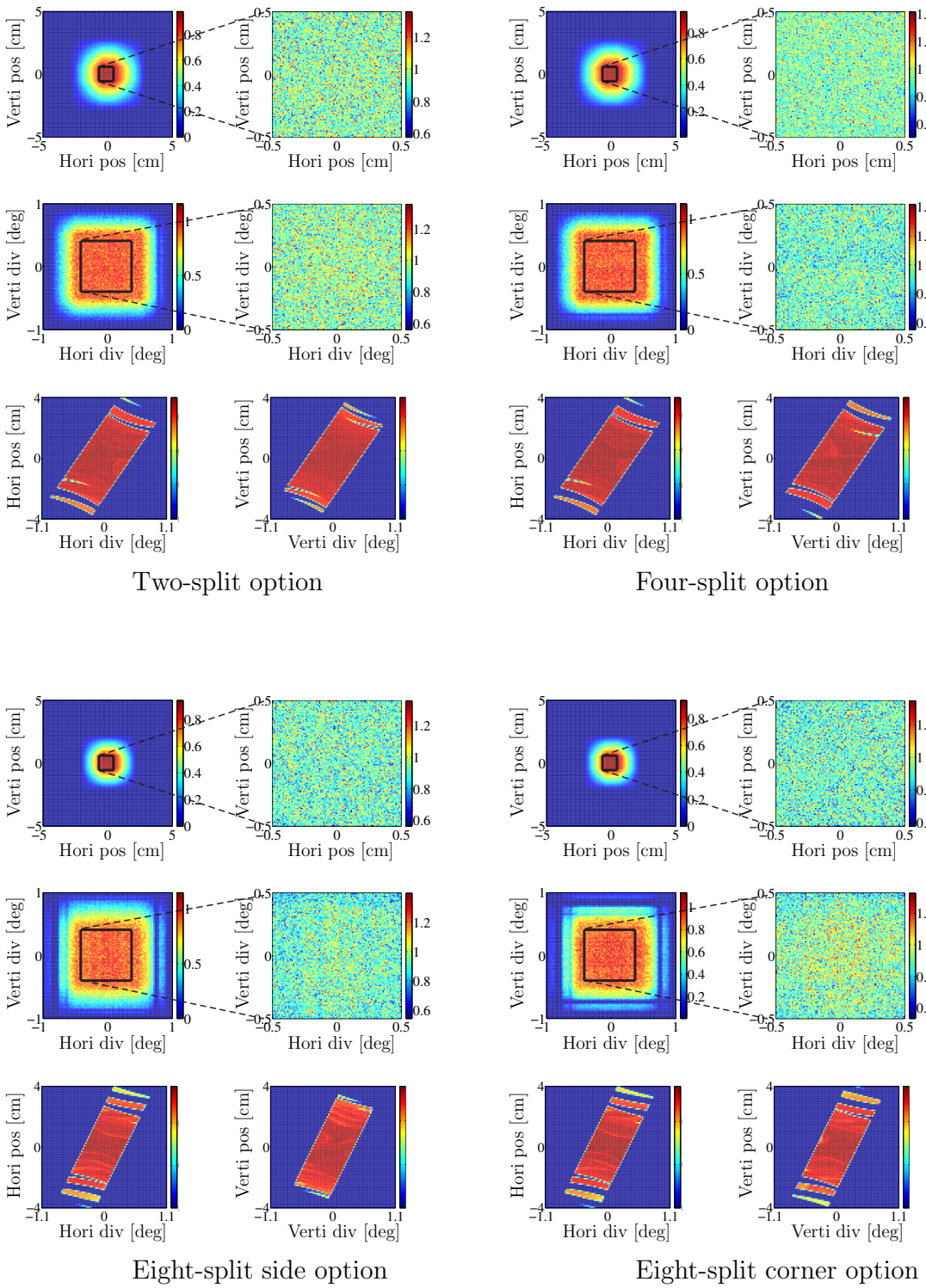

Figure 5.8: Outputs from the position, divergence, and acceptance monitors at the sample position for the four different set-ups. The data has been summed up inside the chosen phase space volume in the dimensions not shown in the 2D plot (±0.5°, 4.25-5.75 Å, 1×1 cm^2). Except the position monitor that accepts all incoming divergences and the divergence monitors are 1×1 cm^2 in size. Their color scales represents the brilliance transfer value.

5.3.4 Performance of guide-split systems

As seen from the data, the idea of guide-splitting is certainly fruitful for the case of two- and four-split elliptical guides. This is judged on the basis of the brilliance transfer values over a large wavelength range, even down to 2 Å. In addition, for the chosen sample size of 1×1 cm^2, the illumination is very smooth both in divergence, position and the correlation of the two. The same is true for the eight-split option, although the brilliance transfer is slightly smaller, in particular towards the shorter wavelengths.

A slightly larger brilliance transfer of the two-split variation is observed (see figure 5.6). This is to be expected, due to the two-split secondary guides being more favorably placed in divergence space. It can be argued that the four split - or even eight-split - options are better choice due to the increased amount of instruments and utilized neutrons. Neither of the variations provides as high a brilliance transfer as a single elliptical guide, although the transmission in excess of 90% for $\lambda > 3$ Å must still be seen as a most satisfactory result. In addition, all variations provide a superior total utilization of the generated neutrons, when the increase in instrument number is considered.

The guide-split concept also works for straight (and curved) secondary guides, although with slightly lower brilliance transfer of ∼80% (data not shown).

In contrast, the elliptical secondary guides have no problem in transporting $\pm 0.5^\circ$ divergence, and can even accommodate slightly higher divergences, even for the present optimization. It is uncertain how well the guide-split set-up will work for higher divergences but it will probably work for long wavelengths. The limiting factor is how large a divergence the primary guide can deliver. This limit is around $\pm 2^\circ$ for $\lambda \sim 5$ Å[43].

5.3.5 Applications of guide-split at ESS

The guide-split set-up facilitates an increased number of instruments at a neutron source. This could be used to build beam-lines that would otherwise not be built at a dedicated beam port, for example;

- Laue stations for crystal alignment.
- In-house test beam-lines for optics and other beam components.
- Dedicated student beam lines for educational purposes.

Also state-of-the art 150 m long cold-neutron instruments could be positioned on a split guide simultaneously, using wavelength bands in the range between roughly $2.5 - 25$ Å. With inspiration from the Technical Design Report for ESS (appendix A.5), a short list of instruments that could be placed on a guide-split is given below.

Monochromator instruments

The monochromator instruments utilize the time-integrated flux of the ESS source, and the usefulness of the split guide for these instruments depends only on the brilliance transfer,

which is excellent (see figure 5.6)

Placing a monochromator instrument at the end of a focused guide requires some care, as the monochromator should not be positioned in the focal point. Rather this point will act as a virtual source point, and a doubly focusing monochromator should be placed a few meters behind this point, see [51].

Inverse-geometry crystal analyzer spectrometer

Simulations of an inverse geometry instrument for ESS with a triple-axis-like backend will be presented in [52], but in general this instrument type is well matched to the wavelength and divergence ranges, and to the limited beam spot size that the guide-split system will provide.

Cold-neutron chopper spectrometer

Conventional chopper instruments would not be suitable for a split guide, since all sibling instrument users operating the instrument would have to agree on how to run the primary chopper close to the source. But if WFM and RRM (explained in section 2.5.1) are combined, it is possible only to have a shared frame-overlap close to the source and have the pulse-shaping chopper just after the guide-split position and a monochromating chopper pair at the end of the second guide.

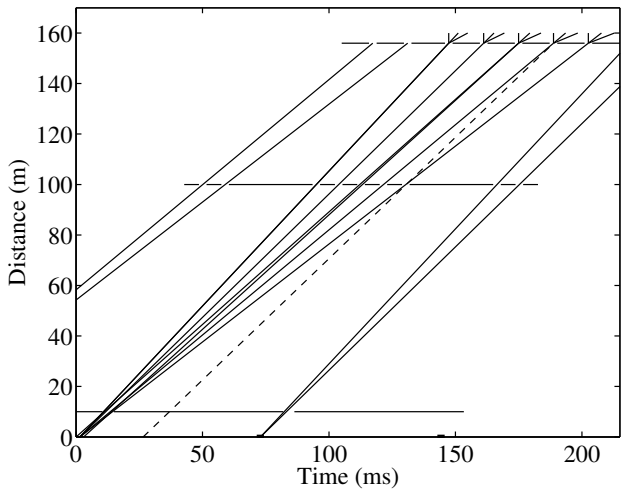

Figure 5.9: Time-distance diagram for the cold neutron chopper spectrometer. The multiple openings of the monochromating chopper just before the sample is typical of the RRM scheme, while the multiple beams from the pulse-shaping chopper is typical of the WFM scheme. The wavelength band of 3.55 Å to 5.3 Å, with 5 monochromatic pulses in this range is shown. Part of the preceding and following source pulses are shown. The dashed line represents a theoretical path a neutron would take to perform "cross-talk" between different chopper channels. The figure is made by Kim Lefmann.

This combination of choppers allows for multiple monochromatic beams on the sample, with slightly different wavelengths, during one single pulse frame. The use of this chopper combination for a time-of-flight spectrometer was first suggested for the IN500 project at LANSCE [53] and is further discussed in [54].

The combination of WFM and RRM is illustrated in a time-distance-diagram, figure 5.9 where the WFM choppers are placed in the beginning of the secondary guide (100 m from the source) and the RRM choppers are, as in a conventional chopper spectrometer, placed close to the sample.

The dashed line in the ToF diagram in figure 5.9 illustrates that the neutrons that may cause "cross-talk" between the designated time-distance channels cannot originate from the main source pulse. It can therefore be seen that the chopper pairs uniquely select the wavelengths of the incoming neutrons.

The cold chopper spectrometer, optimized for the guide-split system at the ESS source, has been simulated and is presented in [55].

5.3.6 Magnetism powder diffractometer

In this section a study of a simple version of a magnetism diffractometer for ESS is presented. The instrument design is based on the Single-Crystal Magnetism Diffractometer described in the Technical Design Report for ESS [56] but placed on a cold, rather than a bi-spectral source. The detector matches that of the WISH instrument at ISIS [57] and is therefore a cylindrical-detector with a height of 1 m and a radius of 2.2 m. There are 855 pixels covering 2π giving a horizontal pixel size of 16 mm.

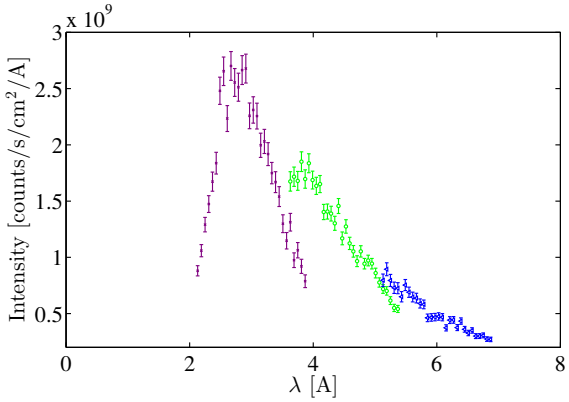

Figure 5.10: Simulated wavelength spectrum at the 1×1 cm^2 sample position for the magnetism diffractometer, running in the wavelength bands $2.1-3.9$ Å, $3.6-5.4$ Å, and $5.1-6.9$ Å.

The instrument is placed at the ESS cold moderator description from 2012 (defined in McStas 2.0 [58]). The maximal width of the wavelength band of the instrument when

using every source pulse is given by $\Delta\lambda = T/(\alpha L) = 1.88$ Å, where $T = 71.4$ ms is the time between pulses and $L = 156$ m. To avoid frame overlap, a slightly smaller wavelength band is used in practice ($\Delta\lambda = 1.80$ Å). In order to cover a larger q-range with the instrument the wavelength band can be shifted by phasing the band choppers. With three wavelength intervals one can cover from 2.1 Å to 6.9 Å, which corresponds to a q-range from 1.29 Å^{-1} to 5.98 Å^{-1} (when using the scattering angles (2θ) between 90° and 180°). In figure 5.10 the simulated flux on the sample is shown for three different wavelength bands.

In the simulations the instrument is placed on the 4-split guide system giving a divergence at the sample position of ±0.5°. The wavelength resolution of the instrument, when using the full pulse, is $\tau = 2.86$ ms, is $\delta\lambda/\lambda = \tau/(\alpha L\lambda) = 1.6\%$ for $\lambda = 4.5$ Å. This is calculated using eq. (6.10).

The total flux on the sample is an impressive $2.5 \cdot 10^9$ n/sec/cm^2 in the wavelength band 2.1 Å -3.9 Å (see figure 5.10).

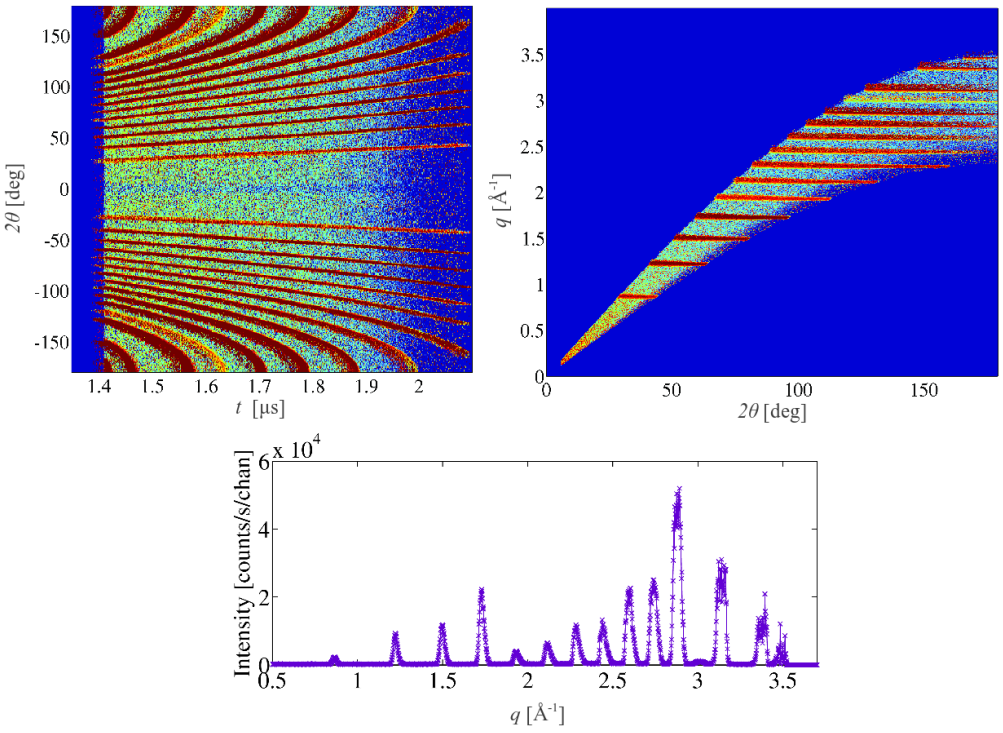

Figure 5.11: Data from a simulation run on the cold powder diffractometer using the wavelength band $3.2 - 5.0$ Å on a NaCaAlF sample (10 mm high cylinder with a 10 mm diameter). The data is plotted in three different ways. The two colour plots are in logarithmic scale to enhance details. **Left:** Raw simulated data $(2\theta, t)$. **Right:** Transformed data $(2\theta, q)$ which is a more useful representation if refinement is desired. **Bottom:** One dimensional data. This is how powder diffraction data is usually analyzed and presented.

To simulate a full experiment, we use a standard NaCaAlF powder sample, including incoherent scattering, [31] in a cylinder with a 10 mm height and a 10 mm diameter. The detector output is shown in figure 5.11 as a $(2\theta, t)$ diagram (raw data output), a $(2\theta, q)$ diagram (data ready to be refined), and the same data collapsed along 2θ onto q. The peak shapes have the expected width of 0.06 Å^{-1} at $q = 3$ Å (calculated from eq. (6.5)) and are seen to have a slight asymmetry at low q, which originates from the pulse shape. The neutron count rate is $5 \cdot 10^6$ s^{-1} for the full spectrum, allowing collection of data with reasonable statistics ($4 \cdot 10^5$ counts) from just one source pulse.

5.3.7 Conclusion on the guide-split concept

It has been shown by simulations that it is feasible to split neutron guides by using a virtual source point from a primary elliptical guide, in particular for cold neutrons with a divergence below $\pm 0.5°$ (1° FWHM) at the sample position. The elliptical set-up variations were found to have the highest brilliance transfer just above 90% for the two-split and four-split systems. The divergence distribution of these variations at the sample position is approximately uniform.

The split-guide set-up offers the possibility of an increased amount of instruments, at the cost of a slightly reduced intensity at the sample position of each instrument. The lower intensity does not originate from a low brilliance transfer, but from a (possibly) reduced maximum divergence. Further studies are needed to quantify this divergence limitation.

The guide-split concept enables several user instruments to share the same beam port at a time-of-flight neutron source. However, the users operating the instruments would have to use the same wavelength band and pulse shaping, as bandwidth and pulse shaping choppers are placed in the shared first part of the guide. However, these bindings will not overshadow the advantage of the increase of the total number of instruments. Furthermore, the cost of individual instruments may be reduced due to the idea of sharing the primary guide and shielding. Yet another advantage of the guide-split idea is that the background can be reduced at the sample station since it furthers the possibility of breaking the line-of-sight from source to sample, even for elliptical guides.

The guide-split has been shown to work well for a full instrument simulation for a cold powder diffractometer.

Chapter 6

The Heimdal diffractometer

Many instruments at ESS will carry the names of gods from the old Nordic Mythology, e.g. Freya, Odin, and Loki[1]. We have chosen to name our instrument Heimdal. In Nordic Mythology, Heimdal of Asgard is the guardian of the rainbow bridge Bifrost. He has the best senses among gods, a vision so powerful that he can see and hear the grass grow in real time.

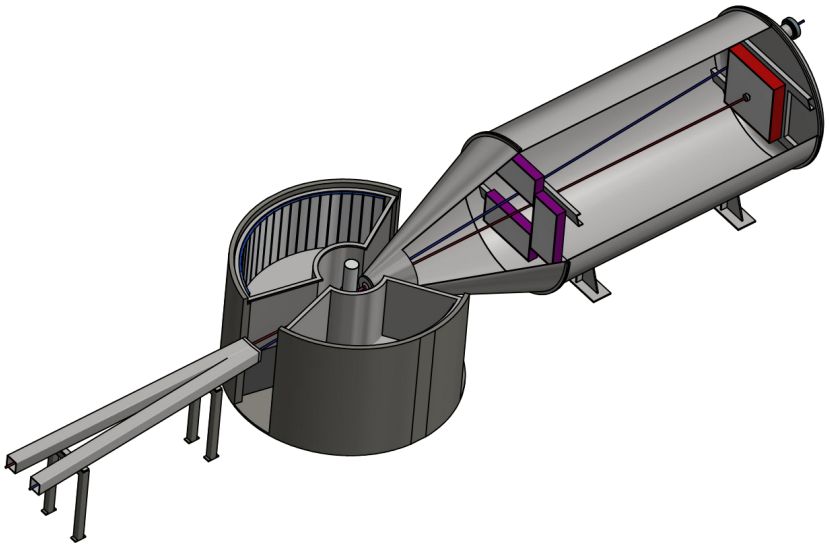

Figure 6.1: 3D drawing of the current design of the Heimdal sample station with two incoming beam tubes (one for cold and one for thermal neutrons), a cylindrical powder diffraction detector around the sample, and a large SANS detector tank with its nose close up to the sample and extending out along the cold neutron beam direction. The imaging set-up is a fairly small insertable box and is not shown in this picture. The image is from the ESS engineering drawing section.

[1] An idea that came to me at a bar after an ESS meeting.

The Heimdal instrument is designed and proposed by the Danish-Swiss work package IV. The team is led by Mogens Christensen (DK) who proposed the instrument concept and has done all the funding work and administration. He is also the main author on the instrument proposal for ESS. Jürg Shefer (CH) and Nadir Aliouane (CH) have done cost estimates of the guides and investigated the feasibility of an imaging insert for the instrument. Mads Bertelsen and Kim Lefmann have simulated the cold neutron guide for the SANS set-up. My work has been to design and simulate the powder diffractometer part of the instrument which is described in detail below.

6.1 The Heimdal instrument

The multipurpose machine, Heimdal, will combine thermal neutron powder diffraction, small angle neutron scattering (SANS), and neutron imaging in one single instrumental setup at ESS. With this instrument it will be possible to follow chemical and physical processes in situ over a very large spatial range (0.01-5 nm (powder diffraction), 2-100 nm (SANS), and 50 μm - 50 mm (imaging)). In other words, the instrument will be capable of simultaneously covering length scales of more than nine orders of magnitude. Heimdal will be able to accommodate modern material research in a broad variety of fields, and the task of the instrument will be to study advanced functional materials in action.

An example of a functional material could be a fuel cell (a device that through a chemical reaction with an oxidizing agent converts chemical energy from a material into electricity) as it has functions working on both different time- and lengths scales. Using the information from Heimdal, it will be possible to optimize the design of the fuel cell.

A thorough review of science cases for this instrument can be found in the ESS Instrument Construction Preproposal in appendix A.4.

In order to combine these three very different neutron techniques some sacrifices in performance must be made in order for everything to come together. The powder diffraction part of the instrument is by far the most demanding due to the high resolution requirements and the long pulsed nature of the source. Therefore the choice was made to design and optimize a high performance powder machine first, and then make minor adjustments to this design in order to make room for the two other instruments around their mutual sample position.

6.2 Thermal powder diffraction

Many overall parameters for the entire instrument suite have already been decided, e.g. the pulse period and length [59]. This combined with a few fundamental choices for the instrument design settles most instrument parameters. In the following sections we shall go through the design choices made for the thermal powder diffraction set-up at the Heimdal instrument and the consequences of these.

6.2.1 Instrument length

When building a high resolution instrument at a long pulsed source, it is necessary to build a very long instrument or make drastic modifications to the pulse shape. We have chosen the latter option with no wavelength frame multiplication [18]. Due to the restrictions arising from the size of the biological shielding around the target station, the first chopper can be placed no closer than 6.5 m from the target. To obtain the largest band width the resolution chopper is placed at this position. We can now calculate the instrument length for which the time window is completely filled without causing frame overlap. Consider the time-of-flight diagram in figure 6.2. The resolution chopper opening time is assumed

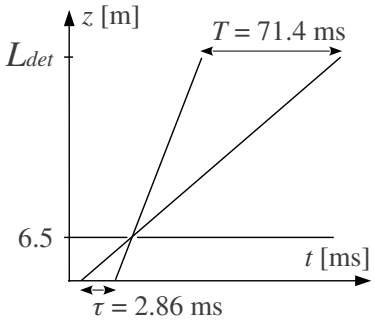

Figure 6.2: ToF diagram displaying the triangles used in the calculations of the instrument length.

to be close to zero for this calculation. So we get

$$L_{det} = \frac{TL_{chop1}}{\tau} + L_{chop1} = \frac{71.4 \text{ ms } 6.5 \text{ m}}{2.86 \text{ ms}} + 6.5 \text{ m} = 168.8 \text{ m} \tag{6.1}$$

where L_{det} is the instrument length, L_{chop1} is the distance from the moderator to the resolution chopper, T is the pulse period, and τ is the pulse length.

6.2.2 Wavelength band

To calculate the bandwidth of the instrument we consider the ToF equation ($t = \alpha L \lambda$). We use the pulse period, T, and refrain from making a small correction of T with the opening time of the resolution choppers, since it is orders of magnitude smaller than the pulse period. The distance from the resolution choppers to the detector is the flight path L. So

$$\Delta\lambda = \frac{T}{\alpha L} = \frac{71.4 \text{ ms}}{0.2528 \ \frac{\text{ms}}{\text{Å m}} \ (168.8 \text{ m} - 6.5 \text{ m})} = 1.74 \text{ Å} \tag{6.2}$$

We have chosen to use 1.5 Å as our mean wavelength and hence a wavelength band from 0.63 Å to 2.37 Å. This also allows us to reach close to the lowest wavelength neutrons feasible for the long ESS guides [43].

6.2.3 Instrument resolution

In this section we calculate the resolution function of the instrument. The overall limiting factor of the instrument resolution is the finite size effect from the sample and pixel size together with the radius of the detector. The other contributions to the resolution function (time uncertainty and maximum divergence on sample) can be adjusted to get the desired instrument resolution (at the cost of neutron flux of course). It will be possible to run Heimdal on different resolution settings, so that the user of the instrument can choose between high resolution or high flux. All numbers in the following sections are calculated for the high resolution case.

Resolution matching

To calculate the size of the contributions to the d-spacing resolution, $\delta d/d$, we use the ToF eq. (**??**) to rewrite Bragg's law

$$\lambda = 2d\sin\theta \quad \Rightarrow \quad t = 2\alpha L d\sin\theta, \tag{6.3}$$

and then use error propagation of this to get

$$\left(\frac{\delta d}{d}\right)^2 = \left(\frac{\delta t}{t}\right)^2 + \left(\frac{\delta\theta}{\tan\theta}\right)^2 + \left(\frac{\delta L}{L}\right)^2. \tag{6.4}$$

The last term in eq. (6.4) is negligible ($\left(\frac{\delta L}{L}\right)^2 = 10^{-9}$) since δL is the sample size of 1-10 mm and $L = L_{det} = 168.8$ m. We also assume that the uncertainty in flight path calculations due to detector thickness is of negligible size. As both the incoming divergence on the sample as well as the sample size together with the detector geometry contribute to $\delta\theta$, the angular contribution is split into two terms:

$$\left(\frac{\delta d}{d}\right)^2 = \left(\frac{\delta t}{t}\right)^2 + \left(\frac{\frac{1}{2}\delta(2\theta_i)}{\tan\theta}\right)^2 + \left(\frac{\frac{1}{2}\delta(2\theta_f)}{\tan\theta}\right)^2. \tag{6.5}$$

The subscripts i and f denote the incoming and outgoing sides with respect to the sample. To obtain resolution matching of the contributions, we let the three terms in eq. (6.5) contribute equally to the resolution and hence it is required that

$$\frac{1}{3}\left(\frac{\sigma_d}{d}\right)^2 = \left(\frac{\frac{1}{2}\sigma_{2\theta_f}}{\tan\theta}\right)^2, \qquad \frac{1}{3}\left(\frac{\sigma_d}{d}\right)^2 = \left(\frac{\frac{1}{2}\sigma_{2\theta_i}}{\tan\theta}\right)^2, \qquad \frac{1}{3}\left(\frac{\sigma_d}{d}\right)^2 = \left(\frac{\sigma_t}{t}\right)^2. \tag{6.6}$$

Calculating $\frac{\sigma_d}{d}$ from sample and pixel size

The limiting factor of the total resolution stems from $\sigma_{2\theta_f}$ which depends on the sizes of the sample, s, and pixels, p, together with the radius of the detector, r (since $\sigma_{2\theta_i}$ and σ_t

are tunable). Hence we can derive the instrument resolution by calculating the resolution contribution from the outgoing beam (from sample to detector).

Neutron detection is currently a very fast progressing field and it is not certain what will be the best detector for Heimdal at the time of its construction, so for these calculations a conservative pixel size of 3 mm and a detector radius of 1.5 m are chosen. We now consider the geometry for distance collimation between sample and detector, drawn in figure 6.3, and obtain

$$\eta_{min} = \text{atan}\left(\frac{s-p}{2r}\right) \approx \frac{|s-p|}{2r}, \tag{6.7}$$

$$\eta_{max} = \text{atan}\left(\frac{s+p}{2r}\right) \approx \frac{s+p}{2r}.$$

We do not take the contribution from the out of plane scattering into account in this calculation since it is a second order effect. When looking at figure 6.3 it is clear that

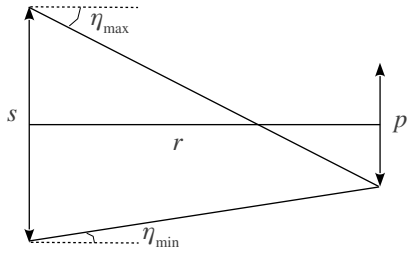

Figure 6.3: A sketch showing the relevant angles arising from the sample size, s, pixel size, p and the detector radius, r.

for divergences smaller than η_{min} the pixel is fully illuminated from the sample (from incoherent scattering) and hence we get the full intensity ($I = I_0$). When the divergence is larger than η_{max} the neutrons do not hit the pixel at all and the intensity is zero. One can derive that the intensity decreases linearly in the interval between η_{min} and η_{max} assuming that the sample scatters equally in all directions. We now have the resolution contribution from the outgoing beam (shown in figure 6.4). We can calculate the variance of this resolution contribution, $I(x)$, with the finite area, A as

$$\sigma^2_{2\theta_f} = \frac{1}{A}\int_{-\infty}^{\infty} I(x)(x-x_0)^2 dx \tag{6.8}$$

$$= \frac{1}{\frac{1}{2}A}\left[\int_0^{\eta_{\min}} (1)(x-x_0)^2 dx + \int_{\eta_{\min}}^{\eta_{\max}} \left(1 + \frac{\eta_{\min}}{\eta_{\max}-\eta_{\min}} - \frac{x}{\eta_{\max}-\eta_{\min}}\right)(x-x_0)^2 dx\right]$$

$$= \frac{\eta^2_{\max}}{6} + \frac{\eta^2_{\min}}{6} = \frac{1}{12}\frac{s^2+p^2}{r^2}.$$

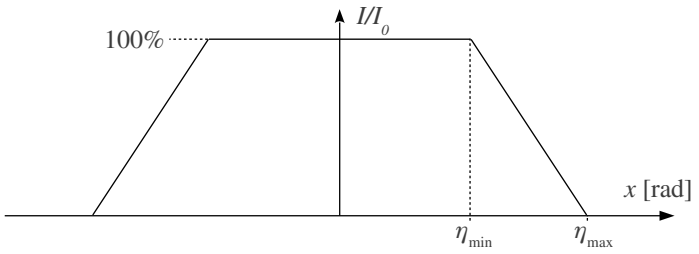

Figure 6.4: Intensity as a function of divergence of the outgoing beam. η_{min} and η_{max} are derived in eq. (6.7).

The full calculation of the integral can be found in appendix B.1. A realistic estimate of how small the pixel size on the detector can be is at the moment 3 mm. We then choose to let the sample size match the pixel size ($p = s = 3$ mm) so that the two terms contribute equally. Since the scattering-angle-part of the resolution eq. (6.5) depends of the scattering angle, we cannot obtain resolution matching for all values of θ. We therefore choose to have resolution matching at $2\theta = 90°$ and from eqs. (6.6) and (6.8) we now calculate the instrument resolution

$$\left(\frac{\sigma_d}{d}\right)^2 = \frac{3}{4}\left(\frac{\frac{1}{12}\frac{s^2+p^2}{r^2}}{\tan^2\theta}\right) = \frac{1}{16}\left(\frac{\frac{2(0.003\ \text{m})^2}{(1.5\ \text{m})^2}}{\tan^2(45°)}\right) = 5.00 \cdot 10^{-7}, \tag{6.9}$$

and $\frac{\sigma_d}{d} = 0.0707\%$ (RMS) corresponding to a FWHM of 0.17% which is the resolution we will have at 90° scattering under resolution matching.

Divergence limit

The optimal horizontal divergence can now be calculated by resolution matching from eq. (6.6) together with the result from eq. (6.9) and again letting $2\theta = 90°$:

$$\sigma_{2\theta_i} = \sigma_{2\theta_f} = \frac{2}{\sqrt{3}}\,\frac{\sigma_d}{d}\,\tan\theta = \frac{2}{\sqrt{3}}\,0.0707\%\,\tan(45°)\,\frac{180°}{\pi} = 0.047° \tag{6.10}$$

which corresponds to a FWHM of 0.11°. Hence we need to collimate the incoming beam as explained below.

Guide to sample distance

One can use distance collimation or slit collimation in order to obtain the desired incoming divergence on the sample. The former is done by ending the guide at an adequate distance from the sample. Applying the same arguments as used in eq. (6.8), we can write

$$\sigma^2_{2\theta_f} = \frac{1}{12}\,\frac{s^2+g^2}{d^2} \tag{6.11}$$

where we replace the pixel size with the guide opening, g, and the radius of the detector with the distance, d, from guide end to sample. The design of the thermal guide system for Heimdal will be discussed in section 6.5, but in order to get a feeling of the collimation distance we can assume that the guide is 6 cm wide and from that calculate the distance.

$$d = \sqrt{\frac{1}{12}\frac{s^2+g^2}{\sigma^2_{2\theta_i}}} = \sqrt{\frac{1}{12}\frac{(0.06^2+0.003^2)\ \mathrm{m}^2}{(0.0707^\circ)^2}} = 21.2\ \mathrm{m}. \tag{6.12}$$

In other words, the last 20 m of the guide will only contribute with transport of unwanted neutrons to the sample area, when running in the high resolution mode. In practice one would probably use a flexible slit system like at WISH at ISIS (as described in section 6.2.4).

Opening time of the resolution chopper

In order to calculate the full opening time of the resolution chopper we first need to find the flight time of the mean wavelength ($\lambda_{mean} = 1.5$Å) from the resolution chopper at L_{chop1} =6.5 m to the detector,

$$t_{chop1\ to\ det} = \alpha(L_{det} - L_{chop1})\lambda_{mean} = 61.53\ \mathrm{ms}\ . \tag{6.13}$$

We now calculate the width (RMS) of the opening time from eq. (6.6).

$$\sigma_t = \frac{1}{\sqrt{3}}\ \frac{\sigma_d}{d}\ t_{chop1\ to\ det} = \frac{1}{\sqrt{3}}\ 0.0707\% \cdot 61.53\ \mathrm{ms} = 25.1\ \mu\mathrm{s} \tag{6.14}$$

The transmission function of a disc chopper with an opening that matches the guide cross section is as drawn in figure 6.5. This function is a special case of eq. (6.8) where we set

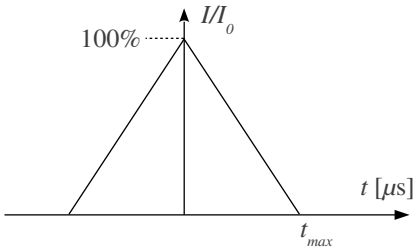

Figure 6.5: Resolution function of the resolution choppers. $t_{\max}$ is the time it takes the choppers to go from fully open to fully closed.

$\eta_{\min}$ to zero. So the ratio between the standard deviation and $t_{\max}$ therefore easily follows as

$$\sigma_t^2 = \frac{1}{6}\ t^2_{\max}\ . \tag{6.15}$$

The full opening time of the resolution chopper should therefore be

$$2t_{\max} = 2\sqrt{6}\ \sigma_t = 2\sqrt{6} \cdot 25.1\ \mu\text{s} = 123.1\ \mu\text{s} \tag{6.16}$$

if we wish to have a balanced ratio between the different contributions to the overall instrument resolution. This opening time is no problem for present day disc choppers with a radius of 35 cm and an opening of 3 cm as the chopper will spin at

$$\nu = \frac{1}{t_{max}} \frac{d}{2\pi R} = 222 \text{ Hz}. \tag{6.17}$$

6.2.4 Instrument resolution settings

The d-spacing resolution of the instrument can be varied to fit the scope of an experiment performed at Heimdal from $\frac{\delta d}{d} = 0.17\% - 1\%$ (FWHM). This is done by adjusting the opening time of the resolution chopper and changing the divergence at the sample position by slitting off the end of the guide and use collimation by distance. This concept with jaw slits has been implemented at the cold-neutron powder machine Wish at ISIS by L. Chapon (see figure 6.6) and we intend to use this system here. In table 6.1, chopper opening times

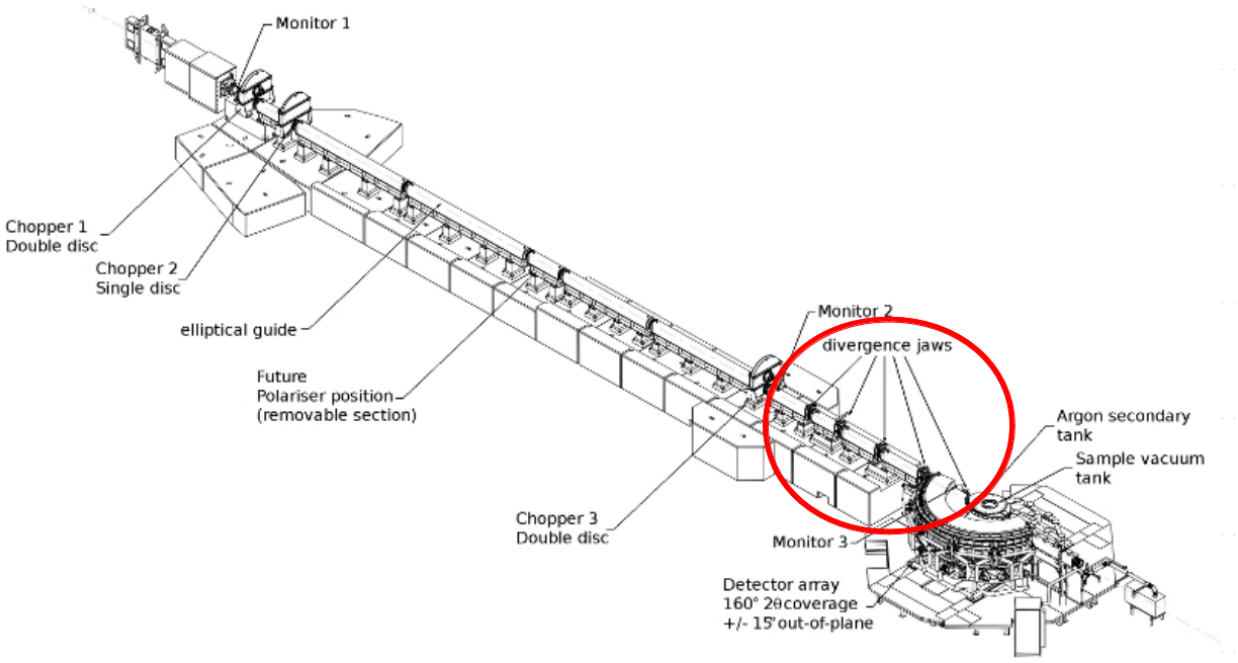

Figure 6.6: A schematic diagram showing the main components of the Wish diffractometer on ISIS TS-2. The five sets of slits are placed in the last part of the guide in order to switch between the high resolution (0.2 degrees), medium resolution (0.4 degrees), and full divergence settings of the instrument. Picture from [57].

and beam divergences are calculated for possible instrument resolution settings where we

abandon the requirement of resolution matching. We can even reach $\delta d/d < 0.17\%$. It will probably not be possible to choose between all the ten calculated settings, due to restrictions in the design of a real resolution chopper and divergence jaws, three or four settings are more realistic.

FWHM d [%]	$\frac{\sigma d}{d}$	Δt [μs]	η_{hori} [°]	$\frac{\sigma\theta}{\theta}$	$\frac{\sigma t}{t}$
0.1	0.0425	72	0.049	0.015	0.028
0.167	**0.0707**	**121**	**0.081**	**0.024**	**0.047**
0.2	0.0849	145	0.097	0.030	0.056
0.3	0.127	217	0.15	0.044	0.084
0.4	0.170	290	0.19	0.059	0.11
0.6	0.255	435	0.29	0.089	0.17
0.8	0.340	580	0.39	0.12	0.22
1	0.425	724	0.49	0.15	0.28

Table 6.1: An overview of possible resolution settings for the Heimdal powder machine. All the numbers are calculated from the equations derived in section 6.1.

6.2.5 Summary of instrument design decisions and calculations

From the decisions and analytical work described above we now have a simple design of a high resolution thermal powder diffractometer. A sketch of this is displayed in figure 6.7. The instrument has a resolution chopper 6.5 m away from the source and wavelength

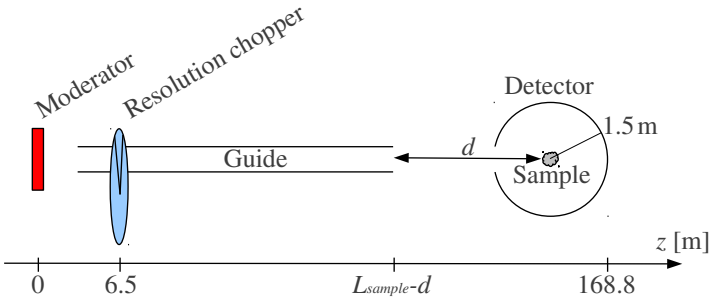

Figure 6.7: A schematic drawing of the simple model of the powder diffractometer for Heimdal. L_{sample} is the distance from the moderator to the sample and d is the distance from the guide end to the sample. The z-axis is not to scale.

frame multiplication is not used. In order to fill the time frame and avoid frame overlap the instrument is 168.8 m long. The detector has a cylindrical shape with a radius of 1.5 m and a pixel resolution of 3×3 mm^2. This gives a natural instrument resolution of $\frac{\sigma_d}{d}$= 0.0707% corresponding to a FWHM of 0.17%, when resolution matching is desired. The mean wavelength is 1.5 Å and the wavelength band is from 0.63 Å to 2.37 Å. The horizontal divergence profile at the sample should have a FWHM of 0.11°. The time

resolution of the instrument is $\sigma_t = 25.1$ μs (FWHM=59.2 μs) which is achieved if the resolution chopper has a full time opening of 123 μs.

6.3 Detector geometry

As the detector technologies presently are undergoing transformative developments and the detectors on a powder machine represent a large part of the instrument cost, it will be unwise to decide on a technology many years prior to the of the instrument construction. But as part of the development of the instrument advanced geometries should be investigated, e.g. the equiangular spiral used at POWGEN at SNS [60] or the multi bank detector concept at GEM [61] (see figure 6.8).

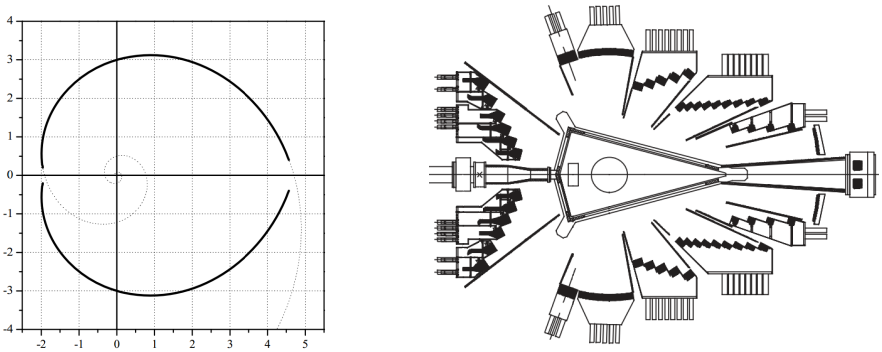

Figure 6.8: Examples of advanced geometries. **Left:** An equiangular spiral used in the design of the detector at POWGEN [60] **Right:** Layout of the GEM diffractometer at ISIS [61].

When choosing the equiangular spiral design one would obtain the same angular resolution in all pixels and it should hence be possible to sum all data together to one 1D dataset with a large q-range [60]. With the multi-bank detector each bank can be summed together obtaining 4-6 1D data sets from one measurement where the q-range and resolution are different for each of them. With the simple cylindrical shape the advantage is that all the detector segments are the same and it will therefore be easy to have spare segments if one should fail. When the data is treated in 2D, it should not a problem that the resolution varies over the different scattering angles as this can be taken into account using data analysis software. In figure 6.9 such a 2D data set from a virtual experiment on the Heimdal diffractometer is displayed.

It should also be investigated how the incoming vertical divergence at the sample in combination with the detector height influences the q-space resolution. When considering the smearing of the Debye-Scherrer rings due to the vertical divergence, we get the highest resolution in $2\theta = 90^\circ$ scattering. In figure 6.10 an idealized drawing of the Debye-Scherrer cone smearing on a cylinder detector is displayed. If the cost of the detector was of no

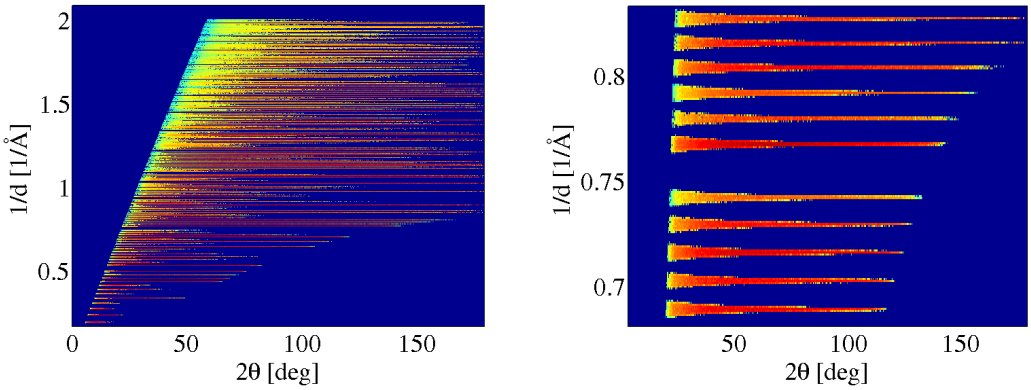

Figure 6.9: A data set using a standard NaCaAlF powder sample on the Heimdal powder diffractometer. **Left:** The full data set from a virtual experiment. The y-axis can be changed by multiplying with 2π in order to obtain q values. **Right:** A zoom in of the y-axis. In this plot it is clear that the resolution changes as a function of the scattering angle when looking a the 2D peak shape.

concern, one could build a tall detector and then, for each experiment performed at the instrument, calculate which part of the detector that should be used in the data analysis in order to get the desired resolution. This, however, is not a very cost efficient solution and a qualitative decision on this matter should be taken.

6.4 SANS machine and imaging insert

As the SANS machine and the imaging set-up have not been part of the work I have done, I will not be presenting it in this thesis. Further reading can be found in internal DK-CH WP4 reports [62].

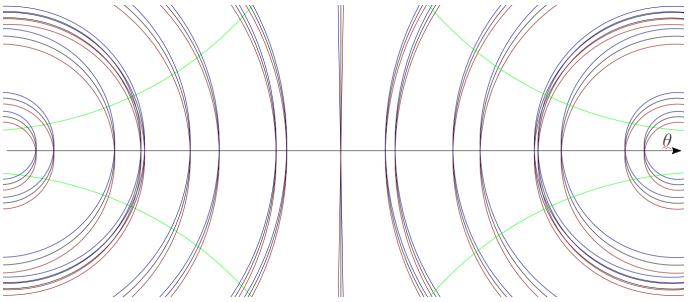

Figure 6.10: Smearing effects of the Debye-Scherrer cones on a cylindrical detector due to an incoming divergence. The effect is largest in forward- and back-scattering. At $2\theta = 90°$ scattering the effect is negligible. The green lines indicate where one could choose the useful area of the detector to be.

6.5 Guide system

The guide systems for ESS are undergoing vast developments and the ongoing task of optimizing the beam delivery system is carried out by the ESS Neutron Optics Group [46] and within the in-kind work done for ESS. Also here in Copenhagen a lot of effort has been made to find solutions to neutron transport issues arising from the long instrument lengths. The new Guide-Bot software written by Mads Bertelsen [49] is an impressive piece of work that performs semi-automatic optimizations of guide systems and hopefully will benefit all scientists working within this field.

When doing optimizations it is important to have a well defined figure of merit together with a set of reasonable physical restrictions. Currently the physical requirements are changing a lot since the moderator design, background reduction measures, beam port sizes, and the cost of component are revised and updated with the ongoing work from the different divisions of ESS. At the moment the guide optimizations have the following requirements

- A needle point ($3\times3\,\mathrm{cm}^2$) at 6.5 m from the moderator in order to fit in the resolution chopper.
- The sample must be placed out of line-of-sight from the moderator, in order to reduce background.
- The guide must end at least 60 cm from the sample position to make room for sample environments.
- A sample size of 10 mm by 30 mm. The spot size can be made smaller with slits.
- Horizontal divergence of $\eta = \pm 0.487°$. Likewise it can be made smaller with slits inside the guide as on WISH [61].
- Vertical divergence is unknown as it is correlated with the height of the detector.
- A wavelength band from 0.6 Å to 2.27 Å.

In the near future, with the Guide-Bot program we hope to be able to determine the effect of the trade off between the flux gain and instrument resolution arising from a large divergence and a tall detector. This is not a trivial task but important in order to get an optimal performance of the thermal powder machine.

Chapter 7

Conclusion

In this master thesis I have given a short introduction to neutron scattering and the Monte Carlo ray tracing program McStas. I have described two projects that have been developed by me and simulated in McStas; the guide-split which is a new guide bundle concept, and a thermal powder diffractometer for ESS.

The two parts of the project have no direct connection as the guide-split does not perform well for thermal neutrons.

The neutron guide-split

I have shown by simulations that it is feasible to split neutron guides by using a virtual source point from a primary elliptical guide. In particular for cold neutrons with a divergence below $\pm 0.5^\circ$ (1° FWHM), and it is possible to get a uniform divergence distribution at the sample position. A high brilliance transfer ($>90\%$) for neutrons with wavelengths above 2.5 Å has been obtained for three different design options; a two-, four-, and eight-split guide-split set-up. This is possible due to the fact that the sibling instruments exploit different parts of the phase space transported by the primary guide. The split guide set-up offers the possibility of an increased amount of instruments at a neutron source, at the cost of a slightly reduced intensity at the sample position for each instrument. A complication for the guide-split is that choppers placed in the first part of the instrument are shared between the sibling instruments. However, this binding will not overshadow the advantage of increasing the total number of instruments and in addition, some instruments will not need to have a chopper in the first part of the guide. Furthermore, the individual instrument cost may be reduced due to the fact that the instruments share the primary guide and shielding. Yet another advantage of the guide-split is that the background at the sample station can be reduced since the guide-split furthers the possibility of breaking the line-of-sight from source to sample.

I have simulated an instrument example that uses the guide-split. It is clear that the concept has an excellent performance for this instrument, a cold powder diffractometer. Other instrument types will also work well with the guide-split.

A thermal powder diffractometer for ESS

The main part of my work on the thermal powder diffractometer has been to develop the overall design of the instrument. The long pulse of ESS stands in contrast to the high resolution requirements of the instrument, which makes the design a difficult task.

The current version of the instrument has a resolution chopper with a full time opening of 123 μs placed 6.5 m from the source. Every source pulse is used, so in order to fill the time frame and avoid frame overlap, the instrument needs to be 168.8 m long. The main wavelength band is from 0.63 Å to 2.37 Å. The detector is kept simple, as the detector technologies are presently undergoing transformative developments. It therefore has a cylindrical shape with a radius of 1.5 m and a pixel resolution of 3×3 mm^2. This gives a natural instrument resolution of $\frac{\sigma_d}{d} = 0.0707\%$, when the requirement of resolution matching is met.

Since simulations and calculations are in agreement, it can be concluded that the assumptions made in order to do the calculations are correct. From the data produced in the simulations it has become clear that new software is needed in order to analyze these 2D data sets, because the resolution varies as a function of scattering angle. A final guide design has not yet been chosen as the physical requirements for an optimization like moderator size, background reduction measures, beam port sizes, and the cost of components are revised and updated with the ongoing work from the different divisions of ESS.

7.1 Outlook

The guide-split concept has been tested using computer simulations and has been shown to work well. The next steps will be to make full instrument designs that utilize the guide-split. As ESS is in the preconstruction phase, this idea is presented at a very convenient time and all cold instrument designs (with wavelengths above 2.5 Å) should have tested whether the instrument would work with a guide-split guide, and if so, the instrument should be built so that sibling instruments can be placed next to the first instrument, on the same primary guide, at a later time.

With this work a feasible design for a thermal powder diffractometer at ESS has been presented. The instrument preproposal for the Heimdal diffractometer is based on this work. If the Heimdal concept is chosen for construction, all parts of the instrument design should be reexamined, but the main idea behind the instrument has been shown to work. One thing that has not been tested is the effect of a large vertical divergence onto the sample combined with a tall detector on the data quality (i.e. peak shape and instrument resolution). The answer to this may change the design and cost of the guide and the detector radically.

Bibliography

[1] E. Rutherford, "The Scattering of alpha and beta Particles by Matter and the Structure of the Atom," *Philosophical Magazine*, vol. 21, no. 6, pp. 669–688, 1911.

[2] J. Chadwick, "Possible Existence of a Neutron," *Nature*, vol. 129, no. 3252, p. 312, 1932.

[3] J. Chadwick, "The Existence of a Neutron," *Proceedings of the Royal Society A: Mathematical, Physical and Engineering Sciences*, vol. 136, pp. 692–708, June 1932.

[4] T. E. Mason, T. J. Gawne, S. E. Nagler, M. B. Nestor, and J. M. Carpenter, "The early development of neutron diffraction: science in the wings of the Manhattan Project.," *Acta crystallographica. Section A, Foundations of crystallography*, vol. 69, pp. 37–44, Jan. 2013.

[5] O. R. N. Laboratory. `http://www.ornl.gov/`, 2013.

[6] C. G. Shull and J. S. Smart, "Detection af Antiferromagnetisn by Neutron Diffraction," *Physical Review*, vol. 76, p. 1256, 1949.

[7] B. N. Brockhouse and P. K. Iyengar, "Normal Modes of Germanium by Neutron Spectrometry," *Physical Review*, vol. 111, no. 3, p. 747, 1958.

[8] Nobel Prize web page. `http://www.nobelprize.org/nobel_prizes/physics/laureates/1994/`, 2013.

[9] Kim Lefmann, "Neutron scattering: Theory, instrumentation, and simulation," 2013.

[10] C. Schanzer, P. Böni, U. Filges, and T. Hils, "Advanced geometries for ballistic neutron guides," *Nuclear Instruments and Methods in Physics Research Section A: Accelerators, Spectrometers, Detectors and Associated Equipment*, vol. 529, pp. 63–68, Aug. 2004.

[11] Quickiwiki. `http://www.quickiwiki.com/en/History_of_the_Earth`, 2013.

[12] Argonne Accelerator Institute web page. `http://www.aai.anl.gov/history/project_pages/ipns.html`, 2013.

[13] K. S. Krane, *Introductory Nuclear Physics*. 1987.

[14] PSI web page. http://www.psi.ch/media/the-sinq-neutron-source, 2013.

[15] HZB web page. http://www.mlz-garching.de/englisch/neutron-research/neutron-source.html, 2013.

[16] W. Stacey, *Nuclear Reactor Physics*. Wiley, 2007.

[17] E. web page. http://ess-scandinavia.eu, 2013.

[18] F. Mezei and M. Russina, "Multiplexing chopper systems for pulsed neutron source instruments," *Proc. SPIE*, vol. 4785, pp. 24–33, 2002.

[19] youtube channel by Anders Kaestners. http://www.youtube.com/watch?v=VESMU7JfVHU, 2013.

[20] O. Park. http://www.overtonpark.org/2013/02/26/know-your-buds, 2013.

[21] P. Robinson, R. J. Harrison, S. A. McEnroe, and R. B. Hargraves, "Lamellar magnetism in the haematiteilmenite series as an explanation for strong remanent magnetization," *Nature*, vol. 418, pp. 517–520, Aug. 2002.

[22] Wikipedia. http://en.wikipedia.org/wiki/Ibn_Sahl, 2013.

[23] Wikipedia. http://en.wikipedia.org/wiki/Snell's_law, 2013.

[24] J. Stahn, "Slides of a talk given at the institut laue-langevin, grenoble, january 18th," *A neutron polariser based on magnetically remanent Fe/Si super-mirrors*, 2006.

[25] Swiss Neutronics. http://www.swissneutronics.ch/, 2013.

[26] H. Jacobsen, K. Lieutenant, C. Zendler, and K. Lefmann, "Bi-spectral extraction through elliptic neutron guides," *Nuclear Instruments and Methods in Physics Research Section A: Accelerators, Spectrometers, Detectors and Associated Equipment*, vol. 717, pp. 69–76, July 2013.

[27] Matter. http://www.matter.org.uk/diffraction/x-ray/powder_method.htm, 2013.

[28] Wikipedia. http://en.wikipedia.org/wiki/Monte_Carlo_method, 2013.

[29] J. von Neumann, "Zur Theorie der Gesellsehaftsspiele," *Math. Annalen.*, vol. 100, pp. 295–320, 1928.

[30] P. L'Ecuyer, "Efficient and Portable Combined Random Number Generators," *Communications of the ACM*, vol. 31, no. 6, pp. 742–750, 1988.

[31] K. Lefmann and K. Nielsen, "McStas, a general software package for neutron ray-tracing simulations," *Neutron News*, vol. 10, pp. 20–23, Jan. 1999.

[32] I. Lux, "Systematic study of some standard variance reduction techniques," *Nucl. Sci. Eng.*, Sep 1978.

[33] B. W. Kernighan, *The C Programming Language*. Prentice Hall Professional Technical Reference, 2nd ed., 1988.

[34] ESS Data Management Center. `http://www.ess-dmsc.eu/`, 2013.

[35] J. Christ and T. Springer, "Über die entwicklung eines neutronleiters am frm-reaktor," *Nukleonik*, vol. 4, pp. 23–25, 1962.

[36] H. Maier-Leibnitz and T. Springer, "The use of neutron optical devices on beam-hole experiments," *J. Nucl. Energy*, vol. 17, p. 217, 1963.

[37] F. Mezei, "Novel polarized neutron devices: supermirror and spin component amplifier," *Comm. Phys.*, vol. 1, pp. 81–85, 1976.

[38] F. Mezei and P. Dagleish, "Corrigendum and experimental evidence on neutron supermirrors," *Comm. Phys.*, vol. 2, pp. 41–43, 1977.

[39] F. Mezei, "Long pulse spallation sources," *Physica B: Condensed Matter*, vol. 234-236, pp. 1227–1232, June 1997.

[40] H. Abele, D. Dubbers, H. Häse, M. Klein, a. Knöpfler, M. Kreuz, T. Lauer, B. Märkisch, D. Mund, V. Nesvizhevsky, a. Petoukhov, C. Schmidt, M. Schumann, and T. Soldner, "Characterization of a ballistic supermirror neutron guide," *Nuclear Instruments and Methods in Physics Research Section A: Accelerators, Spectrometers, Detectors and Associated Equipment*, vol. 562, pp. 407–417, June 2006.

[41] P. Böni, "New concepts for neutron instrumentation," *Nuclear Instruments and Methods in Physics Research Section A: Accelerators, Spectrometers, Detectors and Associated Equipment*, vol. 586, pp. 1–8, Feb. 2008.

[42] D. M. Rodriguez, S. J. Kennedy, and P. M. Bentley, "Properties of elliptical guides for neutron beam transport and applications for new instrumentation concepts," *Journal of Applied Crystallography*, vol. 44, pp. 727–737, June 2011.

[43] K. H. Klenø, K. Lieutenant, K. H. Andersen, and K. Lefmann, "Systematic performance study of common neutron guide geometries," *Nuclear Instruments and Methods in Physics Research Section A: Accelerators, Spectrometers, Detectors and Associated Equipment*, vol. 696, pp. 75–84, Dec. 2012.

[44] J. Liouville, "Note sur la Théorie de la Variation des constantes arbitraires.," *Journal de mathématiques pures et appliquées*, vol. 3, no. 1, pp. 342–349, 1838.

[45] Herbert Goldstein, C. P. P. Jr., and J. L. Safko, *Classical Mecanics*. Pearson, 3 ed., 2002.

[46] P. Bentley *et al.*, "Recent advances in guide design and simulation," *in preparation*, 2013.

[47] P. M. Bentley, P. Fouquet, M. Böhm, I. Sutton, C. D. Dewhurst, and K. H. Andersen, "Global optimization of an entire neutron guide hall," *Journal of Applied Crystallography*, vol. 44, pp. 483–488, May 2011.

[48] DMSC web page. `http://www.ess-dmsc.eu`, 2013.

[49] M. Bertelsen *et al.*, "Exploring performance of neutron guide systems using pinhole beam extraction," *accepted for Nucl. Instr. Meth. A.*, 2013.

[50] F. Mezei and M. Russina, "Neutron beam extraction and delivery at spallation neutron sources," *Physica B: Condensed Matter*, vol. 283, pp. 318–322, June 2000.

[51] K. Lefmann, U. Filges, F. Treue, J. Kirkensgård, B. Plesner, K. Hansen, and K. Klenø, "Optimal shape of a cold-neutron triple-axis spectrometer," *Nuclear Instruments and Methods in Physics Research Section A: Accelerators, Spectrometers, Detectors and Associated Equipment*, vol. 634, pp. S1–S6, Apr. 2011.

[52] J.O. Birk *et al.*, "Camea: An inverse geometry time-of-flight spectrometer. instrument proposal for ess," *in preparation*, 2013.

[53] F. Mezei and M. Russina, "New opportunities in quasi elastic neutron scattering spectroscopy," *Physica B: Condensed Matter*, vol. 301, pp. 94–98, July 2001.

[54] J. Voigt and N. Violini, "Chopper layout for spectrometers at long pulse neutron sources," 2013.

[55] S.L. Holm *et al.*, "Heimdal: A narrow bandwidth time-of-flight diffractometer. instrument proposal for ess," *in preparation*, 2013.

[56] ESS, "Technical Design Report for the European Spallation Source," April 2013.

[57] L. C. Chapon, P. Manuel, P. G. Radaelli, C. Benson, L. Perrott, S. Ansell, N. J. Rhodes, D. Raspino, D. Duxbury, E. Spill, and J. Norris, "Wish: The New Powder and Single Crystal Magnetic Diffractometer on the Second Target Station," *Neutron News*, vol. 22, pp. 22–25, Apr. 2011.

[58] P.K. Willendrup *et al.*, "Mcstas 2.0: A neutron monte-carlo ray-tracing simulation package," *in preparation for J. Appl. Cryst.*, 2013.

[59] K. Lefmann, K. H. Klenoe, J. O. Birk, B. R. Hansen, S. L. Holm, E. Knudsen, K. Lieutenant, L. von Moos, M. Sales, P. K. Willendrup, and K. H. Andersen, "Simulation of a suite of generic long-pulse neutron instruments to optimize the time structure of the European Spallation Source.," *The Review of scientific instruments*, vol. 84, p. 055106, May 2013.

[60] A. Huq, J. P. Hodges, O. Gourdon, and L. Heroux, "Powgen: A third-generation high-resolution high-throughput powder diffraction instrument at the Spallation Neutron Source," *Zeitschrift für Kristallographie Proceedings*, vol. 1, no. EPDIC 2010, pp. 127–135, 2011.

[61] A. C. Hannon, "Results on disordered materials from the GEneral Materials diffractometer, GEM, at ISIS," *Nuclear Instruments and Methods in Physics Research Section A: Accelerators, Spectrometers, Detectors and Associated Equipment*, vol. 551, pp. 88–107, Oct. 2005.

[62] S.L. Holm, M. Bertelsen, and K. Lefmann, "Considerations on the guide and chopper system for the hybrid diffractometer tipsi for ess," *Internal DK-CH WP4 reports*, 2013.

Appendix A

Articles and reports

As written in the preface the articles and reports appended here describe the simulation work I have done as a student assistant from January 2010 to September 2011 (A.1 and A.2) and the work I have done for my master thesis (A.3, A.4, and A.5).

A1: Simulation of a suite of generic long-pulse neutron instruments to optimize the time structure of the ESS. *The Review of scientific instruments, vol. 84, p. 055106, May 2013.* Kim Lefmann, Kaspar H. Klen, Jonas Okkels Birk, Britt R. Hansen, Sonja L. Holm, Erik Knudsen, Klaus Lieutenant, Lars von Moos, Morten Sales, Peter K. Willendrup, and Ken H. Andersen.

A2: Powder Diffractometers at Long-pulsed Sources. *Journal of the Physical Society of Japan vol. 80, p. SB018, 2011.* Morten Sales, Sonja Lindahl Holm, Klaus Lieutenant and Kim Lefmann.

A3: Neutron guide-split: A high performance guide bundle concept for elliptical guides. *In preparation for Journal Appied Crystallography.* Sonja Lindahl Holm, Nina Rasmussen, Louise Høpfner, Jörg Woigt, Ken Andersen, Kim Lefmann.

A4: Time-of-Flight Instrument for Powder diffraction, Small angle scattering and imaging. *ESS Instrument Construction Proposal* Mogens Christensen, Jürg Schefer, Sonja Lindahl Holm, Kim Lefmann, Nadir Aliouane, and Paul Henry .

A5: Technical design report for ESS *Release 3.08, April 23, 2013* S. Peggs et al.

A.1 Simulation of a suite of generic long-pulse neutron instruments to optimize the time structure of the ESS

The former science director of ESS, Christian Vettier, proposed to make a study of the impact of the possible ESS source time structures on the instrument suite. This work would be an important part of the decision process for the final time structure. The work was carried out by the Copenhagen Simulation Task Force Team.

A.1.1 Abstract

We here describe the result of simulations of 15 generic neutron instruments for the long-pulsed European Spallation Source (ESS). All instruments have been simulated for 20 different settings of the source time structure, corresponding to pulse lengths between 1 ms and 2 ms; and repetition frequencies between 10 Hz and 25 Hz. The relative change in performance with time structure is given for each instrument, and an unweighted average is calculated. The performance of the instrument suite is proportional to a) the peak flux and b) the duty cycle to a power of approx. 0.3. This information is an important input to determining the best accelerator parameters. In addition, we find that in our simple guide systems, most neutrons reaching the sample originate from the central 3-5 cm of the moderator. This result can be used as an input in later optimization of the moderator design. We discuss the relevance and validity of defining a single Figure-of-Merit for a full facility and compare with evaluations of the individual instrument classes.

A.1.2 My contribution

My contribution to this article was to simulate a basic cold powder diffractometer to the generic instrument suite for ESS. In order to investigate the impact of the source time structure (frequency and pulse length) on the instrument performance of a powder diffractometer, one needs to optimize the instrument lengths and wavelength bands for each source setting. For this study we simulated 20 settings. More on this can be found in appendix A.2.

A.2 Powder Diffractometers at Long-pulsed Sources

This proceeding article describes the two powder diffractometers simulated for the study of the impact of the ESS source time structure on a generic instrument suite found in appendix A.1.

A.2.1 Abstract

We have investigated the performance of a cold and a thermal neutron powder diffractometer installed at at long-pulsed source with the use of Monte Carlo ray tracing simulations. We show that the cold powder diffractometer will be a very powerful instrument when a relaxed resolution can be accepted - e.g. for magnetic studies. A comparison between a thermal powder diffractometer with and without Wavelength Frame Multiplication (WFM) show that the WFM technique can be used to achieve shorter instrument length without losing flux. The thermal powder diffractometer will be competitive with the existing high resolution powder diffractometers.

A.2.2 My contribution

My contribution to this article was to simulate the cold powder diffractometer for a generic instrument suite at ESS.

A.3 Neutron guide-split: A high performance guide bundle concept for elliptical guides

During the work on the generic instrument suite for ESS a concern regarding the feasibility of long guides (150 m or more) was raised. As this was an unresolved issue a lot of thought and effort was devoted to this question in our group. One of the things that came out of this was the idea of feeding several instruments from the same beam port by splitting the neutron guide.

This appendix is an almost finished draft version of the article that I hope to submit soon.

A.3.1 Abstract

We show that it is possible to feed several cold neutron instruments from the same beam port at a neutron facility by elliptical guides without compromising the neutron flux notably on any of the sample positions. This can be achieved by using the new guide-split concept presented here. Since elliptical guides are capable of transporting an almost completely filled phase space within a large divergence ($\pm 2^\circ$), for cold neutrons, we use the end of a primary guide as a virtual source point. It is therefore possible to place several secondary guides side by side going in slightly different directions, and hence exploit different parts of the transported phase space. In addition the kink between the primary and secondary guide eliminates line of sight. By ray-tracing simulations of three different set-ups (with two, four, and eight secondary guides) we have shown that it is possible to illuminate eight sample positions from one beam port with a brilliance transfer above 90% on each sample, with a sample size of 1×1 cm^2, a maximum divergence of $\pm 0.5^\circ$, and a wavelength band from 4.25 Å to 5.75 Å, on a 150 m long instrument. We show two examples of using this concepts for instruments proposed for the European Spallation Source.

A.3.2 My contribution

The initial idea of the guide-split is mine and I performed the first proof-of-principle simulations. I supervised the students (Nina Rasmussen and Louise Høpfner) doing further optimizations and computer simulation. The simulations of the cold chopper spectrometer example was done by Kim Lefmann and I did the simulations of the cold powder diffractometer example. I wrote most of the text for the paper.

A.4 ESS Instrument Construction Proposal; Time-of-Flight Instrument for Powder diffraction, Small angle scattering and imaging.

This is the final preproposal from the Danish-Swiss work package number four (WP4), to be submitted in the final by October 31. 2013.

A.4.1 Abstract

We propose the construction of an instrument, which combines neutron powder diffraction (NPD), small angle neutron scattering (SANS) and neutron imaging (NI) in a single instrumental setup to be built at ESS. The instrument is designed to have a time resolution sufficient to follow chemical and physical processes in real time over a very broad spatial span. NPD covers the atomic regime in the range from 0.01 to 5 nm, while SANS looks into the nanometer regime covering length scales from 2-100 nm and finally NI reveals the structural features in direct space from 50 μm - 50 mm. In other words the instrument is capable of covering length scale over 9 orders of magnitude and follow in situ processes.

A.4.2 My contribution

Mogens Christensen has written the text and I have done all the analytical calculations and simulations for the thermal powder diffractometer part of the instrument.

A.5 Technical design report for ESS

The Technical design report (TDR) for ESS is a document the will ensure the funding of the whole ESS project from the partner countries. Only an excerpt of the TDR is appended here since the full document contains more than 600 pages.

A.5.1 Abstract

This chapter describes the uses of neutron scattering techniques, their place in the wider science landscape, and the ways in which they complement other experimental techniques. It discusses ESSs strengths in studying and understanding complex materials and presents a reference suite of 22 instruments selected to illustrate capabilities and scientific impact. The chapter also describes the multi-faceted research infrastructure that will surround the facility and enhance its productivity. While the publication of this report marks the end of the design phase for the accelerator and target station, the design phase for the neutron instrument suite will continue past 2020, when the final two instrument concepts are slated for selection. The instruments that will be built are therefore likely to be quite different from the reference suite described here. The phased instrument selection and design process will make it possible to respond flexibly and creatively to changing research needs and to take advantage of evolving technology.

A.5.2 My contribution

My work on the Heimdal powder diffractometer has been used by Paul Henry to write the section on the thermal powder diffractometer for the reference suite in the TDR for ESS (pages 68-69 in the TDR). Also my simulations on the cold powder instrument have been used.

Discussion about data treatment has arisen from the simulations of the thermal powder diffractometer. I have taken an active part in the discussions and on page 144 in the TDR, under the section about the Data Management Center, one of the first data sets from my simulations is displayed.

Simulation of a suite of generic long-pulse neutron instruments to optimize the time structure of the ESS

Kim Lefmann,[1,2] Kaspar H. Klenø,[1,2] Jonas Okkels Birk,[1,2,3] Britt R. Hansen,[4,5] Sonja L. Holm,[1,2] Erik Knudsen,[4,5] Klaus Lieutenant,[6,7,8] Lars von Moos,[1,5,9] Morten Sales,[1,2] Peter K. Willendrup,[4,5] and Ken H. Andersen[10]

[1)] *Nanoscience and eScience Centers, Niels Bohr Institute, University of Copenhagen, Universitetsparken 5, 2100 Copenhagen Ø, Denmark*
[2)] *Danish Workpackage for the ESS Design Update Phase, Universitetsparken 5, 2100 Copenhagen Ø, Denmark*
[3)] *Laboratory for Quantum Magnetism, École Polytecnique Fédérale de Lausanne (EPFL), 1015 Lausanne, Switzerland*
[4)] *Institute of Physics, Technical University of Denmark, 2800 Lyngby, Denmark*
[5)] *Danish Workpackage for the ESS Design Update Phase, 2800 Lyngby, Denmark*
[6)] *Institute for Energy Technology, Instituttveien 18, 2007 Kjeller, Norway*
[7)] *Helmholtz Center for Energy and Materials, Hahn-Meitner Platz, 14109 Berlin, Germany*
[8)] *German Work Package for the ESS Design Update, Hahn-Meitner Platz, 14109 Berlin, Germany*
[9)] *Institute for Energy Conversion, Technical University of Denmark, 4000 Roskilde, Denmark*
[10)] *European Spallation Source ESS AB,22100 Lund, Sweden*

We here describe the result of simulations of 15 generic neutron instruments for the long-pulsed European Spallation Source (ESS). All instruments have been simulated for 20 different settings of the source time structure, corresponding to pulse lenghts between 1 ms and 2 ms; and repetition frequencies between 10 Hz and 25 Hz. The relative change in performance with time structure is given for each instrument, and an unweighted average is calculated. The performance of the instrument suite is proportional to a) the peak flux and b) the duty cycle to a power of approx. 0.3. This information is an important input to determining the best accelerator parameters. In addition, we find that in our simple guide systems, most neutrons reaching the sample originate from the central 3-5 cm of the moderator. This result can be used as an input in later optimization of the moderator design. We discuss the relevance and validity of defining a single Figure-of-Merit for a full facility and compare with evaluations of the individual instrument classes.

I. INTRODUCTION

The European Spallation Source (ESS) is designed to be a long-pulsed spallation neutron source - the first of its kind[1,2]. This opens new territory, including the challenges to design instruments that perform well for a long-pulsed source, to design the optimal moderator for these instruments, and to choose the pulsing time structure that matches these choices. Obviously, these optimizations are coupled, since *e.g.* the instrument design depends upon the pulse length and the optimal moderator design depends on both desired pulse length and on the instrument geometries.

In this article we are concerned with only one part of this optimization problem: the selection of the source time structure, *i.e.* its pulse length (τ) and repetition time (T). The original 2002 design was fixed at $\tau = 2$ ms, and $T = 60$ ms ($f = 16\frac{2}{3}$ Hz)[3], and we have therefore investigated time structures in the neighbourhood of these initial parameters.

In order to perform the time-structure optimization, we have selected a suite of generic instruments, covering a broad range of scientific utilizations. These instruments have then undergone a rough design and optimization for each setting of (T, τ), and the relative merits of the instruments at the different time structures have been compiled and compared.

The simulated instrument suite should not be seen as a draft day-one suite, neither should the individual instruments be seen as being close to their final design. Much design work and careful selection of an initial instrument suite is presently in progress. The present work is merely the first step in a long process.

Below, we present our generic neutron long-pulse instrument suite, the optimization procedure, and the obtained overall results. The simulation results of the 15 individual instruments are available on-line[4] and are or will be published individually in more detailed articles[5–12].

As a result of this and other studies of the ESS time structure, covering its impact on the performance, reliability, construction cost and operation of the facility, the time structure has now been fixed at $\tau = 2.86$ ms and $T = 71$ ms ($f = 14$ Hz). The results presented in this paper were an important input to this decision.

II. THE GENERIC INSTRUMENT SUITE

The instrument suite we discuss here was initiated by the Scientific Advisory Group (SAG) for ESS-

Instrument	L_1[m]	L_2[m]	β
Cold Chopper Spect.	60	100	0
Therm. Chopper Spect.	100	100	0
Cold Triple Axis	40	40	0
Thermal Triple Axis	40	40	0
TOF Triple Axis	60	100	0
Backscatter Spectrometer	151	302	0
Spin Echo Spectrometer	30	30	2.5
Short SANS (bio-)	12 + 1-4		2.5
Medium SANS	18 + 1-10		2.5
Long SANS (materials-)	28 + 2-20		2.5
Horizontal Reflectometer	52	52	4
Vertical Reflectometer	52	52	4
Cold Powder Diffract.	88	176	0
Thermal Powder Diffract.	102	102	0
Single Crystal Diffract.	31	42	0

TABLE I. Properties of 15 generic ESS instruments, suggested by the ESS-S SAG and the ESS SAC. L_1 denotes the length of the instrument for a pulse length of $\tau = 1$ ms, while L_2 is the instrument length for $\tau = 2$ ms, and β is the "Frascati exponent", defined by (1).

Scandinavia, in September 2009. This list was expanded by the slightly different "straw-man-list" of instruments, decided upon by the Scientific Advisory Council for the ESS (SAC) in June 2010. Our starting list was found as a join of these two instrument suites, and is shown in Table I. It should be noted that due to time constraints, neither a tomography instrument, a protein diffractometer, nor a wide-angle spin-echo instrument have been included in these simulations, even though these classes of instruments were present in the straw-man suite.

In the optimizations, we have taken into account that neutrons of different wavelengths may not be equally useful for the individual instruments. In particular, spin-echo spectrometers, reflectometers, and small-angle diffractometers strongly prefer long wavelength neutrons. To account for this fact in a simplified way, we parametrize the relative "value", Q, of each neutron by a simple expression:

$$Q(\lambda) = \lambda^{\beta}. \tag{1}$$

The values of β for different instrument types were selected by an expert meeting in Frascati, August 2009[13], and Table I contains the chosen values of β. Here, a value of zero indicates that all neutrons are considered equally valuable, while a positive value of β gives preference to long-wavelength neutrons.

III. DESIGN AND OPTIMIZATION OF INSTRUMENTS

Over the last decade or more, a number of authors have addressed the issue of long-pulse instrumentation[14–17].

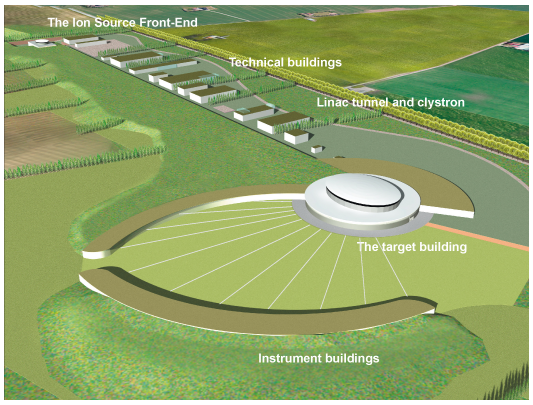

FIG. 1. (Color online) Artists view of the ESS target/instrument buildings seen from above. Note that the long instruments are placed in a hall which is separated from the main target building.

The instrument designs simulated here are in general adapted from the earlier work, except that we have adjusted the instrument lengths as described below and listed in Table I. Most instruments on this list are typical time-of-flight instruments, except the reactor-type triple-axis instruments. One untraditional instrument type, labeled "TOF Triple Axis" has been included in the list. This is a hybrid (or inverted-geometry) spectrometer[11] with a time-of-flight front-end and a triple-axis-like crystal analyzer back-end.

A. Instrument length and resolution

To qualify the discussion, let us first recall the equation for the neutron time-of-flight, t:

$$t = \alpha\lambda L, \tag{2}$$

where L is the flight length and $\alpha = m_{\rm n}/h \approx 252.7\,\mu$s/(m Å). The relative uncertainty of the neutron wavelength can then be expressed by the uncertainty in flight time by

$$\frac{\delta\lambda}{\lambda} = \frac{\delta t}{t} = \frac{\delta t}{\alpha\lambda L}. \tag{3}$$

For long-pulse instruments, δt is either given approximately by the pulse length, τ, (at a long pulsed source, the exponentially decaying tail of the pulse can to first order be neglected compared to τ), or by the opening time of a pulse-defining chopper, as described below. In the latter case, L will be the flight length from the pulse-defining chopper to the detector, in the former it will denote the full instrument length to the detector (for chopper spectrometers, see later).

In analogy, the useful wavelength band, $\Delta\lambda$, of neutrons which can reach the detector without creating

frame overlap is given by

$$\Delta\lambda = \frac{\Delta t}{\alpha L}, \quad (4)$$

where for instruments using the full pulse, $\Delta t = T - \delta t \approx T$.

A number of the simulated instruments cannot directly utilize the full pulse length, τ, since this would result in a too bad resolution, (too large $\delta\lambda/\lambda$). Therefore, pulse shaping must be performed at a fast pulse-defining chopper, close to the source. In this work, the distance between source and chopper is set the the smallest realistic value given by the biological shielding of the moderator: $L_{\rm pc} = 6$ m.) A pulse-defining chopper at the distance $L_{\rm pc}$ effectively selects a wavelength band, given by $\Delta\lambda = \tau/(\alpha L_{\rm pc})$. To let this wavelength band fill the whole time frame, T, at the detector, the instrument must be very long: $L = L_{\rm pc}(1 + T/\tau)$, which for the parameters investigated in this work lies between 126 m and 606 m, since the inverse duty cycle, T/τ, lies in the range 20-100.

B. Wavelength Frame Multiplication and Repetition Rate Multiplication

At some instruments with pulse-defining choppers, we have used an alternative scheme to having very long instruments: A number of closely-spaced shorter pulses is produced at the pulse-defining chopper, which are then kept separated by a number of sub-frame-overlap choppers. This has been denoted "Wavelength Frame Multiplication" (WFM), as first presented by the group of F. Mezei[18,19]. In the present simulations, the WFM method is used at the thermal powder diffractometer and the thermal chopper spectrometer.

The cold chopper spectrometer uses a similar technique, which bears the name "Repetition Rate Multiplication" (RRM). Here, the full pulse length is used, but a monochromating chopper close to the sample produces up to 15 different monochromatic pulses for each moderator pulse[14,20], as simulated in Ref.[5]. Recently, this technique has been experimentally proven feasible at NEAT, HZB[21] and 4SEASONS, J-PARC[22]. In the present simulations, also the thermal chopper spectrometer employs RRM (in addition to using WFM).

C. The source

Lacking precise information about the source power and moderator performance for the different time structures, we have initially considered the two following scenarios.

1. The source has a constant time-average neutron flux.
2. The accelerator is limited by a maximum beam current; *i.e.* the source peak flux is constant.

These two scenarios differ only by a τ/T scaling of the source flux, whence we were able to use the same set of simulations/optimizations. As a reference point at the baseline settings, we use the characteristics of a 12×12 cm^2 moderator with uniform flux distribution, as given in Ref. 23.

D. The guide systems

For the short guide systems (below 60 m), we have everywhere used guides with constant cross section, where fast-neutron background from direct line-of-sight to the moderators is avoided by inserting a kink or curved section. At the reflectometers, we have used elliptical focusing in the direction perpendicular to the sample surface, combined with a kink in the other direction.

For instruments of 60 m and longer, and for the 40 m triple-axis instruments, we have employed elliptical guides for beam transport, since recent experiments and simulations has shown this design to be strongly superior over traditional curved guides[6,24].

For the values of guide reflectivities, we have everywhere used recent information from one supplier[25]. In general, we use $m = 3$ along the main length of all guides, and $m = 6$ in the beginning and end of elliptical guides.

Guides have everywhere been assumed to consist of straight sections, with perfect alignment and zero waviness. The effect of waviness and misalignment of (in particular) long elliptical guides is a topic of future simulations[26]. A similar work was carried out earlier for straight guides[27].

In the optimizations, we have assumed 40 cm as the maximal guide width for the longest guides, relying on information that guides of this width and matching slow frame-overlap choppers can be produced[25,28]. Should it be necessary to place stricter limits on the guide width this will affect the absolute flux values at some instruments[26], but not the relative comparisons relevant for the present work. This statement is valid for most other design parameters.

For the long guides, no attempt has been made to avoid line-of-sight. The key issue is that bending of the guides, as known from traditional guide systems, would disturb the elliptical focusing properties[26], whence a solution to this issue is more involved and was postponed to later studies[29].

An additional possibility to reduce the fast-neutron background would be to insert either a crystal filter or a heavy "straight-beam-block" in the middle of the guide, probably early in the guide[30]. Another possibility for guide design is the combination parabolic-straight-parabolic, where the straight section can be curved. This combination transmists almost as well as an elliptical guide[24].

E. Optimization of instruments by simulation

All present simulations were performed using the Monte-Carlo ray-tracing package McStas v. 1.12[31], where the instrument designs were typically performed on individual computers, while the final optimization and data taking was performed on the computer cluster of the ESS Data-Management Center in Copenhagen. Typical runs used between 10^8 and 10^{11} neutron rays, depending on the type of instrument.

Instruments were first simulated at the baseline time structure settings of $\tau = 2$ ms and $T = 60$ ms. The instrument length and chopper settings were adjusted as to obtain a pre-determined instrumental resolution, while remaining above a certain length limit, relevant for the SANS and spin-echo instruments. Subsequently, the guide system of each instrument was optimized using a Figure-of-Merit (FoM) found from the time average flux, $\Psi(\lambda)$, on the sample position in the useful wavelength band, $[\lambda_{\min}, \lambda_{\max}]$ weighted by $Q(\lambda)$:

$$\mathrm{FoM} = \int_{\lambda_{\min}}^{\lambda_{\max}} \Psi(\lambda) Q(\lambda) d\lambda. \quad (5)$$

Subsequently, the design of each of the 15 instruments was modified and optimized for each of 20 different time structure settings, in principle 300 optimizations and subsequent simulated data. In order to produce comparable simulations, all optimizations for a given instrument were restricted to have certain resolution characteristics. For spectrometers, this was given as $\delta\lambda/\lambda$ at the sample position for a certain value of λ. For diffractometers, this was given as a fixed $\delta\lambda/\lambda$ at the detector for a limited divergence matching this value, to obtain a certain low linewidth in the measured lattice spacing, $\delta d/d$, at a given scattering angle. For a few instrument types (spin-echo spectrometer and SANS), the worst resolution was in all cases deemed "sufficient", so these instruments were not restricted by resolution requirements and were thus simulated at their constant (minimum) lengths.

Since it has been proposed to place triple-axis spectrometers at the long-pulsed ESS, we have included a cold and a thermal instrument in these comparisons. For a triple-axis spectrometer at a pulsed source, the time structure is useful only for filtering of background and higher-order harmonics. Hence, the instrument has identical FoM for all time structure settings, and we needed to simulate only one time structure for each of the two triple-axis spectrometers.

IV. RESULTS OF INSTRUMENT OPTIMIZATIONS

We now present the results of our optimizations over the time structure range, as described above. To exemplify, we begin with the results for two individual instruments, before describing the combined results of the full instrument suite. Finally, we discuss the validity of our FoM approach.

A. Simulation example 1: Cold Chopper Spectrometer

Let us first consider the simulation of the cold-neutron chopper spectrometer, with a design similar to IN5 at ILL. In this present (simple) version of this instrument, the monochromatization is performed by the (full) length of the pulse, in combination with the opening time of fast choppers just before the sample, as illustrated in Fig. 2. The instrument length is determined by the pulse length, to fulfill a constant $\delta\lambda/\lambda = 1.6$ % at 5 Å wavelength. At the baseline time structure settings, the distance between the source and the fast chopper is $L = 100$ m, and the useful band is 2.2 Å wide (here chosen to be 3.9 Å to 6.1 Å). This is described in detail in Ref. 5, where, however, a more simple guide system was used. Our results can thus be seen as an update of the previous publication.

The present cold chopper spectrometer uses an elliptical guide with quadratic cross section, which is 27.3 cm at its widest place. The guide focuses to the sample, which is defined to be 2×2 cm^2. The instrument uses the RRM scheme, as presented earlier This mode allows for each source pulse 9 monochromatic pulses on the sample, with a wavelength difference between neighbouring pulses of 0.25 Å, and 6 ms between pulses. In this way, the instrument reaches a combined monochromatic flux of $1.6 \cdot 10^8$ n/s/cm^2 for the wavelength band mentioned above, centered at 5 Å.

A shorter source pulse will allow for a shorter instrument; for pulses of 1.5 ms, 1.25 ms, and 1.0 ms, the instrument length becomes 80 m, 70 m, and 60 m, respectively. (The finite opening time of the monochromating choppers has the consequence that the 1.0 ms instrument is less than a factor two shorter than the 2.0 ms instrument.) A shorter instrument gives rise to a larger bandwidth and thus more neutrons on the sample (for constant time-average flux). For example, when going from 2 ms to 1 ms pulse length, the increase in FoM is more than 50%, as seen in Table II. A rather similar gain is found from lowering the source frequency from $16\frac{2}{3}$ Hz to 10 Hz, also due to the larger useful bandwidth.

Due to the point-to-point-like focusing of an elliptial guide, most neutrons at the sample originate from the innermost 4×4 cm^2 of the moderator surface, as shown in Fig. 3. Therefore, it would be beneficial if neutrons were emitted preferentailly from the center of the moderator. A simulated hot spot with a factor 2.0 intensity gain over a circle of diameter $d = 3$ cm produces a gain in neutron flux at the sample of 30 %.

Taken at face value, the flux number obtained at the base time structure settings represents an impressive factor 200 gain over IN5. However, care should be taken when comparing these numbers. Firstly, the full gain is possible only if neutrons from all monochromatic pulses are equally useful to the actual experiment. Secondly, much of the flux increase comes from an increased divergence of neutrons in the elliptical guide system (compared to the straight/curved guide at IN5), and this part of the gain would be of value only to particular experi-

T/τ (ms)	N	1.0	1.25	1.5	2.0
100 (10 Hz)	15	2.39	2.24	2.05	1.67
80 (12.5 Hz)	11	2.08	1.83	1.59	1.26
60 (16.67 Hz)	9	1.72	1.48	1.29	1.00
50 (20 Hz)	7	1.35	1.17	0.98	0.76
40 (25 Hz)	5	0.91	0.81	0.68	0.56

TABLE II. Relative Figure-of-Merit (FoM) values for the simulations of the IN5-like cold chopper spectrometer at ESS, under the assumption of constant time-average flux. Simulations are performed for 20 different settings of the time structure, (T, τ). The RRM scheme is parametrized by N, which indicates the number of possible monochromatic pulses at the sample per source pulse.

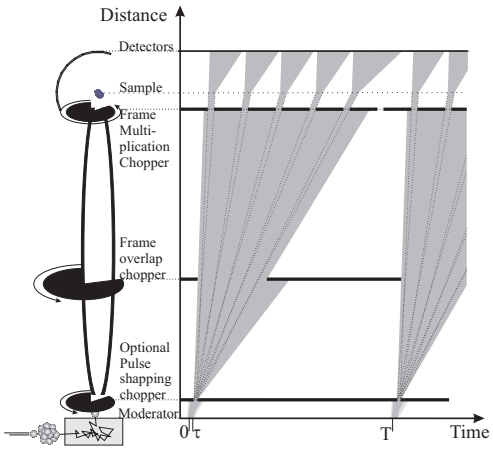

FIG. 2. (left) Sketch of the main elements of the cold chopper spectrometer. Picture is not to scale. (right) Time-of-flight diagram illustrating the selection of neutron pulses by choppers, with the spectrometer running in RRM mode with $N = 5$.

ment types. Hence, the mentioned gain is for this instrument a best case scenario, where a worst case scenario (collimating down to IN5 divergence and using only one RRM frame) would lead to a gain factor of just 5.

B. Simulation example 2: Long SANS instrument

We now consider the longest of the three simulated cold-neutron small-angle scattering instruments. In analogy with the cold chopper spectrometer described above, the wavelength uncertainty is determined by the full pulse length, since the incoming wavelength is determined by the measured time-of-flight in the detector (assuming elastic scattering at the sample).

The length of the instrument is in practice determined by the 20 m long double-pinhole collimator section, combined with an initial 8 m of guide, which includes a kink to avoid direct line-of-sight. The source-sample distance

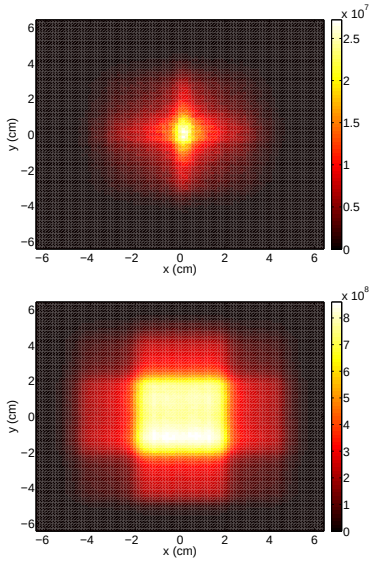

FIG. 3. (Color online). Simulated plots of the moderator surface showing the number of neutrons which reach the sample at the IN5-like chopper spectrometer. Top panel shows the situation with a 60 m guide ($\tau = 1$ ms), while bottom panel shows the results for a 100 m guide ($\tau = 2$ ms).

is thus always 28 m, while the sample-detector distance can vary between 2 m and 20 m. The relevant time-of-flight length, L, thus varies between 30 m and 48 m. At these lengths, the wavelength uncertainty at the SANS instrument at $\lambda = 5$ Å and $\tau = 2$ ms is of the order $\delta\lambda/\lambda \approx 3 - 5\%$, which is almost always "too good", since the double-pinhole collimation of $d_1 = 10.5$ mm and $d_2 = 7.0$ mm has the dominating contribution to the q-resolution.

The bandwidth of the instrument is rather large, of the order 8 Å at the shortest detector setting. In combination with the large angular range covered at the detector, this allows a large q-range detected in the same setting. A sketch of the long SANS instrument and the corresponding wavelength band selection is found in Fig. 4.

In our optimizations, we have employed three settings of the collimation length and the sample-detector distance: $(2 + 2)$ m, $(10 + 10)$ m, and $(20 + 20)$ m. The results presented are an average of the three results, each normalized by the result at the baseline setting. For the baseline setting, the instrument reaches neutron fluxes of $1.8 \cdot 10^8$ n/s/cm^2, $9.0 \cdot 10^5$ n/s/cm^2, and $9.7 \cdot 10^3$ n/s/cm^2 for the three choices of distance, respectively, and the wavelength band centered around 10 Å.

A shorter source pulse will give better wavelength resolution, but the instrument cannot be shortened due to the kink and the collimation section. Therefore, this gives no gain in bandwidth (or integrated flux), but a small improvement in q-resolution. If, on the other hand, the source frequency is lowered, *e.g.* to 10 Hz, at constant

T/τ (ms)	1.0	1.25	1.5	2.0
100 (10 Hz)	1.69	1.69	1.69	1.69
80 (12.5 Hz)	1.34	1.34	1.34	1.34
60 (16.67 Hz)	1.00	1.00	1.00	1.00
50 (20 Hz)	0.83	0.83	0.83	0.83
40 (25 Hz)	0.67	0.67	0.67	0.67

TABLE III. Relative Figure-of-Merit (FoM) values for the simulations of the long SANS instrument at ESS under the assumption of constant time-average flux. Simulations are performed for 20 different settings of the time structure, (T, τ).

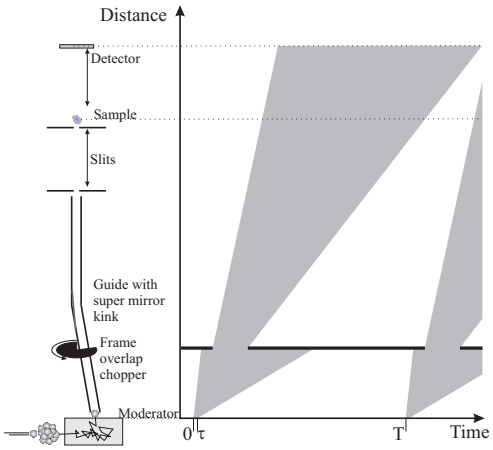

FIG. 4. (left) Sketch of the main elements of the long SANS instrument. Details are not to scale. (right) Time-of-flight diagram illustrating the selection of wavelength band by choppers, with the spectrometer running in the (20+20) m setting.

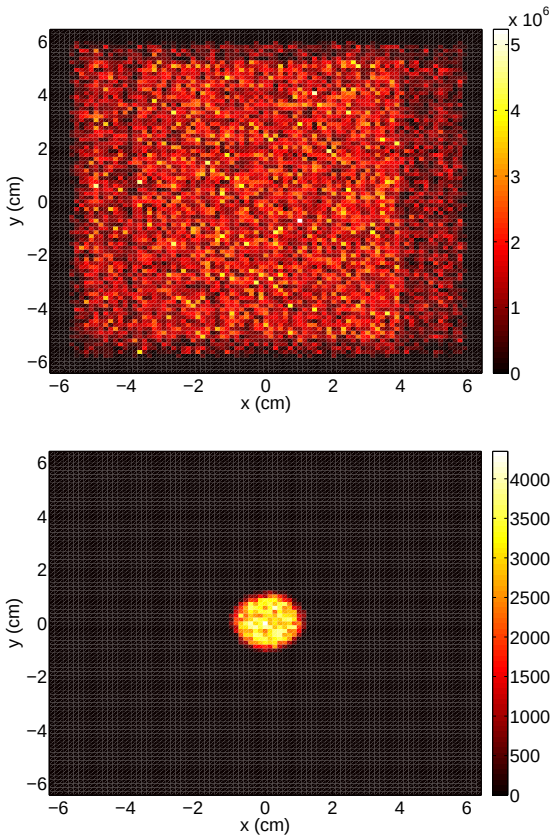

FIG. 5. (Color online). Simulated plots of the moderator surface showing the number of neutrons which reach the sample for the 20 m SANS instrument. The results are valid for any time structure. (top) data for 2 m collimator-detector setting; (bottom) data for 20 m collimator-detector setting.

time-average flux, the instrument will benefit from an increase in useful bandwidth and hence the FoM will increase. All FoM data are displayed in Table III.

At the longest collimation length, all neutrons at the sample originate from a circle of $d \approx 2.5$ cm at the center of the moderator surface. This effect is less pronounced at the shorter collimation lengths. This is illustrated in Fig. 5. On average, a simulated hot spot with a factor 2.0 intensity gain over a circle of diameter $d = 3$ cm produces a gain in neutron flux at the sample of 73%.

C. Optimization of the full instrument suite

After the optimization procedures, we record the resulting values of wavelength, bandwidth, flux at sample position, and FoM for each instrument and time structure setting. The results of the individual simulations are in general similar to the examples shown above 4. The obtained values of FoM have been normalized to the baseline setting of $T = 60$ ms and $\tau = 2$ ms.

For constant time-average flux, almost all instruments perform better towards the upper left-hand corner of the performance matrix. This is as expected, since i) a longer T will allow for a larger useful wavelength band, $\Delta\lambda$, and ii) a smaller τ will either iia) allow L to be smaller, giving an increased $\Delta\lambda$, or iib) allow a higher fraction of the total flux through the pulse-defining choppers.

In contrast, for the constant-peak-flux scenario, most instruments perform better towards the lower right corner of the performance matrix. This is most simply explained by the fact that here, more neutrons are produced in total, overcompensating the advantages of short pulses and low frequencies mentioned above.

To perform a global comparison of the different time structure settings, we use the relative instrument performances for each instrument. A simple arithmetic mean value has been used, since no decision on the relative importance of instruments has been taken. The results for the average performances are listed in Tables IV and V for the constant-time-average-flux and constant-peak-flux scenarios, respectively.

T/τ (ms)	1.0	1.25	1.5	2.0
100 (10 Hz)	2.07	1.81	1.67	1.37
80 (12.5 Hz)	1.89	1.66	1.55	1.19
60 (16.67 Hz)	1.62	1.42	1.24	1.00
50 (20 Hz)	1.53	1.27	1.09	0.88
40 (25 Hz)	1.20	1.05	0.90	0.73

TABLE IV. Average relative Figure-of-Merit for the generic ESS instrument suite at different time structures, under the assumption of constant time-average flux.

T/τ (ms)	1.0	1.25	1.5	2.0
100 (10 Hz)	0.62	0.68	0.75	0.82
80 (12.5 Hz)	0.71	0.78	0.87	0.89
60 (16.67 Hz)	0.81	0.89	0.93	1.00
50 (20 Hz)	0.92	0.95	0.98	1.05
40 (25 Hz)	0.90	0.98	1.01	1.09

TABLE V. Average relative Figure-of-Merit for the generic ESS instrument suite at different time structures, under the assumption of constant peak flux.

We see that the effect of shortening the pulse from 2.0 ms to 1.0 ms is typically around 60% increase at constant time-average flux – or around 20% decrease at constant peak flux. Likewise, the effect of going from 20 Hz to 10 Hz is around a 50% increase at constant time-average flux – or around 30% decrease at constant peak flux.

The data for constant time-average flux is shown as a function of the inverse source duty cycle, T/τ, in Figure 6. It is seen that, except for the very smallest duty cycles, the data fall almost on a common curve, which can be approximately described by

$$\mathrm{FoM} \approx \Psi_{\mathrm{peak}} \left(\frac{\tau}{T}\right)^{\alpha} = \Psi_{\mathrm{peak}}^{1-\alpha} \Psi_{\mathrm{time\,av}}^{\alpha} = \Psi_{\mathrm{time\,av}} \left(\frac{T}{\tau}\right)^{1-\alpha}, \tag{6}$$

with $\alpha = 0.30$. This value confirms the trivial result that the long-pulse source of the ESS is intermediate in nature between a short-pulse source and a continuous source. Instruments at short-pulse sources aim to be optimised to benefit from the peak flux, while instruments at steady-state sources are optimised to benefit from the time-average flux. The exact value of the exponent will clearly depend on the chosen instrument suite, but it is interesting to note firstly that the instrument performance scales more closely with the peak flux than with the time-average flux. Secondly, equation (6) predicts that the global instrument performance depends only on the time-average flux and duty cycle. If both are kept constant, e.g. by changing T and τ simultaneously, the instrument performance should be independent of the time structure.

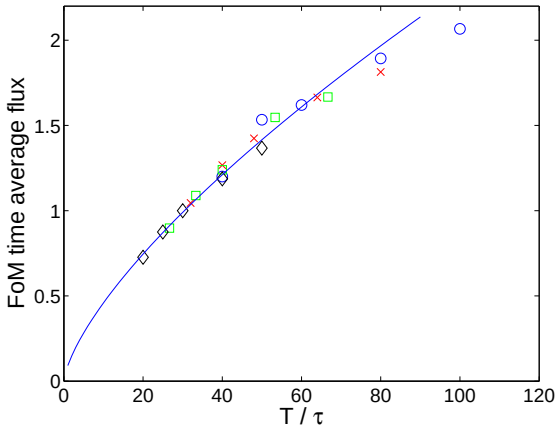

FIG. 6. (Color online). Average Figure-of-Merit for the generic ESS instrument suite at different time structures, plotted as a function of the inverse source duty cycle, under the assumption of constant time-average flux. Diamonds, squares, crosses, and circles represent pulse lengths of 2.0, 1.5, 1.25, and 1.0 ms, respectively. The solid line is a fit to the power law (6), as explained in the text.

D. Considerations beyond a simple Figure-of-Merit

The analysis above is based on the assumption that it is possible to reduce the full scientific usefulness of a facility into one single number, the FoM, and to express its variation by essentially one parameter, the duty ratio τ/T, as illustrated in Figure 6. This assumption shares one problem with most numerical optimization work: Details that cannot be compressed into the FoM are easily overlooked. For this reason, we will look more into some of these details. To simplify the argument, we will consider the effect on the instrument performance under the condition that the duty cycle τ/T is unchanged. The effect of varying the time structure under this boundary condition depends rather sensitively on the type of instrument.

- SANS, reflectometry and spin-echo instruments will benefit from the increased wavelength range which a longer repetition period will give them. Their performance will not suffer significantly from the degraded wavelength resolution, which an associated increase in pulse length would give. Any increase in bandwidth translates directly into improved performance.

- Crystal-monochromator instruments, such as triple-axis spectrometers, do not make much use of the source time structure at all. In these cases, only the time-average flux counts. The time structure has little or no effect.

- Chopper spectrometers, or other instruments that may employ RRM, have a weak preference for

shorter repetition periods. These instruments use the RRM to compensate for the fact that their preferred repetition frequency is higher than the source frequency. Increasing the source frequency reduces the need for RRM and makes their data-collection strategy more similar to existing instruments and simplifies the data analysis.

- Very high-resolution instruments, such as backscattering spectrometers and high-resolution diffraction also have a preference for shorter repetition periods. These instruments cut out only a small fraction of the pulse length to achieve the desired resolution and do not benefit significantly from the increased wavelength range offered by an increase in repetition period.

Overall, it seems clear that an increase in pulse length will translate into an increase in the average length of the instruments, which will result in increased costs for guides and shielding along the guides. On the other hand, with modern ballistic-type guides, the transport of neutrons represents no essential problem[24], while the instrument space becomes less restricted at the same time as the general background level decreases. In addition, certain combinations of T and τ may result in instruments with lengths which allow them to be grouped together in common instrument halls, rather than requiting separate buildings. In such a scenario, the cost savings associated with the reduction in the number of instrument buildings could cancel out the cost increase of the longer guides, as well as providing other benefits in terms of upgradeability and flexibility.

E. Optimizing the moderator parameters

The design and simulation of the target/moderator is much more computationally demanding than that of the instruments. Hence, one aim of the instrument simulations has been to assist the moderator optimizations towards an improved functionality of the full ESS. We here describe the results obtained in this direction.

Often, the figure-of-merit in moderator optimizations is the number of neutrons produced, possibly in a given wavelength interval and for a given moderator size. However, the moderator simulations produce more detailed information than this. The result of each simulation is given as a history of neutron events, each event having 6 parameters: position at moderator surface ($\mathbf{r}$), time of emittance (t), wavelength (λ), and divergence ($\boldsymbol{\eta}$). By means of instrument simulations it was found possible to represent the transmission probability of a neutron from moderator surface to sample as

$$T(\mathbf{r},\lambda) \approx T_r(\mathbf{r})T_\lambda(\lambda). \quad (7)$$

Here, the dependence on divergence has been integrated out, since the moderator flux (even with complex geometries) is expected to vary insignificantly over the rather small solid angle of the guide entry, Furthermore, we have neglected the emission time, which corresponds to ignoring the tails from the moderators. For a total target/moderator optimization, the figure-of-merit to optimize is thus for each of the moderators (*e.g.* a cold and a thermal):

$$\mathrm{FoM}_{\mathrm{mod}} = \sum_j W_j \int N(\mathbf{r},\lambda,t,\boldsymbol{\eta})Q_j(\lambda) \times T_{j,r}(\mathbf{r})T_{j,\lambda}(\lambda)d^2\mathbf{r}d\lambda d^2\boldsymbol{\eta}dt, \quad (8)$$

where the summation label, j, represents the instruments at the moderator, W_j is a normalization and weighting constant for each instrument, N is the simulated density of neutrons from the moderator, and $Q_j(\lambda)$ is given in (1).

We have for each instrument calculated the spatial transmission function, $T_r(\mathbf{r})$, as shown in the examples above, and listed in Ref. 4. The results show that for most instruments, the transmission peaks strongly in a 3-5 cm diameter circle (or square) in the center of the moderator. This effect results for some instruments from the use of elliptical guides, for others from using tight collimation and straight guides. Thus, it can for these simple guide systems be advantageous to concentrate the flux in a hot spot, while the size of the emitting part of the moderator can be limited, *e.g.* by reflectors. In this way, it should be possible to simultaneously increase the useful neutron flux and decrease the emission of fast neutrons. For each instrument, we have calculated the effect of producing a circular, 3 cm diameter, hot spot with 100% higher emittance - while maintaining the total emittance of the moderator. This set-up is close to what was presented in Ref.[32]. For most instruments, the gain factor of such a hot spot is around 30%, while few instruments show a full 100% gain.

It should be added that more elaborate guide systems, in particular an optimized guide extraction system for instruments with a pulse shaping chopper close to the moderator, will modify this picture. This problem will be addressed by further simulation work[29].

V. CONCLUSION

We have performed a series of systematic ray-tracing simulations of the performance of a generic instrument suite for the ESS. These simulations were carried out for a large number of time structure settings, for constant, typical instrument resolutions. The performance parameters were found to increase with increasing peak flux, as well as with increasing time-average flux, while varying only weakly with the details of the time structure.

The variation with time-average and peak flux can be expressed as $\mathrm{FoM} \propto \Psi_{\mathrm{peak}}\,(\tau/T)^{\alpha}$, with $\alpha = 0.30$. If both the peak flux and the duty cycle are kept constant, the average instrument performance is largely independent

of pulse-length or frequency, within the frequency range of the current study.

Since most instruments use tight collimations or (elliptical) focusing guides, most neutrons hitting the sample stem from a central part of the moderator of a diameter 3-5 cm. We suggest to use this knowledge for the optimization of the moderator design, in particular by considering "hot spots" at the moderator. However, this can be finalized only when the guide systems of the instruments are designed.

A. Implications for design of long-pulsed sources, e.g. ESS

As part of the study which resulted in the decision to fix the time structure of the ESS to $\tau = 2.86$ ms and $T = 71$ ms ($f = 14$ Hz), two boundary conditions were considered: 1) the time-average power is planned to be 5 MW. 2) the peak accelerator current cannot exceed 50 mA. The 5 MW number is judged to be important, so as to at least match the best existing instruments over the largest possible range. The limitation on the peak current results from a judgement, based on the experience of the SNS linear accelerator, as to the optimal compromise between performance, reliability and cost. In the interest of maximizing the instrument performance, it is clearly advantageous to push for the highest peak flux which the accelerator and target assembly can provide. We can therefore consider the 50 mA peak current as our specification, rather than an upper limit. These boundary conditions reduce the number of degrees of freedom when choosing τ and T from 2 to 1, as follows. The peak power on target is given by the product of the peak current and proton energy of 2.5 GeV. At 50 mA peak current, the instantaneous power is 125 MW. In order to achieve a time-average power of 5 MW, the source therefore needs to operate at a duty cycle τ/T of 5 MW/125 MW= 1/25, as a direct consequence of our two boundary conditions. If we set the repetition period to 100 ms (10 Hz), the pulse length will be 4 ms. At $T = 50$ ms repetition period ($f = 20$ Hz), the pulse length is 2 ms. The range of τ and T covered in the present study only overlaps partially with the duty cycle $\tau/T = 1/25$. In order to study the instrument performance over the 10-25 Hz frequency range, while maintaining a duty cycle of 1/25, we extrapolate based on the data in Tables IV and V and eq. (6) that the performance of the instrument suite does not depend upon the value of the source frequency.

In general, our results imply that factors other than the flux-related FoM used here should be decisive when determining the time structure for a long-pulse spallation source. For the case of ESS, the time structure has now been locked to $\tau = 2.86$ ms and $f = 14$ Hz, as the best compromise between performance, reliability and cost. The detailed considerations are outside the scope of this article.

B. Further design and optimization of ESS instruments

The instrument design work for ESS is currently taking place in a setting which is very different from when the design work described in the present paper was taking place. A large number of the neutron laboratories and university groups working in neutron scattering in Europe are now engaged in the process of designing instruments for the ESS and the number is still increasing. About 40 different concepts for instruments are currently being optimized, some pursued by researchers in partner countries and some by ESS instrument scientists. A subset of these concepts has been assembled into a reference suite of instruments which is described in the ESS Technical Design Report[33]. The reference suite has been chosen to maximize the scientific impact of the ESS by addressing a broad science case while in each case being fully optimized to benefit from the natural strengths of the long-pulse concept. The choice of instruments to be built at the ESS will take place as a staged process in consultation with the European scientific community and will result in the reference suite gradually evolving into the actual instrument which will be available at the ESS.

ACKNOWLEDGEMENTS

First of all we are strongly indepted to Ch. Vettier for initiating this project and to D. Argyriou for keeping up the urgency of the simulations. We would further like to thank the ESSS SAG, the ESS SAC, and H.M. Rønnow for illuminating discussions.

This project was supported by the Danish, Norwegian, and German contributions to the Design Update phase of the ESS. J.O. Birk was supported by PSI and the Danish Research Council through the graduate school C:O:N:T.

REFERENCES

[1] See the home page for the ESS project: `www.ess-scandinavia.eu`
[2] D. Richter (ed.), *The ESS Project* (Jülich Research Center 2002), Vol I
[3] D. Richter (ed.), *The ESS Project* (Jülich Research Center 2002), Vol IV
[4] See the home page `sim.esss.dk`
[5] K. Lefmann, H. Schober, and F. Mezei, Meas. Sci. Techn., **19**, 034025 (2008)
[6] K. Lefmann, U. Filges, F. Treue, J.J.K. Kirkensgård, B. Plesner, K.S. Hansen, and K.H. Klenø, Nucl. Instr. Meth. A **634**, S1 (2011)
[7] M. Sales, S.L. Holm, K. Lieutenant, and K. Lefmann, J. Phys. Soc. Jpn., **80**, SB018 (2011)
[8] K.H. Klenø and K. Lefmann, J. Phys. Soc. Jpn., **80**, SB004 (2011)
[9] K.H. Klenø, P.K. Willendrup, E. Knudsen, and K. Lefmann, Nucl. Instr. Meth. A **634**, S100 (2011)

[10]K.H. Klenø *et al.*, *Small-angle scattering instruments for a long-pulsed spallation source*, in preparation (2013)
[11]J.O. Birk *et al.*, *An inverse-geometry time-of-flight spectrometer for ESS*, in preparation (2013)
[12]A. Vickery *et al.*, *Comparing thermal spectrometers for a long-pulse spallation source*, in preparation (2013)
[13]R.K. Crawford *et al.*, *Report of the Long-pulse Neutron Instrumentation Workshop, Frascati, August 2009* (2010)
[14]F. Mezei, Journal of Neutron Research **6**, 3 (1997)
[15]G. Zsigmond *et al.*, Appl. Phys. A **74**, S224 (2002)
[16]H. Schober *et al.*, Nucl. Instr. Meth. A **589**, 34 (2008)
[17]K. Lefmann *et al.*, Report from the Ven 2008 meeting (unpublished)
[18]K. Lieutenant and F. Mezei, J. Neutron Res. **14**, 177 (2006)
[19]M. Russina and F. Mezei, Proc. SPIE (Int. Soc. f. Opt. Eng.) **4785**, 24 (2002)
[20]F. Mezei, M. Russina, and S. Schorr, Physica B, **276**, 128 (2000)
[21]M. Russina and F. Mezei, Nucl. Instr. Meth. A **604**, 624 (2009)
[22]M. Nokamura *et al.*, J. Phys. Soc. Jpn. **78**, 093002 (2009)
[23]F. Mezei, *ESS reference moderator characteristics for generic instrument performance evaluation*, (ESS Project, Jülich, December 2000); see also `http://rencurel.essworkshop.org/documents/ess_itg/ESS-moderators.pdf`
[24]K.H. Klenø , K. Lieutenant, K.H. Andersen, and K. Lefmann, Nucl. Instr. Meth. A **696**, 75 (2012)
[25]SwissNeutronics A.G., personal communication (2010); see also `www.swissneutronics.ch`
[26]K.H. Klenø *et al.*, *Effects of non-idealities in long neutron guides*, in preparation (2013)
[27]P. Allenspach, P. Böni, and K. Lefmann, Proceedings of SPIE 4509 (2001)
[28]Mirrotron Ltd., personal communication (2010); see also `www.mirrotron.kfkipark.hu`
[29]M. Bertelsen *et al.*, *Exploring performance of neutron guide systems using pinhole beam extraction*, in preparation (2013)
[30]U. Filges, personal communication (2012)
[31]K. Lefmann and K. Nielsen, Neutron News **10/3**, 20 (1999); see also `www.mcstas.org`
[32]Y. Kiyanagi *et al.*, Proceedings of the ICANS conference, PSI report (2010)
[33]S. Peggs (ed.), *ESS Technical Design Report* (European Spallation Source ESS AB 2013), in preparation

Proc. Int. Workshop Neutron Applications on Strongly Correlated Electron Systems 2011
J. Phys. Soc. Jpn. **80** (2011) SBNASCES11-019

Powder Diffractometers at Long-pulsed Sources

Morten Sales[1,2], Sonja Lindahl Holm[1,2], Klaus Lieutenant[3] and Kim Lefmann[1,2]

[1]*European Spallation Source, St. Algaten 4, 223 50 Lund, Sweden*
[2]*Niels Bohr Institute, Universitetsparken 5, 2100 Copenhagen, Denmark*
[3]*Helmholtz Zentrum Berlin, Hahn-Meitner-Platz 1, 14109 Berlin, Germany*

We have investigated the performance of a cold and a thermal neutron powder diffractometer installed at at long-pulsed source with the use of Monte Carlo ray tracing simulations. We show that the cold powder diffractometer will be a very powerful instrument when a relaxed resolution can be accepted - e.g. for magnetic studies. A comparison between a thermal powder diffractometer with and without Wavelength Frame Multiplication (WFM) show that the WFM technique can be used to achieve shorter instrument length without losing flux. The thermal powder diffractometer will be competitive with the existing high resolution powder diffractometers.

KEYWORDS: Instrumentation, Powder diffractometer, ESS, Wavelength Frame Multiplication, Monte Carlo ray tracing, McStas

1. Introduction

Neutron instrumentation for long-pulsed target stations (LPTS) is a rather new field of study, spawned by the forthcoming construction of the European Spallation Source[1,2] (ESS); the first long-pulsed spallation source ever to be built.

At short-pulsed target stations (SPTS), powder diffractometers have a natural high resolution that is not immediately realised by installing conventional powder diffractometers at a LPTS. However, in order to accommodate a broad user community for ESS, it is highly desirable to include diffraction studies in the ESS design. Hence, to achieve high resolution for powder diffractometers installed at the ESS, it is necessary to cut the pulse by using a pulse shaping chopper.

Earlier studies comparing the performance of a powder diffractometer at a SPTS to its performance if installed at a LPTS has been performed by Lieutenant and Mezei.[3] In their design of the LPTS instrument they used a technique called Wavelength Frame Multiplication (WFM)[4] where the pulse shaping chopper creates several sub-pulses per source period in this way cutting the pulse to get higher resolution, shorter instrument, and larger wavelength band.

The work we here present is an investigation of the performance of two different types of powder diffractometers:

- A Cold Powder Diffractometer (CPD) with low resolution designed to study magnetic structures and phase transitions.[5]
- Two Thermal Powder Diffractometers (TPD) with a high resolution for structural analysis.

The TPD simulation will include an evaluation of the benefits of WFM. The instruments studied are fairly long and have been simulated with an elliptical guide design that excels when long flight paths are needed.[6]

The Monte Carlo simulations and instrument optimisations have been done using the McStas[7] software package.

2. Cold Powder Diffractometer

This prototype high-flux low-resolution diffractometer is meant for magnetic structure determination and phase transition studies, possibly under extreme environments.[5] The wavelength band is fixed around $\lambda_{mean} = 4.5$ Å which means that this instrument should use neutrons coming from a cold (H_2) moderator. The wavelength resolution of this instrument is set to be $\delta\lambda/\lambda = 0.01$ at λ_{mean}. The CPD is a simple instrument using the full pulse length and using choppers only to avoid frame overlap. Due to the instrument length an elliptical guide is used to transport the neutrons from the source to the sample. The guide has m = 6 at the end parts and m = 1 in the middle.[6] The detector is a cylindrical time of flight detector with a radius of 2 m. For the base line setting of the source (period, $T = 60$ ms and pulse length, $\tau = 2.0$ ms) the length of the CPD is $L = 175.7$ m and the wavelength band goes from $\lambda_{min} = 3.85$ Å to $\lambda_{max} = 5.15$ Å.

2.1 Design and Simulations

The layout of the instrument is shown in figure 1.

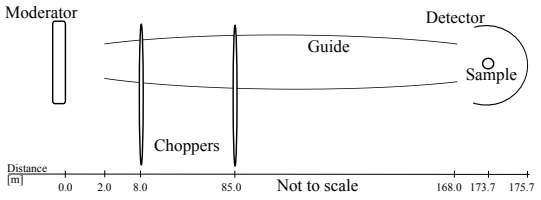

Fig. 1. Layout of the CPD when using the full pulse length of 2 ms. The 175.7 m long instrument with an elliptical guide has two choppers to avoid frame overlap. The sample size is 1×1 cm^2 and the detector is a cylindrical time of flight detector with a radius of 2 m. The length of the CPD varies with the choice of the pulse length. The layout is not to scale.

The length of the instrument at constant wavelength resolution ($\delta\lambda/\lambda = 0.01$ at $\lambda = 4.5$ Å) depends of the pulse length. The length (L) of the instrument depends on the pulse length, as derived from the time-of-flight equation:

$$t = \alpha L \lambda \tag{1}$$

J. Phys. Soc. Jpn. **80** (2011) SBNASCES11-019 **SBNASCES11-019-2**

where $\alpha = 2.528 \cdot 10^{-4} \frac{\text{s}}{\text{mÅ}}$.

$$norm = \frac{n\frac{\tau}{T}}{n_B\frac{\tau_B}{T_B}} \quad (2)$$

The lengths from moderator to detector of the CPD for the four investigated values of τ are shown in table I. The wavelength band will change with both pulse length and period and can be calculated by using:

Table I. Instrument lengths from moderator to detector of the CPD as a function of pulse length and with constant wavelength resolution ($\delta\lambda/\lambda$ = 0.01 at λ = 4.5 Å).

τ [ms]	1.0	1.25	1.5	2.0
L [m]	87.9	109.9	131.9	175.8

$$\lambda_{max} - \lambda_{min} = \frac{T - \tau}{\alpha L} \quad (3)$$

The band widths are shown in table II for 20 different moderator settings studied for the ESS design update.[8)]
The maximum allowed divergence at the sample is set to ±0.45° for the CPD. This is derived with error propagation of the Bragg law:

$$\left(\frac{\delta d}{d}\right)^2 = \left(\frac{\delta\lambda}{\lambda}\right)^2 + \left(\frac{\delta\theta}{\tan\theta}\right)^2 \quad (4)$$

So for $(\delta\lambda/\lambda) \approx (\delta\theta/\tan\theta)$, $\delta\lambda/\lambda = 0.01$ and a scattering angle, 2θ, of 115°, thereby aiming to simulate typical, not best, wavelength resolution, this gives $\delta\theta = 0.9° = \pm 0.45°$. This result should be seen as an approximation, since the correct uncertainties in divergence and wavelength can only be achieved from analysing their distribution functions at the sample.

Table II. Width of wavelength bands [Å] of the CPD for 20 different moderator time structures.

T/τ [ms]	1.0	1.25	1.5	2.0
100	4.46	3.56	2.96	2.21
80	3.56	2.84	2.36	1.76
60	2.66	2.12	1.76	1.31
50	2.21	1.76	1.46	1.08
40	1.76	1.40	1.16	0.86

We used an elliptical guide for neutron transport and chose to terminate the guide 6 m before the sample position because there is no significant intensity loss of neutrons with a divergence below ±0.45°. However, by doing so the background of neutrons with a higher divergence is strongly reduced, since it is the last part of the elliptical guide that is responsible for these neutrons. Only neutrons with a divergence lower than the limit of ±0.45° were included in the flux values given in section 2.2. The shape of the guide is optimised to make neutrons with a divergence below the divergence threshold hit a sample with the size of 1×1 cm^2 coming from a moderator that emits an uniformly distributed flux from a 12×12 cm^2 surface area. The broadest section of the guide in figure 1 is 20×20 cm^2. The wavelength distribution from the moderator is described by the McStas ESS long-pulsed cold source.[9)]

2.2 *Performance*

The CPD has a very good performance at a long-pulsed source. We have investigated the performance of the CPD for a number of time structures for the ESS moderator, assuming that the peak moderator flux is constant.[8)] Here, the instrument length has been adjusted by the value of τ to obtain the same $\delta\lambda/\lambda$ wavelength resolution for all simulations. For the base line time structure of the moderator the neutron flux at the sample (1×1 cm^2) is $5.89(10)\cdot10^8$ neutrons/s/cm^2. For the other moderator time structures investigated, the neutron flux values have been normalised to the base line flux and are displayed in table III.

Table III. Relative flux values for the CPD with constant peak flux, normalised to the moderator base line setting value.

T/τ [ms]	1.0	1.25	1.5	2.0
100	1.2	1.2	1.2	1.0
80	1.2	1.1	1.1	1.0
60	1.2	1.1	1.1	1
50	1.1	1.0	1.0	1.0
40	1.1	1.0	1.0	1.0

2.3 *Effect of moderator hot spot*

It has been shown that grooved moderators with hot spots can be useful for long-pulsed spallation sources,[10)] and so we have studied the point of origin in the CPD of useful neutrons (with a divergence below ±0.45°) that hits the sample. Results are shown in figure 2. It is seen that the CPD would benefit from a neutron hot spot at the center of the moderator surface since most neutrons stem from the central part of the moderator as a consequence of the elliptical guide shape. To quantify this, the uniformly distributed moderator has been replaced by a moderator with the same overall summed flux but a hot spot with a diameter of 3 cm and twice the intensity. For the baseline setting the CPD gains 28 % more flux on the sample by having such a moderator hot spot.

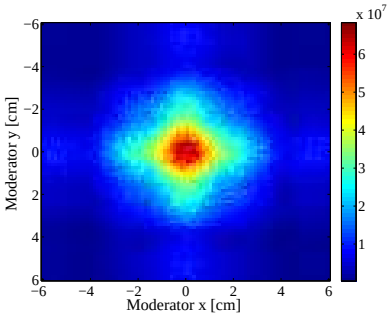

Fig. 2. Colour plot of the moderator surface showing how the useful neutrons (with a divergence below ±0.45°) hitting the sample are distributed for the CPD. This origin plot is made from the simulation of the moderator base line setting. Colour bar is in neutrons/second/pixel.

J. Phys. Soc. Jpn. **80** (2011) SBNASCES11-019 **SBNASCES11-019-3**

3. Thermal Powder Diffractometer

The TPD is a work horse instrument at any neutron facility, used for the study of crystal structure and chemical phases of materials. We chose to investigate such an instrument with a wavelength resolution of $\delta\lambda/\lambda = 0.1$ % and almost 4π detector coverage comparable to GEM at ISIS.[11)]

To obtain this high resolution a diffractometer needs to be adequately long or use a short pulse; e.g. a diffractometer using neutrons with wavelengths around 1.5 Å, 0.1 % wavelength resolution, a pulse length of 2 ms, and filling the whole time frame, will need to be more than 5 kilometres long! So in order to have a reasonable instrument length the pulse needs to be shortened by a pulse shaping chopper.

3.1 *Wavelength Frame Multiplication*

In order to fill the time frame, the instrument length is $L = L_{ps} \cdot T/\tau$, where L_{ps} is the distance from the moderator to the pulse shaping chopper. For the baseline source time structure and the shortest possible value of $L_{ps} = 6$ m the instrument length will be 186 m. A further shortening of the instrument length can be obtained by implementing the WFM[4)] method where several short pulses in combination fill the frame as shown in figure 3.

The main ideas behind the design of the instrument using WFM is taken from an article by K. Lieutenant and F. Mezei.[3)] The fast rotating pulse shaping chopper acts as a new virtual short-pulsed source with shorter pulse length and period. The aim of this investigation is to give an overview of the benefits and disadvantages of using WFM.

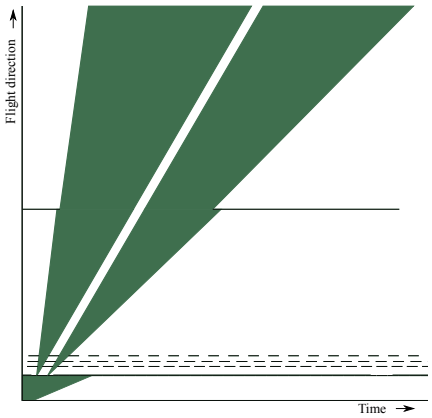

Fig. 3. Time of flight diagram showing the principle Wavelength Frame Multiplication for $n = 2$. The tail of the source pulse has not been included.

3.2 *Design and Simulations*

We have investigated the powder diffractometer both with and without WFM.

The overall layout of the instrument is similar to the CPD and can be seen in figure 4. The 12×12 cm^2 moderator has been simulated with a wavelength distribution described by the McStas ESS long-pulsed thermal source.[9)] The first chopper is the fast rotating pulse shaping chopper that creates several sub-pulses per source period. Its opening time, τ', is calculated to match the required wavelength resolution:

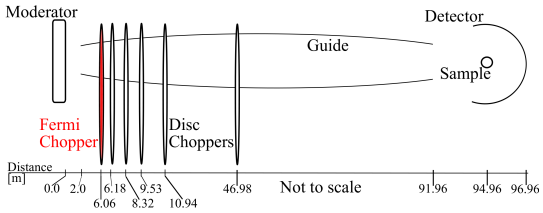

Fig. 4. Layout of the thermal powder diffractometer with WFM. The guide is elliptical with m = 6 at the guide ends and m = 1 in the middle section.[6)] The detector is cylindrical and placed 2 m from the 1×1 cm^2 sample.

$$\tau' = \alpha\left(L - L_{\mathrm{ps}}\right)\lambda\frac{\delta\lambda}{\lambda} \tag{5}$$

λ is the wavelength for which the required wavelength resolution is wanted. This has for the TPD been set to 1.5Å. The maximum allowed divergence on the sample is set to match the wavelength resolution ($\pm 0.045°$ for $\delta\lambda/\lambda = 1 \cdot 10^{-3}$ and $2\theta = 115°$) calculated in the same way as for the CPD (see equation (4)).

Just after the pulse shaping chopper the pulse selecting chopper is situated. This chopper is rotating with the same period as the source, T, and it picks out the required number of pulses, n.

$$\mathrm{n} = \left\lceil \frac{T}{\tau} \cdot \frac{L_{\mathrm{ps}}}{L - L_{\mathrm{ps}}} \right\rceil \tag{6}$$

See table IV for the number of frames used for different combinations of T and τ.

The rest of choppers further defines the pulses, prevents frame overlap between pulses or sub-pulses and eliminates cross talk.[3)] Figure 4 depicts an instrument using WFM and having a length of $L_{\mathrm{Total}} = 96.96$ m. To obtain the same wavelength resolution without WFM the length would have been: $L_{\mathrm{no\ WFM}} = (L - L_{\mathrm{ps}}) \cdot \mathrm{n}$. The wavelength bandwidth for the TPD using WFM is given by $T/(\alpha \cdot (L - L_{\mathrm{ps}}))$ and is presented in table V.

Table IV. Number of sub pulses per original pulse, n, using WFM and keeping the instrument length at 96.96 m.

T/τ [ms]	1.0	1.25	1.5	2.0
100	7	6	5	4
80	6	5	4	3
60	4	4	3	2
50	4	3	3	2
40	3	3	2	2

Table V. Width of wavelength band with $L_{\mathrm{Total}} = 96.96$ m and using WFM

T [ms]	100	80	60	50	40
Wavelength bandwidth [Å]	4.40	3.52	2.64	2.20	1.76

J. Phys. Soc. Jpn. **80** (2011) SBNASCES11-019 **SBNASCES11-019-4**

3.3 Performance

For the baseline setting the flux at the sample position is found to be $3.25(4) \cdot 10^5$ neutrons/second/cm^2 for $\delta\lambda/\lambda = 1 \cdot 10^{-3}$ and using WFM. Without the use of WFM for the same wavelength resolution and source time structure, the flux at the sample is higher: $5.137(18) \cdot 10^5$ neutrons/second/cm^2. Without WFM the bandwidth is halved and the higher flux is caused by a narrower wavelength band with more intense wavelengths being selected. For an instrument without WFM at the baseline time structure to have the same wavelength band as the instrument with WFM, it needs to be run with two different time delays of the choppers. In this case the average flux at the sample position is $3.256(9) \cdot 10^5$ neutrons/second/cm^2. So if the wavelength band is unimportant, using WFM will give a loss of 37 % of the useful neutrons. However, comparing instruments with the same wavelength band the instrument length is halved and the flux is the same when using WFM. The downside is that more choppers are needed to use WFM and that data analysis may become more difficult.

Figure 5 shows the flux at the sample for the baseline setting with WFM for different wavelength resolutions. It can be seen that a significant gain in intensity at the sample can be achieved by relaxing the resolution. Comparing to the GEM[11,12] instrument at ISIS that for a resolution of $\delta d/d$ of $\sim 4 \cdot 10^{-3}$ at 115° scattering angle has a flux of $\sim 2 \cdot 10^6$ neutrons/second/cm^2 our simulations show a powerful instrument with around four times the flux.

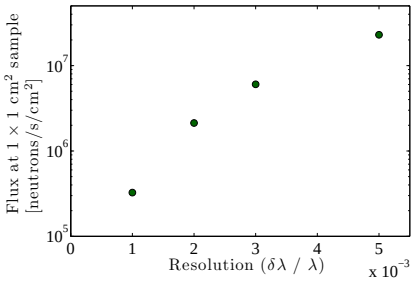

Fig. 5. Flux at sample position for the thermal powder diffractometer with WFM and $T = 60$ ms, $\tau = 2$ ms. Simulations are performed for different wavelength resolutions with matching divergence limitations (at $2\theta = 115°$) on the sample.

Table VI shows the relative flux at the sample position simulated for different combination of T and τ.

Table VI. Flux at sample position (1×1 cm^2) for the TPD with WFM for constant peak flux and normalised by the $T = 60$ ms and $\tau = 2$ ms result. $\delta\lambda/\lambda = 1 \cdot 10^{-3}$ and maximum divergence at the sample is ±0.045°.

T/τ [ms]	1.0	1.25	1.5	2.0
100	0.38	0.45	0.51	0.61
80	0.48	0.57	0.63	0.79
60	0.63	0.74	0.83	1.00
50	0.74	0.86	0.96	1.10
40	0.89	1.02	1.09	1.18

3.4 Effect of moderator hot spot

As with the CPD we have studied the effect of having a moderator hot spot. Figure 6 shows from what part of the moderator surface the useful neutrons originate. It is seen that almost all the neutrons originate from the central 3×3 cm^2 of the moderator. So by having a moderator hot spot with a diameter of 3 cm and twice the intensity (but still keeping the same overall intensity) the flux at the sample position is found to rise by 93 % in the case of $T = 60$ ms, $\tau = 2$ ms and using WFM. Simulations of the longer instrument without WFM show that it will gain 100 % in flux at the sample from having a moderator hot spot.

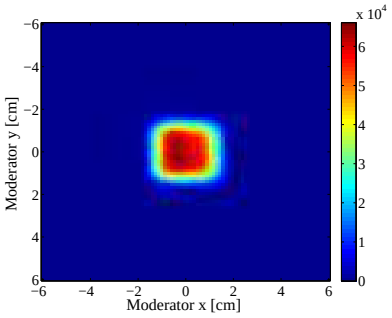

Fig. 6. Origin plot for the TPD with WFM, $T = 60$ ms, $\tau = 2$ ms and $\frac{\delta\lambda}{\lambda} = 10^{-3}$. Colour bar is in neutrons/second/pixel.

4. Conclusion

Our simulations show that it is feasible to install powder diffractometers at a long-pulsed source like the ESS.

The cold powder diffractometer with relaxed resolution is a very potent instrument with a tremendous flux and is due to utilise the full pulse.

A high resolution thermal powder diffractometer can use wavelength frame multiplication to shorten the instrument length, without losing flux at the sample. If only a narrow wavelength band is needed, however, an instrument without WFM has the highest flux at the sample position.

For both the cold and the thermal powder diffractometers there is a significant gain by having a moderator with a 3 cm diameter, factor 2 hot spot. Our simulations show that this can increase the flux at the sample position significantly up to a full factor 2.

1) H. Schober et al. Nuclear Instruments and Methods in Physics Research A 589 (2008) 34-46. 2008.
2) F. Mezei. J. Neutron Research, Vol. 6, pp. 332. 1997.
3) K. Lieutenant and F. Mezei. *Journal of Neutron Research*, 14(2):177–191, June 2006.
4) M. Russina and F. Mezei, Proc. SPIE (Int. Soc. f. Opt. Eng.) 4785 24 (2002).
5) The ESS design report, Vol III, Jülich 2002.
6) K.H. Klenø et al, in preparation (2011).
7) P.K. Willendrup, E. Farhi, K. Lefmann, Physica B 350, e735 (2004).
8) K. Lefmann et al. to be submitted (2011).
9) The McStas library. http://www.mcstas.org/.
10) Y. Ogawa et al. J. Neutron Research, Vol. 6, pp. 197-204.
11) W.G. Williams et al. Physica B 241 243 (1998) 234 236.
12) A.W. Hewat. Physica B 385-386 (2006) 979-984.

1

Abstract

We show that it is possible to feed several cold neutron instruments from the same beam port at a neutron facility by elliptical guides without compromising the neutron flux notably on any of the sample positions. This can be achieved by using the new guide-split concept presented here. Since elliptical guides are capable of transporting an almost completely filled phase space within a large divergence ($\pm 2^\circ$), for cold neutrons, we use the end of a primary guide as a virtual source point. It is therefore possible to place several secondary guides side by side going in slightly different directions, and hence exploit different parts of the transported phase space. In addition the kink between the primary and secondary guide eliminates line of sight. By ray-tracing simulations of three different set-ups (with two, four, and eight secondary guides) we have shown that it is possible to illuminate eight sample positions from one beam port with a brilliance transfer above 90% on each sample, with a sample size of 1×1 cm^2, a maximum divergence of $\pm 0.5^\circ$, and a wavelength band from 4.25 Å to 5.75 Å, on a 150 m long instrument. We show two examples of using this concepts for instruments proposed for the European Spallation Source.

IUCr macros version 2.1.6: 2013/03/28

2

Neutron guide-split: A high performance guide bundle concept for elliptical guides

[1]Nano-science Center, Niels Bohr Institute, University of Copenhagen, Denmark

Sonja Holm[1,2], Nina Rasmussen[1,2], Louise Høpfner[1,2], Jörg Voigt[3], Ken Andersen[4], Kim Lefmann[1,2]

[2]*ESS Design update program, Denmark,* [3]*Jülich Centre for Neutron Science JCNS, 52425 Jülich, Germany, and* [4]*European Spallation Source ESS AB,22100 Lund, Sweden*

1. Introduction

With the construction of the European Spallation Source (ESS) (web page, 2013), the field of neutron scattering is on the verge of entering a new era. As the world's first long-pulsed source, ESS offers a great number of new possibilities. Nevertheless, a natural limit for the number of instruments exists due to the geometry of the source. A limit that might prevent the realization of new advanced instrument ideas. However it is possible to increase the ESS instrument capacity with a new guide system design described in this article.

The design of neutron guides has gone through many transformations since the first straight guides of the sixties (Christ & Springer, 1962; Maier-Leibnitz & Springer, 1963). The realization that a removal of the sample from the line of sight leads to a significant reduction of the background noise from fast neutrons and gamma radiation, made a slightly curved version of the straight guide the standard of contemporary guide design (Christ & Springer, 1962; Maier-Leibnitz & Springer, 1963). With the addition

of the supermirror coating in the seventies (Mezei, 1976; Mezei & Dagleish, 1977), another vital step in the improvement of neutron guides was taken. In the recent years ballistic guides with straight tapering (Mezei, 1997; H. Abele *et al.*, 2006), parabolic tapering (C. Schanzer *et al.*, 2004) and full elliptical (Boeni, 2008; Rodriguez *et al.*, 2011; *et al.*, 2012) geometries have all been investigated with the aim of reducing transport losses in guide systems.

We present the idea to implement split elliptical guides, where a shared primary guide feeds a number of secondary guides with each of the instruments out of line-of-sight from source, and show a few examples of instruments that can benefit fully from the split guide concept. This idea facilitates an increase in the instrument capacity of a neutron source by allowing several instruments to use the same beam port without compromising the instrument performance of the individual instruments.

2. The concept of split elliptical guides

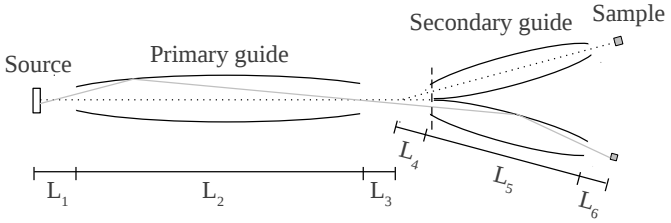

Fig. 1. Layout of the guide split set-up with two secondary guides. The dotted line represents the primary axis through one instrument. The gray line is an example of a neutron path through the guide system. The dashed line marks the junction of the secondary guides. The cross section of the junction area is shown in figure 3. L_i represents the naming of the lengths in the set-ups.

The basic feature in our guide system is the occurrence of two elliptical guides in series, where the second guide is slightly rotated around a point near to their closely spaced focal points. In turn, this rotation enables the possibility of placing several secondary guides after the primary guide. An illustration of this arrangement is shown

in figure 1.

The concept of having several instruments on the same beam port is well known from straight or curved guides of constant cross section. These *guide bundles* are *e.g.* found at ILL (*et al.*, 2011).

Each of the sibling instruments on the secondary guides exploits different parts of the phase space transported by the primary guide, and thus retains a high brilliance transfer ($\sim$ 90%) for each sibling instrument. The brilliance transfer is defined as the transmission of the four dimensional (2D position, 2D divergence) phase space through the guide system to the samples (P. Bentley *et al.*, 2013) within a certain wavelength band. According to the Liouville theorem this transfer cannot exceed unity (Klenø, 2013).

This new idea can be realized in numerous variations with many different shapes of the primary and secondary guides in different combinations, *e.g.* elliptic, parabolic or ballistic with different taperings. However, we here explain only the double ellipse case.

3. Set-up and simulations

We have investigated three guide split set-ups where the guide junction supports two, four, or eight secondary guides each with a total length of 150 m. The cross section of the guide junctions are illustrated in figure 3. In this study the primary guides are chosen to be elliptical and 98 m long and the secondary guide lengths were optimized. Other guide length ratios are also feasible (*e.g.* 75 m primary guide).

5

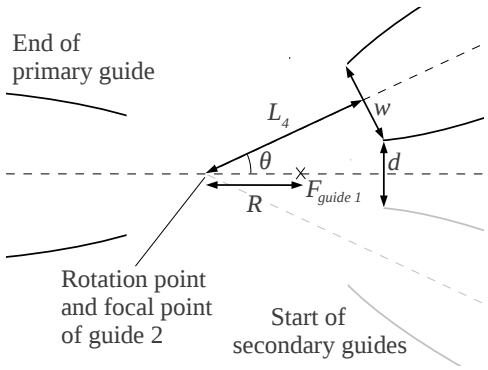

Fig. 2. Top view of the guide junction of the two-split set-up. θ is the rotation angle of the secondary guide, R is the rotation displacement length, F_{guide1} is the focal point of the primary guide, L_4 is the length from the rotation point to the secondary guide entrance, w is the with of the secondary guide entrance, and d is the distance between the secondary guides. The focal point of the primary guide and the rotation point is not necessarily the same (for detailed information see table 1).

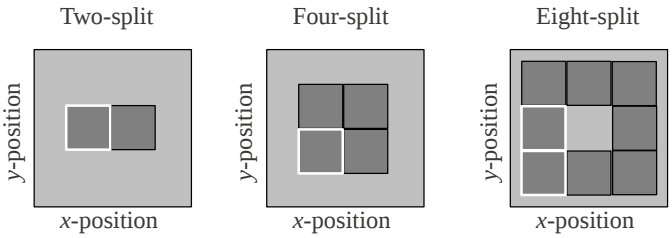

Fig. 3. Sketch of the cross sections of the secondary guide junction for the two-, four- and eight-split variations of the set-up. The position of this cross section is marked as L_4 in figure 1. The guide positions marked with white outlines are simulated and the results presented in this article. The two positions in the eight split option are referred to as the side and the corner positions.

The guide parameters of the set-up are restricted by the requirement that the secondary guides can not overlap. An illustration used in the geometrical considerations of a two-split set-up is shown in figure 2.

The relation between the distance from the focal point to the start of the secondary guides (L_4 shown in figure 1) and the rotation angle (θ) of the secondary guides is

$$\theta = \operatorname{atan}\left(\frac{w}{2L_4}\right) + \operatorname{asin}\left(\frac{d}{2\sqrt{\frac{1}{4}w^2 + L_4^2}}\right) \approx \frac{w+d}{2L_4} \tag{1}$$

where w is the width and height of the secondary guides and d is the distance between the secondary guides at their starting points.

For the two- and four-split set-up we have chosen to let the secondary guide openings be joined at the primary axis (ignoring the substrate thickness, we use $d = 0$, see figure 3) and in the eight-split option we fix $d = w$ in order to reduce the number of free parameters. Another parameter reduction was done by locking the focal point of the second ellipses to the rotation point (see figure 2). The rotation angles are small ($\sim 0.4^\circ$, for detailed information see table 1) in all three test cases. Due to the symmetric nature of the set-up we present only selected simulated data: the guide rotated to the left in the two-split version, the lower left corner of the four-split, and the middle and lower left guides in the eight-split set-up as highlighted in figure 3. The effect of gravity, which breaks the symmetry in the vertical dimension is minor and will not be discussed here. No guide is placed in the middle of the eight-split variation, due to the line-of-sight considerations. It is most likely, however, that a curved guide will perform adequately in this position.

The optimizations were performed using the Monte Carlo ray-tracing package McStas v. 1.12 (Lefmann & Nielsen, 1999) and run at the computer cluster of the ESS Data Management and Software Center cluster (DMSC web page, 2013). The optimized phase space was chosen to have a divergence within $\pm 0.5^\circ$ a cold wavelength band (4.25-5.75 Å) and a sample size of $1{\times}1$ cm^2. For the two- and four-split option, and in the two eight-split cases, the same guide parameters were chosen. The elliptical guide component used in the simulation, has a perfect elliptical shape in the x- and y-direction and a quadratic cross section (M. Bertelsen *et al.*, 2013). For simplicity the m-value is set to be $m = 6$ for all guides. When doing a specific case study of an instrument, coating should be cost optimized (M. Bertelsen *et al.*, 2013). The moderator used has a surface of 12×12 cm^2. The wavelength distribution is described by

the McStas ESS long-pulsed cold source from 2000 (Mezei, 2000).

During the optimization we found that the parameter space (lengths, focal points, angles) have several plateaus with high brilliance transfer (>90%) and hence we chose the final parameters such that we get a smooth divergence distribution at the sample position. The hereby obtained parameters of the guides are listed in table 1.

Layout option	**Two- and Four-split**	**Eight-split**
Parameters of the primary guide		
L_1, distance from moderator to guide entrance	2.0 m	2.0 m
L_2, length of the primary guide	92.0 m	96.0 m
L_3, distance from exit to rotation point	0.897 m	2.780 m
Width and height at guide entrance	0.105 m	0.105 m
Entrance focal length	2.5 m	1.3 m
Exit focal length	1.7 m	3.0 m
Parameters of the secondary guide		
R, rotation point displacement	-0.8 m	-0.2 m
θ, angular rotation of secondary guides	0.39 °	0.41 °
L_4, distance from rotation point to entrance	2.7 m	4.9 m
L_5, length of the secondary guide	51.3 m	46.1 m
L_6, distance from guide exit to sample	1.4 m	1.0 m
Width and height at guide entrance	0.037 m	0.035 m
Entrance focal length	2.7 m	5.3 m
Exit focal length	2.33 m	2.89 m

Table 1. *The optimized parameters for the different variations of the set-up. The parameters for the two- and four-split variations are identical, whereas the parameters for the eight-split differ. See figure 1 for a graphical explanation of the lengths.*

4. Results

Our main result is the wavelength dependence of the brilliance transfer for the four optimized guide systems. These data are shown in figure 4. It is clear that the guide-split concept shows excellent performance for cold neutrons ($\lambda > 3$Å). The brilliance transfers obtained in the optimizations are 94% for the two-split, 93% for the four-split, and 89%, 90% for the two eight-split options, respectively. At $\lambda = 1.47$Å the brilliance transfer is 62% for the two-split, 58% for the four-split, and 48%, 47% for the two eight-split options.

8

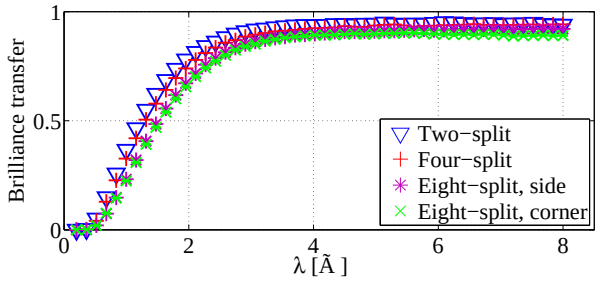

Fig. 4. The brilliance transfer to the sample position for the one of the two-, four-, or eight-split options as a function of wavelength. Wavelength scans performed using iFit (E. Farhi *et al.*, 2013).

It is desirable to have a homogeneously filled four dimensional phase space at the sample position within the optimized wavelength band. We show the brilliance transfer as a function of each of the four parameters in figure 5. We assume that the horizontal position and vertical divergence are uncorrelated and vice versa and hence display the four other correlations in figure 6. The results are simulated for neutrons within the wavelength interval for which the set-ups have been optimized (4.25-5.75 Å).

The optimizations obtain a flat divergence distribution in the desired divergence range ($\pm 0.5°$) in all four test cases (see figure 5). In the eight-split cases there are small features (40%) on the sides of the central peak, at $\pm 0.9°$. This can also be seen in figure 6. These features can be removed by smaller collimators, pinhole collimation, or distance collimation.

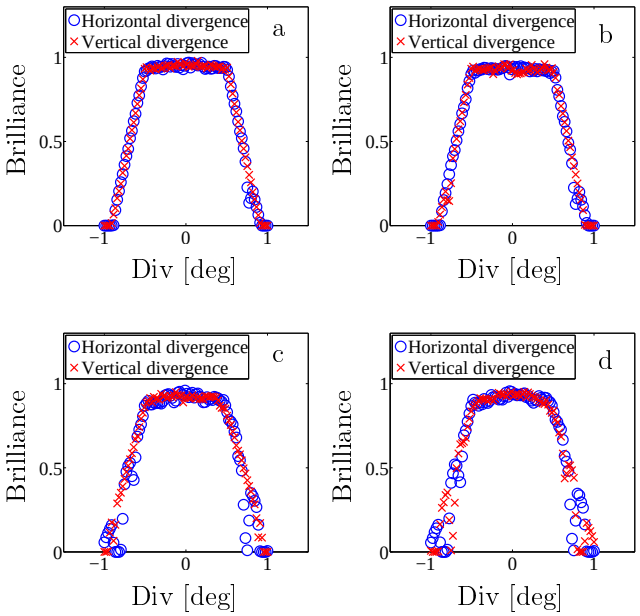

Fig. 5. Horizontal and vertical divergence distributions summed from -0.5° to 0.5° perpendicular to the displayed direction at the sample position for neutrons with wavelengths within 4.25-5.75 Å. **a:** Two split. **b:** Four-split. **c:** Eight-split side. **d:** Eight-split corner.

10

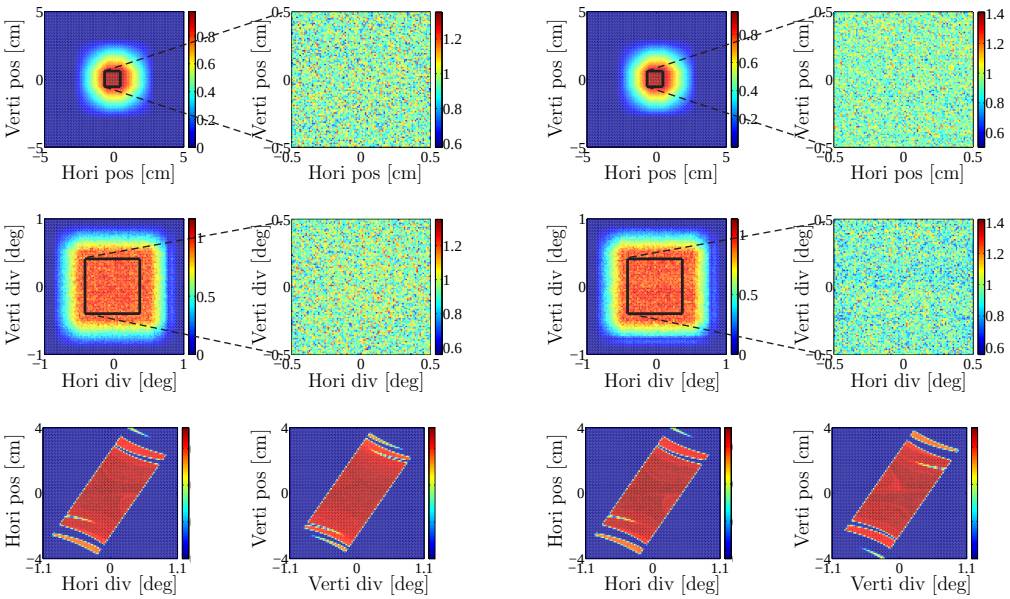

Two-split option

Four-split option

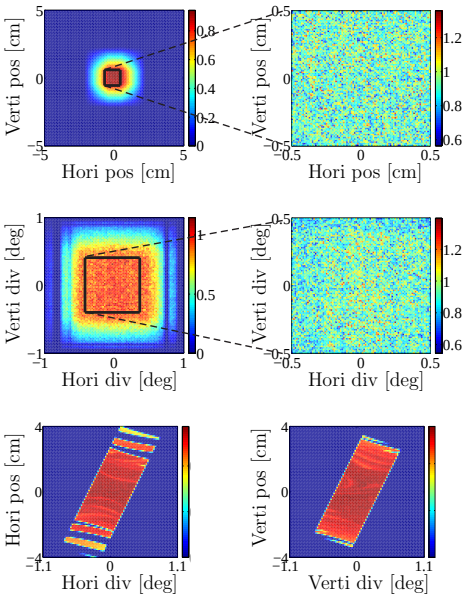

Eight-split side option

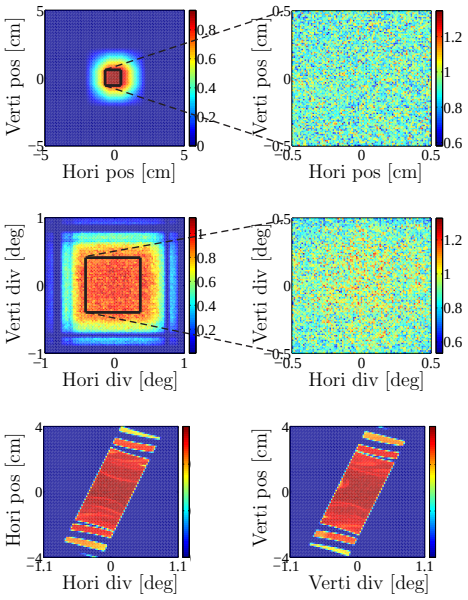

Eight-split corner option

Fig. 6. Outputs from the position, divergence, and acceptance monitors at the sample position for the four different set-ups. The position monitor accepts all incoming divergences and the divergence monitors are 1×1 cm^2 in size. Their color scales represents the brilliance transfer value.

In figure 6, we show the performance of the guide-split set-ups with regard to sample illumination, divergence distribution, and their correlations. In all four test cases we show the same four correlations. The two zoom-ins on the right side display the neutrons within our phase space restrictions only. On the left side we show how the illumination and divergence distribution looks outside the boundaries. The two bottom plots show the horizontal and vertical position *vs.* divergence correlations, also known as *acceptance diagrams*. We observe that for all four guide set-ups and all correlations monitored, the neutron phase space is quite uniformly filled within the set requirements.

5. Performance of guide split systems

As seen from our data, the idea of guide splitting is certainly fruitful for the case of two- and four-split elliptical guides. We judge this on the brilliance transfer values over a large wavelength range, even down to 2 Å. In addition, for the chosen sample size of 1×1 cm^2, the illumination is very smooth both in divergence, position and the correlation of the two. The same is true for the eight-split option, although the brilliance transfer is slightly smaller, in particular towards the shorter wavelengths.

We observe a slightly larger brilliance transfer of the two-split variation. This is to be expected, due to the two-split secondary guides being more favorably placed in the divergence space. It can be argued that the four split - or even eight-split - options are a better choice due to the increased amount of instruments and utilized neutrons. Neither of the variations provides as high a brilliance transfer as a single elliptical guide, although the transmission in excess of 90% for $\lambda > 3$ Å must still be seen as a most satisfactory result. In addition, all variations provides a superior total utilization of the generated neutrons, when the increase in instrument number is considered.

We have tested that the guide split concept also works for straight (and curved)

secondary guides, although with slightly lower brilliance transfer of $\tilde{8}0\%$ (data not shown). The discrepancy is mostly caused by the lower effective divergence from the straight guide type.

In contrast, the elliptical secondary guides have no problem in transporting $\pm 0.5^\circ$ divergence, and can even accommodate slightly higher divergences, even for the present optimization. We did not attempt to perform an optimization for higher total divergence, but from the present data we believe that good transmission of divergences up to around $\pm 1^\circ$ should be possible for neutrons of wavelengths of 3 Å and above.

6. Applications of guide-split at instruments

The guide-split set-up facilitates an increased number of instruments at a neutron source. This could be used to build beam-lines that would not always be allowed a dedicated beam port, for example;

- Laue stations for crystal alignment.
- In-house test beam-lines for optics and other beam components.
- Dedicated student beam lines for educational purposes.

More significantly however, we believe that the guide split concept enables several user instruments to share the same beam port at a time-of-flight neutron source, despite the fact that the instruments would need to agree on the use of wavelength band (bandwidth choppers are placed in the common first part of the guide). Another complication is that a possible pulse shaping chopper, relevant at a long-pulsed source like ESS, must in some cases be shared between the instruments. However, we believe that these bindings will not overshadow the advantage of increasing the total number of instruments.

As an example, we present a number of state-of-the art 150 m long cold-neutron instruments for ESS that could be positioned on a split guide simultaneously, using a

wavelength band of around $4-6$ Å (although wavelengths down to around 2.5 Å can be used with the present guide system on a cold source).

A similar list could be made for bispectral instruments (working wavelength range $1.5-3.5$ Å), including macromolecular Laue diffraction. It was recently shown that bispectral extraction feeds well into elliptical guides (Jacobsen *et al.*, 2013; Zendler *et al.*, 2012). However thermal neutrons (wavelengths below 1.5 Å) do not seem to be well transported by the split guides, although we can not exclude that future developments will enable this.

6.1. Monochromator instruments

The monochromator instruments utilize the time-integrated flux of the ESS source, and the usefulness of the split guide for these instruments depend only on the brilliance transfer - which is excellent - and on the amount of divergence transported - which is sufficient for most monochromator instruments.

Placing a monochromator instrument at the end of a focused guide requires some care, as the monochromator should not be positioned in the focal point. Rather this point will act as a virtual source point, and a doubly focusing monochromator should be placed a few meters behind this point. This is simulated and discussed in Ref. (K. Lefmann *et al.*, 2011).

6.2. Inverse-geometry crystal analyzer spectrometer

Simulations of an inverse geometry instrument for ESS with a triple-axis-like back-end will be presented elsewhere (J.O. Birk *et al.*, 2013), but in general this instrument type is well matched to the wavelength and divergence ranges, and to the limited beam spot size that the guide-split system will provide.

6.3. Magnetism diffractometer

We here present a simple version of the magnetism diffractometer described in the Technical Design Report for the ESS (ESS, 2013) but placed on a cold, rather that a bispectral source.

The maximal width of the wavelength band of the instrument when using every source pulse is given by $\Delta\lambda = T/(\alpha L) = 1.88$ Å, where $T = 71.4$ ms is the time between pulses, $\alpha = 253\,\mu$s/m/Å, and $L = 150$ m as before. However, to avoid frame overlap, a slightly smaller band is used in practice; we take $\Delta\lambda = 1.80$ Å. In order to cover a larger q-range with the instrument the wavelength band can be shifted by phasing the band choppers. With three wavelength intervals one can cover from 2.1 Å to 6.9 Å, which correspond to a q-range from 1.29 1/Å to 5.98 1/Å, (when using the scattering angles (2θ) between 90° and 180°). In figure 7 the flux on the sample is shown for three different wavelength bands.

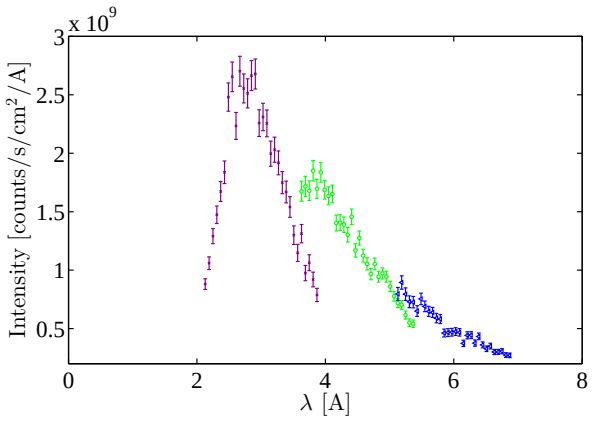

Fig. 7. Simulated wavelength spectrum at the 1×1 cm^2 sample position for the magnetism diffractometer, running in the wavelength bands 2.1 – 3.9 Å, 3.6 – 5.4 Å, and 5.1 – 6.9 Å.

In the simulations of this simple instrument we use the 4-split guide system placed on the ESS cold moderator description from 2012 (defined in McStas 2.0 (P.K. Willendrup *et al.*, 2013)). We use a cylindrical detector of radius 1 m and height 10 cm, with

10×10 mm^2 pixel resolution, which would give a secondary resolution contribution to $\delta d/d$ of 1.0% (S.L. Holm *et al.*, 2013). The wavelength resolution of the instrument when using the full pulse, $\tau = 2.86$ ms, is $\delta\lambda/\lambda = \tau/(\alpha L\lambda) = 1.6\%$ for $\lambda = 4.5$ Å. A better resolution would require a shorter pulse. For example, for 1.0% resolution, we would require a 1.7 ms pulse width. A shorter pulse width can be obtained with the use of a pulse shaping chopper approximately 6 m from the source, which still would allow the full 1.8 Å wavelength band to hit the sample. We perform the simulation in the simple case without the pulse shaping chopper, somewhat similar to what was presented in Ref. (Sales *et al.*, 2011). The total flux on the sample is an impressive $1.5 \cdot 10^9$ n/sec/cm^2 in the wavelength band 2.1 Å -3.9 Å (see figure 7).

To simulate a full experiment, we use a standard NaCaAlF powder sample (Lefmann & Nielsen, 1999) in a cylinder of 10 mm height and 10 mm diameter. The detector output is shown in figure 8 as a $(2\theta, t)$ diagram (raw data output) and a $(2\theta, q)$ diagram (data ready to be refined) in figure 9. In figure 10 we show the same data collapsed along 2θ onto q.

The peak shapes have the expected width 0.06 Å^{-1} at $q = 3$ Å and are seen to have a slight asymmetry at low q, which originates from the pulse shape. The neutron count rate is $5 \cdot 10^6$ s^{-1} for the full spectrum, allowing collection of data with reasonable statistics from just one source pulse.

16

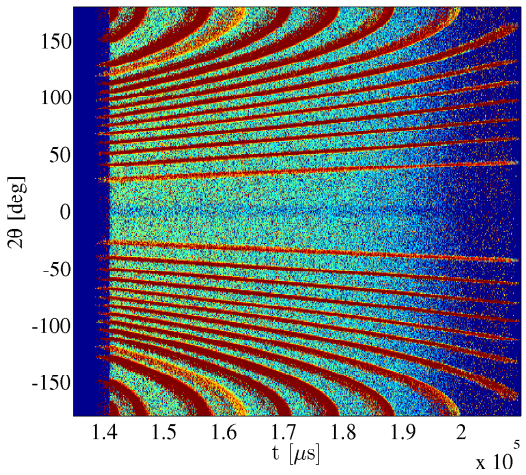

Fig. 8. Raw simulated data $(2\theta, t)$, from a run in the wavelength band $3.2 - 5.0$ Åwith a NaCaAlF sample (10 mm height cylinder width 10 mm diameter).

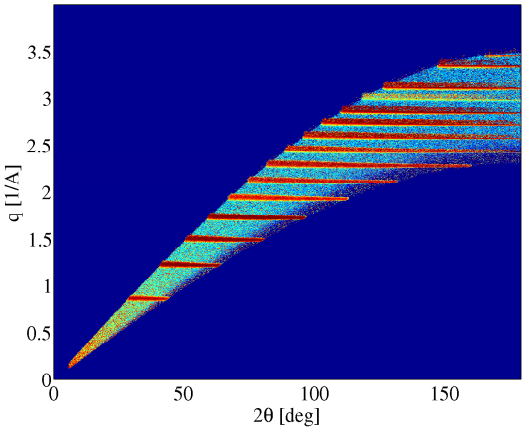

Fig. 9. Transformed data $(2\theta, q)$, from a run in the wavelength band $3.2 - 5.0$ Åwith a NaCaAlF sample (10 mm height cylinder width 10 mm diameter). It is the same data as in figure 8 but displayed in a more useful representation.

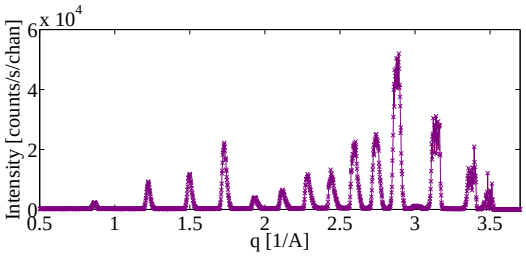

Fig. 10. Simulated one dimensional data, from a run in the wavelength band 3.2 – 5.0 Åwith a NaCaAlF sample (10 mm height cylinder width 10 mm diameter).

6.4. Cold-neutron chopper spectrometer

We here present a simple version of a cold chopper spectrometer, optimized for a split guide system at a long-pulsed source with the ESS time structure.

The instrument has a counter-rotating pulse-shaping chopper pair just after the guide split position and a monochromating pair of counter-rotating choppers at the end of the second guide. This combination of choppers allows for multiple monochromatic beams on the sample, with slightly different wavelength, during one single pulse frame. This scheme is known as *repetition rate multiplication*, or RRM (Mezei & Russina, 2002). In our design, the monochromating pulses stem from subsequent bursts of the pulse shaping choppers; a feature that is reminiscent of the wavelength-frame multiplication (WFM) scheme (M. Russina and F. Mezei, 2002).

The combination of WFM and RRM is illustrated in a time-distance-diagram, fig. 11. As illustrated by the dashed line in this diagram, the neutrons that may provide "cross-talk" between the designated time-distance channels of this scheme cannot originate from the main source pulse. This is explained by the pulse-shaping chopper being situated far from the moderator. Thus, we can sen that the chopper pair uniquely selects the wavelength of the incoming neutrons, without use of additional choppers as on same WFM schemes. The use of this chopper combination for a time-of-flight spectrometer was first suggested for the IN500 project at LANSCE (F.

Mezei and M. Russina, 2001) and is further discussed in ref. (*et al.*, 2013).

In our set-up, there is a need for choppers to avoid frame-overlap by slow neutrons from previous moderator pulses. This task can be carried out rather simply by frame defining choppers in the first part of the guide. In fig. 11, this happens at a distance of 10 m. This scheme leaves room only for very long wavelength neutrons, as also sketched in the figure. These slow neutrons can be removed by one additional chopper, to be placed after the frame defining chopper or by seperating the two frame defining choppers by a fraction of a meter. In the simulations of the present instrument, we have not taken long-wavelength frame overlap into account.

In our set-up, the monochromating choppers have a radius of $R_{\rm c} = 0.35$ m with an opening angle of 3.5°, spinning at 98 Hz or 196 Hz. For the former option, we use two openings in the disks to obtain in both cases a 5 ms time interval between bursts. These chopper settings give opening times of 20.7 μs (10.2 μs) simulated RMS, corresponding to 48.7 μs (24.0 μs) FWHM.

The monochromating choppers are placed $L_{\rm cs} = 1.0$ m before the sample, which has an area of 1×1 cm^2, while the sample-detector distance is $L_{\rm sd}$ =4 m.

The pulse-shaping choppers run at 154 Hz (308 Hz) and have an opening of 60°, giving an opening time of 264μs (133μs) simulated RMS, corresponding to 624 μs (313 μs) FWHM.

The ratio of the two opening times (a factor 11) equals the ratio of the primary and secondary flightpaths plus one, which in turn makes the primary and secondary wavelength resolutions match (*et al.*, 2013; Lefmann *et al.*, 2008).

Apart from the position of the pulse-shaping chopper, the instrument is quite similar to the cold chopper spectrometer foreseen for ESS (ESS, 2013), and also rather similar to other suggestions for ESS long-pulsed chopper spectrometers, simulated earlier (*et al.*, 2013; Lefmann *et al.*, 2008).

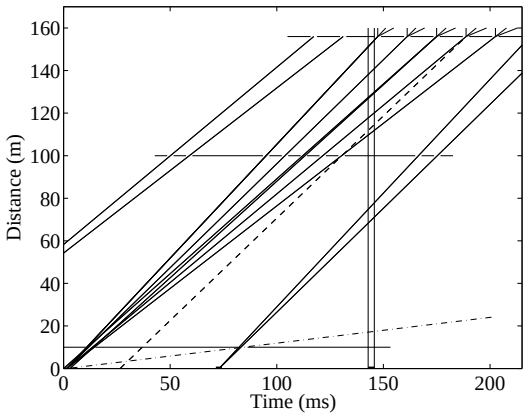

Fig. 11. Time-distance diagram for the cold neutron chopper spectrometer. The multiple openings of the monochromating chopper just before the sample is typical of the RRM scheme, while the multiple beams from the pulse-shaping chopper is typical of the WFM scheme, as explained in the text. We show the wavelength band of 3.55 Å to 5.3 Å, with 5 monochromatic pulses in this range. Part of the preceding and following source pulses are shown. The dashed line represents a theoretical path a neutron would take to perform "cross-talk" between different chopper channels. However, this line does not originate at the source pulse and is hence irrelevant. The dashed-dotted line shows a possible path for slow-neutron frame overlap, which survives the single frame-overlap chopper at 10 m. The vertical lines at 145 ms represent one fast-neutron prompt pulse from the moderator.

We have simulated this instrument by creating a simple model in McStas, which adds the pulse shaping and monochromating chopper pairs to the guide system. In addition, we have placed a sample and a detector after the guide system to carry out simple virtual experiments.

Figure 12 shows the wavelength distribution on the sample for the low-resolution setting. Th typical multiple-peak structure of the RRM scheme is seen.

Figure 13 shows an energy resolution scan on a 10 mm tall, 10 mm diameter vanadium sample, taken with only the 5 Å peak, using both settings described earlier. Unlike in our previous study, the line shape is here seen to be free from skew tails and is almost Gaussian. The absence of tails is an effect of the pulse-shaping chopper. The width of the elastic line in this setting is 43.9 μeV (23.2 μeV) RMS, corresponding

to 103 μeV (55 μeV) FWHM, which is rather similar to the 120 μeV (FWHM) in the previous simulations (Lefmann *et al.*, 2008). The flux at the sample position for a single wavelength pulse of 5 Å is found to $9.4(2)(2.6(2)) \cdot 10^5$ n/s/cm^2. This should be compared to our earlier findings (Lefmann *et al.*, 2008), where a similar spectrometer at a straight guide was found to have a 5 Å flux at the sample position some 15 times higher: $1.39 \cdot 10^7$ n/s/cm^2. To explain this large flux difference, we first notice the 20% increase in resolution width in the old data, which corresponds to a factor 1.4 increase in flux. Secondly, in the present work, the divergence has a FWHM of 1° in both directions, whereas the earlier spectrometer had a value of the order 4° in each direction. This would explain the remaining factor of 10 in flux.

A more realistic approach for a spectrometer would be to allow a larger divergence. With a two-split guide, a larger vertical divergence should pose no problems, while a larger horizontal divergence seem possible, but still needs more optimization (K. Klenø*et al.*, 2013).

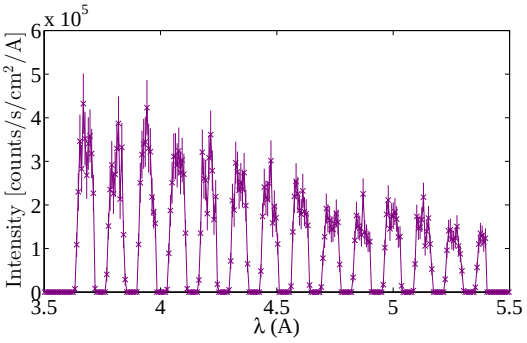

Fig. 12. Simulated flux at the sample from the cold-neutron chopper spectrometer, running at a wavelength band of 3.5 Å -5.3 Å

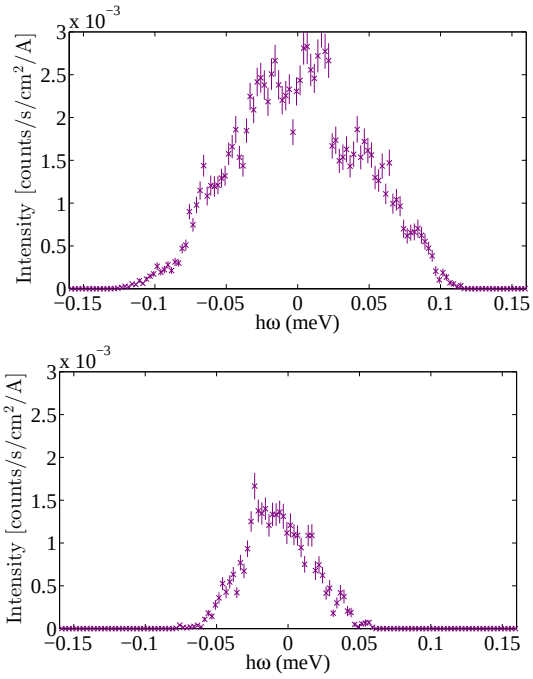

Fig. 13. Simulated vanadium data from the 5 Å pulse only, and with the resolution choppers running at 98(196) Hz. Left frame shows data from the low resolution mode while the right frame shows data from the high resolution mode.

7. Conclusions

In this paper, we have shown by simulations that it is feasible to split neutron guides by using a virtual source point from a primary elliptical guide. In particular, we have demonstrated this concept for cold neutrons with a divergence below $\pm 0.5^\circ$ (1° FWHM) at the sample position. The elliptical set-up variations were found to have the highest brilliance transfer just above 90% for the two-split and four-split systems. The divergence distribution of these variations at the sample position is approximately uniform.

We have demonstrated the use of this guide system by full simulations of two instruments, related to ESS. The cold-neutron diffractometer is rather close to the ESS design for a magnetism diffractometer. Also the cold-neutron chopper spectrometer

has characteristics similar to a foreseen ESS instrument, although a realistic cold shopper spectrometer would likely use a higher neutron divergence, of the order $\pm 1°$, which is likely achievable for cold neutrons (wavelengths from 3 Å and higher) through a re-optimization of the split guide system.

The split guide set-up offers the possibility of an increased amount of instruments, at the cost of a reduced intensity at the sample position at each instrument. The lower intensity does not originate from a low brilliance transfer, but from a (possibly) reduced maximum divergence. Further studies are needed to quantify this divergence limitation.

References

Boeni, P. (2008). *Nucl. Instr. Meth. A*, **586**, 1–8.
C. Schanzer *et al.* (2004). *Nucl. Instr. Meth. A*, **529**, 63.
Christ, J. & Springer, T. (1962). *Nukleonik*, **4**, 23.
DMSC web page, (2013). `http://www.ess-dmsc.eu`.
E. Farhi *et al.* (2013). *J. Neutr. Res.* **17**.
ESS, (2013). Technical Design Report for the European Spallation Source.
et al., J. V. (2013). *submitted to Nucl. Instr. Meth. A*.
et al., K. K. (2012). *Nucl. Instr. Meth. A*, **696**, 75–84.
et al., P. M. B. (2011). *J. Appl. Cryst.* **44**, 483–488.
F. Mezei and M. Russina (2001). *Physica B 310, 94*.
H. Abele *et al.* (2006). *Nucl. Instr. Meth. A*, **562**, 407.
Jacobsen, H., Lieutenant, K., Zendler, C. & Lefmann, K. (2013). *Nucl. Instr. Meth. A*, **717**, 69–76.
J.O. Birk *et al.* (2013). *in preparation*.
K. Klenø*et al.* (2013). *in preparation for J. Appl. Cryst.* .
K. Lefmann *et al.* (2011). *Nucl. Instr. Meth. A*, **634**, S1.
Klenø, K. (2013). *Ph.D. theisis, Uni. Copenhagen*, p. Submitted.
Lefmann, K. & Nielsen, K. (1999). *Neutron News*, **10**, 20.
Lefmann, K., Schober, H. & Mezei, F. (2008). *Meas. Sci. Techn.* **19**, 034025.
M. Bertelsen *et al.* (2013). *in preparation for Nucl. Instr. Meth. A*.
M. Russina and F. Mezei (2002). *Proc. SPIE 4785, 24*.
Maier-Leibnitz, H. & Springer, T. (1963). *J. Nucl. Energy*, **17**, 217.
Mezei, F. (1976). *Comm. Phys.* **1**, 81.
Mezei, F. (1997). *J. Neutr.Res.* **6**, 3.
Mezei, F. (2000). *ESS report*.
Mezei, F. & Dagleish, P. (1977). *Comm. Phys.* **2**, 41.
Mezei, F. & Russina, M. (2002). *Proc. SPIE*, **4785**, 24.
P. Bentley *et al.* (2013). *in preparation*.

web page, E., (2013). `http://ess-scandinavia.eu`.

P.K. Willendrup *et al.* (2013). *in preparation for J. Appl. Cryst.* .

Rodriguez, D., Kennedy, S. & Bentley, P. (2011). *J. Appl. Cryst.* **44**, 727.

Sales, M., Holm, S., Lieutenant, K. & Lefmann, K. (2011). *J. Phys. Soc. Japan*, **80**, SB018.

S.L. Holm *et al.* (2013). *in preparation*.

Zendler, C., Lieutenant, K., Nekrassov, D., Cussen, L. & Strobl, M. (2012). *Nucl. Instr. Meth. A*, pp. 1–8.

EUROPEAN SPALLATION SOURCE

MXType.Localized	
Document Number	MXName
Project Name	<<project name>>
Date	12/08/2013
Revision	MXRevision MXPrinted Version
State	MXCurrent

ESS Instrument Construction Proposal
Time-of-Flight Instrument for Powder diffraction, Small angle scattering and imaging.

	Name	Affiliation
Main proposer	Mogens Christensen	Center for Materials Crystallgraphy iNANO & Department of Chemistry Aarhus University DK-8000 Aarhus
Co-proposers	Kim Lefmann Jürg Schefer	Niels Bohr Institutet, Universitetsparken 5, DK-2100 København Ø Laboratory for Neutron Scattering Paul Scherrer Institut CH-5232 Villigen PSI
ESS coordinator	Paul Henry	European Spallation Source ESS AB Box 176 S-221 00 Lund

The following table is used to track the ESS internal distribution of the submitted proposal.

	Name	Affiliation
Document reviewer	Ken Andersen	ESS
Document approver	Oliver Kirstein	ESS
Distribution (list names)		

European Spallation Source ESS AB
Visiting address: ESS, Tunavägen 24
P.O. Box 176
SE-221 00 Lund
SWEDEN

www.esss.se

MXType.Localized	
Document Number	MXName
Project Name	<<project name>>
Date	12/08/2013

ENCLOSURES

<< file name>>

EXECUTIVE SUMMARY [1-2 PAGES]

We propose the construction of an instrument, which combines neutron powder diffraction (NPD), small angle neutron scattering (SANS) and neutron imaging (NI) in a single instrumental setup to be built at ESS. The instrument is designed to have a time resolution sufficient to follow chemical and physical processes in real time over a very broad spatial span. NPD covers the atomic regime in the range from 0.01 to 5 nm, while SANS looks into the nanometer regime covering length scales from 2-100 nm and finally NI reveals the structural features in direct space from 50 μm-50 mm. In other words the instrument is capable of covering length scale over 9 orders of magnitude and follow *in situ* processes.

The aim of the multi length scale instrument is to study advanced functional materials in action. The material properties are determined by the structural characteristics on multiple length scales i.e. the combined atomic-, nano-, meso-, and microstructure in parallel. Covering a large spatial span is crucial as understanding of advanced functional materials in action often involves external stimuli such as gas flow or temperature, and recreating the exact conditions in different experiments can be difficult. A classical example is heterogeneous catalysts: Here the atomic structure of catalytic nanoparticles is placed in a microporous matrix. All length scales are relevant for the efficiency of the catalytic process. Therefore in-depth insight into the structure and functionality requires multiple length scale coverage, with a sufficiently high time resolution. Commonly, information on different length scales on advanced functional materials is collected separately and quite often in the equilibrium state i.e. after external *stimuli* has taken place. The proposed instrument would be ideal for studying advanced materials in function under real life working conditions. The structural understanding of advanced functional materials is a prerequisite for designing new and improved materials.

The different experimental neutron techniques, NPD, SANS, and NI have highly different requirements to the incoming neutron beam. That is why all instruments existing today are focused towards one or the other technique; a few instruments have the capability of covering large length scales like NOVA, i-Materia, HI-SANS at J-Parc or NOMAD at ISIS, however they are still optimized for either NPD or SANS. To overcome the largely different requirements for the different techniques we propose an entirely new concept, where two guides are viewing the cold and thermal part of a bispectral moderator. The two beams are extracted from the same beamport and transported to the sample through two independent guides. The thermal guide will be optimized for NPD, while the cold guide will be optimized for SANS and NI. By having two guides it is possible to individually optimize the beam condition. Compromises will still have to be made even though the challenge has been separated into two independent problems. The setup requires individual detectors for NPD, SANS and NI, therefore the cost of this instrument is expected to become larger compared to a conventional single technique instruments, but significantly less than three separate instruments. Popularly said - get 3 for the price of 1.5.

MXType.Localized
Document Number MXName
Project Name <<project name>>
Date 12/08/2013

The proposed instrument is largely relying on existing technology with respect to detectors, guides and choppers. The largest challenge for the instrument is the extremely crammed space around the source at the beginning for the instrument.

The trend of looking at multiple length scale at fast time scales is currently being built-up at synchrotron facilities, where most new synchrotron sources are building dedicated SAXS/WAXS (small angle X-ray scattering/wide angle x-ray scattering) beamlines. The proposed multi length scale instrument will be a game changer in neutron scattering for looking into multi dimensions and fast time scales. Topics of interest are here light elements in energy materials, composites materials, matrix embedded systems, phase transition and nucleation and materials with magnetic properties like multiferroics: The materials for the next decades.

TABLE OF CONTENTS

1. INSTRUMENT PROPOSAL [APP. 20 PAGES]

1.1 Scientific Case [5 pages]

Functional materials have at all times driven our civilization in search for prosperity and superiority. This fact is reflected by names associated with different periods in history i.e. Stone Age, Bronze Age, Iron Age etc. Today, it could be said that we are approaching the end of the Silicon Age, as we reach the density limit for transistors on chips. Research efforts have developed new functional materials extending Moore's law.[1] The hot topic in science in 2025 and beyond is hard to predict, but functional materials are certain to play a key role in driving our society.

To meet the great scientific challenge of understanding advanced functional materials in action - *in situ* or *in operandi* information is needed at multiple length scales. We therefore propose the construction of an instrument for the ESS, combining neutron powder diffraction (NPD), small angle neutron scattering (SANS) and neutron imaging (NI) in a single instrumental setup to cover this gap. The designed instrument allows quasi simultaneous coverage of multiple lengths scales with a time resolution sufficient to follow chemical and physical processes in real time. The concept is completely novel and uses a single beamport to extract a cold and a thermal beam that converge at the sample position. The instrument

will be referred to as TIPSI, because it is a Time-of-Flight Instrument for Powder diffraction, Small angle scattering and Imaging. The instrument is unique in combining different techniques and simultaneous operation, without strongly compromising any of the techniques.

Combining NPD, SANS and NI in a single instrument allows studying multiple length scales simultaneously and obtaining information on the atomic-, nano-, meso-, and microstructure scale. If we wish to understand and improve functional materials it is paramount to understand the structure at all length scales and with sufficient time resolution to follow physical and chemical processes. Until now, different length scale information is collected separately and quite often *post mortem* i.e. after the process have taken place. Such experiments allow scientists to make educated guesses for the processes taking place in the material. However, the proposed multi length scale instrument will be a game changer as it allows insight into time dependent processes at all length scales at the same time and from the same sample.

Studying functional materials implies multi-component systems that vary with applied conditions, such as pressure, magnetic field, gas flow, etc. Moreover, solely using a single neutron scattering method of investigation cannot deliver comprehensive understanding. This is especially true when the sample preparation is difficult and individual experiments cannot be compared directly, as they are often separated considerably in time. Current investigations with neutron scattering often focus on measuring phases and structures mainly in equilibrium and static environments. For science of the future, altering and grouping of conditions will be a necessity to study material behaviour.

The scientific focus areas of the instrument are related to the strengths of neutron scattering in comparison with X-ray. Contrast between light and heavy elements, magnetic materials, use of bulky sample environment and measurements of samples with sizes comparable with those used in applications. The research areas, where TIPSI will excel can be divided into four different groups:

- Light elements and energy related materials.
- Composites, scaffolds or matrix embedded systems.
- Phase transition and nucleation.
- Materials with magnetic properties.

1.1.1 Light elements and energy related materials:

Neutrons can provide unique information about energy storage materials, which are becoming increasingly important as renewable energy takes over from conventional energy sources. Developing such materials to become available at reasonable price may be the only solution to overcome the green house effect/CO_2 problem.[2] Two elements are of particular interest in energy storage namely lithium and hydrogen. Both of which are difficult to observe using X-ray scattering, due to their low number of electrons. Lithium is the key component in Li-ion batteries, whereas H is the active element in hydrogen storage materials. For neutron scattering these elements hold special potential as they have good contrast with respect to other elements and the attenuation coefficients and the scattering length can be tuned by using different isotopes giving access to contrast methods. Different length scales effects the performance of both hydrogen storage and battery materials. The time dependence of intercalation and deintercalation of Li in such batteries and hydrogenation and dehydrogenation is crucial for cyclability and durability for materials applications.

Another area, where energy research can benefit from neutron investigations is oxygen containing compounds. Typical applications of such oxides are membranes of oxygen fuel cells,[3] catalyst support materials, superconductors, ceramic filters, thermoelectric materials etc. Information about oxygen is difficult to extract from X-ray diffraction data, when heavy elements are present, however in the case of neutrons, oxygen has an appreciably neutron scattering length.[4] Ceramic materials are often porous materials and information about the pore structure extractable from small angle scattering is crucial for the functionality of the material e.g. in oxygen fuel cells, and catalyst support materials.

1.1.2 Composite, scaffold or matrix embedded systems

Hydrogen storage and Li-ion batteries can be interpreted as matrix embedded systems, where the Li or H is placed in a host matrix from which it can be inserted or extracted. Other important compounds can be represented as matrix embedded systems including heterogonous catalysts, molecules in porous matrix, drug transport, magnetic materials, etc.

Improvement of catalytic processes in such materials requires knowledge about different length and time scales. Heterogeneous catalysis often relies on liquid or gas reactions in the presence of a nanocrystalline catalyst embedded in a porous support matrix. The atomic structure of catalysts, pore volume and size of the matrix determines the catalytic properties[5-7]. The catalytic performance is a function of temperature, gas flow, fouling atoms concentration, etc. Obtaining *in operandi* data for catalytic systems allow mapping performance against external *stimuli*.

Photoswitchable molecules are another guest suitable for composite materials where molecules are embedded in a porous matrix.[8] They have potential applications as optical data storage materials or even in cancer therapy by delivering radicals. Combining powder diffraction, small angle scattering and imaging is crucial for extracting full information about pore size and embedded molecules, being on a different length scale. The photoswitchable molecules are unstable and change over time, therefore it is essential to collect data at different length scales during the same experiment at the same time.

Biological inspired systems are also examples of multiple length scales systems, which would benefit from simultaneous data collection as preparing the exact same state of biological samples, can be difficult. Biomineralization has importance for artificial bone and in an environmental context.[9, 10]

1.1.3 Phase transition and nucleation

The wide and small angle scattering capabilities of TIPSI allow following chemical synthesis, i.e. follow nucleation and investigate metastable phases. Phase transitions occurring during variation of thermodynamic conditions such as temperature, pressure, volume, or composition. Metastable transitions are highly sensitive to the history of the external *stimuli*, which can be difficult to control. Thus simultaneously or quasi-simultaneously data collection of the different length scale is vital for achieving a full picture. This *in situ* information is crucial for determining critical parameters for optimal synthesis conditions. The TIPSI instrument will be of general interest when studying *in situ* chemistry, e.g. solid-state, liquid-to-solid-state, gas-to-solid-state, solvothermal and supercritical reactions[11-14]. Common for these synthesis are a precrystalline states, where agglomerates form before they begin crystallizing[14]. Small angle scattering and low resolution total scattering can give information about the pre-crystalline state, while diffraction provides structural information as it has crystallized and starts to grow. Following chemical synthesis has a broad fundamental

science appeal; however there are also example with high technological importance such as curing of cement[15-20] and nucleation of clathrate hydrates in oil pipes[21-27]. These systems have already been extensively studied using neutron techniques, however, again the studies have been limited either due to the length scale of small angle scattering, powder diffraction or imaging. Combining all techniques to look at the same sample will provide much more profound information about the processes happening as function of time.

Nucleation and aging processes of grain boundary and crystalline phase under temperature, pressure or magnetic field for ceramics, metal and alloy are extremely important for material performance. TIPSI will be well suited for studies of phase transition in multicomponent materials and phase separation.

1.1.4 Materials with magnetic properties

Multiferroics have in recent years attracted increasing attention. These modern magnetic systems couple magnetism with either electrical, mechanical, thermal, or optical properties [28]. Multiferroics are of great technologic interest as they raise the possibility of controlling the magnetic properties[29, 30] with an electrical field, pressure or vice-versa[31]. Spintronics[32, 33] as this field is aiming at spin domain manipulation in half metal ferromagnetic systems. These materials are either realised in single chemical phase compounds or composite materials. Topologically ferroic systems are physical systems, which are governed by its domain structure[34, 35]. The domains structure and the topology of the domain wall are susceptible to chemical effects[36], size effects and magnetic interactions. Establishing the correlation between local atomic structure and long/short range magnetic ordering requires data collection on all length scales i.e. diffraction, small angle scattering and imaging.

An example of multi-length scale studies are colossal magneto-resistance perovskites structures[37]. The perovskites possesses a metal-insulator transition and phase separation promoted by electron/hole doping via chemical substitution[38, 39]. Fundamental[40] and technological applications[41] rely on understanding the coupling of these different length scales and the degrees of freedom. Aging, phase transitions, percolation phenomena, defects mobility, phase homogeneity, domains wall pining, atomic and magnetic structure, are key parameters in the improvement of magneto-memory shape alloys[42], spintronics, magnetocaloric and magnetocapacitance materials[43]. Multidimensional length scales collected simultaneously as offered by TIPSI would greatly aid the understanding of this interesting class of materials.

TIPSI with its multi-length-scale data collection capacity will be able to tackle scientific challenges in this frontier area and will be able to identify also the magnetic properties more accurately especially *in operandi* for magnetic phase separation, quantum criticality in magnetic and superconductor materials, ferroic/multiferroic systems[43], and high performance magnetic coupled materials[42].

1.1.5 The size and impact for existing and potential user

The main user community consists of users doing *in situ* experiments on advanced functional materials at existing NPD, SANS and NI instruments. Today, *in situ* experiments are routinely performed at numerous instruments, which will be described in more detail in the next section. The interest in performing *in situ* studies appears to be increasing, when considering the new instruments coming online at SNS, J-Parc and FRM-II. TIPSI will extend the information *in situ* users may extract from their experiments through observation of a broader length scales. The extractable information per experiment may therefore be largely enhanced and add crucially understanding to the science being investigated.

The potential user community is quite large when looking towards the synchrotron world. A quick search at Web of Science for 'SAXS WAXS' resulted in 1232 publications including all years, with a strongly increasing trend. The current rate is just below 100 publications per year. A brief visit to different synchrotron homepages reveal more than 20 beamlines worldwide offer simultaneous SAXS/WAXS studies. The majority of these beamlines are dedicated to SAXS/WAXS studies, especially the more recent built beamlines. Therefore a high impact to the user group of TIPSI can be found in the synchrotron community. The demand for doing combined studies is also reflected by PANalytical since the fall 2012 offers a setup for doing SAXS/WAXS in the home laboratory. Needless to say if SAXS/WAXS becomes a standard home laboratory technique it will also be demanded that large facilities can before these kind of experiments.

An X-ray powder diffraction and imaging beamline has been proposed for MAX-IV. This experimental setup using X-ray would be highly complementary to the capabilities of TIPSI and great synergies between X-ray and neutron measured are expected due to the close proximity of the two instruments.

Finally the instrument TIPSI will be of interest for industry for looking at different length scales of commercial samples. The combination of imaging with diffraction/small angle scattering is potentially of particular interest. The instrument would also offer industry oriented groups a single point of entry for performing a broad range of experiments. Special care must be taken to allow an easy and transparent operation and data visualization for these non expert users.

1.1.6 Comparison with similar existing instruments:

A number of instrument at various facilities are performing fast *in situ* powder diffraction experiments e.g. D20 at ILL, GEM, Polaris, and Nimrod at ISIS, Powgen and Nomad at SNS, NOVA and i-Materia at J-Parc, Wombat at ANSTO and the foreseen instrument PowTex at FRM-II. It is difficult to compare the different instruments, but the main characteristics of a powder neutron diffractometer are resolution and flux at the sample position plus covered q-range. The inherent property of a short pulse source largely determines flux and resolution. The advantage of a Time-of-Flight (TOF) neutron powder diffractometer is the option for increase flux at a relaxed the resolution. But the performance of long pulsed TOF NPD instruments will be similar to the performance of short pulse sources, at high resolution. However the possibility of tuning resolution and flux is a great advantage for *in situ* experiments at long pulse spallation sources such as ESS.

In general the SANS instrument at long pulsed sources will hugely benefit as SANS can cope with a resolution of $\Delta\lambda/\lambda = 10\%$. The length of the TIPSI setup gives results in a resolution of about $\Delta\lambda/\lambda = 1\%$, therefore the SANS performance of TIPSI will be comparable to the best SANS instruments at sources such as ILL.

Only a few instruments have the capability to cover multiple length scales. However all existing instruments are focused primarily towards one technique with some capability of measuring non-ideal data for the other technique. The instruments in questions for SANS/NPD are D16 at ILL, Nimrod at ISIS and three instruments at J-Parc, HI-SANS, Nova and i-Materia. For combination of NPD and NI are two instruments under construction IMAT at ISIS and VULCAN at SNS. Through the use of two guides TIPSI will outperform the combined instrument at other facilities. TIPSI will have a comparable performance compared to the other NPD instruments, while the long instrument length will reduce the SANS

performance compared to other ESS SANS instruments. However the long distance from the source is expected to give TIPSI and extremely low background and therefore a significantly better signal to noise ratio then, what can be expected from the short instruments.

1.1.7 Infrastructure and supporting facilities:

TIPSI will need heavy support for sample environment, as the experiments are considered to be *in situ* or *in operando* therefore large variation in samples are expected for the instrument. It is also foreseen that the instrument should have a sample environment built up station, comparable to the real instrument, so that users can setup and test their sample environment off-line before the experiment including all electrical, gas or water cooling connections necessary. This will ensure that a minimum of neutrons are lost during the experiment. Chemical preparation laboratories should also be present to prepare samples for experiments on side.

1.2 Description of Instrument Concept and Performance [10 pages]

The instrument description is divided into two parts: The first part gives an overall introduction of the instrument followed by a detailed description of individual components:

Introduction: The proposed instrument combines NPD, SANS and NI. The technical challenge is the highly different requirements to the incoming neutron beam for the different techniques. For NDP, it is favorable to have a wavelength resolution ($\Delta\lambda/\lambda$) < 0.5%, as this produces sharp powder diffraction peaks. Small angle scattering on the other hand can easily accept $\Delta\lambda/\lambda$ ~10%. Small angle scattering also requires a highly collimated beam, whereas powder diffraction can have a flux benefit by increasing the divergence. Finally, a short wavelength is advantageous for NPD as this allows large coverage of reciprocal space and is necessary for pair distribution function analysis (PDF). Small angle scattering typically uses long neutron wavelength to obtain better resolution at short Q. Therefore we suggest a new concept, where two guides - a cold and a thermal guide – are extracted from the same beamport and transported to the sample position. Whereas the thermal guide is optimized for NPD, the cold guide is optimized for SANS and partially for NI. The two guides are separated by an angle of 5° to leave sufficient space for optical components and avoid the direct thermal beam hitting the SANS detector.

Due to the complexity in working with two guides, we are immediately rule out the possibility of having a shortened instrument by Wavelength Frame Multiplication. Hence, the optimal instrument length is determined by the ratio of the source repetition rate (T = 71.4 ms) and the pulse duration (τ = 2.86 ms) and the distance between moderator and pulse shaping chopper (L_{ps} = 6.5 m). The 6.5 m is given by the necessary biological shielding in front of the moderator. The pulse duration τ is "magnified" through the chopper opening like a pinhole camera, see Figure 5. The natural instrument length is therefore $T/\tau = (L-L_{ps})/L_{ps}$, resulting in L = 169 m. This instrument length represents a compromise between the needs for powder diffraction and small angle scattering and the needed distance to have the two beams converging with an angle of 5° at the sample position. The instrument length together with the pulse repetition rate gives a usable wavelength band: $T = \alpha(L-L_{ps})\Delta\lambda$, (where α =0.2528 ms/Åm) giving $\Delta\lambda$ ~1.73 Å, which is sufficient for powder diffraction, but a broader wavelength range with decreased resolution $\Delta\lambda/\lambda$ would be advantageous for SANS. A length of 169 m, results in a natural wavelength resolution of $\Delta\lambda/\lambda = \pi/(\alpha L\lambda)$, equal to 4.5%, 1.5% and 0.8% for 1.5, 4.5, and 8 Å neutrons, respectively. For NPD it is necessary to reduce the pulse length to increase the resolution, while the full pulse can be accepted for

MXType.Localized
Document Number MXName
Project Name <<project name>>
Date 12/08/2013

the SANS setup. Having two guides allows chopping the thermal beam for powder diffraction, while leaving the cold beam unperturbed. This would not be possible by using a bispectral extraction, through one guide. Furthermore having two guides allow having a divergent beam for NPD, while the SANS beam can be strongly collimated.

Instrument simulations show the feasibility of extracting two beams from the same beamport and having the beams converging at the samples position at an angle of ~5°. The instrument would in normal operation mode send either a thermal or cold pulse towards the sample. After the sample position the instrument can be divided into three main components: Diffraction detectors placed 1.5 m from the samples covering an angle from 20-170°, the primary SANS detector placed 7 m from the sample behind the cold beam and the NI setup, see Figure 1 (NI is not shown). The detection system is divided into five different detectors, three of which are in place for the SANS signal: A1) zero angle detector at the beamstop position of the cold beam, A2) low q-SANS flat panel detector positioned 7 m from the sample at the center of the cold beam, A3) high q-SANS placed 3 m from the sample around the cold beam. The diffraction detectors A4) are placed cylindrically around the sample. Finally the imaging detector A5) is placed just behind the sample and can moved in and out of the beam path. The thermal beam passes through the SANS detector tank and is dumped behind the SANS detector.

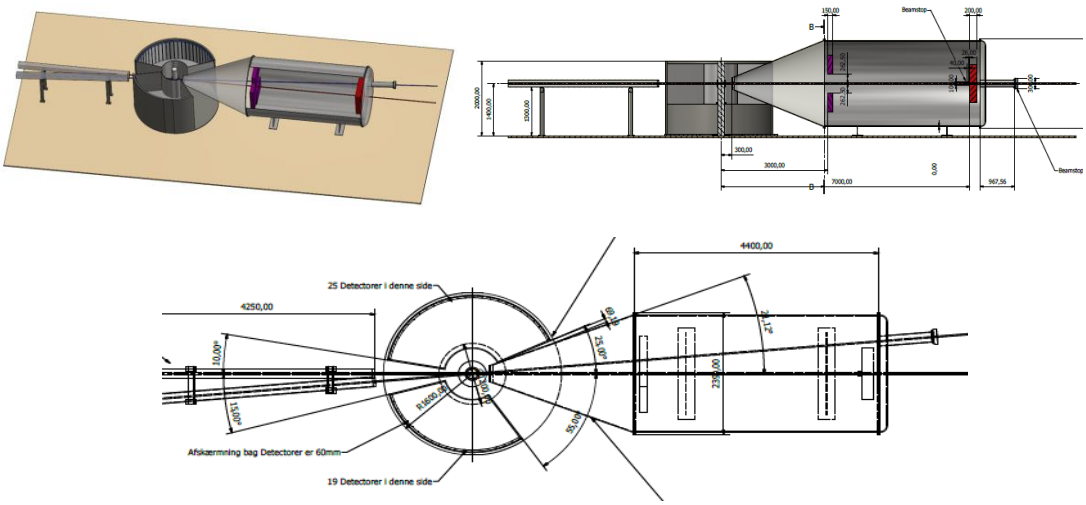

Figure 1 Instrumental setup seen from different angles.

The cylindrical diffraction detectors cover an angular range from 20-170°, corresponding to q-space coverage of ~1-21 $Å^{-1}$ for an incoming wavelength band of 0.6-2.3 Å. Lower q-values can potentially be obtained from diffraction signal on the SANS detectors. The PND q-range provides excellent data for refinement of structural features including thermal vibrations. The covered range is even sufficient for performing low resolution pair distribution function analysis, with an atom pair resolution $\Delta r=\pi/q_{max}$~0.15 Å. The covered length scale is approximately 0.01-5 nm.

The SANS and NPD detectors coverage as function of wavelength of the different detectors is illustrated in Figure 2. A beamstop of 3 cm diameter is placed 20 cm from the detector surface i.e. the calculation is made without the zero angle detector. When including the A4 diffraction detectors a possible q-range ($q=4\pi\sin\theta/\lambda$) coverage from the cold guide is q_{min}(11.7Å, A2) = 0.003 $Å^{-1}$ to q_{max}(3Å, A4) = 4 $Å^{-1}$. Using only a single pulse with the wavelength range 10-11.7 Å gives full coverage in the region 0.003-1.2 $Å^{-1}$. A calculation of

MXType.Localized
Document Number MXName
Project Name <<project name>>
Date 12/08/2013

the detector coverage using 10-11.75Å wavelength band is shown in Figure 3. The scattering curve is calculated for a hard sphere with radius 2 nm and 100 nm, with an assumed polydispersivity of 10%. The small angle scattering covers the length scale from ~1-100 nm.

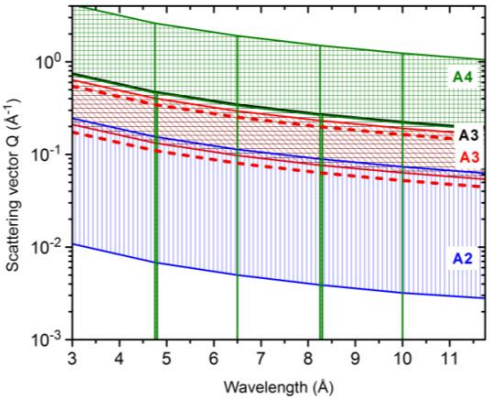

Figure 2 The detector coverage for the cold guide depending on wavelength and detector. The red dashed line show the limit of full coverage or pseudo full coverage, due to the square shape of the detector.

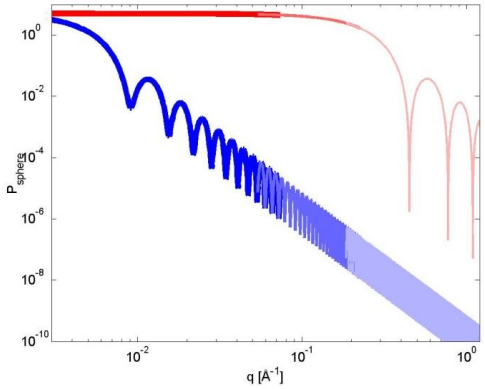

Figure 3 Calculation of two spherical particles of diameter 2 nm (red) and 100 nm (blue) using the wavelength range from 10-11.7 Å. The different color and line width represents different detectors.

Based on the above calculations a single narrow wavelength band is sufficient for collection of SANS data. If necessary a larger wavelength band can be obtained through pulse suppression. Pulse suppression is also used to separate the individual pulses from powder and small angle scattering i.e. the time window on the detector will be dedicated to either small angle scattering or powder diffraction.

The imaging detector is placed as close to the sample as possible and allows real space images of the sample with a resolution down ~50 µm for samples of sizes smaller than 5x5 cm^2. The intention is to use a time resolved imaging detector, which allows Bragg-edge imaging. The Bragg-edge imaging will inherently have good resolution $\Delta\lambda/\lambda$=1.5% at 4.5 Å.

The two different guides and the three different techniques NPD, SANS, and NI allow information to be obtained within a size range spanning 9 orders of magnitude. The following describes the individual components of the instrument in larger detail:

- Beam extraction.
- Thermal guide.
- Cold guide.
- Sample position.
- Diffraction detectors.
- Small angle scattering detectors.
- Imaging station.

1.2.1 Beam extraction

The exact positions of the moderators are still under discussion; the following description is based on information from 2012. At ESS the center of the cold and thermal moderators are separated horizontally by a distance of 12 cm. The two beams must go through different openings as only the thermal beam should see the pulse defining chopper, placed after the biological shielding. The current plug dimensions of 90×90 mm^2 allow the two beams to be displaced vertically. It is likely that the plug area can be larger in the vertical direction and

towards the end of the biological shielding. The thermal guide is passed through the plug by a feeder starting at dimensions of 60x30 mm^2 at a distance 2 m from the moderator surface and shrinking to 40×20 mm^2 at the resolution chopper position, 6.5 m from the moderator. The cold guide is 20x20 mm^2 and it is straight all the way from its beginning to the end of the biological shielding. This could cause some near-collision of guide, but an angling of the guide in the horizontal direction leaves sufficient space to accommodate both guides within the same plug. Figure 4 illustrates the geometry of this set-up and shows the absence of guide collision. Assuming conservatively that the outer guide dimensions in each direction are 10 mm larger than the inner dimensions due to substrate etc. In total, this leaves up to 20 mm space between the two guides at the chopper position.

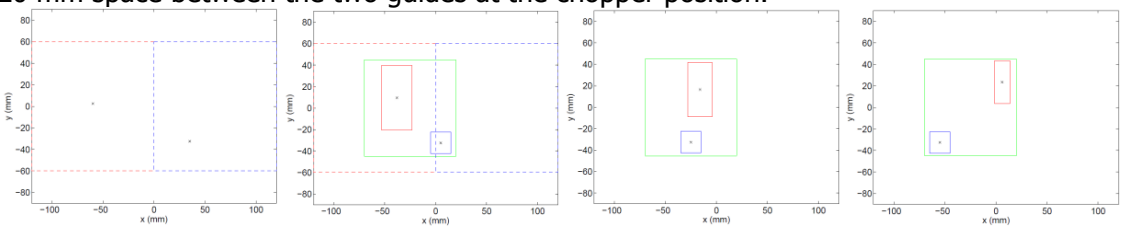

Figure 4: The beam extraction from the cold and thermal moderator. Red is the thermal moderator, while blue is the cold moderator. The figures are different distances to the moderator, z = 0, 2, 4 and 6 m (from left to right). The figure illustrates the possibility of extracting a cold and a thermal beam from the moderator using a single beam port of only 90x90 mm^2 size. The scales are in [mm]

The beam extraction solution introduces an initial angular deviation between the two guides of 1.8°, the guides must be brought together at the sample position with a separation of about 5°. Due to the difficulty of guiding thermal neutrons the angular change will be obtained through curving the cold guide. The setup is illustrated in Figure 6. The cold guide is curved by 8.1° over 98.8 m before ending in a 14 m straight section. The thermal guide is double ellipse with approximate dimensions of ~80 + 80 m) with a small kink of 0.2° between the ellipses, to avoid line-of-sight between moderator and sample. The simulations of the individual guides are described in detail in the following.

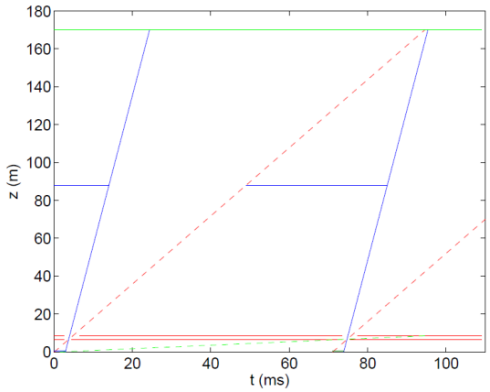

Figure 5 Time-of-flight diagram of a 170 m long diffraction instrument with a pulse shaping chopper. The neutron position (z) is plotted as a function of flight time, t. Neutrons from two ESS pulses are shown; straight blue lines representing λ = 0.5 Å, dashed red lines representing λ = 2.2 Å.

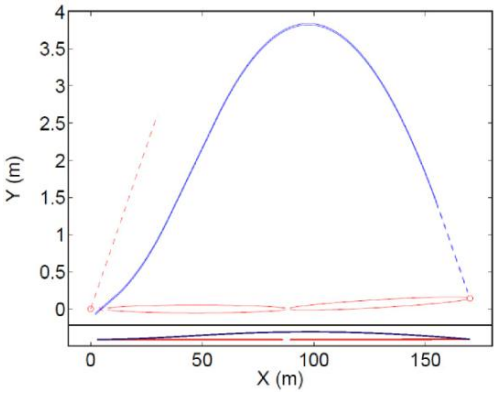

Figure 6 Illustration of the cold (blue) and thermal (red) guide system when taken from a single beam port. The figure above shows enlarged y-axis for clarity, below is the guide showed with equal scaling of X and Y.

MXType.Localized
Document Number MXName
Project Name <<project name>>
Date 12/08/2013

1.2.2 The thermal guide

The instrument is aiming at *in situ* studies with large q-space coverage and a minimum wavelength of λ_{min} = 0.6 Å. Shorter wavelengths are not considered, due to guide transport efficiency and source flux spectrum. The d-space resolution ($\delta d/d$) at 2θ = 90° for λ_{mean} ~1.5 Å is tunable between $(\delta d/d)_{FWHM}$ = 0.2 - 1%. Achieving this resolution requires the pulse shaping chopper position at 6.5 m to be open for 145 µs (~1/20 pulse length) for a 0.2% resolution and 725 µs (~1/4 pulse length) for a 1% resolution. The wavelength resolution must be matched with the beam divergence and the sample size. We choose the optimal sample size to be 5x15 mm^2. The horizontal and vertical beam divergences are uncoupled and can be controlled individually. The horizontal divergence is limited to ±0.5° matching the lowest d-space resolution, while a larger divergence of ±1.5° can be allowed in the vertical direction, due to the detector arrangement. Furthermore, it was recently required by the ESS that the sample should be twice out of line-of-sight of the moderator, however our current simulations is only out of sight once. A first approximation to the beam delivery system is obtained by running the GuideBot software written by Mads Bertelsen[44]. The GuideBot does not consider guide cost and offers rather crude supermirror coating considerations. Nevertheless it gives a good starting point for further guide optimization. The guide optimization is still ongoing work at the time of writing. The result from GuideBot is shown in Figure 7 . Two elliptical guides are obtained separated by a straight section at the kink position.

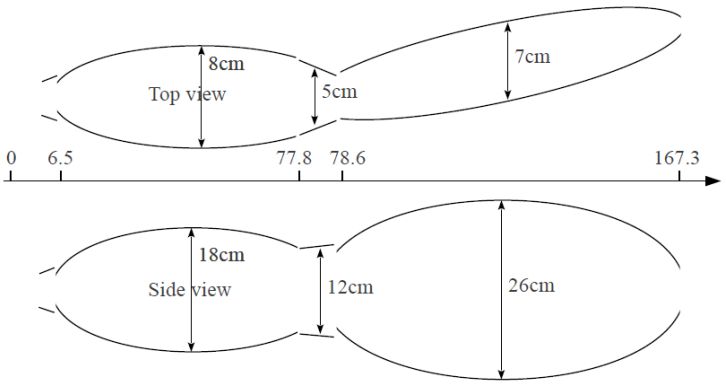

Figure 7 Results from GuideBot optimization. The upper figure is the horizontal plane, while the lower figure represents the vertical plane. The difference in height and width reflects the different divergence requirements.

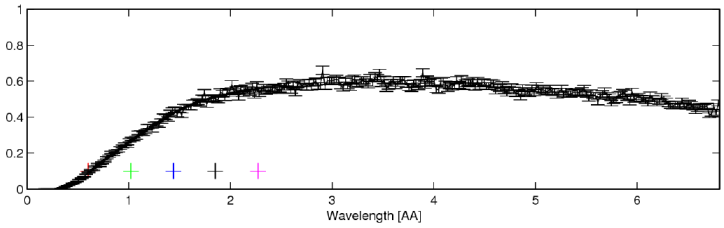

Figure 8 McStas simulation of the brilliance (defined as neutron intensity within a certain interval in wavelength, position, and divergence)**.**

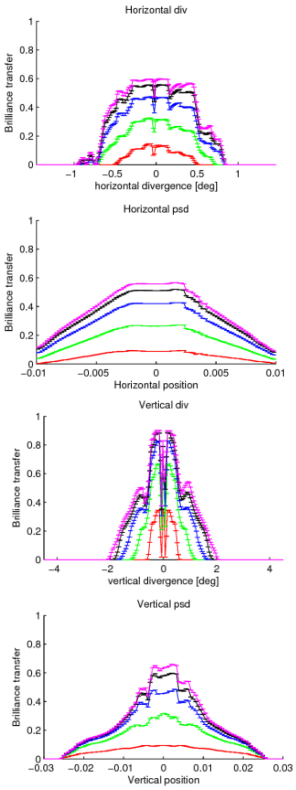

Figure 9 Brilliance transfer as function of divergence and position.

The guide is optimized for maximum brilliance transfer, shown in Figure 8, it is clear that long guides have difficulty in transporting short wavelength neutrons. The brilliance transfer is about 60% at 2 Å and decreases to about 30% for 1 Å. To obtain the flux at the sample the brilliance transfer is multiplied with the source brightness. It may be advantageous to reduce the vertical divergence to reduce the guide height and produce better brilliance transfer at lower divergence, this point is still under investigation. The position and divergence dependence of the brilliance transfer is shown in Figure 9.

Thermal guide chopper system: The thermal guide will have three choppers; CT1) pulse shaping chopper, CT2) pulse selection chopper, and CT3) frame overlap chopper.

CT1) Pulse shaping chopper: The pulse shaping chopper is placed at 6.5 m from the moderator, i.e. just after the biological shielding of the source. The pulse shaping chopper is a fast counter rotating double disc chopper running at 280 Hz, below the limit of today's choppers of f_{max} = 350 Hz. The opening time (dt) should be variable between 145 μs and 725 μs to obtain a wavelength resolution of 0.2-1% (FWHM). The maximum opening of the chopper d can be calculated from the disc radius (r) and the opening angle ($d\varphi = 2\pi f dt$). Fast choppers typically have a radius maximum of about 350 mm. Setting the beam height to 320 mm and the rotation frequency to 280 Hz, gives a chopper opening of d_{max} = 45 mm. Spinning the pulse shaping chopper at lower speed increases the pulse length. Running the pulse shaping chopper at 280 Hz produces an opening every 3.57 ms and therefore allows unwanted neutrons with longer wavelengths to enter the guide system. The long wavelength neutrons can be suppressed by placing a slow rotating pulse selection chopper at 7 m (CT2).

CT2) Pulse selection chopper: The pulse selection chopper is placed at 7 m and has two functions: suppressing the long wavelength neutrons allowed by the pulse shaping chopper CT1 and pulse suppression of the entire pulse for allowing the cold neutron pulse from the second guide to reach the sample. The pulse selection chopper will be rotating at low speed, at most identical with the source frequency of 14 Hz. The slow frequency allows the use of a disk with large diameter R = 640 mm. Using a chopper window of ~40 mm allows a fully open time of 1.3 ms and a partial opening time of 2 ms, sufficient to allow a single thermal pulse and suppress the longer neutron wavelengths.

Having the first two choppers rather close together and also close to the moderator will produce "blurry" edges in the wavelength distribution, e.g. from the neutrons emitted in the time-tail of the moderator. We remove these neutrons by a wavelength definition chopper located half way down the instrument CT3.

CT3) Frame overlap chopper: The frame overlap chopper is placed at the neck of the kink region, around 78.6 m from the moderator. The frame overlap chopper CT3 will have an opening angle of 175° and be spinning at the source frequency of 14 Hz. In this guide system, frame overlap is found when neutrons from one source pulse reach the pulse-shaping burst from the next pulse. i.e. neutrons with wavelengths around 45 Å may reach the sample. However, the flux from the thermal source at this wavelength will be low and the d-spacing has to be >65 Å to fulfil Bragg conditions. The chopper system has not been included in our simulations. A summary of the chopper system can be found in Table I.

Thermal guide optics: At the converging end of the second guide, an aperture system consisting of four individual apertures is controlling the beam size as well as the beam divergence at the sample position as on WISH at ISIS. The last aperture is placed at the end of the guide, about 600 mm before the sample.

MXType.Localized
Document Number MXName
Project Name <<project name>>
Date 12/08/2013

1.2.3 The cold guide

As described above the cold guide is rather peculiar, due to the need of bending the guide with respect to the thermal guide. The cold neutrons are extracted by a 20x20 mm^2 guide placed 2 m from the moderator. The beam extraction introduces an initial angular offset of 1.8° between the two guides. The first 11 m are straight. Hereafter follows a 2.1° bend achieved over 24 m followed by a straight section of 21.2 m length, before bending the guide an additional 8.1° over a distance of 98.9 m. Finally the guide ends in a straight section of 14 m. This configuration allows a double pinhole setup in front of the sample as illustrated in Figure 6. The brilliance transfer has been simulated using McStas for different mirror-coatings m = 2 and 3. The coatings are in both cases assumed to be near to ideal with reflectivity equal to unity and a supermirror degradation α = 1. The curved shape is made by piecing 5 cm guide parts together and the brilliance transfer curves are found for a divergence up to ±0.5°. The results are shown in Figure 10. The brilliance transfer for neutrons with wavelength longer than 4 Å is almost independent of the guide coating, while below 4 Å it drops rapidly with lower coating value. The guide curvature does not allow transmission of short wavelength neutrons, due to the higher number of reflections experienced by the neutron in the guide.

The divergence profile for the very narrow wavelength band of 4 to 4.01 Å at the sample position in an area of 10x10 mm^2 is shown in Figure 11. Vertical stripes are clearly visible, originating from strongly bend. Such a divergence profile is not particularly suited for imaging purposes. However, the final guide design for the cold setup is still in progress to overcome such problems.

In summary, the simulations provided clearly reveal the possibility of combining two guides from a single beamport.

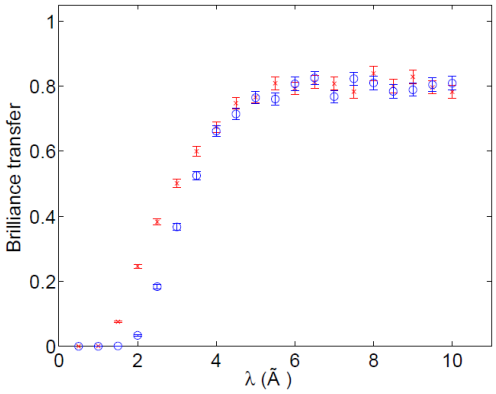

Figure 10 Brilliance transfer for the cold guide shown as a function of the wavelength, λ for two m-values: 2 (blue circles) and 3 (red crosses). The brilliance is collected over an area 10 × 10 mm^2 and the divergence limits are ±0.5° in both directions.

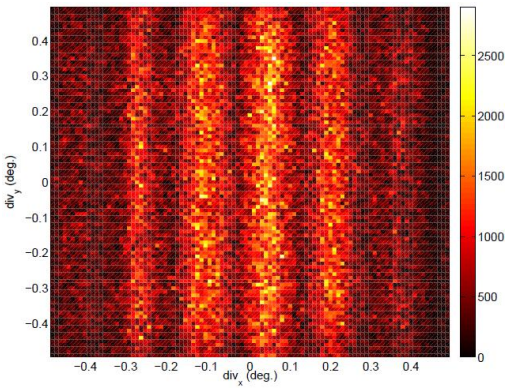

Figure 11 Divergence profile of the beam at the 10 × 10 mm^2 sample position for λ = 4 Å, using an m = 2 coating. The briliance transfer is 65%.

Cold guide chopper system: As mentioned in the introduction the wavelength resolution at 4.5 Å is already $\Delta\lambda/\lambda$ = 1.5%, better than needed for SANS. Therefore, no pulse shaping chopper is necessary. However, three choppers are necessary to achieve our needs CC1) wavelength band definition chopper, CC2) frame overlap chopper, CC3) frame overlap chopper.

CC1) *Wavelength band definition chopper*: This chopper must be placed within the first half of the instrument length and as close to the moderator as possible. To avoid interference with the choppers in the thermal guide, we chose to place this wavelength band definition chopper 9 m away from the moderator in the straight section of the guide. The chopper will spin at source frequency 14 Hz and have a disk radius of 640 mm. The chopper should allow the full 2.86 ms pulse to reach the sample. At 9 m the pulse width is about ~6.6 ms with 14 Hz rotation frequency this gives an opening angle of ~33**°.**

CC2) *Frame overlap chopper #1*: Like for the thermal instrument a frame overlap chopper will be placed half way between the moderator and the sample. This chopper is again spinning at source frequency and has a radius of 640 mm. The opening angle of the frame overlap chopper is just below 180°. Frame overlap is found when slow neutrons from one pulse match the burst time of the wavelength definition chopper meant for neutrons from the next pulse. The wavelength in the wrong frame is 25 Å higher than that of the first frame.

CC3) *Frame overlap chopper #2*: This chopper is placed 13 m from the source and will prevent the neutrons with wavelength +25 Å to pass through the two previously described choppers CC1 and CC3.

In case a wider wavelength range is needed for the cold guide, some moderator pulses have to be skipped. This can be done by the first band definition chopper (CC1) - and by running all other choppers (CC2 and CC3), at a slower frequency of *f/n*, where *n* is an integer (*f*=14 Hz). For our chopper system, the maximal suppression comes at *n* = 6, above which the chopper system begins to leak neighbor pulses into the guide. A suppression of 6 pulses corresponds to a wavelength band of Δλ ~ 12 Å, which should be more than sufficient, for the detector arrangement envisioned. Conclusively three choppers are sufficient for the SANS system. A summary of all the chopper system can be found in Table I.

	Purpose	Guide	Position [m]	v [Hz]	Radius [mm	Opening time [μs]	Opening Length L_{max} [mm or °]	Pulse length [ms]
CT1	Pulse shaping	thermal	6.5	280	350	145-725	45	3.57
CT2	Pulse selection	thermal	7.0	14	680	-	20	2.0
CT3	Frame overlap	thermal	78.6	14		-	175°	-
CC1	Band definition	cold	9	14	640	-	33°	6.6
CC2	Frame overlap	cold	78	14	640	-	175°	-
CC3	Frame overlap	cold	13	14	640	-	175°	-

Table I: Summary of the chopper system need for the thermal and cold guide

Cold guide optics: The SANS setup is envisioned with double pinhole collimation and a collimation length of ~7 m – identical to the sample to detector distance. By removing the front aperture, a single pinhole camera can be made with a L/D = 350 using a 20 mm aperture. A ±0.5° divergence gives an illuminated area of approximately 120 mm. The beam divergence could be reduced by using an aperture just in front of the sample.

1.2.4 The sample environment

The intention of studying multiple length scales in different functional materials *in operandi* requires special and flexible sample environment as users are expected to come from different scientific areas bringing their own equipment. The sample space is 1 m in diameter allowing most kinds of sample environment to fit inside the instrument. The sample environment should be mounted so that it can be translated along xyz and rotated around omega for tomography and spatial resolved studies. The incident optical components and radial collimation should be easily interchangeable to allow the use of sample environment brought in from user laboratories. The sample space should be easily accessible from the top, bottom and the side. It should be possible to set up the next sample environment close to the instrument and easily transfer the entire setup to the beam position, while the prior experiment is running. This way the dead time between experiments is minimized. It is envisaged that the complete experimental setup of the sample environment can be tested off-line and all cables can be setup and the functionality of the sample environment can be tested without beam. As the previous beamtime ends the entire sample environment can be pulled out of the instrument and the next sample environment can be inserted with a minimum of setup time and cable connection. In this fashion, it could also be imagined, that long term experiments could be inserted at various times without removing the sample from the sample environment.

Around the sample space will be mounted a moving radial collimator system. Different collimators will be available depending on the size of the sample environment. It will ideally be possible to build the collimators into the sample environment and make it easily interchangeable.

1.2.5 Powder diffraction detectors

Powder diffraction detectors are grouped into three sections around the sample area: The low 2Θ section interesting for magnetic investigations, the medium group around 2Θ=90° for solving problems depending on the highest flux and the backscattering detector bank for archiving the highest resolution. The range covered by one side can reach 150°. Low and medium detector banks will only cover one side at the start-up with a maximum height of 1 m and a radius of 1.50 m. Scintillation detectors[45] are the most straightforward solution for our needs. Replacing photomultipliers by avalanche-photo-diodes (APD's) such as developed by PSI for the new POLDI detectors at PSI can further improve such detectors, making the primary electronics less sensitive to stray fields from magnets. Our budgeting also foresees upgrade options to extend these banks such as completing the second side as far as sample access is not disturbed. We intend to start with closed to 4 m^2 detector area on day 1.

1.2.6 Small angle scattering detectors

Small-angle detectors have to fulfil two tasks and two boundary conditions: Most important is covering the small and high q-range simultaneously. We want to fulfil this by a cascade detector,[46] which can withstand high counting rate of the direct beam. The cascade detector will cover the low q-range and stop the direct cold beam. The high q-detector is divided into

three partially overlapping sectors. 1) A flat panel detector placed 7 m from the sample with a size of 1x1 m^2, 2) three half sized flat panel detectors (1x0.5 m^2) placed 3 m from the sample. The fourth detectors are missing and allow lost beam tube geometry for the direct beam from the thermal guide. 3) The diffraction detectors maybe used to extend the q-range of the experimental setup. Flat panel detector will be base on present ESS developments with ^{3}He detectors as a backup option.

1.2.7 Imaging station

The imaging option is operated as an add-on unit, which can be activated on demand, but not operated in sequence with the 14 Hz ESS pulse frequency. The imaging camera will be placed within the sample chamber normally kept under vacuum. For the operation of the SANS option, the camera has to be moved completely out of the beam area. This can be solved by approaching a parking position, which is beyond the beam, but still within the vacuum chamber. In the operating position, the camera should be placed as close to the sample as possible to avoid loss of resolution. The design will allow both neutron beams (thermal and cold) arriving at different angles to be used for imaging. Possible detectors are the Medipix [47] detector or a small imaging detector built at PSI (using a CCD camera viewing a scintillation plate over an optical mirror). The two different setups are shown in Figure 12. The Medipix detector has two main advantages: 1) it allows time resolved Bragg edge imaging and 2) it can be placed much closer to sample, due to the absence of spacious mirror setups, which consequently gives higher resolution. The limitation of the present Medipix detector is the relative small active area (28x28 mm^2), however increasing this area requires limited R&D.

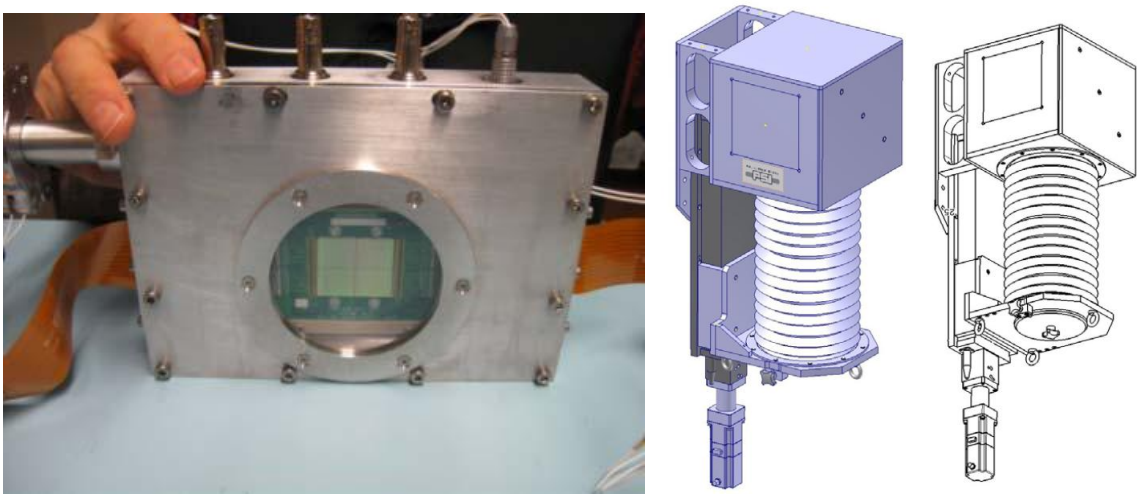

Figure 12 (*left*) the medipix detector with an active area of ~ 28x28 mm^2 and a sampling rate of about 1200 samplings per second. (*right*) classical imaging setup made with fluorescent screen mirror and CCD.

1.2.8 Summary of the TIPSI detectors

This list is summarizing the detector specifications of TIPSI. A future upgrade option is the extended area for the powder diffraction banks.

MXType.Localized
Document Number MXName
Project Name <<project name>>
Date 12/08/2013

	pieces	Size Horizontal Vertical [cm]	Total Area [m^2]	Resolution horizontal/vertical [mm]	Max. overall counting rate ($c/s/cm^2$)	Max. counting rate on spot, spot size ($c/s/cm^2$)	Efficiency
SANS Low q	1	7x7	.005	1x1	10^4	10^8	60%@10Å
SANS High q	1 3	100x100 50x100	1 1.5	5x5	10^4	10^4	75%@5Å
NPD	#	400-800* 50-100*	4-8	3x10	10^4	10^5	50%@1Å 75%@5Å 100%@10Å
NI	1	3x5 (.8x2.8)	.002	0.05x0.05	Not Critical	Not Critical	Not critical

Table II Summary of the detector specifications of TIPSI
*) upgrading options for NPD detector banks: height and size
#) a maximum of 2 banks covering up to 150° in 2Θ

1.3 Technical Maturity [3 pages]

The concept of the multiple-length scale instrument TIPSI is based on existing instrument concepts for powder diffraction, small angle scattering and imaging. The challenge is merging these concepts into a single instrument.

1.3.1 Guide system:

Using two guides from the same beam port converging at the sample position is a new and challenging concept. The guides have to be optimized individually. The thermal guide for diffraction is challenging (double elliptical double ellipse with high m=6 at some places compared to m=3 for HRPD build by SwissNeutronics). The large curvature on the cold guide is not a standard solution. These concepts must be tested on smaller scales e.g. using the BOA beamline at SINQ.

1.3.2 Chopper systems:

All chopper parameters are all in the range of operating instruments and only space limitations due to the two guides and also neighbouring guides will become a challenge. The general setup of choppers close to the source at ESS will be challenging.

1.3.3 Beam stops:

The two-guide-design needs special attention to stop the beams. Lost-beam-geometry seems to be an appropriate approach, but is challenging, as space is limited. The challenge here is avoiding interference to the small angle detectors.

1.3.4 Alternative pulse-use for the thermal and cold guide:

This concept needs clear separation of the pulses and taking care of the background from "secondary" sources such as the prompt pulse, choppers, slits efficiently. A special effort must be placed on the sector from 6.5 to 11.5 m distance from the source to reduce the background. The calculations for this concept has been successfully applied to the shielding

of instruments such as EIGER@SINQ and experimental results have proven it's maturity on a instrument facing a similar neutron spectra as at ESS.

1.3.5 Detectors:

The availability of huge area detectors may be the most limiting factor as for a majority of ESS instruments. The prize can limit here the affordable area and in consequence the performance of the instrument. Stability and background sensitivity (γ-suppression) of the detectors can be a limiting factor for TIPSI with its relatively open geometry and unpredictable sample equipment brought-in by the user. However, the detectors have fall-back options using present technologies, but here unpredictable cost can limit this option.

1.3.6 Sample environment:

On one hand, using an evacuated sample area reduces the background, but may limit the user-access with dedicated auxiliary equipment. Special care must be taken here to fulfil different needs.

In summary, the maturity of the instrument TIPSI is given. All the single components have been realized at least on a smaller scale or in another combination elsewhere, but merging them will be highly challenging. Major limitations – as for any ESS instrument – could be the choppers placed close to the biological shielding in a very cramped space, the availability of large and economic area detectors with sufficient resolution, sensitivity and stability. Reducing the background from the source, our own beam optics and the neighbouring instruments needs a major effort.

1.4 Costing [2 pages]

The cost estimates for TIPSI can be divided into six main parts:

- Neutron guide system
- Choppers including electronics
- Sample surrounding (slits, sample positioning, sample chamber, sample mechanics)
- Detectors (including mechanic, electronics)
- General electronics and computing
- Shielding (primary 5° sector and Instrument)

1.4.1 Neutron guides system

TIPSI uses two guides, each 170 m long. Whereas the cold guide is coated fully by m=2 and has an open size of 2 cm by 2 cm, the thermal guide consists of 2 double-elliptical sections, eventually with a feeding section. The coating will likely be m=6 in parts of the guide, with a potential to use sections with lower (and consequently less expensive) coating. Our calculations are based on a pseudo-trapezoidal approximation of the elliptical shape. We expect here cost of 1 Mio Euro (the price includes 0.5 Mio Euro for the mechanical support) for the cold guide and 1.7 Mio Euro for the thermal guide (includes 0.75 Mio Euro for the mechanical support).

1.4.2 Choppers including electronics

6 choppers are necessary with an average cost of 50 kEuro, adding up to 300 kEuro and 200kEuoro for the electronics.

1.4.3 Sample surrounding/instrument mechanics

The sample environment contains a vacuum tank, xyz table for the sample positioning, and a positioning system for the imaging camera. All materials chosen for this area have low magnetic permeability. The costs are expected to be around 300 kEuro. We add here 300kEuro for sample auxiliary.

1.4.4 Detectors and detector electronics

For the SANS detectors, a vacuum tank made of aluminum of approximately 30 m^3 volume is necessary. Detector electronics inside has to be cooled from the outside. Expected costs are around 300 kEuro for the mechanics only.

Detectors cost itself are difficult to estimate as many development projects are on going. We are starting with coverage of approximately $5m^2$. Extrapolating the price of the HRPT-detector at SINQ (1 m^2), we expect here costs in the range of 5 MEuro. Detector mechanics is included in this numbers. Upgrades will mostly focus at increasing the detector area for powder diffraction.

1.4.5 Electronics (motor drives, computing, security system)

Operating this 3-in-1 instrument will need significantly more electronics compared to a standard instrument. State-of-the-art electronics will be around 400 kEuro including computers. Electronics also includes the instrument safety system.

1.4.6 Shielding costs

Shielding is separated into three main parts:

Secondary shielding: This includes the remaining guide shielding (160m) and the sample area shielding and will be mostly low cost concrete ($1000m^3$). Expected costs are 1.5 Mio Euro. Special care and more expensive shielding are needed for the beam-entrance to the sample area (0.2 Mio Euro) with materials similar to the primary sector described later in 3) for the 5^o sector closest to the source.

Shielding of the detectors: 300 kEuro will be needed for specialized shielding material, which is materials such as borated alu-matrix-materials, respectively borated plastic materials for shielding against thermal neutrons.

Primary shielding: The 5m thick shielding of the 5 degree sector starts at a radius of 6.5m and ending at 11.5m. It covers 1.5m above and below the beam level. We need here a composite shielding with high accuracy as many mechanical parts such as chopper, filters, slits, e.g. are located here and their background has to be eliminated. We are using here the effective costs spent for the EIGER spectrometer built at SINQ to get the costs per volume, as this existing spectrometer is facing a similar radiation spectrum as TIPSI at ESS. The volume of this sector for TIPSI sums up to 12 m^3 and we expect cost of 1.5 Mio Euro. This seems high, but high precision machining of heavy parts, which involves steps, limiting gaps, access to choppers, etc.). Not only TIPSI, but also the neighboring instruments will benefit from a high-quality shielding of this sector, and the cost are therefore taken out of the TIPSI Budget and listed separately.

MXType.Localized
Document Number MXName
Project Name <<project name>>
Date 12/08/2013

1.4.7 Manpower

The project needs a Postdoc for 3 years/fulltime, 1 year of a senior scientist for supervision, 6 years/50% of a leading scientist for the full period, adding up to 7 person-years or approximately 1.5 MEuro based on full-costs basis.

The personals costs of a lead engineer (6 years), a designer (6 years) as well as 2 technicians (12 years in total) are included in the costs below as the numbers are showing full-costs. Building it internally by a university would reduce the costs accordingly. Upgrade phase 1 and 2 are expected to need 1.5 person for 1 year each.

Investment	**Day 1**	**Upgrade 1**	**Upgrade 2**
Guides (thermal and cold)	3		
Shielding TIPSI (instrument only)	1.8	0.5	0.5
Detectors including support/vacuum chambers	5.3	2.5	2.5
Electronics	0.5	0.2	
Sample Area, Instrument Mechanics	0.6		
Choppers	0.5		
Total TIPSI	**11.7**	**3.2**	**2.7**
Shielding primary 5^{o} sector	1.5		
Total TIPSI Sector	**13.2**	**3.2**	**2.7**
Personnel			
Manpower	**1.5**	**0.2**	**0.2**

Table III Summary of the costs to build TISPI (numbers based on full-cost-calculations, in MEuro)

2. LIST OF ABBREVIATIONS

Abbreviation	**Explanation of abbreviation**

PROPOSAL HISTORY

Version	Reason for revision	Date
2.0	Incorporate lessons from 2012 proposal round	31.10.2013
1.0	New Document	2012

1. G. E. Moore, Cramming more components onto integrated circuits, Reprinted from Electronics, volume 38, number 8, April 19, 1965, pp.114 ff. *Solid-State Circuits Society Newsletter, IEEE* **11**, 33-35 (2006).
2. L. Bjørn, *The Skeptical Environmentalist: Measuring the Real State of the World*. (Cambridge University Press, 1998).

3. G. Amow, S. J. Skinner, Recent developments in Ruddlesden-Popper nickelate systems for solid oxide fuel cell cathodes. *J. Solid State Electrochem.* **10**, 538-546 (2006).

4. A. W. Hewat *et al.*, High resolution neutron powder diffraction investigation of temperature and pressure effects on the structure of the high-Tc superconductor Y2Ba4Cu7O15. *Physica C: Superconductivity* **167**, 579-590 (1990).

5. J. D. Grunwaldt, A. M. Molenbroek, N. Y. Topsoe, H. Topsoe, B. S. Clausen, In situ investigations of structural changes in Cu/ZnO catalysts. *Journal of Catalysis* **194**, 452-460 (2000).

6. T. Kandemir *et al.*, In situ neutron diffraction under high pressure-Providing an insight into working catalysts. *Nucl. Instrum. Methods Phys. Res. Sect. A-Accel. Spectrom. Dect. Assoc. Equip.* **673**, 51-55 (2012).

7. B. S. Clausen *et al.*, In situ cell for combined XRD and on-line catalysis tests: Studies of Cu-based water gas shift and methanol catalysts. *Journal of Catalysis* **132**, 524-535 (1991).

8. A. Cervellino, J. Schefer, L. Keller, T. Woike, D. Schaniel, Identification of single photoswitchable molecules in nanopores of silica xerogels using powder diffraction. *Journal of Applied Crystallography* **43**, 1040-1045 (2010).

9. S. L. S. Stipp *et al.*, Behaviour of Fe-oxides relevant to contaminant uptake in the environment. *Chemical Geology* **190**, 321-337 (2002).

10. B. C. Christiansen, T. Balic-Zunic, K. Dideriksen, S. L. S. Stipp, Identification of Green Rust in Groundwater. *Environmental Science & Technology* **43**, 3436-3441 (2009).

11. M. Bremholm, M. Felicissimo, B. B. Iversen, Time-Resolved In Situ Synchrotron X-ray Study and Large-Scale Production of Magnetite Nanoparticles in Supercritical Water. *Angew. Chem.-Int. Edit.* **48**, 4788-4791 (2009).

12. V. Middelkoop *et al.*, Imaging the inside of a Continuous Nanoceramic Synthesizer under Supercritical Water Conditions Using High-Energy Synchrotron X-Radiation. *Chem. Mat.* **21**, 2430-2435 (2009).

13. S. Takami *et al.*, Neutron radiography on tubular flow reactor for hydrothermal synthesis: In situ monitoring of mixing behavior of supercritical water and room-temperature water. *Journal of Supercritical Fluids* **63**, 46-51 (2012).

14. C. Tyrsted *et al.*, Watching Nanoparticles Form: An In Situ (Small-/Wide-Angle X-ray Scattering/Total Scattering) Study of the Growth of Yttria-Stabilised Zirconia in Supercritical Fluids. *Chemistry – A European Journal*, 5759-5766 (2012).

15. R. A. Livingston, D. A. Neumann, A. J. Allen, S. A. Fitzgerald, R. Berliner, Application of neutron scattering to Portland cement. *Neutron News* **11**, 18-24 (2000).

16. J. W. Phair, Green chemistry for sustainable cement production and use. *Green Chemistry* **8**, 763-780 (2006).

17. M. P. Fang, P. E. Sokol, J. Y. Jehng, W. P. Halperin, Neutron Diffraction Study of Cement. *Journal of Porous Materials* **6**, 95-99 (1999).

18. M. Castellote, C. Andrade, X. Turrillas, J. Campo, G. J. Cuello, Accelerated carbonation of cement pastes in situ monitored by neutron diffraction. *Cement and Concrete Research* **38**, 1365-1373 (2008).

19. I. P. Swainson, E. M. Schulson, A neutron diffraction study of ice and water within a hardened cement paste during freeze–thaw. *Cement and Concrete Research* **31**, 1821-1830 (2001).

20. P. J. McGlinn *et al.*, Appraisal of a cementitious material for waste disposal: Neutron imaging studies of pore structure and sorptivity. *Cement and Concrete Research* **40**, 1320-1326 (2010).

21. W. F. Kuhs, A. Klapproth, F. Gotthardt, K. Techmer, T. Heinrichs, The formation of meso- and macroporous gas hydrates. *Geophysical Research Letters* **27**, 2929-2932 (2000).

22. W. F. Kuhs, T. C. Hansen, in *Neutron Scattering in Earth Sciences,* H. R. Wenk, Ed. (2006), vol. 63, pp. 171-204.

23. E. D. Sloan, Fundamental principles and applications of natural gas hydrates. *Nature* **426**, 353-359 (2003).

24. M. A. Kelland, History of the development of low dosage hydrate inhibitors. *Energy Fuels* **20**, 825-847 (2006).

25. B. Chazallon, W. F. Kuhs, In situ structural properties of N2-, O2-, and air-clathrates by neutron diffraction. *The Journal of Chemical Physics* **117**, 308-320 (2002).

26. H. Ohno, I. Moudrakovski, R. Gordienko, J. Ripmeester, V. K. Walker, Structures of Hydrocarbon Hydrates during Formation with and without Inhibitors. *Journal of Physical Chemistry A* **116**, 1337-1343 (2012).

27. D. K. Staykova, W. F. Kuhs, A. N. Salamatin, T. Hansen, Formation of porous gas hydrates from ice powders: Diffraction experiments and multistage model. *J. Phys. Chem. B* **107**, 10299-10311 (2003).

28. M. Fiebig, Revival of the magnetoelectric effect. *J. Phys. D-Appl. Phys.* **38**, R123-R152 (2005).

29. T. Lottermoser *et al.*, Magnetic phase control by an electric field. *Nature* **430**, 541-544 (2004).

30. M. Daraktchiev, G. Catalan, J. F. Scott, Landau theory of domain wall magnetoelectricity. *Physical Review B* **81**, 224118 (2010).

31. M. Kenzelmann *et al.*, Magnetic Inversion Symmetry Breaking and Ferroelectricity in TbMnO_{3}. *Physical Review Letters* **95**, 087206 (2005).

32. H. Ohno, - A window on the future of spintronics. **- 9**, - 954 (2010).

33. S. i. o. Spintronics, Open access. *Nat Mater* **11**, 353-476 (2012).

34. G. Catalan, J. F. Scott, A. Schilling, J. M. Gregg, Wall thickness dependence of the scaling law for ferroic stripe domains. *J. Phys.-Condes. Matter* **19**, (2007).

35. G. Catalan *et al.*, Fractal Dimension and Size Scaling of Domains in Thin Films of Multiferroic BiFeO_{3}. *Physical Review Letters* **100**, 027602 (2008).

36. B. Ravel, M. P. Raphael, V. G. Harris, Q. Huang, EXAFS and neutron diffraction study of the Heusler alloy Co_{2}MnSi. *Physical Review B* **65**, 184431 (2002).

37. J. M. DeTeresa *et al.*, Evidence for magnetic polarons in the magnetoresistive perovskites. *Nature* **386**, 256-259 (1997).

38. P. G. Radaelli *et al.*, Mesoscopic and microscopic phase segregation in manganese perovskites. *Physical Review B* **63**, 172419 (2001).

39. G. H. Rao *et al.*, Magnetic phase transitions in Pr_{5}Ge_{4}. *Physical Review B* **69**, 094430 (2004).

40. J. Seidel *et al.*, Conduction at domain walls in oxide multiferroics. **8**, 229 - 234 (2009).

41. E. A. Eliseev *et al.*, Linear magnetoelectric coupling and ferroelectricity induced by the flexomagnetic effect in ferroics. *Physical Review B* **84**, 174112 (2011).

42. K. P. Bhatti, S. El-Khatib, V. Srivastava, R. D. James, C. Leighton, Small-angle neutron scattering study of magnetic ordering and inhomogeneity across the martensitic phase transformation in Ni_{50−x}Co_{x}Mn_{40}Sn_{10} alloys. *Physical Review B* **85**, 134450 (2012).

43. W. Kleemann, V. V. Shvartsman, P. Borisov, A. Kania, Coexistence of Antiferromagnetic and Spin Cluster Glass Order in the Magnetoelectric Relaxor Multiferroic PbFe_{0.5}Nb_{0.5}O_{3}. *Physical Review Letters* **105**, 257202 (2010).

44. M. Bertelsen,GuideBot Software Package (2013)

45. N. J. Rhodes, Scientific Reviews: Status and Future Development of Neutron Scintillation Detectors. *Neutron News* **17**, 16-18 (2006).

46. C. J. Schmidt, F. Groitl, M. Klein, U. Schmidt, W. Häussler, CASCADE with NRSE: Fast Intensity Modulation Techniques used in Quasielastic Neutron Scattering. *J. Phys., Conf. Ser.* **251**, 012067 (2010).

47. http://medipix.web.cern.ch/medipix/pages/images.php

ESS Technical Design Report

Release 3.08

April 23, 2013

Executive editor: S. Peggs[1].

Structural editor: R. Kreier[1].

Contributing editors: C. Carlile[1], R. Miyamoto[1], A. Påhlsson[2], M. Trojer[2], J. G. Weisend II[1].

Chapter editors: M.-L. Ainalem[1], K. H. Andersen[1], K. Batkov[1], P. Carlsson[1], D. Ene[1], B. Hedén[1], K. Hedin[1], A. J. Jackson[1], P. Jacobsson[1], O. Kirstein[1], G. Lanfranco[1], Y. Lee[1], M. Lindroos[1], J. Malovrh Rebec[3], G. Trahern[1], J. Yeck[1].

Contributors: M. Åberg[1], N. Ahlfors[1], R. Ainsworth[4], C. Alba-Simionesco[5], S. Alimov[6] N. Aliouane[7] B. Alling[8], K. Andersson[9], M. Andersson[1], N. H. Andersen[9], D. Anevski[10], S. Ansell[11], V. Antonelli[12], D. Argyriou[1], L. Arleth[13], E. Babcock[14], S. Barbanotti[15], F. Beckmann[16], P. M. Bentley[1], P. Beran[17], L. Bérden[1], F. Bergstedt[1], J. Bermejo[18], M. Berrada[14], M. Bertelsen[13], Y. Beßler[14], T. Bigault[19], J. Birch[8], J. O. Birk[13], J. Bobnar[3], C. Böhme[1], A. Bollhalder[7], P. Böni[12], H. N. Bordallo[13], P. Bosland[5], S. Bousson[20], W. G. Bouwman[21], G. Brandl[12], S. Brault[20], J. Brinch[21], R. Brinkmann[15], H. Brueck[15], T. Brückel[14], J. C. Buffet[19], M. Bulat[6], R. Bürge[7], I. Bustinduy[18], M. Butzek[14], X. X. Cai[22], R. Caniello[23], M. Cardenas[13], G. Castro[24], H. Carlsen[13], L. Celona[21], Y. Chen[25], N. Cherkashyna[1], S. Choroba[15], B. Cheymol[1], M. Christensen[26], N. B. Christensen[27], E. P. Cippo[28], A. Class[25], K. Clausen[19], U. Clemens[14], J. F. Clergeau[19], M. Comunian[21], C. Cooper-Jensen[1], J. Correa[19], G. Croci[23], G. Čuk[3], L. Cussen[6], Y. Dai[7], H. Danared[1], D. Dancila[29], C. Darve[1], T. Davenne[11], P. de Vicente[18], P. P. Deen[1], M. Dell'Anno Boulton[1], S. Deledda[22], C. Densham[11], R. De Prisco[1], M. Desmons[5], G. Devanz[5], F. M. Dominguez[18], P. Duchesne[20], R. Duperrier[1], P. Duthil[20], H. Eckerlebe[16], S. Eckert[30], H.-J. Eckholt[15], T. Ekelöf[29], J. Embs[7], M. Eneroth[1], R. Engels[14], C. Engling[15], M. Eshraqi[1], R. Fabbri[14], C. Fazio[25], J. Fenske[16], J. Fetzer[25], U. Filges[7], U. Fischer[25], K. G. Fissum[10], M. Forster[7], A. France[5], A. Franciosi[31], P. Freeman[6,32], H. Frielinghaus[14], C. Fröjdh[33], C. Frost[11], T. Gahl[1], S. Gallimore[1], S. Gammino[21], N. Gandalfo[20], R. Georgii[12], G. Gerbeth[30], G. Gervasini[23], B.-E. Ghidersa[25], A. Ghiglino[18], L. Giacomelli[28], O. Gonzalez[18], G. Gorini[28], V. Goryashiko[29], M. Göhran[1], K. Gajewski[29], A. Goukassov[26], D. Graf[7], F. Grespan[24], A. Gromov[7], G. Grosso[23], U. Greuter[7], C. Grünzweig[7], B. Guérard[19], S. Gysin[1], K. Habicht[6], H. Hahn[1], E. A. L. Håkansson[34], S. Hall[1,10], R. Hall-Wilton[1], B. R. Hansen[9], U. B. Hansen[35], T. Hansson[1], T. Haraldsen[22], V. Haramus[16], C.-H. Hårdh[1], H. Hassan[1], H. Hassanzadegan[1], B. C. Hauback[22], W. Häussler[12], W. Hees[1], G. Helgesen[22], P. Henry[1], L. Hermansson[29], A. Hiess[1], A. Hilger[6], T. Hofmann[6], C. Höglund[1,8], L. Hoitzner[7], A. I. S. Holm[27], S. Holm[36], L. Høpfner[35], C. Horstmann[16], A. Houben[37], L. Hultman[8], M. Imam[1,8], A. Ioffe[14], J. Iversen[15], S. Iyengar[34], P. Jacobs[37], C. L. Jacobsen[35], H. Jacobsen[35], J. Jacobsen[13], A. Jansson[1], K. Jensch[15], J. Jensen[8], M. Jensen[9], X. J. Jin[25], A. J. Johansson[34], R. Jongeling[1], F. Juranyi[7], C. Kagi[7], R. Kampmann[16], K. Kanaki[1], N. Kardjilov[6], S. Kecskes[25], P. Keller[7], G. Kemmerling[14], M. Kenzelmann[7], A. Khaplanov[1], C. Kharoua[1], I. Khokhriakov[16], K. Kiefer[6], B. Kildetoft[1], T. Kittelmann[1], H. Kleines[14], K. Klenø[35], E. B. Klinkby[9], B. Klösgen[38], E. B. Knudsen[9], K. Knudsen[22], J. Kohlbrecher[7], M. Könnecke[7], A. Konobeev[25], P. Korelis[7], T. Köttig[1], L. Krämer[12], J. Krašna[3], J. Krebs[7], Ž. Kroflič[3], V. Krsjak[39], S. Kynde[13], B. Laatsch[14], P. Ladd[1], E. Laface[1], B. Lauritzen[9], R. E. Lechner[1], K. Lefmann[35], E. Lehmann[7], M. Lehmann[7], F. Leseigneur[20], K. Lieutenant[6], L. Lilje[15], R. Linander[1], H. Lindblad[1], B. Lindenau[14], I. Llamas-Jansa[22], T. Lofnes[29], W. Lohstroh[12], D. Lott[16], P. Lukáš[17], J. Lundgren[1], M. Lundin[40], H. Möller[1], M. Maǵan[18], I. Manke[6], M. Marko[7], N. Martin[12], D. Mascali[24], A. Matheisen[15], S. Mattauch[14], D. McGinnis[1], M. Meissner[1], P. Mereu[24], M. Meshkian[34], F. Mezei[1], W.-D. Moeller[15], J. Molander[1], S. Molloy[1], K. Mortensen[13], J.-F. Moulin[16], A. Milocco[28], M. Monkenbusch[14], M. Morgano[7], T. Mühlebach[7], M. Müller[16], J. L. Muñoz[18], G. Nagy[7], D. Nekrassov[6], L. Neri[24], K. Neuhaus[15], J. Neuhausen[7], C. Niedermayer[7], J. B. Nielsen[9], S. Nielsen[9], B. Nilsson[40], P. Nilsson[1], E. Noah[1], E. Nonboel[9], P. Norby[9], A. Nordt[1], G. Nowak[16], E. Oksanen[1], G. Olivier[20], G. Olry[20], T. Panzner[7], S. Pape-Møller[27], C. Pappas[21], T. Parker[1], S. Pasini[14], H. Pedersen[8], S. Peetermans[7], J. Persson[1], B. Petersen[15], S. Petersson[33], S. Petersson Årsköld[1], J. Pieper[41], A. Pietropaolo[23], J. Pilch[17], A. Piquet[5], F. Piscitelli[19], A. Pisent[24], E. Platacis[25], F. Plewinski[1], J. Plomp[21], J. Plouin[5], A. Ponton[1], S. Pospisil[42], B. Pottin[5], H. F. Poulsen[9], S. O. Poulsen[9], P. Rådahl[1], P. K. Pranzas[16], M. Proell[15], O. Prokhnenko[6], K. Prokeš[6], E. Rampnoux[20], E. Rantsiou[7], N. Rasmussen[35], O. Rasmussen[9], K. Rathsman[1], M. Rebai[28], T. Reiss[7], M. Reščič[3], D. Reschke[15], C. Rethfeldt[6], M. Reungoat[44], D. Reynet[20], D. Richter[14], M. Rieth[25], T. H. Rod[35], D. M. Rodriguez[1], I. Rodriguez[1,14] K. Rolfs[6], M. Rouijaa[16], R. Ruber[29], U. Rücker[14], C. Rüegg[7], H. Rønnow[32], M. Russina[6], A. Ryberg[29], P. Sabbagh[1], A. Sadeghzadeh[1],

M. Sales[6,36], Z. Salhi[14], R. Santiago-Kern[29], J. Šaroun[17], T. Satogata[45], F. Saxild[9], J. Schaffran[15], J. Schefer[7], J. Scherzinger[10], M. Schild[7], B. Schillinger[12], H. Schlarb[15], P. Schmakat[12], A. Schreyer[16], W. Schroeder[14], P. Schurtenberger[10], C. Schulz[6], M. Schulz[12], W. Schweika[1,14], M. Seifert[12], G. Severin[9], R. Seviour[1], M. Sharp[1], T. Shea[1], P. Sievers[1], L. Silvi[12], G. G. Simeoni[12], W. Singer[15], P. Šittner[46], R. Sjöholm[1], N. Skar-Gislinge[13], S. Skelboe[35], F. Sordo[18], J. Stahn[7], P. Staron[16], I. Stefanescu[12], F. Stefani[30], W.-D. Stein[6], R. Steitz[6], H. Stelzer[14], A. Steuwer[1], M. Störmer[16], M. Strobl[1,6], P. Stronciwilk[14], P. Strunz[17], A. Sukhanova[14], I. Sutton[1], K. Svedin[1], H. Svensson[40], A. Takibayev[1], V. Talanov[7], M. Tardocchi[23], L. Tchelidze[1], M. Telling[11], S. Terron[18], K. Theodor[35], J-P. Thermeau[20], H. D. Thomsen[27], K. Thomsen[7], A. Tibbelin[1], C. Tiemann[14], M. Trapp[6], N. Tsapatsaris[1], L. Udby[13], A. Ushakov[6], P. Van Esch[19], L. Van Eijck[21], S. van Waasen[14], A. A. Van Well[21], C. Vasi[48], E. Vassallo[23], C. Vettier[1], A. Vickery[35], N. Violini[14], M. Vitorovič[3], R. Vivanco[18], E. Vogel[15], J. Voigt[14], L. Von Moos[13], H. P. Wacklin[1], X. Wang[15], X. L. Wang[1], T. Weber[12], R. Wedberg[29], S. Weichselbaumer[12], B. Weinhorst[25], H. Weise[15], A. Weisenburger[25], P. K. Willendrup[9], R. Willumeit[16], T. Wilpert[6], A. Wischnewski[14], M. Wohlmuther[7], J. Wolters[14], R. A. Yogi[29], L. Zanini[1], K. Žagar[3], K. Zeitelhack[12], C. Zendler[6], R. Zeng[1], V. Ziemann[29], M. Zoppi[49], A. Zugazaga[18].

[1]European Spallation Source
[2]ÅF Consult
[3]Control System Laboratory
[4]Royal Holloway, University of London
[5]Commissariat à l'Énergie Atomique et aux énergies alternatives
[6]Helmholtz-Zentrum Berlin für Materialien und Energie
[7]Paul Scherrer Institut
[8]Linköping University
[9]Technical University of Denmark
[10]Lund University
[11]Science and Technology Facilities Council
[12]Technische Universität Mnchen
[13]Københavns Universitet
[14]Forschungszentrum Jülich
[15]Deutsches Elektronen-Synkrotron
[16]Helmholtz-Zentrum Geesthacht
[17]Nuclear Physics Institute ASCR, Řež
[18]European Spallation Source – Bilbao
[19]Institut Laue-Langevin
[20]Institut de Physique Nucléaire
[21]Delft University of Technology
[22]Institute for Energy Technology
[23]Consiglio Nazionale delle Ricerche – Milano
[24]Istituto Nazionale di Fisica Nucleare
[25]Karlsruhe Institute of Technology
[26]Laboratoire Léon Brillouin
[27]Aarhus University
[28]Milano-Bicocca University
[29]Uppsala University
[30]Helmholtz-Zentrum Dresden-Rossendorf
[31]Sincrotrone Trieste S.C.p.A. di interesse nazionale
[32]École Polytechnique Fédérale de Lausanne
[33]Mid Sweden University
[34]Lunds Tekniska Högskola
[35]Niels Bohr Institute
[36]Copenhagen University
[37]Rheinisch-Westfälische Technische Hochschule Aachen
[38]University of Southern Denmark
[39]Slovak University of Technology, Bratislava
[40]The MAX IV Laboratory
[41]University of Tartu
[42]Czech Technical University in Prague
[43]Institute of Nuclear Techniques – Budapest
[44]Centrum výzkumu Řež s.r.o.
[45]Thomas Jefferson National Accelerator Facility
[46]Institute of Physics of the ASCR, Prague
[47]IHEP – Protvino
[48]Consiglio Nazionale delle Ricerche – Messina
[49]Consiglio Nazionale delle Ricerche – Firenze

Chapter 2

Neutron Science and Instruments

Chapter abstract

Summary: This chapter describes the uses of neutron scattering techniques, their place in the wider science landscape, and the ways in which they complement other experimental techniques. It discusses ESS's strengths in studying and understanding complex materials and presents a reference suite of 22 instruments selected to illustrate capabilities and scientific impact. The chapter also describes the multi-faceted research infrastructure that will surround the facility and enhance its productivity. While the publication of this report marks the end of the design phase for the accelerator and target station, the design phase for the neutron instrument suite will continue past 2020, when the final two instrument concepts are slated for selection. The instruments that will be built are therefore likely to be quite different from the reference suite described here. The phased instrument selection and design process will make it possible to respond flexibly and creatively to changing research needs and to take advantage of evolving technology.

Neutron science makes it possible to explore the complexity of condensed matter, furthering both technological progress, and humanity's understanding of nature. While no single probe can cover the whole span of time and length scales required for scientific enquiry, neutrons are a crucially important research tool. Neutron scattering techniques can, among other things, probe the molecular basis of superconductivity, guide the development of new materials or "look inside" an operating car engine.

ESS will push the frontiers of neutron science due to its capabilities in two key areas: Its unique characteristics as a neutron source, and an integrated scientific and computing infrastructure. It will be able to study a broad range of structures and time scales, offering neutron beams of unparallelled brightness, delivering more neutrons than the world's most powerful reactor-based neutron source with higher peak intensities than other spallation sources. Its user infrastructure will include sample preparation, characterisation, and specialised synthesis laboratories; detector and sample environment systems; and information technology and computational support designed for a broad range of disciplines.

State-of-the-art neutron scattering instruments depend on sophisticated hardware components, such as choppers, detectors, neutron guides, advanced neutron optics and sophisticated shielding. Progress in defining and developing these technologies is described here, and is illustrated by a science-driven, 22-instrument reference suite that matches the capabilities of individual instruments to specific areas of societal, scientific and technological interest.

Software and data management infrastructure will harness the scientific potential of the instruments and their sophisticated technology, integrating the control of each neutron instrument and its sample environment with the processing, real-time visualisation, analysis and preparation for publication of the data. This infrastructure also will provide for permanent storage and public access to the data, and will make neutron techniques more accessible to researchers from fields that do not have long histories using these tools, but for which neutrons hold significant promise of yielding new insights.

quantum states of neutrons in the gravitational field are interesting topics for related experiments at ESS. Many such experiments require ultra-cold neutrons, which can be efficiently produced at ESS.

Neutron bound beta decay

Neutron decay has been the subject of intense studies for many years, as it reveals detailed information about the structure of the weak interaction [193]. Using the two-body neutron β-decay into a hydrogen atom and an electron antineutrino, the hyperfine population of the emerging hydrogen atom can be investigated [194]. By investigating the spin states, beyond-Standard Model quantities can be accessed and tested [195–198].

2.3 Design drivers for the instrument suite

Based on the analysis of the science drivers in the preceding section, a number of key instrument themes have been identified, mapping the science drivers onto the inherent instrumentation advantages presented by the long-pulse concept:

1. **Flexibility.** Many of the problems that ESS will address require the measurement of structures or dynamics over several length or time scales. Being able to tailor the resolution and bandwidth of the measurement to the sample behaviour is key. The long-pulse concept is inherently advantageous for designing such flexibility into instrument performance. At long-pulse sources, the resolution is often set by controlling the opening time of a pulse-shaping chopper, instead of hard-wiring the resolution into the moderator line-shape as is done for instruments at a short-pulse source. The systematic use of repetition-rate multiplication and wavelength-frame multiplication allows the full time-frame to be used, while tailoring the bandwidth of the measurement to the requirements of each experiment.

2. **Small sample volumes.** ESS's high flux is well suited for accessing small sample volumes, particularly when combined with the latest advances in focusing optics. By designing instruments to probe smaller volumes than can be reached now, it will be possible to measure materials that are only available in small quantities, which is often the case for newly-developed materials and for biological and soft-matter systems for which the use of larger sample volumes can be prohibitively costly or time-consuming. The ability to investigate smaller volumes will also make it possible to scan for local variations across larger samples, for example when measuring systems under flow, and to reach more extreme conditions using complex sample environments, such as high pressure or high magnetic fields.

3. **Cold and bispectral neutron beams.** Cold neutrons are required to elucidate the structures and dynamics of biological and soft-matter systems, and of many types and aspects of hard condensed matter, as well. ESS's source brightness and time structure are particularly well suited to cold neutrons, providing high flux and a wide dynamic range. The dynamic range is especially important for hierarchical systems and other systems that need to be covered over multiple length or time scales. Instruments using a bispectral extraction system will be able to access an unprecedented dynamic range. The spectral brightness of thermal neutrons will also be world-leading.

4. **Polarised neutrons.** The inherent strengths of neutrons in being able to see hydrogen atoms and magnetism can be significantly enhanced by manipulating the neutron spin. This has applications throughout biology, soft matter, chemistry and physics. The use of polarised beams and polarisation analysis allows the unambiguous separation of structural, magnetic and incoherent scattering contributions. ESS's high brightness will greatly enhance the feasibility of this inherently flux-demanding technique.

Instruments optimised for a long-pulse neutron source are in many ways intermediate between those on a short-pulse source and those on a continuous source. Short-pulse instruments benefit from the high peak brightness of the short pulse, but are constrained by the need to match their requirements to the time-widths imposed by the choice of moderator. Time-of-flight instruments at continuous sources offer complete freedom to choose their time structures using chopper systems, but make it necessary to live with the inherently lower peak brightness imposed by their sources. A comparison of the peak brightnesses of

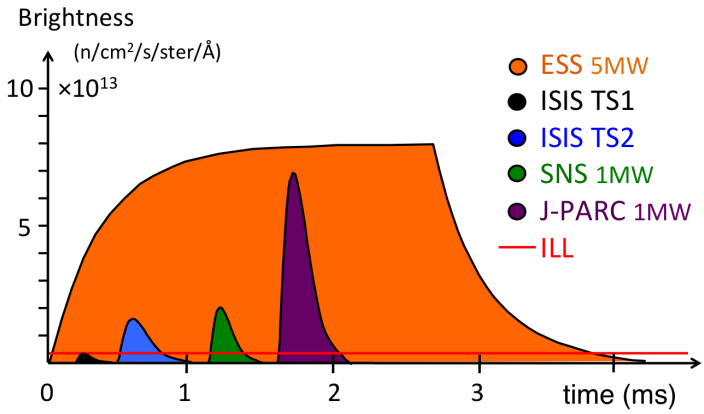

Figure 2.19: Single-pulse source brightness as a function of time at a wavelength of 5 Å at ESS, ILL, SNS, J-PARC and ISIS target stations 1 and 2. In each case, the cold moderator with the highest peak brightness is shown.

the world's leading neutron facilities is made in Figure 2.19. The peak brightness at ESS will be higher than that of any of the short pulse sources, and will be more than an order of magnitude higher than that of the world's leading continuous source. The time-integrated brightness at ESS will also be one to two orders of magnitude larger than is the case at today's leading pulsed sources.

The designs of instruments at ESS will be less limited by the time-structure of their long-pulse source than are instruments at short-pulse sources. They will benefit from a substantially higher peak brightness, combined with a time-average brightness which is much higher than that at any short-pulse source, while retaining much of the flexibility of continuous-source instruments.

Many of the instruments will be substantially longer than their counterparts at short-pulse sources. The underlying reason is the requirement for good wavelength resolution; the pulse length at the source represents the uncertainty in the emission time of the neutrons, which can be reduced compared to their time-of-flight by making the instrument longer. However, the instrument length also directly affects the bandwidth; that is, the longest wavelength that can be measured from a particular source pulse before it overlaps in time with the shortest wavelength emitted from the following pulse. Pulse-shaping choppers are an alternative method of improving wavelength resolution. Placed close to the source, they effectively reduce the pulse length, and hence the resolution, without making it necessary to increase instrument length. A large part of the optimisation of the instrument suite consists of balancing resolution and bandwidth considerations through appropriate combinations of instrument lengths and chopper systems.

2.3.1 White-beam instruments

The majority of the instruments at ESS will use a substantial part of the full white beam. Their bandwidth will be limited by their length and choice of pulse suppression, and it will be possible to tailor their resolution using a pulse-shaping chopper. They fall into two categories – large pulse width and small pulse width – depending on the required pulse width compared to the intrinsic length, $\tau = 2.86$ ms, of the neutron pulse.

Full pulse width $\simeq \tau$

SANS, spin-echo, macromolecular crystallography, and particle physics: There are seven instruments in this category in the ESS reference suite, all of which are well suited to the long-pulse time structure. They can use the full ESS pulse width and thus benefit from the high peak and time-average brightness. The ESS instruments will significantly outperform equivalent present-day instruments, due to the often unnecessarily good wavelength resolution of those instruments at contemporary short-pulse sources, and to the inherently lower peak brightness available to instruments at continuous sources.

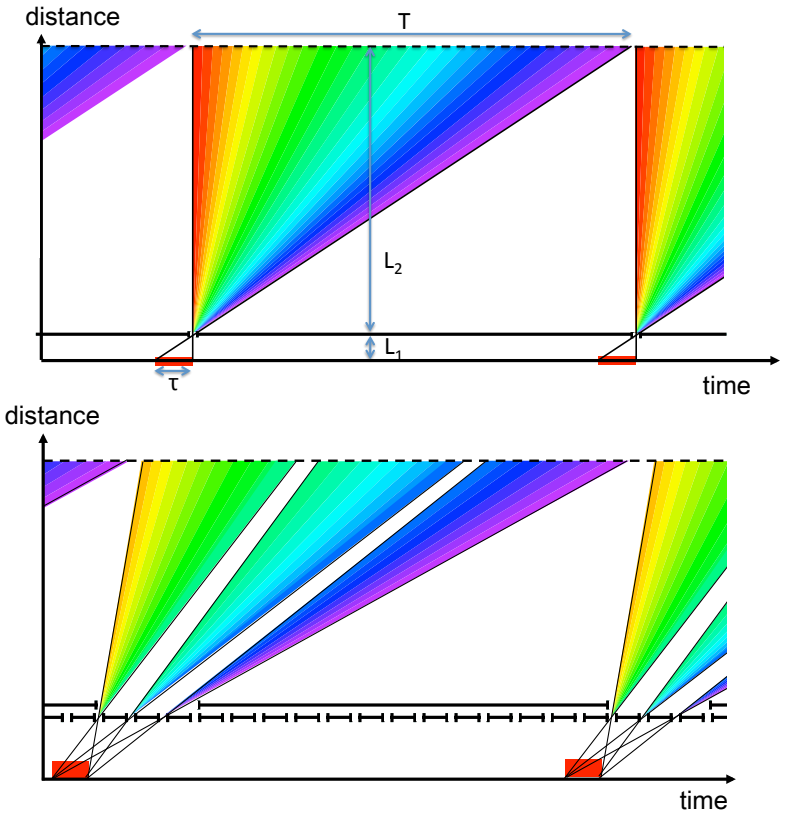

Figure 2.20: Time-distance diagrams for white-beam instruments. Top: An instrument with a pulse-shaping chopper, where τ and T are the source pulse width and repetition period, and L_1 and L_2 are the source-to-chopper and chopper-to-detector distances. The figure shows the "natural" length that fully fills the time frame without wavelength-frame multiplication for an instrument with a pulse-shaping chopper. Bottom: An instrument with a pulse-shaping chopper and triple wavelength-frame multiplication.

Flexible pulse width $< \tau$

Single-crystal and powder diffraction, crystal-analyser spectroscopy, reflectometers, backscattering, imaging: This will be the largest group of instruments at ESS, and so 11 of the 22 instruments selected for the reference suite fall into this category. These instruments employ a pulse-shaping chopper to reduce the length of the source pulse in order to achieve the required wavelength resolution. This makes them intrinsically very flexible, as it is possible to make them gain flux by relaxing resolution when appropriate. The pulse-shaping chopper is placed as close to the source as possible, which at ESS will be at the edge of the target monolith, at 6 m from the moderator. It can be seen from Figure 2.20 (top) that the pulse-shaping chopper, in addition to improving the resolution, also has the effect of reducing the bandwidth. When the instrument length after the chopper reaches 150 m, this bandwidth is sufficient to fill the full time frame (T) between adjacent pulses. The instrument length of 156 m is therefore considered the "natural" length for an instrument with a pulse-shaping chopper, which is achieved when $L_1/\tau = L_2/T$, where L_1 and L_2 are the source-to-chopper and chopper-to-detector distances, respectively. Instruments shorter than the natural length require wavelength-frame multiplication (WFM) in order to fill the time-frame, as shown in the bottom panel of Figure 2.20 for an instrument that is one third of the natural length. Detailed WFM calculations have demonstrated the feasibility of the method in simulations. Test experiments and prototyping are well under way at the time of writing.

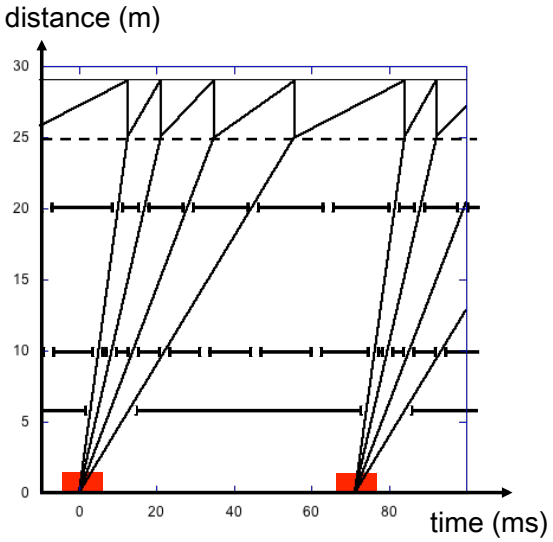

Figure 2.21: Time-distance diagram of a 25 m chopper spectrometer, using 4-fold repetition-rate multiplication (RRM) to cover incident energies from 1 to 20 meV in a single measurement.

2.3.2 Monochromatic instruments

There are three **chopper spectrometers** in the reference suite, ranging in length from 25 m to 156 m. These instruments will employ repetition-rate multiplication (RRM) in order to make full use of the long repetition period of ESS, as illustrated in Figure 2.21. The figure illustrates the need for using different frame lengths for each of the individual neutron energies selected in the incident beam. Several different chopper schemes for RRM have been identified that can achieve this effect, and whose study and optimisation are in process. In general, it is clear that both short and long instruments will be able to perform survey measurements using RRM, covering several orders of magnitude in energy scales in a single measurement, while the longer instruments will also be able to select smaller ranges of incident energy to provide very high counting rates over a smaller Q-energy area.

Only one instrument in the reference suite uses a **crystal monochromator**: The pulsed monochromatic powder diffractometer. This type of instrument is envisaged to function in a similar manner to analogous instruments at continuous sources. However, the ESS time structure allows several new modes of operation: Using the higher orders from the monochromator to provide separate data sets, similarly to what is done with RRM; separating elastic from incoherent-inelastic scattering from hydrogenous samples by time-of-flight; or performing ms-resolution stroboscopic or kinetic measurements which would make use of the very high flux on the sample for the duration of the pulse.

2.3.3 Neutron optics and transport

Considerable effort is going into the development of novel concepts for optimising the long-pulse performance, while ensuring the appropriate balance between novelty and low risk. Particular emphasis is being placed on studying chopper systems for RRM and WFM, as described in the previous two sub-sections, and also on optimising the performance of the many long guides which will be required. The work is still on-going, but it is already clear that the feasibility of transporting neutrons over very long distances is limited essentially by the cost of the guides and shielding, rather than by any fundamental or technical problem. Cold and thermal neutron guides on the order of 100 m already exist at today's reactor and spallation sources, and recent simulation work has shown that guides as long as 300 m can deliver almost perfect brightness transfer up to the sample for realistic beam divergences of both thermal and cold neutrons [199].

Many of the instruments employ an "eye-of-the-needle" concept for beam extraction, in which the relatively large area (12 cm $\times$ 12 cm) of the moderator is viewed through a small aperture at the edge of the target monolith 6 m away. When more divergence is required than such a setup can allow, a focusing

in-pile guide section is used, commonly referred to as a "feeder" section. There are several advantages to such a setup:

1. **Lower fast-neutron background.** The solid-angle acceptance for high-energy neutrons which might otherwise contribute to the background on the instrument is greatly reduced.

2. **Improved resolution and flux.** Instruments that use a pulse-shaping chopper should place it at the position of minimum beam size in order to reduce the sweep time across the beam, thus allowing shorter opening times, which in turn make it possible to reach higher resolution and allow for a more rectangular opening function, which provides a considerably higher flux than the typical triangular opening functions obtained when the sweep time is similar to the opening time.

3. **Improved Q-resolution and slow-neutron background.** By an appropriate choice of guide geometry, such as a single or two sequential ellipses, it is possible to image the beam profile and divergence at the target monolith exit on the sample. This results in a very uniform beam distribution at the sample, both in space and divergence, with clear benefits for Q-resolution. It also minimises the halo around the beam, which can be an additional source of background.

Further enhancement of the signal over noise will be achieved by designing-in suppression of fast neutrons and other sources of background, using a combination of shielding, heavy choppers and various types of kinked and curved guides. The count rates, spatial resolution, area coverage, efficiency and availability of neutron detectors are also the subject of intense study and R&D. Technical aspects associated with all the neutron technology components required for the various instruments are addressed in Section 2.7.

2.4 The reference instrument suite

A total of 22 public instruments will be built at ESS to serve the neutron user community, with the initial seven instruments coming online in 2019, and the full suite operational by 2025. To deliver the required instrument designs, around 40 instrument concepts are currently in various stages of design by ESS scientists and scientific partners around Europe. From among these concepts, a reference suite of 22 instruments has been assembled here to showcase ESS capabilities and to serve as a basis for the costing and planning of the facility. The selection of instruments in the reference suite focuses on the natural strengths of the long-pulse concept in order to maximise scientific output, while addressing a broad science base and employing state-of-the-art instrument techniques. The reference suite is not identical with the instruments that ultimately will be built.

Selection of instruments

The choice of instruments to build will take place as an ongoing process in which a number of concepts are selected every year, starting in 2013. This staged approach will allow ESS to remain engaged with the European neutron community and to choose instrument designs that are state-of-the-art and scientifically relevant when they enter user operation. As mentioned above, about 40 instrument concepts are currently under study. Other conceptual studies will be added as ideas and resources progress. As each conceptual study reaches a sufficient level of maturity, a proposal will be submitted for its construction. The proposals will be evaluated each year by review panels which will make recommendations for construction to ESS management. The evaluation criteria are scientific impact, user base and demand, instrument performance, strategy and uniqueness, technical maturity and costing. It is important to stress that the instruments that will be built have not yet been chosen. The reference suite described here does not, and cannot, represent the precise instrument suite that actually will be built, as the process for selection of instruments will run over several years and has only just begun.

Presentation of the reference suite

The instruments of the reference suite are presented in this and the following section. They can be categorised by instrument class, with the coverage of length- and time-scales accessed by each instrument class shown in Figure 2.1. A selection of the scientific areas addressed by the various instrument types is indicated in the plot, illustrating the mapping between scientific needs and instrumental capabilities. Also

shown are the analogous areas for selected complementary techniques, such as microscopy and synchrotron x-ray scattering.

Neutron imaging

Neutron imaging is a real-space technique examining the inner structure of potentially highly complex components by looking at the transmitted beam. The **multi-purpose imaging beamline** pushes spatial resolutions down to the micron range thanks to the high brightness of ESS, coupled with ongoing advances in detector technology. The pulsed nature of the source will give access to wavelength-resolved information, yielding a qualitative informational advance over the state-of-the-art today. The instrument offers its users a variety of imaging techniques for the characterisation of objects, covering cultural heritage, energy materials, magnetic phenomena and fuel cells as well as inspection of engineering components. Different imaging techniques, from traditional attenuation-based imaging to advanced dark field or Bragg edge imaging, are available with unprecedented efficiency and detail. The instrument concept takes full advantage of the flexibility made possible by the ESS time structure, allowing wavelength resolution, bandwidth and collimation to be tuned for each application.

Small angle neutron scattering

Small angle neutron scattering (SANS) provides access to the largest length scales possible with neutron scattering. SANS instruments are white-beam instruments requiring a large pulse-width, as described in Section 2.3.1, and so are perfectly adapted to the long-pulse ESS time structure. As an illustration, Figure 2.22 shows a comparison between a SANS instrument adapted to the ESS source and a present-day world-leading SANS instrument. Not only is the counting rate for the ESS instrument higher by an order of magnitude, but the Q-range covered in a single measurement is also an order of magnitude greater. There are three SANS instruments in the reference suite. The **general-purpose polarized SANS instrument** simultaneously covers the Q-range of current conventional SANS instruments, 10^{-3} Å^{-1} to 0.1 Å^{-1}, using multiple detector banks. It is particularly powerful when high resolution is needed, and for industrial processes requiring bulky sample environment. The instrument will have flexible resolution and bandwidth and will make available the option of reaching very low Q, possibly using specialised optics for accessing the very-small-angle regime. The **broadband small sample SANS instrument** is a shorter instrument and covers a very large Q-range in a single measurement. It is a lower-resolution instrument optimised for very high counting rates and smaller samples. The key science areas are in soft matter and

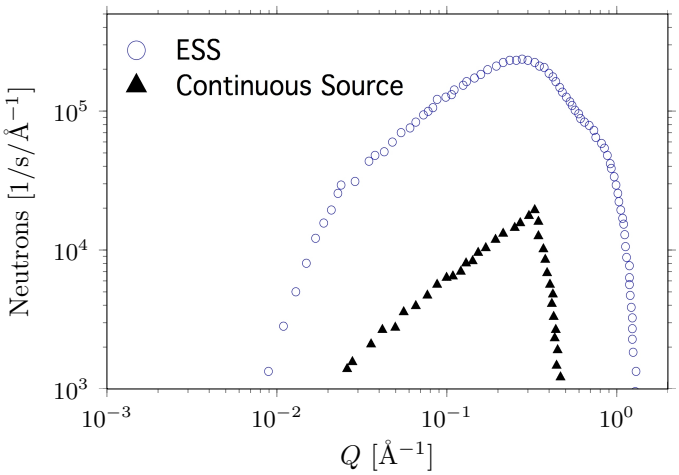

Figure 2.22: A comparison of the count rate obtained as a function of Q on a SANS instrument at ESS and on a world-leading SANS instrument at a continuous source. The curves were generated using simulations of isotropic scattering from 1 mm of water. Using the entire long pulse and cold spectrum, SANS at the ESS gains as neutrons of all wavelengths contribute to scattering at all Q values, whereas at a continuous source a narrow wavelength band must be selected using a velocity selector.

biology. The high counting rate will also make it a very powerful instrument for parametric studies, e.g. temperature, electric and magnetic fields, and pH. While the SANS community today is primarily focused on bulk samples, it is expected that the high source brightness of ESS will allow many of these studies to be extended to surface structures. The **surface scattering instrument** will probe the lateral topology of surfaces with a controlled penetration depth. By adjusting the incident angle of the beam, it will be possible to measure the structure of horizontal sample surfaces, opening grazing-incidence SANS to the study of free liquid interfaces, an area which is only just beginning to be explored at existing facilities.

Neutron reflectometry

Neutron reflectometry is used to probe the structure of surfaces and interfaces in the Å to micron range. The **horizontal reflectometer** uses an inclined beam to measure horizontal surfaces, particularly liquid-air interfaces, covering the full Q-range of interest without moving the sample. The instrument is optimised for very fast measurements with moderate resolution, with particular applications for kinetics of structural changes in biological systems and soft matter. The **vertical reflectometer** is a versatile instrument for measuring solid interfaces with high resolution and on small samples. It employs a novel double-elliptical mirror setup which allows flexible tailoring of the beam divergence to the resolution and background requirements of the samples. The beam size can be adapted to the measurement of mm-sized samples which are inaccessible on current instruments.

Powder diffraction

Powder diffraction is covered by five instruments in the reference suite. ESS's unique pulse structure makes possible a very wide dynamic range, while the inherent long-pulse flexibility allows the resolution to be tuned to the requirements of each experiment by adjusting the opening time of the pulse-shaping chopper. This capability is illustrated in Figure 2.23, which shows the resolution and intensity of a range

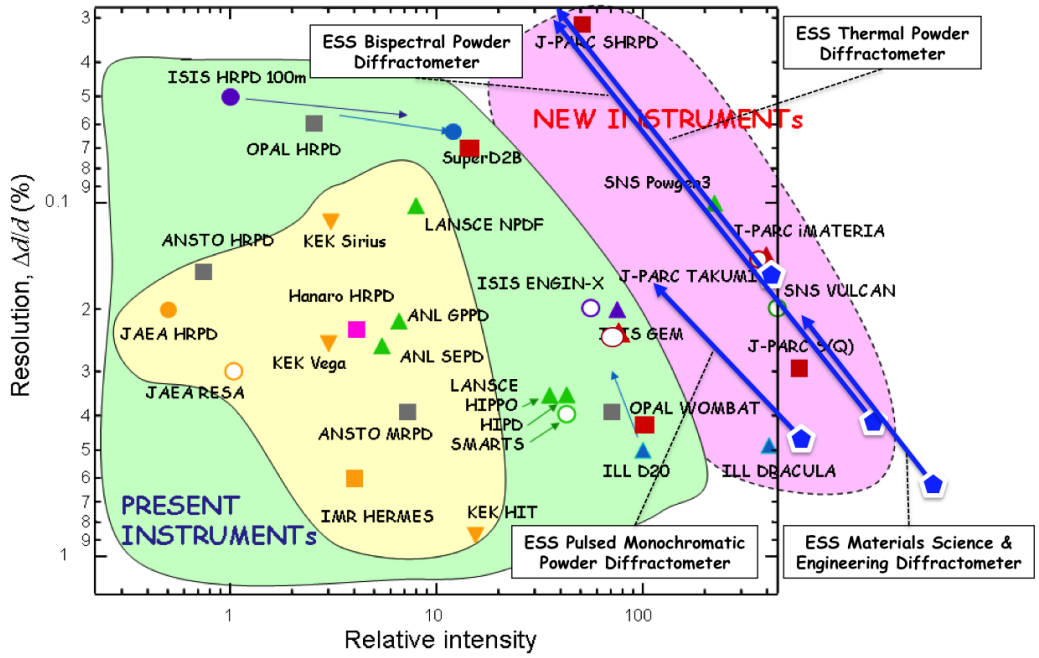

Figure 2.23: Performance of powder diffractometers at leading large-scale facilities (adapted from Kamiyama [200]) with the expected performance of reference suite diffractometers marked as blue pentagons with extended arrows to illustrate the count rate/resolution flexibility afforded by tuning the pulse width for the time-of-flight diffractometers, or the monochromator takeoff angle for the pulsed monochromatic diffractometer. The instruments in the area labelled "New Instruments" are currently in various stages of commissioning and have not yet reached the performance shown here.

of neutron powder diffractometers at leading large-scale facilities around the world. The performance of current instruments and their specialisation for high flux or high resolution are shown by various symbols, while continuous lines show how instrument performance can be selected depending on the needs of the experiment, for four of the five powder diffractometers in the reference suite. (The extreme conditions instrument is not shown.) The reference suite instruments match the projected best performance of today's new instruments, though there are limitations in comparison to short-pulse sources at large Q, which do not appear in such a figure.

The **thermal powder diffractometer** covers the core crystallography and *in situ* processing science case for thermal neutrons up to a Q_{max} of around 25 Å^{-1}. The pulse-shaping chopper allows the wavelength resolution to be matched to experimental requirements over a very wide range, in the best case achieving a resolution of $< 0.01\%$. The **bispectral powder diffractometer** can access longer wavelengths and hence, larger d-spacings in backscattering. It is well suited for powder magnetic structure determination, larger unit cell powder crystallography and *in situ* experiments in the intermediate Q range ($Q_{max} <$ 13 Å^{-1}). The **pulsed monochromatic powder diffractometer** is a high-throughput instrument for *in situ* chemical processing, crystallography, pole figures, high time-resolution kinetics and hydrogen-containing materials, with the option for variable resolution inelastic scattering mapping. It uses a set of crystal monochromators with access to a wide range of takeoff angles to tune the accessible Q range, flux and instrument resolution. The **materials science & engineering diffractometer** allows users to study mechanical and micro-structural properties, texture, phase transformations and kinetics in engineering and functional/smart materials. Dedicated sample environments allow a wide range of conditions to be probed. Structural studies include the determination of residual stresses in engineering materials and components, an important area in welding and joining R&D. The **extreme conditions instrument** is built around bulky, complex sample environments (high pressure, high magnetic field) and the limitations that imposes on detector coverage and geometry. It is a multi-role instrument to perform diffraction, spectroscopy, SANS and imaging experiments. For all the diffraction instruments, the resolution and bandwidth can be tailored to each application.

Single-crystal diffraction

Single-crystal diffraction is required for solving complex or large unit cell structures and profits largely from the the ESS long pulse structure. The **single-crystal magnetism diffractometer** has a polarised incoming beam with optional full polarisation analysis. It is optimised for the determination of complex magnetic structures, spin density distributions, local susceptibility measurements and diffuse scattering. The **macromolecular diffractometer** is dedicated to biological crystallography and is optimised for sub-millimetre single-crystal samples with large unit cells. The flux increase made possible by the use of the full pulse allows the study of systems such as membrane proteins which currently cannot be addressed with neutrons. The objective is to bring neutrons into the mainstream of protein crystallography, currently addressed almost exclusively by synchrotron light sources.

Time-of-flight and crystal spectroscopy

Time-of-flight and crystal spectroscopy is carried out by two types of instruments: Chopper spectrometers and crystal-analyser instruments. There are three chopper spectrometers in the reference suite which are designed for optimised RRM for all experiments, as described in Section 2.3.2, using sophisticated multiplexing chopper systems. The range of incident energies for these types of instruments will be adapted to the range of time scales that need to be covered, while the spacing between adjacent incident energies will be adjusted to cover the width of the inelastic scattering. Due to the very high ESS peak brightness, the flux of each individual wavelength frame incident on the sample will be significantly higher than on today's world-leading chopper spectrometers. The additional pulses arising from the RRM system will bring the total flux on the sample up to more than an order of magnitude greater than what is possible today while simultaneously probing a far larger dynamic range in both Q and energy. The **cold chopper spectrometer** is specialised for cold neutrons and the measurement of single-crystal samples. It is optimised for low background and high resolution and is thus ideally suited for probing weak signals and collective excitations. The **bispectral chopper spectrometer** provides a one-shot measuring technique for covering dynamics over a very wide simultaneous energy range of $0.1 - 100$ meV. It is a wide-mapping instrument optimised for quasi-elastic scattering on small samples, allowing more than three orders of magnitude in fluctuation

times to be covered in a single measurement. The **thermal chopper spectrometer** is a high-resolution, narrow-bandwidth instrument for fast dynamics. It allows incident energies up to 150 meV with flexible resolution both in energy and Q. The beam optics are tunable, allowing efficient focusing for small samples as well high Q-resolution single-crystal measurements. The **cold crystal-analyser spectrometer** uses graphite crystals to cover a quasi-continuous range of scattering angles in the horizontal plane. This a high-flux instrument, particularly well suited for measuring samples in constrained horizontal geometries that are imposed by high-field or high-pressure sample environment. The **instrument for vibrational spectroscopy** will have variable resolution to allow measurements up to 300 meV, with a variable energy resolution down to 2% with very little energy-dependence. The instrument characteristics are well suited to the mapping of molecular vibrational modes and collective excitations of hydrogenated materials in heterogeneous catalysis, energy storage systems and hydrogen-bonded scaffolds in pharmaceuticals.

Backscattering

The **backscattering spectrometer** provides access to a unique combination of high energy resolution, intermediate Q, and large dynamic range. It uses Si 111 and Si 311 analyser crystals arranged in near-backscattering geometry, and the flexible chopper cascade is matched to the source time structure to allow a continuous variation of the energy resolution between 2 μeV and 300 μeV together with a variable dynamic range down to about 1 meV. ESS's low repetition rate provides the instrument with an unparallelled dynamic range that is perfectly suited for studies of localised relaxational atomic motions with overlapping collective long-range motions, as well as quantum-mechanical tunnelling. It addresses all disciplines of condensed matter from physics to chemistry and biology via soft matter and energy materials.

Spin-echo spectroscopy

Spin-echo spectroscopy reaches the longest time scales accessible with neutrons, allowing the measurement of polymer and protein dynamics, membrane fluctuations, confined liquids, micro-emulsions and magnetism. This type of instrument will accept the full pulse width of ESS, giving rise to a very large improvement in performance compared to the best instruments available today. The **high-resolution spin echo spectrometer** provides the highest energy resolution available in the reference suite. It measures dynamics, predominantly of large-scale structures, with fluctuation times of up to 1 μs, covering a dynamic range of six decades. The **wide-angle spin echo spectrometer** provides the bridge in fluctuation times between the backscattering and cold chopper spectrometers at one end, and high-resolution spin-echo spectrometers at the other. By covering a large range of Q, it is able to probe nanosecond fluctuations over many length-scales simultaneously, while the large solid-angle coverage of the analysers and detectors provides a counting rate two orders of magnitude higher than any comparable instrument today.

Particle physics

Particle physics is covered by the **fundamental and particle physics beamline**, which addresses precision tests of the Standard Model, and searches for new interactions and symmetries. The range of Standard Model tests and searches that such a beamline could competitively address is wide. Therefore, the instrument is designed to be highly configurable, analogous to similar beamlines at current sources.

2.4.1 A balanced reference suite

Table 2.1 provides an overview of the reference suite instruments, including instrument lengths and the main science drivers relevant to each instrument. The reference suite has been chosen to cover a broad range of science, as well as a broad range of instrument types and degrees of specialisation and complexity. Some instruments have a narrowly focused science case, while others address a diverse user community. Some are workhorse instruments, which will have very high throughput and a limited degree of configurability, while others will need to be configured specifically for each experiment, requiring strong scientific collaborations between users and ESS scientific staff. In all cases, the instruments will be accessible by both non-expert and expert users, placing strong requirements on beam access, staff quality and software.

Instrument length is a key performance driver, determining constraints on bandwidth and resolution. It also drives the instrument layout on the ESS site, which is shown in Figure 2.24 at the beginning of Section 2.5. Due to the design of the moderator-reflector assembly and the beam extraction within the

Instrument name	**Moderator to sample distance** [m]	**Sample to detectors distance** [m]	**Science drivers**
Multi-purpose imaging	50	10	LIF, SOF, MAG, ENG
General-purpose polarized SANS	30	20	MAG, SOF, CHE, NRG
Broadband small sample SANS	20	10	SOF, LIF
Surface scattering	30	15	SOF, LIF, CHE, MAG
Horizontal reflectometer	27	3	SOF, LIF, CHE
Vertical reflectometer	52	6	MAG, CHE, NRG, SOF
Thermal powder diffractometer	156	2	CHE, NRG, ENG, MAG
Bispectral powder diffractometer	75	1.5	MAG, CHE, NRG, ENG
Pulsed monochromatic powder diffractometer	46+4	2.5	CHE, NRG, MAG
Materials science & engineering diffractometer	156	2	ENG, CHE
Extreme conditions instrument	156	4	ENG, MAG, CHE
Single-crystal magnetism diffractometer	156	1	MAG, CHE
Macromolecular diffractometer	156	1	LIF
Cold chopper spectrometer	156	4	LIF, CHE, MAG
Bispectral chopper spectrometer	25	4	LIF, SOF, CHE, MAG
Thermal chopper spectrometer	156	6	CHE, NRG, MAG
Cold crystal-analyser spectrometer	156	3	CHE, NRG, MAG, ENG
Vibrational spectroscopy	60	1	CHE, NRG, MAG
Backscattering spectrometer	156	5	LIF, SOF, CHE
High-resolution spin echo	30	5	LIF, SOF, CHE, NRG
Wide-angle spin echo	50	3.5	NRG, MAG, LIF, SOF
Fundamental & particle physics	70	30	FUN

Table 2.1: Instrument names and lengths, as shown in Figure 2.24. For the *pulsed monochromatic powder diffractometer*, the first distance is shown as a two-term sum, indicating the distance from the moderator to the monochromator and then to the sample. The science drivers for each instrument are listed in order of decreasing importance. The acronyms are as follows. LIF: Life science, SOF: Soft condensed matter, CHE: Chemistry of materials, NRG: Energy research, MAG: Magnetism and superconductivity, ENG: Engineering materials and geosciences, ARC: Archaeology and heritage conservation, FUN: Fundamental and particle physics.

target monolith, all beamlines have the freedom to view either a cold or a thermal source, or a combination of the two. All beamlines also will view roughly the same time structure, as the long-pulse time structure of the proton beam means that there is no need for decoupled or poisoned moderators, such as are used at short-pulse sources. The choice of beam port for each instrument is therefore primarily driven by operational convenience and the desire to save cost, with little or no compromise on performance.

The nine instruments in the reference suite which are 156 m long are housed together in the west experimental hall, where they can comfortably be accommodated next to each other with 5° of beamline separation. Instruments between 50 m and 80 m long are in the south experimental hall, while the short ($<$ 50m) instruments are arranged in two sectors – one each in the north and east experimental halls – that are adjacent to the incoming proton beam, where the fast-neutron background is expected to be the lowest. The distribution of instruments in the north and east halls has been determined first by the need to allow them sufficient lateral space for shielding and convenient operation (as has been done for all the instruments), and then by the need to separate the spin-echo spectrometers from instruments that are likely to need large superconducting magnets for their sample environment. The floor of the hall in the north sector, where the spin-echo and non-magnetic instruments are housed, has also been made 1 m lower than that of the other halls, in order to provide a magnetically cleaner environment for the spin-echo instruments. The grey area around the target monolith in Figure 2.24 shows the common bunker in which the first sections of the guides outside the target monolith are housed. This allows for an effective shielding assembly enclosing the guides, choppers and optical elements near the monolith.

2.5 Catalogue: The reference suite

This catalogue presents the 22-instrument reference suite. Its layout is shown in Figure 2.24, while the instrument names and lengths are summarised in Table 2.1. The reference suite has been assembled to showcase the scientific and technical capabilities that ESS is expected to have, and also to provide a basis for costing and planning the facility. It does not represent the precise instrument suite that will actually be built, since the process of choosing those instruments has only just started at the time of writing and will continue until 2020. The reference instrument suite is discussed at length in Section 2.4.

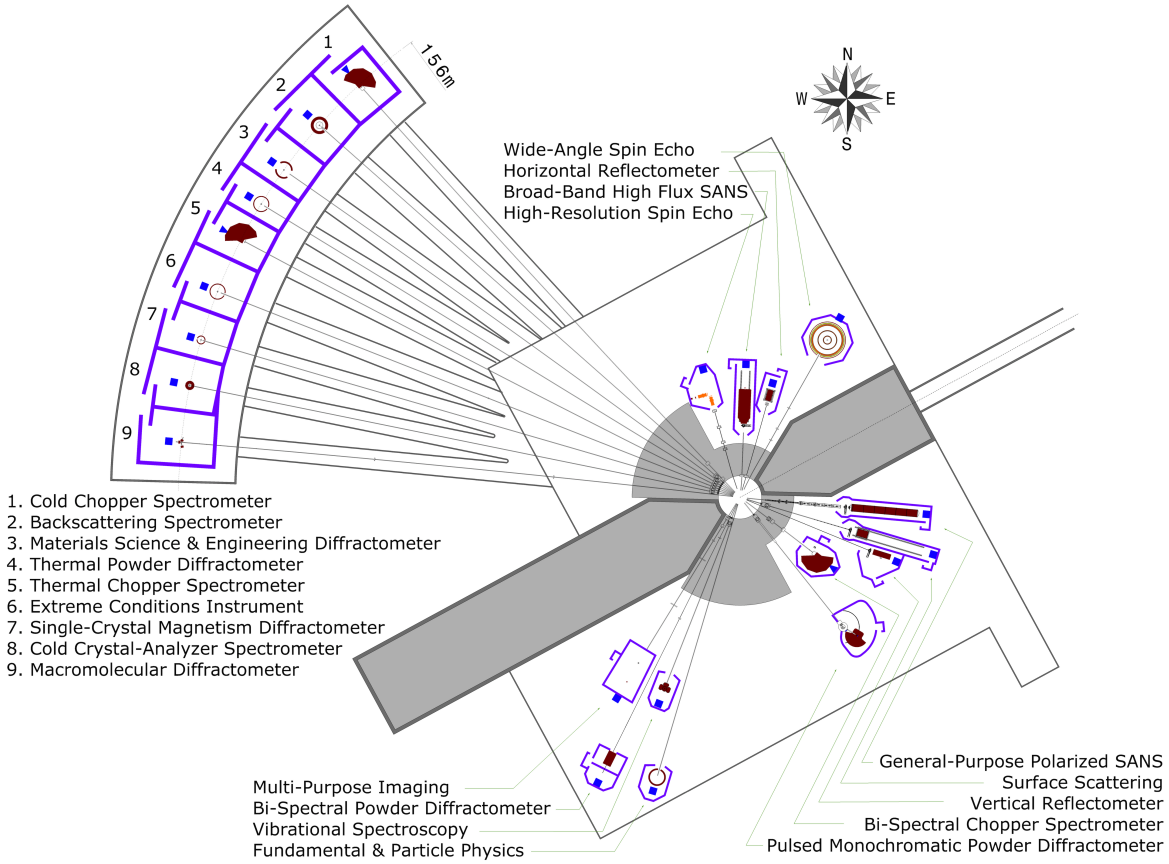

Figure 2.24: Neutron beamline and instrument layout of the reference instrument suite.

Thermal Powder Diffractometer

Thermal Powder Diffractometer

Structure & in-situ processing
Catalytically-active materials
Novel materials
Health & pharmaceuticals
Fuel cells
Battery materials
Gas storage materials
Solar cells & photovoltaics
Engineering & geosciences
Archeology & heritage conservation

This is a thermal neutron, time-of-flight diffractometer with variable wavelength resolution ($\Delta\lambda/\lambda$ from $\approx$ 0.02% to 5%), provided by a pulse shaping chopper, and a useful Q_{max} of $\approx$ 25 Å^{-1} for medium and high-resolution powder crystallography. The usable wavelength band in the time-frame is 1.9 Å (normal operational mode λ = 0.5 - 2.4 Å) and is optimised for shorter wavelengths for structural characterisation and *in situ* processing when extended Q-data are required. The flexibility of the instrument allows a wide-range of materials to be investigated. While the instrument is optimised for thermal neutron powder diffraction, it can also perform single crystal diffraction measurements in a quasi-Laue mode.

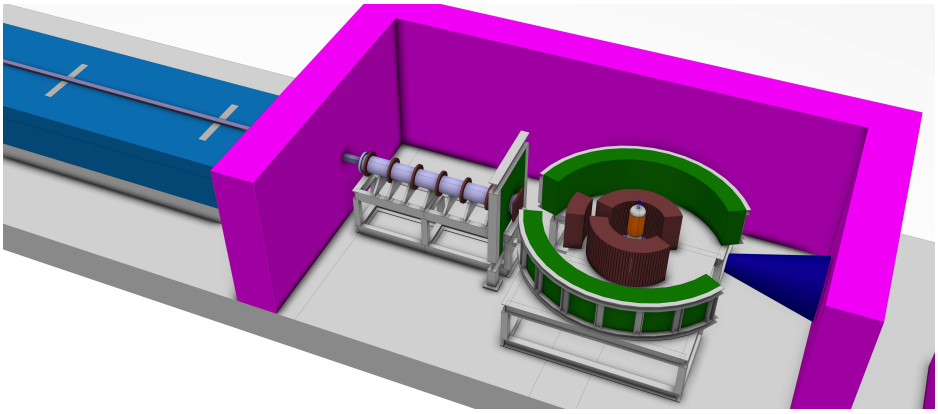

Instrument Description

The beam transport system is based on a kinked double ellipse geometry, in order to avoid line-of-sight from the thermal moderator. A pulse shaping chopper allows the wavelength resolution to be tuned from 0.02% to 5% for the central wavelength of 1.45 Å. The guide is optimised for the transport of short wavelength neutrons, giving the standard operational mode wavelength band of 0.5 - 2.4 Å, ideal for small to intermediate unit cell crystallography. Using short wavelengths also avoids problems with the prompt pulse for almost the entire wavelength band. The wavelength band can be tuned across the range available from the thermal moderator (0.5 - 6 Å) but, for longer wavelength bands, the *bispectral powder diffractometer* is preferred. Vertical focussing of the guide means that cylindrical sample geometry is preferred. A large cylindrical 2-D detector ($10° < 2\theta < 160°$) with a height of at least 1 m and high spatial resolution (2 mm in the scattering plane, 5 mm in the vertical plane) matches the sample geometry, allowing both angle dispersive and time-of-flight information to be collected across a wide angular range. A backscattering detector array is also envisaged for high resolution studies. The ability to tune the instrument resolution to the experimental system is a key advantage of the ESS suite. The combination of the very flexible instrument set-up, event mode data acquisition and optimised sample environments are key to the impact of this instrument across a broad range of science. Additionally, the cylindrical detector geometry will allow single crystal data collection using the quasi-Laue technique but the instrument is not optimised for this purpose. Polarisation of the incoming beam is also foreseen as an upgrade path.

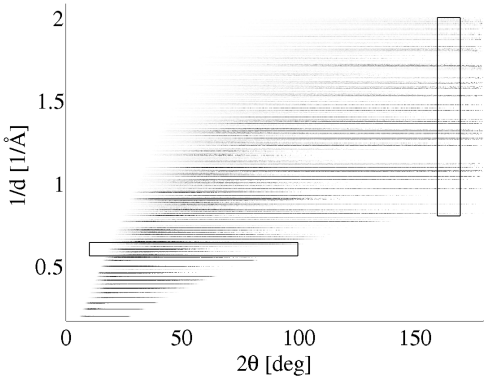

Simulation of powder diffraction data for a NaCaAlF standard for a two-dimensional detector over the full detector scattering angle.

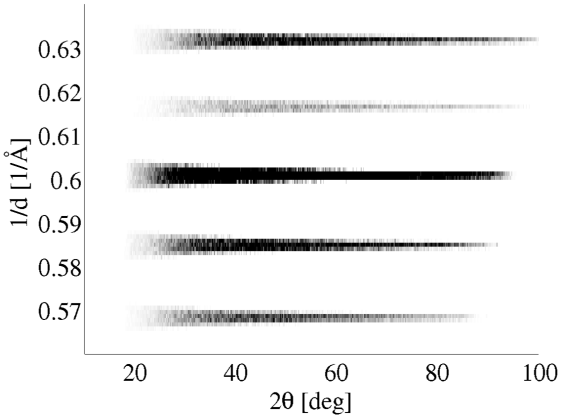

Bragg diffraction peak width as a function of detector scattering angle showing the variation in the instrument resolution function.

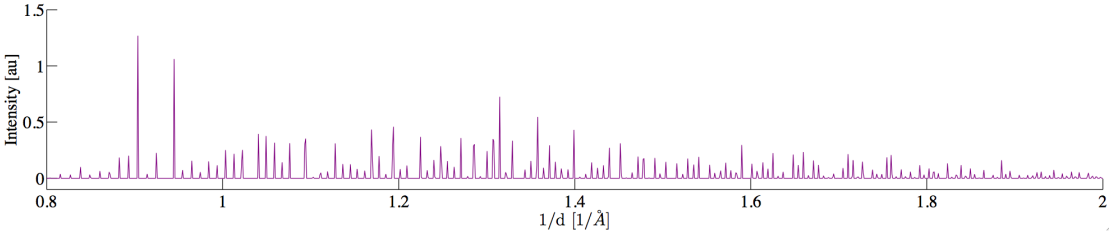

Standard one-dimensional powder diffraction pattern obtained by summation of the data within the box at high scattering angle (160-170°) in the above left figure.

Diffraction data is simulated above assuming a cylindrical detector geometry and plotted in 1/d in order to illustrate the instrument characteristics (Figure top left). Detector summing over a restricted scattering angle range to give one-dimensional data is the usual method to produce data for Rietveld refinement (Figure bottom) but summing the data into one-dimension across a larger detector angle leads to broader Bragg reflections (Figure top right) and the loss of information due to increased peak overlap. The goal is to develop multi-dimensional Rietveld analysis software to refine the full detector image, where the variation in the instrument resolution as a function of detector scattering angle can be modelled.

Instrument Parameters	
Moderator	thermal
Moderator - Sample distance	156 m
Wavelength Range	0.5 - 2.4 Å in standard mode; full range 0.5 - 6 Å
Wavelength Resolution	≈0.02% (10 μs) - 5% (full pulse) at λ = 1.45 Å
d-range	0.25 - 14 Å in standard mode; full range 0.25 - 35 Å
Q-range	0.5 - 25 Å^{-1} in standard mode
Beam Size at sample	full beamsize 2 × 1 cm^2 with optional additional focussing (0.5 × 0.5 cm^2)
Sample to Detector distance	wide angle bank - 2 m, backscattering bank - up to 2.5 m
Detector Technology	Boron-10 or wavelength shifting fibre, spatial resolution ≈ 2 mm in scattering plane and 5 mm in vertical plane, efficiency > 50% (for $\lambda > 1$ Å)
Detector Coverage	$10° < 2\theta < 160°$ on both sides with separate backscattering detector array from 160-180°

Bispectral Powder Diffractometer

Bispectral Powder Diffractometer

Novel &materials
Structure & in-situ processing
Catalytically-active materials
Fuel cells
Battery materials
Solar cells & photovoltaics
Novel states of matter
Engineering & geosciences
Archeology & heritage conservation
Earth & environmental sciences

This time-of-flight diffractometer combines the flux of a thermal and coupled cold moderator for an efficient use of a broad wavelength band with flexible time resolution, which makes it ideal to determine larger units cells of complex materials, or magnetic superstructures simultaneously with the atomic structure including light elements. The instrument is 75 m long and uses two wavelength frames with a total bandwidth of 3.8 Å. The choppers will typically be phased to select 0.8 to 4.6 Å, yielding a Q_{max} of 15 $Å^{-1}$ and can be tuned to provide wavelengths up to 10 Å. The pulse shaping chopper system provides a flexible time resolution and efficient wavelength frame multiplication, in addition to the ability to shift the wavelength band and to suppress the background of the prompt pulse. The beam divergence and detector resolution are also well adapted to single crystal diffraction studies. With an optional monochromating chopper, the instrument can be converted to a special multispectral spectrometer optimized for small samples and low divergence.

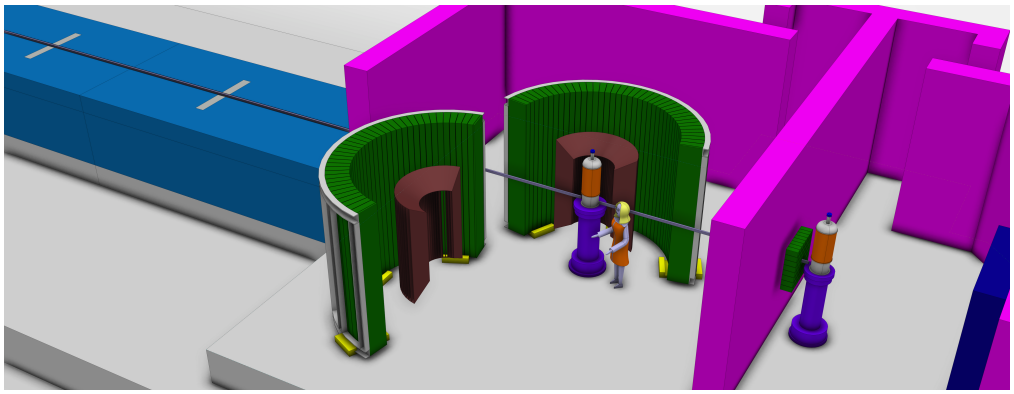

Instrument Description

The bispectral extraction system, consisting of a super-mirror stack inserted in the monolith, allows the instrument to view simultaneously both the thermal and cold moderators. The pulse shaping chopper (PSC) uses the eye-of-the-needle concept in both space and time and is placed at the first focal point of the double elliptic guide system, mirroring the phase space density at the PSC to the sample position.

The final section of the guide will contain exchangeable parts to vary the beam size and divergence at the sample position. The detector system covers a large solid angle with 2D position sensitivity at 3 mm spatial resolution and will likely be composed of units based on wavelength shifting fiber scintillation detectors. A cylindrical detector geometry with the cylinder axis along beam and a dedicated backscattering detector are foreseen. The measurements provide angle and wavelength dispersive data for powder diffraction, as illustrated for the *Thermal powder diffractometer*, and multi-dimensional Rietveld analysis software, currently under development, will be used for data analysis. The beam is further guided out of the experimental section to a second station, which can use the transmitted beam for neutron Laue characterization and test experiments.

Time resolution options

$\delta t(\lambda_1)$	$\delta t(\lambda_1 + 1.9\text{Å})$	(Hz) : (Hz)
27.5 μs	82.5 μs	84 : 70
60.6 μs	181.8 μs	45 : 28
151.5 μs	353.5 μs	28 : 14
227.4 μs	606.3 μs	14 : 14
378.8 μs	681.8 μs	0 : 14

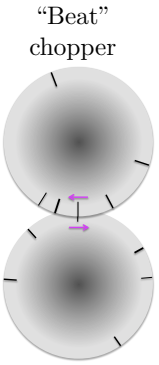

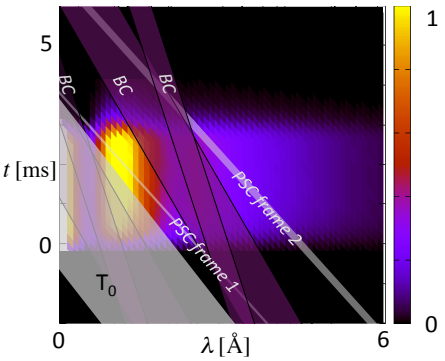

The pulse shaping chopper consists of two counter-rotating discs of 75 cm diameter rotating with different multiples of the source frequency to produce short pulses as a 14 Hz"beat" of the ESS source frequency. The choice of slit pair provides a large flexibility in time/wavelength resolution: for high resolution backscattering diffraction $\delta t/t$ can be tuned to the range of 10^{-3} to 10^{-4} and can be relaxed to increase flux in fine incremental steps up to 1% resolution. The acceptance diagram (right-hand figure) shows the selection of the chopper system from the bispectral moderator distribution. The stripes indicate the opening time of the PSC and the closing time for the Bandwidth Control (BC) choppers and the T_0 chopper. The BC choppers remove the background from the long time decay of the source pulse, while a massive T_0 chopper suppresses the prompt pulse. For a typical medium resolution setting of $\delta d/d \sim 0.005$ at $2\theta = 90°$, a pulse width of 100 to 600 μs, depending on wavelength, matches the divergence given by the instrument geometry and detector specification. The wavelength band can easily be shifted by phase-shifting the choppers to match the required Q-range.

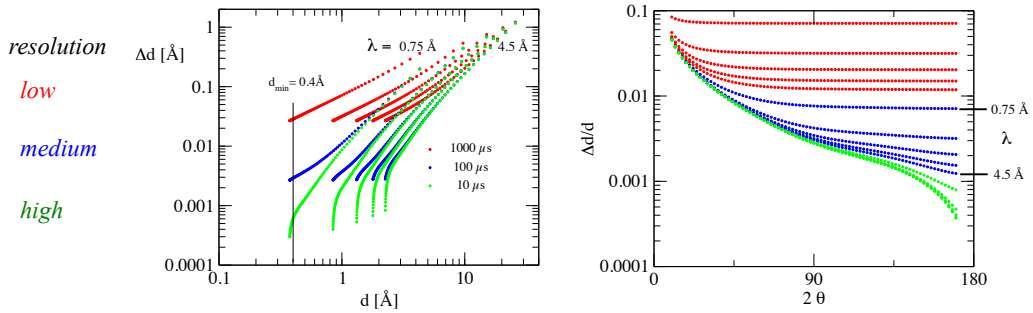

Instrument Parameters	
Moderator	bispectral cold/thermal
Moderator - Sample distance	75 m
Wavelength Range	0.8 - 10 Å
d-range	0.4 - 30 Å
Q-range	0.2 -15 Å^{-1}
Beam size at sample	full beamsize 1 × 1 cm^2 with optional focussing (0.5 × 0.5 cm^2)
Background suppression	T_0 chopper
Sample to Detector distance	about 1.5 m
Detector Technology	Wavelength shifting fibre, Boron-10 blade, or $^{10}BF_3$ volume spatial resolution 3 mm, efficiency > 50% (for $\lambda > 1$ Å)
Detector Coverage	$10° < 2\theta < 170°$

Bispectral Powder Diffractometer

Pulsed Monochromatic Powder Diffractometer

Pulsed Monochromatic Powder Diffractometer

Structure & in-situ processing
Fuel cells
Battery materials
Gas storage materials
Solar cells & photovoltaics
Catalytically-active materials
Novel materials
Health & pharmaceuticals
Novel states of matter
Engineering & geosciences
Paleoclimatology & climate change
Earth & environmental sciences

The instrument is a thermal neutron, crystal monochromator diffractometer with variable $\Delta d/d$ resolution from $> 1\%$ to $< 0.1\%$ covering a Q-range up to ≈ 12.5 Å^{-1}. The complete diffraction pattern over a scattering angle of 160° can be obtained in a few seconds, ideal for parametric investigations, and the out-of-plane scattering angle coverage is matched to the requirements of complex sample environments. The variable take-off angle to the monochromators (continuous from 40° to $\approx$ 130°) increases the flexibility of the instrument, allowing trade of flux for resolution. Several additional modes of operation are foreseen to take advatnage of the pulsed source: simultaneous multiple wavelength data collection, the possibility to separate the inelastic incoherent scattering contribution from hydrogenous materials and fixed incident energy inelastic scattering mapping.

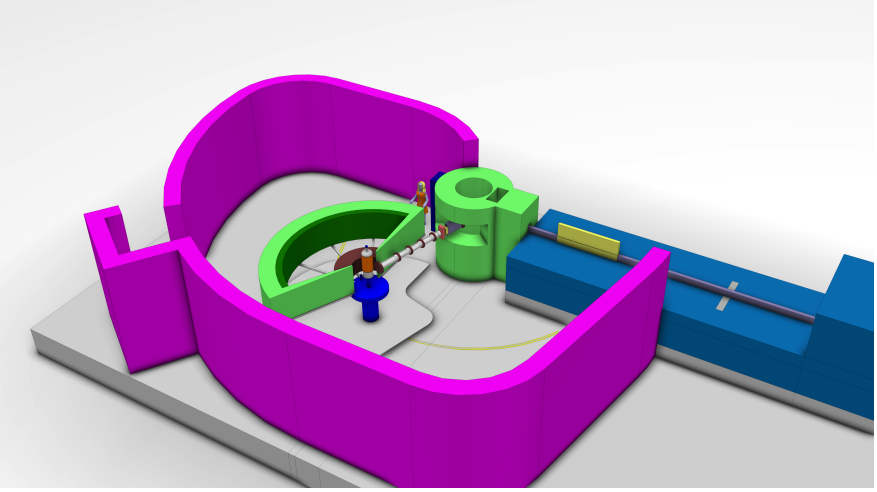

Instrument Description

The beam transport system will be optimised for thermal neutrons and starts with an in-pile feeder focussing through a 4 cm × 4 cm aperture at 6 m. A half-elliptical guide section (horizontal and vertical directions) will transport the neutrons to a point where the guide will be split, allowing an upgrade path to several instruments on the same beamport as, for this instrument, only 1/3 of the guide is required (horizontally). In the near future, we shall evaluate an angled straight guide section after the splitting point to avoid direct line-of-sight of the monochromator to the moderator, so as to reduce background. The total flight-path length from the moderator surface to the monochromator face is 46 m, allowing full illumination of at least a 30 cm high vertically-focussing (variable curvature) monochromator through the aperture at 6 m (natural divergence of ± 0.2°). A fixed-collimation carousel will determine the divergence acceptance onto the monochromator and a carousel with several monochromators offers flexibility. The operational take-off angle to the monochromators can be varied between 40° and 130°. The secondary evacuated flight path length (monochromator to sample) is 4 m with variable apertures to vary the beam divergence at the sample position, followed by a final set of beam-defining jaws. The sample - detector distance is 2.5 m, including a radial oscillating collimator (to suppress parasitic sample environment scattering) at the detector entrance and an evacuated detector housing (to reduce air scattering).

Crystal Mono.	d-spacing (Å)	Wavelength (Å) ($2\theta = 90°$)	Wavelength (Å) ($2\theta = 40°$)
HOPG(002)	3.355	4.743	2.295
HOPG(004)	1.677	2.372	1.147
Ge(220)	2.000	2.828	1.368
Ge(440)	1.000	1.414	0.684
Ge(400)	1.414	2.000	0.967

Table showing some possible composite monochromators based on HOPG and Ge.

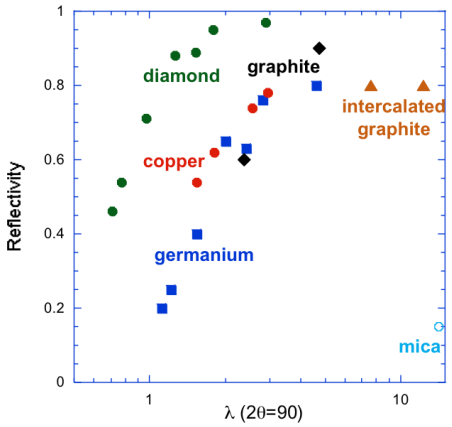

Comparison of diamond reflectivity (green) to other materials for crystal monochromators - Ge (blue), Cu (red) and graphite (black).

The instrument is similar to a conventional reactor-based diffractometer, such as D20 at the ILL, in the single wavelength mode of operation, as the time-averaged flux of the ESS is comparable to that of the ILL. However, the background is reduced *cf.* existing reactor instruments by discarding events outside the elastic line boundary time-of-flight conditions, increasing the effective signal-to-background ratio. Furthermore, multiple monochromatic wavelengths can be generated from monochromators (through co-aligned reflecting planes and/or higher order reflections) or by developing composite sandwich monochromators (see Table above left). The individual pulsed wavelengths are separated at the detector using the total path-length time-of-flight difference, not possible at a continuous source. Other monochromator materials will be investigated, such as diamond for its superior reflectivity in the wavelength range of interest (see Figure right) and layered materials (more higher order reflections). The monochromatic pulse structure is also well matched to fast kinetic measurements (sampling rate 4-5 ms at 14 Hz) and has potential with triggered cyclic measurements under extreme conditions, such as pulsed high-magnetic fields. The sample - detector flight-path can be used to separate inelastic incoherent scattering contributions, in time-of-flight, from elastic scattering in hydrogenous materials. Fixed incident energy inelastic scattering mapping can be performed with the full pulse (low energy resolution) or with a shaped pulse (variable energy resolution) using the optional chopper placed before the monochromator, offering a variable pulse-width from tens of μs to the full pulse-width. RRM-like measurements can also be replicated using the composite monochromator and/or higher order reflection set-up. Thus, while optimised for diffraction and *in situ* processing, several additional modes of operation are envisaged.

Instrument Parameters	
Moderator	Thermal
Moderator – monochromator distance	46 m
Monochromator – sample distance	4 m
Sample – detector distance	2.5 m
Q-range	0.1 -12.5 Å^{-1}
Beam size at sample position	maximum 40 mm height × 15 mm width
Normal Monochromators	diamond(111), diamond(220), Ge(113), HOPG(002)
Composite Monochromators	Example - Ge(220) / Ge(440) / Ge(400)
Detector technology	$^{1}0B$ or wavelength shifting fibre, resolution 2.5 mm
Detector coverage	160° 2-D cylindrical detector of 30 cm height (± 6.8° acceptance)

Pulsed Monochromatic Powder Diffractometer

Materials Science & Engineering Diffractometer

Materials Science & Engineering Diffractometer

Materials science
Engineering materials
Structure & in-situ processing
Residual stress & texture
Novel materials
Geosciences
Earth & environment sciences
Archeology & heritage conservation

A unique instrument for a broad range of scientific and industrial applications with a special emphasis on in-situ investigations of mainly engineering materials. The user will have the choice of multiplexing for fast time-resolved measurements or to trade resolution, divergence, beam size etc. versus flux in a single-frame pulse shaping mode. Flexible resolution is achieved by utilizing a double chopper system for pulse shaping, where different distances between the two chopper discs can be chosen. It will have the option of standard pulse shaping on a natural length instrument (Complex Environment Engineering Diffractometer "CEED" concept) or applying the structured pulse modulating (SPEED) concept. The latter allows modulation of the broad ESS pulse and thus to multiplication of the signal and efficiency especially for high-symmetry materials and strain measurements. Other concepts such as pulse-overlap are also being considered.

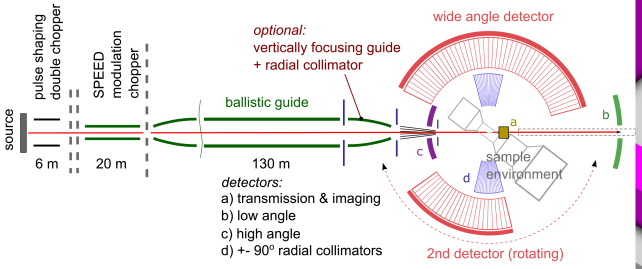

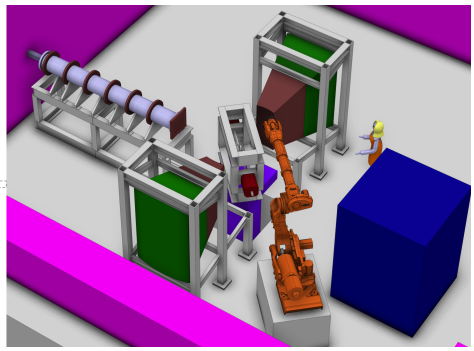

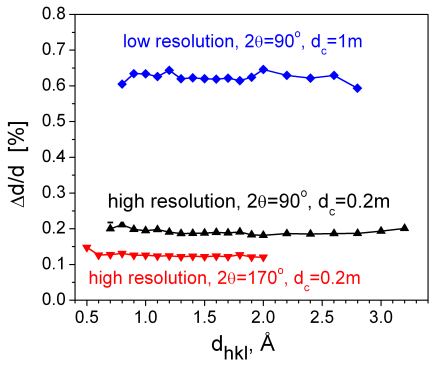

Nearly constant $\Delta\lambda/\lambda$ resolution as produced by the double chopper for different distances, d_c, between the chopper discs (simulation for pulse suppression mode with double band width).

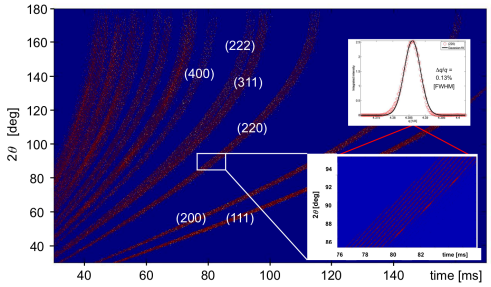

A diffraction pattern simulated in the SPEED mode displays the modulation of the broad source pulse for each Bragg peak. The top inset shows the high intensity and resolution obtained by integrating over the range shown in the lower inset.

Instrument Description

In addition to the pulse shaping and frame overlap choppers the instrument will possess the option to run a modulation chopper positioned in the first third of the instrument's total length of about 160 m. This device allows for chopping the beam into short subframes i.e. pulses, which then overlap at the detector position. Nevertheless the signal can be separated in many cases, especially when highly symmetric crystal lattices are under investigation, due to the corresponding angular offset of the Bragg peaks registered by the detector. In this way the signal is multiplied independently of the resolution, which may boost the efficiency for many engineering applications.

The instrument will be equipped with a wide range of sample environments dedicated for in-situ testing and characterization of engineering materials exposed to complex thermal, mechanical and electric or magnetic field loading. Under particular consideration are (i) physical simulations of fabrication and processing of engineering materials, (ii) long-lasting creep and fatigue experiments, (iii) investigation of magnetic materials in pulsed magnetic field and (iv) combination of in-situ diffraction and micro-imaging. Physical simulation of materials fabrication, processing and/or end use involves the exact laboratory reproduction of the thermal and mechanical processes that the engineering material is subjected to in the large scale production or end use. In-situ neutron diffraction during the physical simulation provides supplemental information about the evolution of texture, preferred orientation of martensitic variants, elastic and plastic anisotropy, dislocations and many other aspects. This additional information is expected to significantly improve the chance of achieving the optimisation of material performance through physical simulation. The instrument will also be used for texture and residual stress measurements in engineering components which are of major interest for industry. The basic instrument concept involves conventional detector banks located at right angles to the incident beam, coupled with flexible radial collimators (thus providing two distinct Q-vectors or independent directions of strain). Together with the incident slits, these define a gauge volume that allows spatially resolved measurements (of strain, texture etc) by moving the sample. Extension of the 90° banks to include back-scattering or forward scattering are to be considered. This would give better coverage for texture measurements and more directions of strain, but has to be balanced with the spatial and logistical requirements demanded from the advanced and potentially bulky sample environment. For residual stress measurements, the resolution and vertical divergence can be relaxed considerably (up to 1%) in order to gain flux.

Instrument Parameters	
Moderator	Thermal &Cold Bi-spectral
Moderator - Sample distance	156 m
Wavelength Range	0.5-5Å(0.5%)
Resolution	0.1% to 1% at 90°
Beam Size at sample	$0.5 \times 0.5\text{mm}^2$ to $10 \times 20\text{mm}^2$
Detector Technology	Boron-10, with mm spatial resolution
Detector Coverage	Initially 2θ=90° ± 20°, two banks but with extensions, possibly transmission detector
Sample environment	In-situ materials testing equipment, stress rigs, furnaces, cryo-cooling, robotics

Extreme Conditions Instrument

Extreme Conditions Instrument

Novel materials
Structure & in-situ processing
Geosciences
High-Tc superconductivity
Molecular magnets
Novel states of matter
Earth & environmental sciences

This instrument is optimised for effective use of state-of-the-art sample environments, in particular high-field ($\geq$ 25 T) magnets or high-pressure cells, including multi-anvil presses high temperature presses (up to 30 GPa at 2000 K). It can perform diffraction and spectroscopy measurements, and has additional SANS capabilities with bispectral extraction from the moderators to cover the widest possible Q/energy range. For wide angle diffraction the useful Q_{max} is 12 Å^{-1} and the usable wavelength band is 1.9 Å. For the spectroscopy option, the instrument covers an energy range of 1 - 80 meV with a variable energy resolution of up to 5%. The detector set-up is modular and will be matched to the sample environment. The instrument has a broad range of applications ranging from the physics and chemistry of materials to applied science.

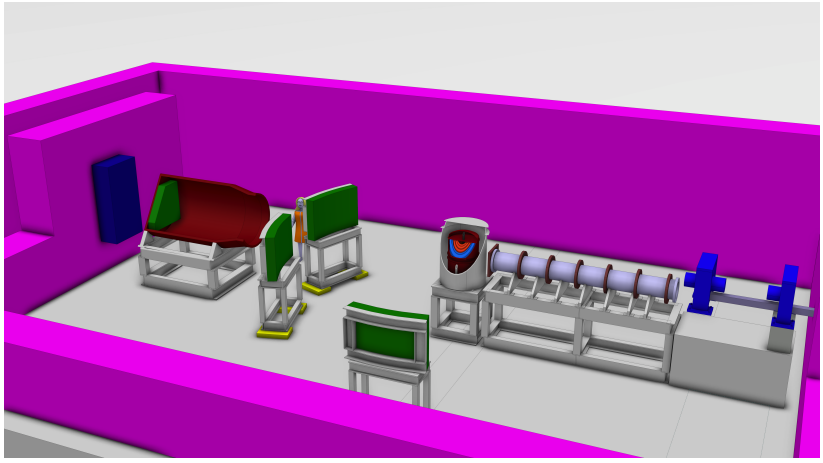

Instrument Description

The primary instrument is very flexible, due to the quite different requirements for diffraction, spectroscopy and SANS, while the secondary instrument matches the sample environment. Bispectral extraction from both moderators significantly expands the range of wavelengths accessible at the instrument and allows conventional diffraction, cold spectroscopy or SANS under the same experimental conditions. The wavelength resolution can be tuned by choppers from <0.1% to several % depending on the incident wavelength band, the former resolution is preferred for diffraction and the latter for SANS. For the spectroscopy option, either full or shaped pulse operation is foreseen depending on the required energy resolution. The direct spectrometer mode gives flexibility in choosing the incident energy from an extended energy range of 1 to 80 meV with a resolution that can be varied between 1 and 5%, enhanced by RRM. The beam delivery system has a kinked double ellipse geometry, similar to that proposed for the *thermal powder diffractometer* in order to bend out of the line-of-sight of the moderator to reduce background. The final section of the guide will contain slit systems to optimise the spatial and divergence acceptances at the sample position, offering great flexibility to tune the instrument set-up to those required by the experiment. Extreme conditions mean small sample sizes and/or severely restricted sample geometry and the maximum beam size is 1×1 cm^2, with optional focusing to reduce the beam to mm dimensions.

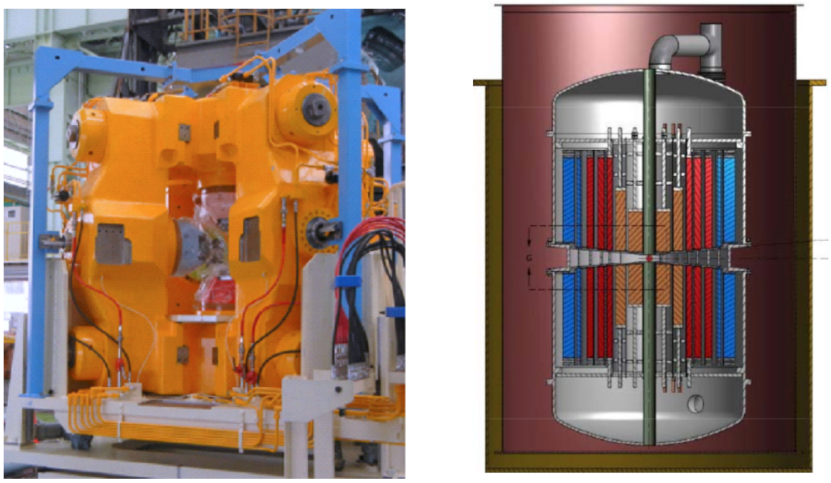

Possible sample environment types: (left) Multi-anvil pressure apparatus installed at PLANET (J-Parc) and (right) 25 T high-field split-pair magnet. Other alternatives include split magnets with wedge openings or superconducting horizontal magnets (not shown).

The secondary instrument is adapted to the dedicated sample environment (see Figure). Depending on the type of magnet, the scattering angle can be either limited to 30° in- and out-of-plane in forward and backscattering directions or be as wide as 300° in-plane but only a few degrees out-of-plane. For a high-pressure apparatus, the most useful scattering angle is around 90°, whereas forward and backward scattering positions are similar to those for the high-field magnet. For the system robustness, a modular detector panel configuration is planned for all the diffraction and spectroscopy modes, with an additional SANS detector bank in forward scattering that can be installed at a distance of 6 - 8 m from the sample position. To define the gauge volume and avoid parasitic scattering from the sample environment, a high degree of collimation is required in the secondary instrument. The non-magnetic and evacuated detector chambers will therefore incorporate radial collimation (not shown in the instrument overview). Combined with the long distance from the source and the kinked guide, this will provide a very low background and maximize the signal-to-noise ratio, crucial for small sample volumes.

Instrument Parameters	
Moderator	bispectral cold/thermal
Moderator - sample distance	156 m
Wavelength range	1 - 15 Å
d-range (Q-range)	0.5 - 600 Å (0.01 - 12 $Å^{-1}$) including SANS mode
Energy range (resolution)	1 - 80 meV (1 - 5%)
Beam size at sample	1×1 cm^2 (optional focusing)
Sample - detector distance	up to 4 m
Detector technology	Diffraction/spectroscopy: Boron-10 or wavelength shifting fibres, spatial resolution 2.5 mm, efficiency > 50% (for $\lambda > 1$ Å); SANS: (see Broad-band small sample SANS)
Detector Coverage	modular detector panels 1.5×1 m^2, SANS detector 1×1 m^2
Dedicated sample environment	superconducting high field magnet (>25T), multi-anvil press (6-axis press with max. load 500 ton/axis), diamond anvil pressure cells

Single-Crystal Magnetism Diffractometer

Single-Crystal Magnetism Diffractometer

Highly frustrated magnetism and emergent phenomena
Structure & in-situ processing
Molecular magnets & nanoparticles
Novel states of matter
Spin densities
Site susceptibilities

A time-of-flight (TOF) Laue instrument with the option to use polarized neutrons and full polarization analysis. Applications include magnetic structure determination for small single crystals including polarimetry, site susceptibilities, spin density distributions, hydrogen bonding, diffuse magnetic scattering, parametric real-time exploration of reciprocal space and monitoring the order parameters of weak signals.

The instrument takes full advantage of the ESS long pulse structure, its high flexibility and low background allowing to measure very small samples. Measurements using the TOF Laue method can very efficiently cover the reciprocal space of interest by a single or just a few sample settings.

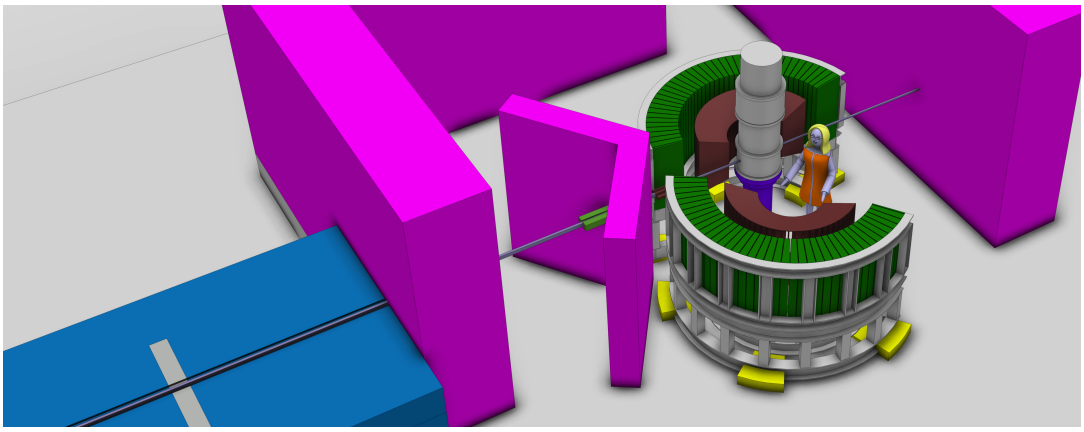

Instrument Description

Details on site susceptibilities and spin density distributions are obtained by polarized *thermal* neutron diffraction under magnetic field reversal, whereas *cold* polarized neutrons with polarization analysis can favourably be used for complex magnetic ordering and diffuse magnetic scattering. In order to enable both of these two standard modes of operation, the wavelength band can be shifted within the spectrum of a bi-spectral moderator, a flexibility which also allows efficient survey measurements, as well as parametric studies focused on small regions of reciprocal space.

With a simple spin-echo technique, it is possible to set a common coordinate system for the polarization analysis in *white* beam TOF Laue polarimetry, a method that rigorously disentangles the various nuclear and magnetic scattering terms on the full measured range of Bragg peaks in a single shot.

The spectrum of a bi-spectral moderator feeds a neutron guide system avoiding direct line of sight. The background is minimized by elliptic guide elements for focusing on small samples. Beam polarization is achieved by super mirrors. Half-polarized experiments with thermal neutrons can be performed with a 10 T asymmetric split-coil magnet giving large access to solid angle and reciprocal space. Polarization analysis and polarimetry are applied for separating magnetic, nuclear coherent, spin-incoherent scattering and interference terms.

The detector at 1 m distance from the sample, 1 m high, will be based on a thin film $^{10}B_4C$ converter, with 50% efficiency at 1 Å, which can achieve a spatial resolution of 2.5 mm fitting to a crystal mosaicity of 0.15°.

The user may benefit from the versatility of the instrument by adjusting wavelength band, pulse duration and focusing to the required reciprocal space, resolution and sample size. A large section of reciprocal space can be covered in a single sample setting, or alternatively, a continuous sample rotation can be chosen for data acquisition. The choice of a 156 m long instrument using a single wavelength frame gives a simple, adaptable time structure. For most needs the instrument exploits the full long source pulse. In order to resolve Bragg peaks at large Q with constant high resolution, the thermal spectrum of the pulse can be adapted to the unit cell dimensions, using a pulse-shaping chopper to provide a wavelength-dependent pulse length, as shown in the figure below.

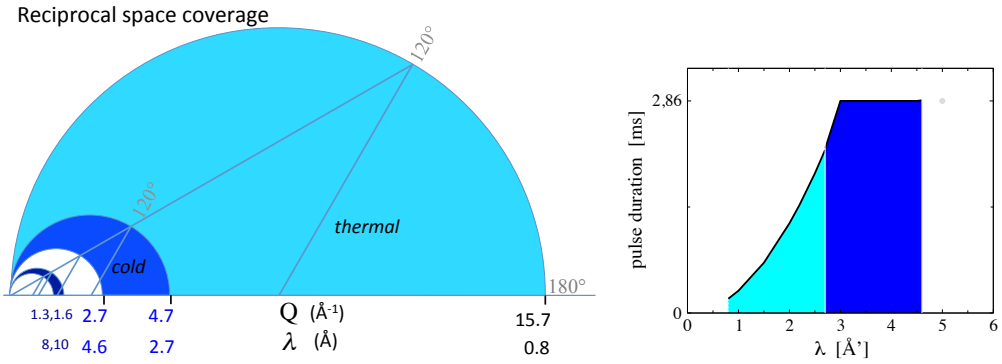

The left figure, a cut through the Ewald sphere, displays the reciprocal space coverage for different selected wavelength bands, with thermal (cyan) and cold (blue) choices and scattering angles up to 180°. The 2D detector also gives access to vertical Q-components (< 2.7 Å^{-1}) and completes the picture to both sides of the incoming beam.
The right figure shows the pulse-shaping required for a constant absolute resolution of $\Delta k_i \leq 0.05$Å^{-1}; for cold neutrons the resolution improves considerably even using the full pulse. At a wavelength resolution of 1%, the flux at the sample position will be 5×10^8n/cm^{2}s.

Instrument Parameters	
Moderator	bispectral cold/thermal
Moderator - sample distance	156 m
Wavelength range	0.8 - 10 Å
d-range (resolution)	0.4 - 60 Å ($\sim 1\%$)
Q-range (resolution)	0.1 -15 Å^{-1}
	($\sim 1\%$, flexible $\Delta Q \leq 0.05$Å^{-1})
divergence	$0.3° - 0.6°$ (thermal−cold, FWHM)
Background	no direct line of sight
Beam size at sample	typical $< 0.5 \times 0.5$ cm^2
Sample size	0.1 - 10 mm^3
Sample to detector distance	1 m
Detector technology	^{10}B-foil, efficiency $> 50\%$ for $\lambda > 1$Å
	spatial resolution 2.5 mm
Detector coverage	horizontal $10° < 2\theta < 170°$
	vertical $-20° < \chi < 20°$
Special sample environment	asymmetric vertical 10 T magnet for half-polarized setup
wide angle polarization analysis	^{3}He spin-filter cell applying for full the 2D detector or,
and neutron polarimetry	super mirror analyzer for applied fields, high polarization
	and 25° vertical acceptance, ($\lambda = 2 - 10$Å)

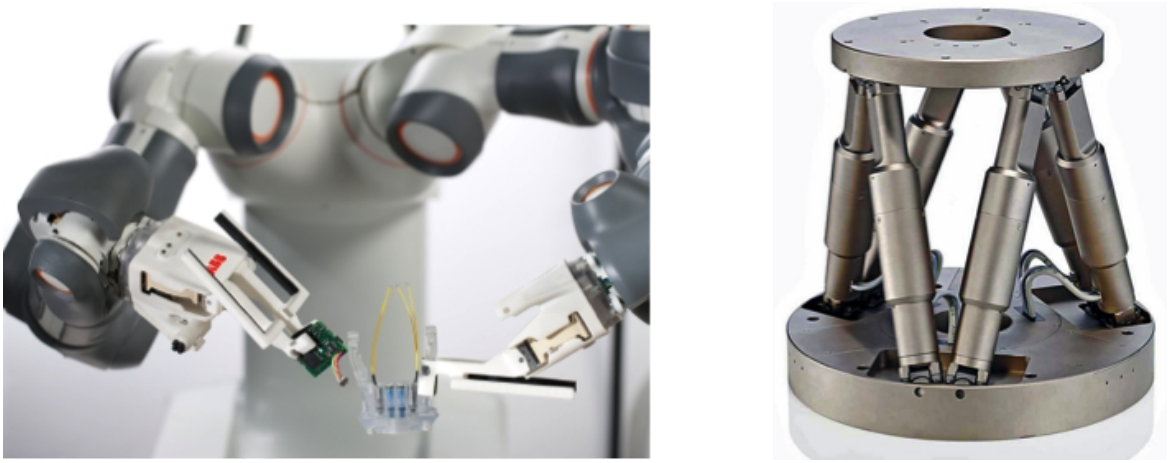

Figure 2.47: Multi-axis robotic and hexapod sample tables. Left: Conceptual robot FRIDA [260]. Courtesy of ABB. Right: A Hexapod robotics system for sample positioning [261]. Courtesy of Physikalische Instrumente.

control of complex hardware at optimised cost-to-performance ratios with a high degree of scalability. Examples of multi-axis robotic and hexapod sample tables are shown in Figure 2.47.

2.8 Data management and software for instruments and users

To fully exploit the information power of ESS, a new approach for software and data management is needed that intuitively integrates control of the neutron instrument and its sample environment; data processing, visualisation, analysis and publication; and permanent storage and public access. Realising this vision of a fully integrated e-science solution from idea to publication will be one of ESS's major contributions. The ESS-Data Management and Software Centre (DMSC) will tackle this e-science challenge, delivering a 24/7 e-science service programme to cover the complete research cycle from idea to publication as illustrated in Figure 2.48. The programme will provide an Internet-based system for interactions of the user community with ESS. It will include a user proposal system and peer review management; high-end tools for virtual experiments in order to plan, optimise and model measurements; a homogeneous instrument control platform across the instrument suite, which will be fully integrated with sample environments and ancillary measurements that generate meta data. It will also provide tools to enable researchers to interact remotely with experiments and ESS staff in real time; a platform that seamlessly integrates neutron and meta data and facilitates data reduction, visualisation and analysis in an intuitive manner; and state-of-the-art computational tools and computing platforms integrated with theoretical support in order to exploit the full scientific potential of ESS measurements. Finally, the programme will provide state-of-the-art data archiving and e-science tools to make data available to the scientific community in an appropriate form.

ESS-DMSC will be an integral part of ESS, located on the campus of University of Copenhagen in Denmark where it will host the ESS staff and IT equipment required to achieve its mission. Figure 2.49 provides an overview ESS-DMSC linkages. Reliability, usability, maintainability, and high quality will be ensured by using best practices in the development of the IT infrastructure. The complex IT infrastructure that is required to support scientific activities will be composed of dedicated networks, work stations, supercomputers, file systems, and long term storage. Figure 2.49 shows how the different components of the IT infrastructure will be distributed between the different physical locations in Lund and in Copenhagen. DMSC will provide and maintain updated infrastructure for high-performance computing during the construction phase for instrument simulations, simulations of the target, and for the online model of the accelerator. The use of this infrastructure will naturally extend into the operation phase, where it will form the starting point for the computational infrastructure required by the instruments and user programme. Moreover, DMSC will ensure that the McStas [262] software that is used for instrument simulations is properly maintained and further developed. Software development environments will also

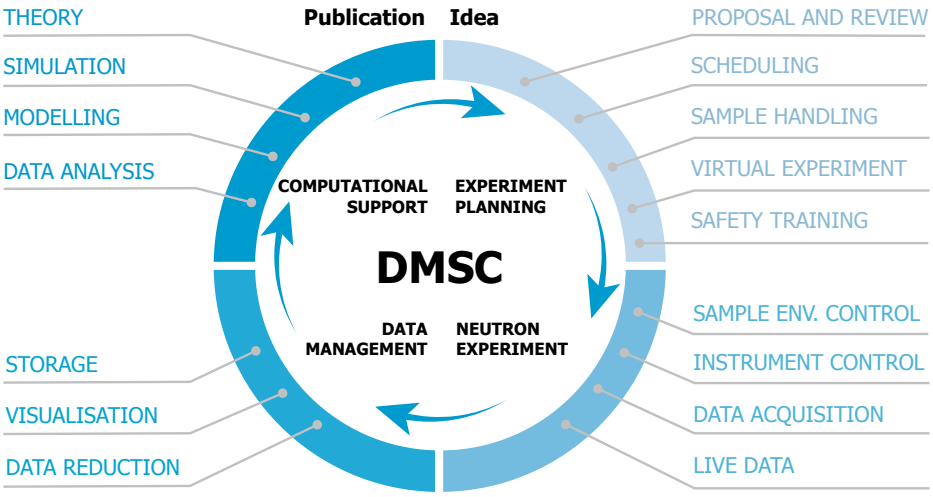

Figure 2.48: IT services and infrastructure provided by the Data Management and Software Centre, in each step of the research cycle from idea to publication, beginning with experiment planning, followed by the actual neutron experiment, data management, and finally computational support. This in turn may result in publications as well as new ideas and experiments.

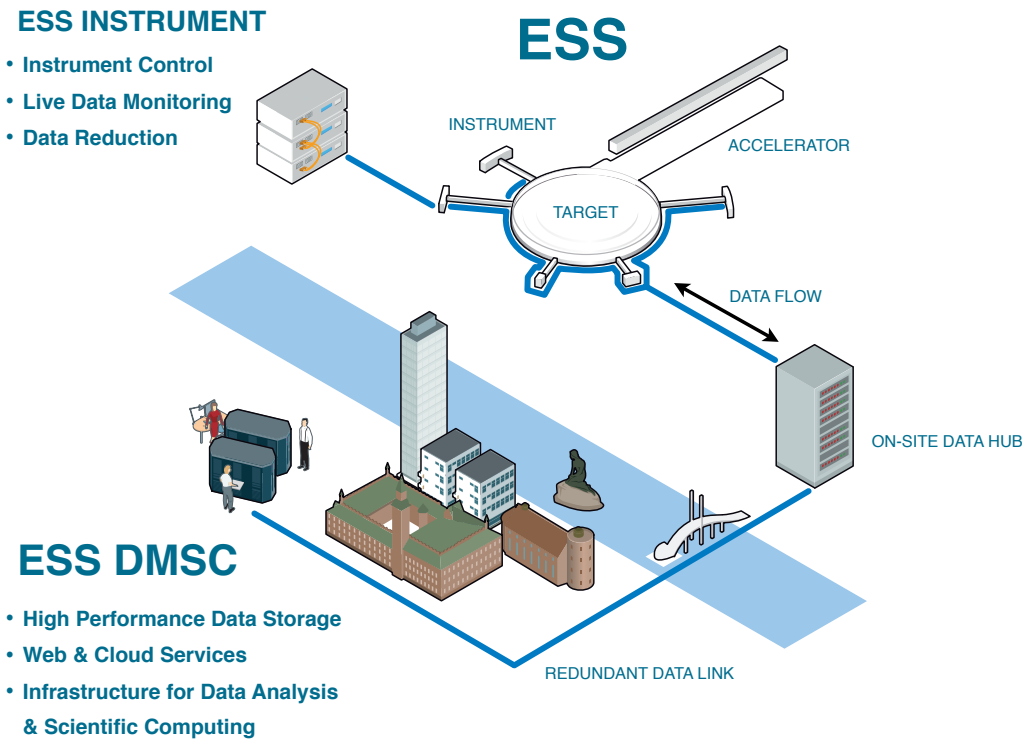

Figure 2.49: The relationship between the ESS-DMSC in Copenhagen, and ESS in Lund.

be required for research and development in the Detector Group and in the Integrated Control System group.

2.8.1 Requirements

In order to reach its full potential, ESS will need software and IT infrastructure for its instruments and user programme that are reliable, maintainable, usable, and supportable. Given the multi-decade duration of the ESS project and the rapid pace of technological change, ongoing software projects may easily span successive generations of technological developments. ESS will need the flexibility to cater for changing user requirements over its life time, and to interface to new or user-supplied equipment. In particular, the software provided through the user programme must be easy to learn and use for users with vastly different backgrounds and experiences in order to reduce the burden of support and avoid waste of beam time.

Instrument user interfaces

ESS will offer different instrument user interfaces in order to support researchers who will have very different backgrounds. For example, visiting scientists are likely to include both archaeologists who may visit the facility once a year for a few days, and physicists who visit on a regular basis. Interfaces will support users who need to perform complicated tasks as well as those requiring routine services, including software developers, instrument scientists, and support staff. To cater for these different types of users, an application programming interface (API) will be developed, as well as a domain specific command line interface (CLI) and a graphical user interface (GUI), as is common in modern scientific software. The interface will also support users who are not comfortable with command line interfaces in setting up sequences of operations. It will be possible to use a sequencer table interface, which resembles a spreadsheet in look-and-feel and functionality, to set up a sequence of operations for execution. The sequencer table will be an integral part of the graphical user interface. A uniform look-and-feel will be maintained across the software suite, and different programs will work seamlessly together. This will save user time, and increase the research productivity of the facility.

Software architecture

The same architecture will be used for all components of the software suite used across the entire research cycle from idea to publication, as is illustrated in Figure 2.48. This uniformity is important for building an efficient software development organisation, and will make it easier and cheaper to ensure that different components of the software suite indeed work together seamlessly. A software architecture that spans the needs is outlined in Figure 2.50. The central component is an API that will be used to interface to various libraries, including graphical components, databases, and third-party applications. The API will in turn be used to develop domain-specific command line interfaces, graphical user interfaces, and browser-based services. The preferred option for the implementation is based on Python for the API, C++ for performance intensive libraries, and Qt as a graphical library, as shown in Figure 2.50. This approach is becoming a standard software framework for scientific applications, in part due to the extensive selection of scientific libraries. Many facilities already use, or have plans to use Python as a scripting language, including the Diamond Light Source, ISIS, and SNS. This architecture also is used by the data reduction and analysis program, Mantid [263]. For this reason, Mantid has been selected as a cornerstone of the software suite. Many other programs of relevance for ESS-DMSC are also based on this architectural choice, such as the Python-based Hierarchical ENvironment for Integrated Xtallography (PHENIX) for macromolecular structure solution [264]. Some level of web development (which could be based on HTML5, for example) will take place because some components of the software solution, such as the user office software, must be browse- based. Indeed, ideally, the software suite as a whole will work as a web application.

Command line interface

A command line interface will be made available for instrument control, data reduction and data analysis. It will be possible to use the command line interface interactively as well as to execute scripts consisting of several lines of codes, a capability already available in Python. Users will be able to generate their own scripts, test that they work as intended through a dry-run, and save them for later use or for distribution

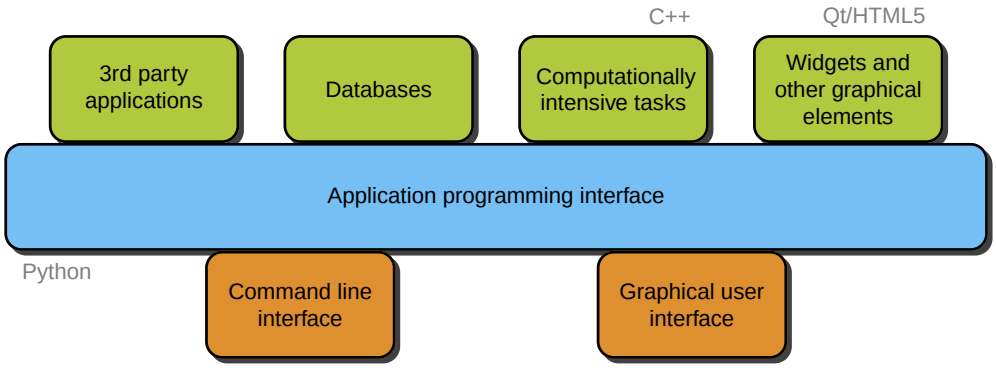

Figure 2.50: The architecture that will be used for the software suite that will support users from idea to publication. Python, C++, Qt, and HTML5 are the current preferred options. Language use locations are indicated.

to other users. The latter makes it possible for instrument scientists to optimise the path from idea to publication for specific types of experiments by scripting predefined procedures for the user community. Whether run interactively on the command line, through a script, or via the graphical user interface, all steps will be time stamped and logged as a new script. This will make it easy for users to repeat the various steps of an experiment (instrument control, reduction, or analysis), or to make variations over the same experiment by modifying the logged script. The time stamping will also make possible the alignments of logged commands with data acquired from the experiment, facilitating the creation of a detailed log book from the experiment.

Graphical user interface

The graphical user interface will be self-explanatory for the users of the instruments. It will be customised for each instrument. It will be possible for the instrument scientist, users, and technical support staff to selectively enable features for a given experiment. The graphical user interface will support advanced tasks through a shell for executing commands of the command line interface, a library of predefined scripts, and a sequencer table interface, which will allow the execution of commands via a spreadsheet-like interface. The sequencer table interface is expected to appeal to many users because it resembles the spreadsheet interfaces that they are already familiar with, and because it will enable them to do fairly complicated tasks without scripting through the command line interface.

Remote access and web applications

Users will be given secure remote access to software services. In fact, much of the software required by ESS will be developed as web applications, including types of software that traditionally have been thought of as standalone applications. Web applications offer many advantages. Web-based solutions will enable DMSC to avoid providing support for a multitude of current and future hardware platforms and operating systems. Web applications will also spare users the hassle of software installation. In addition, web applications will make in-house resources available to users remotely. It will be possible to analyse experimental data by means of computers and software running with a minimum of data transfer.

Security and access control

Many of the risks related to remote access, if not all, can be mitigated by implementing proper authorisation policies and security measures. DMSC has a strategy to monitor developments in IT security, hacking, and network penetration techniques and will ensure that the systems in place remain at the forefront of recommended practice. The final line of defence for a successful penetration will be the provision of an operation mode under which ESS is completely disconnected from the Internet. To avoid unwanted intrusions into the ESS network, user credentials (such as user name and password) will be required to

access DMSC software services. A single set of credentials will give access to all services that the user has permission to use. Moreover, single sign on (SSO) [265] will be used for all web applications, such as user office services, data access, and remote monitoring of experiments. Where feasible, SSO will also be used for software programs that are not web applications. It is currently the plan to mesh SSO with existing methods, developed as part of PaNData [266], CRISP [267], and eduroam [268]. Authentication (the ability for users to prove who they are) and authorisation (the different rights a user has in the system) are discussed in more detail in relation to user office software in Section 2.8.2.

2.8.2 Experiment planning and the user office

A number of administrative and planning tasks need to be completed before an experiment can take place. First, the experiment must be approved for beam time. Subsequently, scheduling, sample handling, and safety training (among other procedures) must be taken care of. The user office, which will be under the responsibility of the Neutron Science Division, will play a pivotal role in accomplishing these practical tasks. It will be the user's primary point of entry to ESS. The functionality of the user office software that DMSC will provide will have a significant impact on the efficiency of the user office and on the user's experience at ESS. Besides administrative matters, both visiting users and ESS staff involved in an experiment, may plan the execution of the experiment in detail, and practice operation of the instrument and its associated software through virtual instruments, for instance through computer simulations. The user office will have both an online and a physical presence which will come into play during experiment planning, and at other stages of the user's involvement with the facility. The user office will offer both end-users (visitors) and staff a simple and comprehensive gateway to the information required to make the visiting scientist's stay successful. The gateway will be a mostly paperless, integrated solution that does not duplicate information across various systems or require constant manual re-entry of information already in the system. The user office software will play a central role at the facility since the information gathered by the user office will feed into many systems across the facility. Such information exchange is required, for example, to facilitate scheduling and planning. In developing the user office software, special care will therefore be taken to identify and manage information exchange. European data protection laws, in addition to Swedish and Danish regulations, provide very specific requirements for the collection and retention of data, and DMSC will adhere to these standards. The scope of the user office software is quite broad, as also are the different areas of responsibility within the user office, including a user database, proposal system, scheduling, invitation procedure, sample handling, and post-experiment activities.

Instrument user database

Users will have to be registered in the instrument user database in order to access various services at the facility. There will be different kinds of users at the facility, including external users who visit the facility to conduct experiments and permanent staff, who also will need to access various functions of the user office systems. Provision may also be made for other classes of users, such as those proposal reviewers who may be neither staff nor visitor. The instrument user database will provide both authentication (the ability for users to prove who they are) and authorisation (the different rights a user has in the system). The information required to authenticate and authorise a user will vary depending on the level of access they are granted to the facility. An external user will be able to create an online account for the purpose of submitting proposals without providing proof of identity. However, such proof, for example through the provision of identity papers, will be required before a user is granted further access to the facility. The status of trust in a user's identity will be kept updated in the system. Identity information may also come from other sources, such as other trusted facilities or through a federated identity management service.

Proposal system

During calls for proposals, registered users will be able to create, view, edit, submit, and withdraw proposals. A given user may have one or more active proposals. For each proposal, users will be able to enter various types of information, for example, title, type, instrument, the purpose of the data collected (e.g., whether it is used for thesis work), subject and research areas, abstract, related proposals, information about the team, samples and sample environment. Users also will be able to attach files with supporting material. Once a proposal has been submitted, a proposal ID will be allocated, which the user will be

able to use to view and track the proposal as it makes its way through the review process. During the submission process, users may be required to agree to various conditions before being allowed to submit proposals, including conditions governing access to data generated at the facility, intent to publish, and compliance with safety procedures. Once a user has submitted a proposal, it will be possible for administrators to view it and to assign reviewers to it. The reviewers will be able to view the contents of the proposal and submit evaluations, which initially will not be visible to the proposer. Before the results are released, the successful proposals will be ranked and scheduled. Once the review deadline has passed, users will be informed of the result of the review of their proposal. If review results are favourable, the proposing team will receive an invitation to visit the facility to conduct its experiment. At that point, proposers also will be able to view the details of the evaluation.

Scheduling

Scheduling is an integral part of the proposal process. The schedule of each instrument will be stored and will be query-able, and alterable. In addition to the instruments, other components will also be scheduled, including sample environment and the instrument team. Care will be taken to make sure that crucially important scheduling information is disseminated correctly throughout the facility.

Invitation procedure

Once a successful proposal has been scheduled, the proposing user will be formally invited to the facility. Invitation procedures involve informing the user of the invitation, of course, but also ensuring that the proposer and other members of the scientific team are ready to visit the facility. Along with the invitation there are a number of practical matters that the proposal system will be equipped to deal with, including booking, confirming, and providing opportunity to review accommodations at the facility; travel arrangements, when required; ensuring that site access is granted for the duration of the experiment and that conditions for granting that access have been met, such as the completion of safety and instrument training, submission of health certificates, and dosimetry handling. These procedural matters will be addressed during the period of time between the issuing of the invitation and the beginning of the experiment. In some cases, such as travel arrangements, activity will be initiated by the user, but will usually require action from user office staff. Other matters can be entirely automated, such as safety training. It is important to ensure that these practical matters do not become burdensome for staff and visitors.

Sample handling

Some users will send in their samples, rather than showing up physically at the facility. The system will be able to handle the registration of samples, shipping, storage, safety evaluation, and location tracking at the facility, using identifying markers such as barcodes, QR codes, or electronic tags. Both users and ESS personnel will be able to add, view, and update information about samples, and this information will be automatically included in the metadata of an experiment. If the user is off-site, the system will also grant remote access to the instrument during scheduled beam time. Once the sample has been exposed to the beam, it may need to be quarantined for some time before being returned or disposed of. The software will keep track of the location of the sample, as well as the custodian who should be contacted once the sample has been released from storage.

Post-experiment activities

Although many responsibilities of the user office are related to experiment planning, there are also a number of post-experiment activities that the system will enable the user to complete. The user office system will be able to handle the creation, editing, and approval or rejection of reimbursement forms, and to facilitate communication about these forms where clarification is required. The user office software will make it possible to attach necessary documentation to the reimbursement forms. A simple and well documented workflow will be established for completing these forms. The software will also make provisions to elicit feedback from users at the conclusion of their stays. After the user has published or otherwise made use of the experimental data collected at ESS, data about outcomes will be recorded in the system. While some users may take the initiative themselves to collect and track this information, user office staff will often play this role. Outcomes of interest might be reports, publications, or intellectual property

such as patents attributable to the research carried out at the facility. Along with the specific services above, the user office will provide some generic services in order to support day-to-day functions, such as content management for training materials, instructions, and help related to user office procedures; and a method to administer tests and provide feedback forms. The user office will play a central role in user authentication and authorisation. This will apply to both electronic and physical access to the facility. Electronic access will encompass the various user office facilities and remote access to instruments, which will be limited to the period during which the user is scheduled to use the instrument ,and to data once the experiment has concluded. Physical access to the facility will also be limited to the period during which the user is scheduled to use the instrument.

Training

Besides safety training, training in performing an experiment at ESS will be provided to novices before the experiment takes place. This will avoid unnecessary waste of beam time. Training may take the form of face-to-face workshops at DMSC or of electronic courses, including online courses. In either case, users in the training sessions will engage with software identical to that which they will need to use during the experiment to operate the instrument and analyse resulting data. They will be given the opportunity to perform dry runs using the software with artificial data.

Virtual experiments

Monte Carlo ray-tracing simulations using programs like McStas [262] or Vitess [269] have already been deployed in the design update phase for evaluation and design of instruments, neutron optics and time structure of the ESS source. For each instrument constructed, ESS will develop a detailed instrument model that mimics the real instruments. A limited number of sample models for McStas exists today. This library of sample models will be expanded significantly in the future, based partly on a systematic development chain from quantum chemistry calculations (for example, density functional theory) to McStas model. With a model of instrument, sample environment and sample in hand, it will be possible to simulate a complete experiment, which in turn will become a tool for training users and staff in how to operate the instrument and perform data analysis. Users may also employ the virtual instruments to evaluate experiment ideas and to optimise experimental procedures prior to scheduled beam time. In the long term, it may become common practice to include complete simulations of experiments in applications for beam time.

2.8.3 Instrument control and data acquisition software

Software is required for controlling the instrument and sample environments, and also for acquiring neutron and metadata from ancillary measurements. Live data processing will enable experimentalists to better control the experiment to increase research productivity. The term “instrument control” is used here exclusively to refer to the process of controlling the instrument through commands (slow control), while the term “data acquisition” is used to refer to the process of acquiring data from sensors or detectors, whether it is neutron data (fast control) or metadata (typically slow control).

Instrument control software

The devices that need to be controlled in order to perform an experiment are associated with the neutron scattering instruments, sample environments, or detectors. Technical details for these systems are discussed in Section 2.7, and layouts for specific instruments in the reference instrument suite are discussed in Section 2.4. Neutron scattering instruments typically are associated with a number of controllable devices, including choppers (as discussed in Section 2.7.2); motors for positioning and aligning the sample and for operating the shutter; and associated sensors for monitoring frequency and phase of the choppers, position of the motors, intensity of the neutron beam, and pressure (to verify the existence of vacuum in the beamline). Vendor-supplied goniometer systems and robots for picking up samples and aligning them in the beam may also be part of a neutron scattering instrument. Depending on the specific instrument, there may be other components along the beam line that need to be controlled via motors, such as collimators and removable polarisers. In some cases, highly integrated motion control systems with complex trajectories and/or a high number of coupled axes maybe needed, as discussed in Section 2.7.5. A complete list of

devices will be available only after the instruments have been selected for construction and completely designed.

Sample environments are discussed in Section 2.7.4. They will have vastly different configurations depending on their purpose. They may be equipped with temperature, pressure or applied force regulation; magnetic and electric fields; and/or access for chemicals, for instance by means of syringes in stopped flow experiments or valves for gases. At a lower level, this implies the existence of heaters, coolers, cryostats, magnets, pumps, motors, and various sensors, including thermometers, pressure sensors, pH-meters, and flow-meters. In addition to instrument-specific sample environments, there will also exist a set of standardised sample environments that will be compatible with several instruments. Furthermore, some users are expected to provide their own sample environment equipment, and ESS will provide standard interfaces to facilitate these experiments. The sample environment will be controllable by the same means and through the same user interface as the beamline instrument, and thus the sample environment will be plug and play. All detectors will need to be controlled and will require monitoring of magnitudes such as voltage and gas-related settings. Furthermore, whilst the majority of instruments will have a fixed geometry, some instruments may have movable detector banks requiring motors, as is the case for the materials science and engineering diffractometer in the reference suite. Detection of neutron events will take place in hardware systems, and is discussed in detail in Section 2.7.1. The various devices will be controlled by a user through a control console. Control consoles ready for use will be available in the main control room, and also in satellite control areas associated with each neutron scattering instrument, and via a mobile device. This is discussed further in Section 5.1.2.

Integrated control system

The instrument control will be part of the integrated control system (ICS), which in addition to the instruments also will control the accelerator, target, and conventional facilities. The integrated control system will facilitate standardisation and collaboration, for example, on driver development, across ESS. Moreover, required information from the accelerator and target will be provided by ICS, such as moderator temperature and flux of the proton pulse. Time signals from the master oscillator, machine protection system (MPS) and personnel protection system (PPS) also will be provided by ICS. ICS will be based on EPICS [259] for the device layer (drivers) and EPICS channel access middleware for communication between devices and between devices and control units. Control boxes will be employed to ensure modularisation and standardisation across ESS, as described in detail in Section 5.3.

Requirements for instrument control

The general requirements outlined in Section 2.8.1 are also valid for the instrument control software. Both a command line interface and a graphical user interface will be available. The same software will be implemented on all beamlines in order to reduce development and maintenance costs and to facilitate the transfer of knowledge and experience among instruments. Other software will only be implemented for instrument control where there are substantial benefits that balance the additional cost of supporting multiple solutions. Examples of such exceptions might be the existence of a standard solution within a given technique or a desire to support cross-facility experiments, for instance between ESS and MAX-lab, in which case it will be desirable for users to encounter the same software at the two facilities. There is no *de facto* standard for instrument control user interfaces at neutron scattering facilities, and no interface currently fulfils all the required specifications described above. ESS will monitor developments in existing projects and will decide to what extent it will be advantageous to use existing solutions in the near future.

Data acquisition

In order to fully preserve all the information from an experiment and allow for more powerful and flexible data analysis, instrument data acquisition will be based on event mode as far as possible and appropriate. In event mode, a detected event is time stamped with a value from the central timing system provided by ICS, as described in Section 5.2.6. ICS will employ current practices of accurate timekeeping, in partnership with the chopper and instrument groups, to ensure that recorded data are accurate and reliable and properly aligned in time with other events across the facility. Three categories of data events will be generated for experiments: Neutron data, metadata events, and absolute time records. Neutron data will be sent from the detector electronics in a binary data format containing the relative timing information

and the index of the detectors being hit by a neutron, as described in Section 2.7.1. Metadata events will be provided by the control boxes associated with the relevant devices in a binary format containing the required information about parameter, time, and value. The exceptions from this are user, sample, and proposal tags which will be obtained from the software suite provided by DMSC, as will be the case for the user office. Absolute time records will contain absolute time and will be provided by the central timing system.

Data transfer will take place by means of two types of data streams. One will contain neutron data events and the other will contain metadata events. In both cases, the streams also will contain absolute time records in order to ensure that all events can be properly aligned on an absolute time scale. Details about the data format can be found in [270]. A non-exhaustive list of relevant metadata includes experiment data on users, team members, local contact, and system under study; proton pulse data; moderator temperature; neutron flux; chopper settings; measured speed and phase; position of detector banks; instrument settings and sample positions including motor axle positions; pressure, humidity, temperature, and alignment on optical systems; beam monitor counts. For sample environment, metadata will include temperature, pressure, magnetic field, mechanical strain; and user-supplied commands, as discussed in Section 2.8.1. All data will be streamed to the live-processing system, which is discussed below, and to the data storage system discussed in Section 2.8.4, where they will be saved in the form of NeXus files, with a NeXus file for each experiment or measurement performed.

Live-acquisition processing, visualisation and automation

Live-acquisition processing and visualisation will enable researchers to get feedback in real time during their experiments. Data processing and visualisation are discussed in more detail in the next section. An efficient infrastructure will be developed to give fast access to stored data and sufficient CPU power

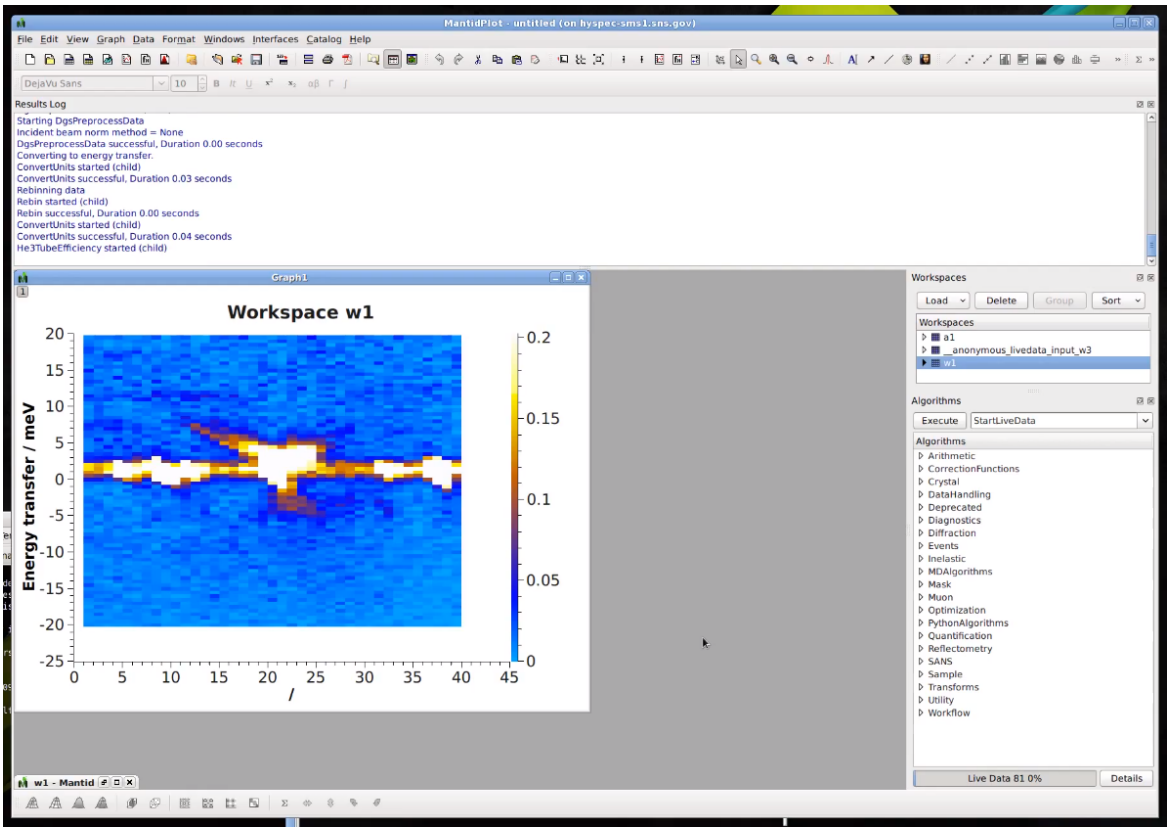

Figure 2.51: Snapshot of live streaming data reduction with Mantid and the ADARA system developed at Oak Ridge National Laboratory [271, 272].

for live-acquisition processing as well as for post-acquisition processing. Given the high neutron fluxes, significant computer resources will be required on site in Lund for processing of acquired data in real time. The ADARA system shown in Figure 2.51, which was developed at ORNL, will be used for live processing, and further developed so that it will be able to cope with ESS's high data flow rates. It may be possible to use libraries from the ROOT data handling system at CERN [273], which can handle data streams on the same order as may be required at ESS. Various levels of automation will be employed. Scripting and the sequencer table interface will provide the means to do so and the software will make it possible to use data from the live-acquisition processing to automatically advance to the next step in a sequence of measurements once sufficient statistics have been obtained. This will enable scientists to concentrate on the scientific aspects of the experiment rather than the technical details of running routine tasks on the instrument.

2.8.4 Data management

An experiment or sequence of experiments generally results in a large number of documents, simulation results, measurement data, analysis results and scientific papers. All this information will be stored at DMSC and DMSC will provide tools and services to ensure that researchers are able to access the data and the required computational resources to manipulate this data at all stages of the scientific process in accordance with the security policies described in Section 2.8.1. Much of the information will be made browsable and searchable, including metadata. Besides metadata and raw neutron data originating from measurements, logs of applied data analysis and information about the employed software and resulting publications also will be stored in the data management system.

Data reduction

Data reduction describes the process of correcting and transforming acquired raw data into physically interpretable data. It is an essential part of an experiment. The algorithms for data reduction are instrument-specific, and software for reducing data acquired at a given instrument will thus be considered an integral part of that instrument. Preliminary data reduction and real time analysis and visualisation will assist users in performing an experiment as described in the previous section. However, at any given time after the experiment, a user also will be able to access the data and process them or visualise them without transferring the data out of the facility. Thus data reduction is intimately linked to data management. That being said, the user will also be able to copy data to the home institution, where a user will be able to use his or her own software or software provided by DMSC, which will be open source to the extent feasible.

Data reduction consists of filtering, correction, mathematical operations, binning and presentation. Filtering ensures that only data that fulfils specification will be used in the subsequent processing. Data may fail to meet specifications for a variety of reasons. For example, data generated before choppers have settled to the specified speed and phase will be rejected, as will be data generated when sample environment conditions have not yet met specifications, or when neutron pulses are of inferior quality. All raw data will be stored, so no data will actually be discarded in the filtering process. Data will be corrected to compensate for spurious effects. This may include, but will not be limited to, normalising a data set by the incident flux; determining variations in detector sensitivity using a vanadium sample and normalising data accordingly; or correcting for background obtained by measurement. Data sets may also be corrected for scattering from the instrument itself or from the sample environment or corrected for multiple scattering effects by measurement or instrument simulations using, for example, Monte Carlo ray-tracing codes.

Mathematical operations will be used to slice, project, interpolate or otherwise manipulate data into a scientifically appropriate form. The extensive use of wavelength frame multiplication and repetition rate multiplication at ESS will augment the complexity of this task, which underscores the importance of providing adequately reduced data in order to realise the full potential of the long-pulsed source. Binning is a procedure that converts the set of remaining events to histograms that may be multidimensional. In the general case, events will be converted to a histogram depicting neutron intensities (event counts) as a function of parameters of interest. The accumulated data from each detector pixel will be presented to the user graphically, and it will be possible to replay the accumulation of data over time. It will be possible

to plot graphs and histograms in one and two dimensions, and also to visualise data in 3, 4 or even more dimensions, based on the slicing and projection of data for final presentation on a graphics terminal.

Virtual instruments for data reduction

Virtual instruments based on Monte Carlo ray-tracing software will play an important role in the development of data reduction and analysis software for the instruments while the real instruments are being constructed. This will be particularly important for researching and developing algorithms for data reduction and analysis for wavelength frame and repetition rate multiplication where no standard methods exist at the present time. The use of virtual instruments will make it possible to develop and test software for data reduction even though the instruments have not yet been constructed and put into operation. This, in turn, reduces the risk that adequate software will not be ready once the target instruments enter the commissioning phase. Virtual instruments are also expected to play an important role during the operational phase. Advanced data reduction can be performed with a realistic sample model, making it possible to simulate the complete experiment to obtain good agreement between simulation and experiment. Once that has been obtained, the individual contributions to the observed scattering pattern can be separated, as illustrated in Figure 2.52. With the single coherent, incoherent and multiple scattering patterns available, more reliable data analysis can be performed. Furthermore, simulations can be used to estimate contributions from the surrounding sample container and cryostat.

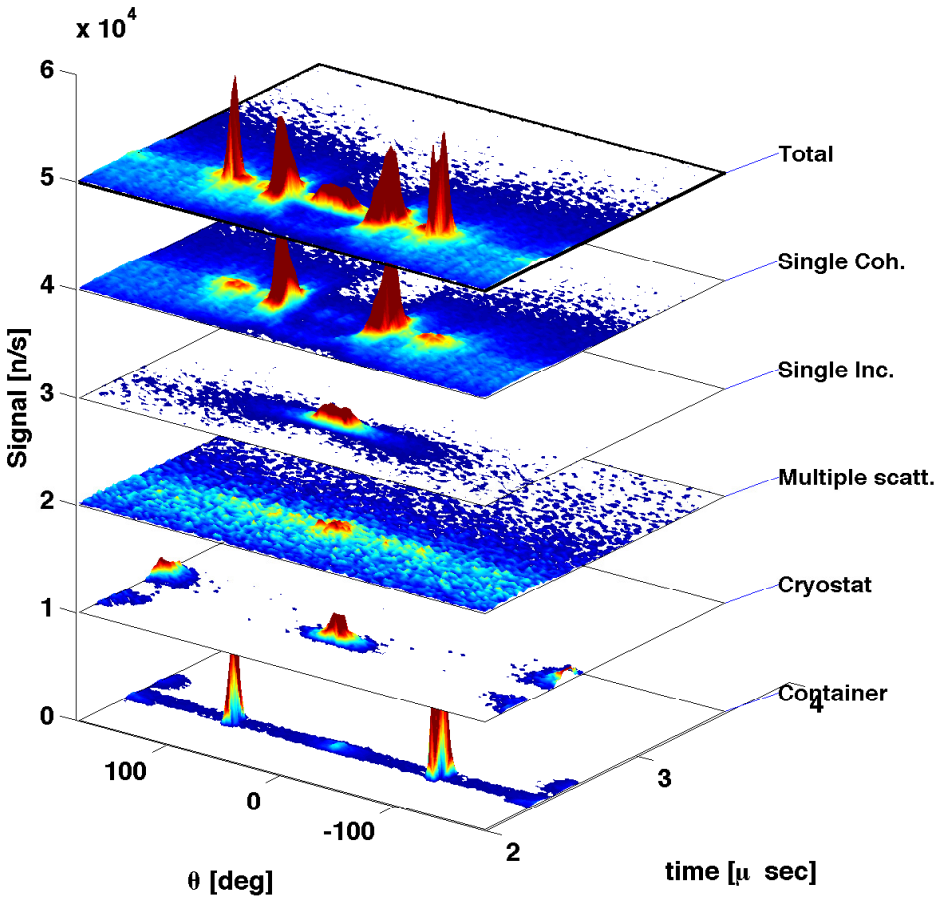

Figure 2.52: Simulated total signal from l-Rb at 350 K separated into coherent, incoherent, multiple scattering, cryostat, and container contributions. The cryostat and multiple scattering signals are multiplied by a factor of ten.

Options and system architecture for data management

The preferred option for a data format for storage is the NeXUS file format [274], which is a customisation of the HDF format to data from neutron scattering experiments. ICAT [275] is an example of a data management system that could be used, in which all metadata are stored in a relational database and made browsable and searchable. Links to the raw data files are stored, and in this way a single point of entry to information from the experiment from idea to publication is obtained. Solutions for data reduction and visualisation will likely be developed in the Mantid framework, which fulfils most requirements with respect to architecture, user interfaces, and development as discussed in Section 2.8.1. Mantid, which has both a graphical user interface and a command line interface, is being developed for reduction, analysis, and visualisation of data acquired at ISIS and at SNS [263], and may be adopted by J-PARC [276] and ILL. Thus, by joining the Mantid project, ESS will be able to deploy data reduction software with which users are already very familiar. Mantid can already be used for processing live data streams [277], has excellent visualisation capabilities, and can handle data of high dimensionality [263]. A project has been launched to connect McStas and Mantid so that algorithms in Mantid can be applied to data generated in silico by McStas. This would make possible the use of virtual instruments in the software development process.

The data management system will reside on a high performance file system at DMSC. A data volume of the order of multiple petabytes per year is expected. The file system will be based on both disk and tape to assure fast access to frequently used data and reliable storage for all data. A total backup of the storage system will be located in Lund to assure physical separation of the master data and the backup data. Data will be transferred between Copenhagen and Lund over a dedicated fibre connection that will be doubled for reliability reasons; one fibre will pass over the Öresund bridge and one fibre will pass under the Öresund between Denmark and Sweden. If all connections between Lund and Copenhagen fail, data will remain in the back-up facility in Lund until the connection is reestablished. A high performance computing cluster for post-acquisition processing will interface directly with the data storage system to ensure the highest data-transfer bandwidth during reduction and analysis and will make it possible for users to process their data with a minimum level of data transfer out of the IT infrastructure.

2.8.5 Computational support for analysis

Data analysis will require new sophisticated software, powerful computing hardware, and expert knowledge in scientific computing if ESS is to reach its full potential. Two examples of how scientific computing can be used in the data analysis process are given in Figure 2.53. DMSC will prioritise making it easy to integrate new data analysis methods and algorithms into the software to increase research productivity and the potential for new breakthroughs in experimental techniques. Indeed, scientific computation and theory will be critical in providing added value to the data measured at ESS. Recent development of supercomputing infrastructures (e.g. the Cray XT5 computer at Oak Ridge National Laboratory) has allowed the timescale and system size attainable by molecular dynamics simulations to reach timescales on the order of 1 μs and sizes in the order of 10 million atoms. Extrapolation of this performance indicates that it probably will become possible to perform molecular dynamics simulations of systems of 10 billion explicit interacting atoms (i.e., approximately the size of a living cell) within the time frame of ESS's operational life [281]. Simulations at this level will complement the length and timescales of systems that can be characterised by the instruments at ESS, as discussed in Section 2.2. This rapid development in computing power will thus bring unprecedented capabilities to scientific computing and make it possible to employ new algorithms for analysis, for instance based on quantum chemical calculations or molecular dynamics simulations.

In most cases, data analysis consists of resolving a spectrum into individual peaks or other curve forms by means of curve fitting followed by modelling. Data analysis allowing for multi-dimensional fitting will be particularly important for ESS because data will be acquired in event mode. Figure 2.54 illustrates this in the (simulated) case of a powder diffraction pattern, where existing analysis tools only use a tiny fraction of the available information. By developing methods that use all data, the beam time required to obtain sufficient statistics can be drastically reduced. In some cases, the subsequent modelling step is more or less standardised, and users will be able to go from data acquisition to resolved structures in a single step through reduction, fitting, and modelling. However, this only works for perfect crystal structures, whereas structures with defects or amorphous and porous materials (for example, polymers and concrete) are more

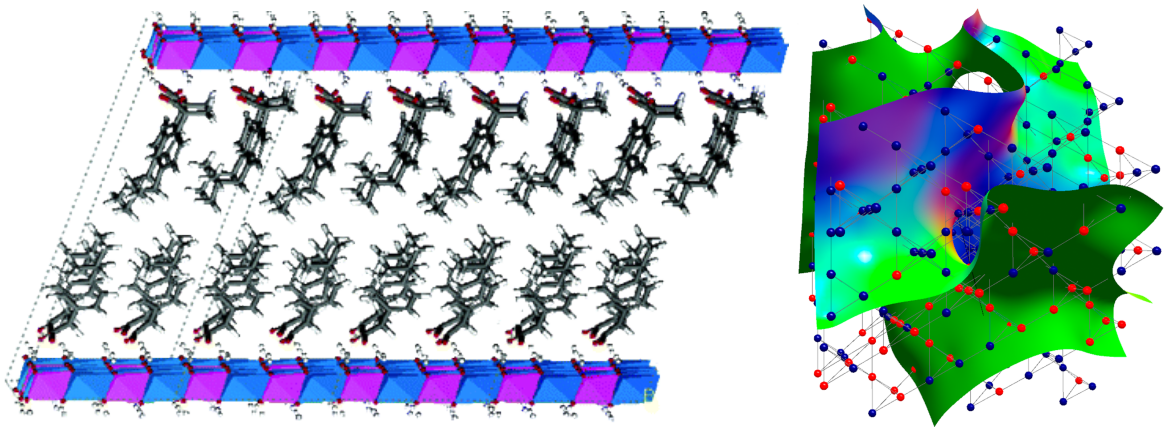

Figure 2.53: Two examples of how intensive computing can be used in data interpretation. Left: Snapshots of the simulation of Mg-Al intercalated drug hybrids, in this case ibuprofen (indicated by sticks). Dashed lines indicate the initial simulation unit cell. Colour code: Blue N, green Cl, red O, gray C, white H, pink Al, and blue-green Mg [278]. Neutron scattering data is indispensable to confirm or constrain these simulations. Right: Computer reconstruction of the surface morphology of a percolation cluster surface in $Y(Mn_{1-x}Fe_x)_2$. Colour code: Red Fe and blue Mn. Magnetic small angle neutron scattering experiments show that the morphology is similar to that of microemulsions [279].

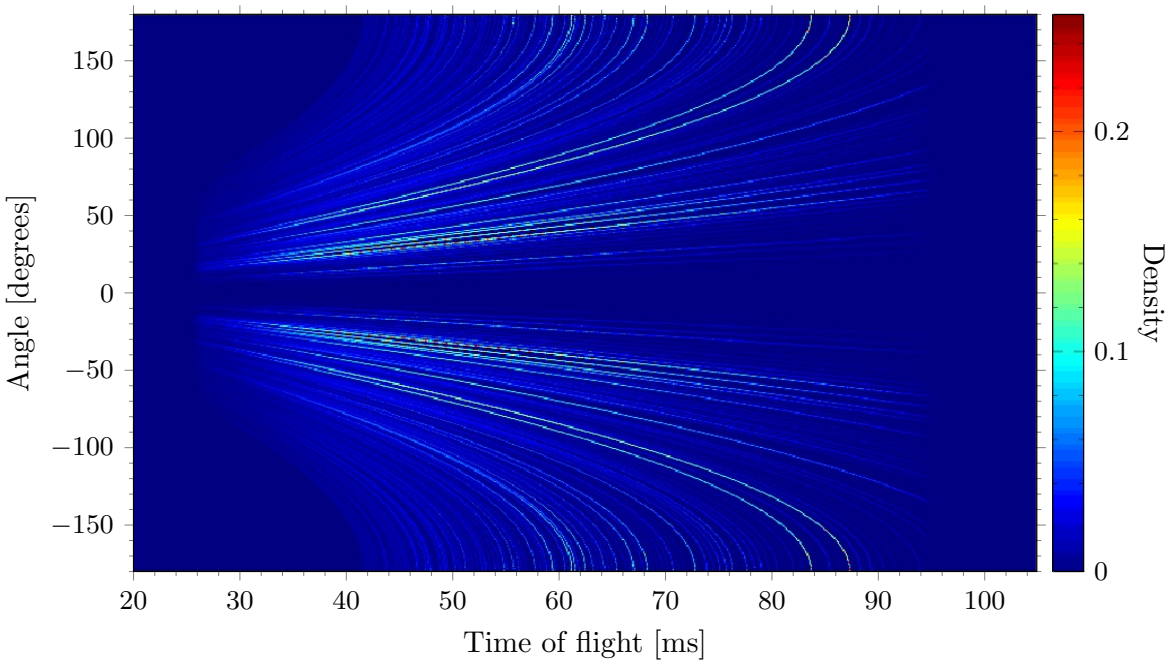

Figure 2.54: Simulated density plot based on ray tracing simulations showing intensity of detected neutrons as function of scattering angle and time-of-flight for a thermal powder diffractometer. Bragg's law ($\lambda = 2d\sin\theta$) manifests itself in the shape of the curves. Each curve corresponds to one value of the lattice plane distance d [280]. Existing analysis tools only use a tiny fraction of the available information.

Appendix B

Appendix; Calculations

B.1 Calculation of the resolution function

$$\sigma^2_{2\theta_f} = \frac{1}{A}\int_{-\infty}^{\infty} f(x)(x-x_0)^2 dx$$

$$= \frac{1}{\frac{1}{2}A}\left[\int_0^{\eta_{\min}} (1)(x-x_0)^2 dx + \int_{\eta_{\min}}^{\eta_{\max}} \left(1 + \frac{\eta_{\min}}{\eta_{\max}-\eta_{\min}} - \frac{1}{\eta_{\max}-\eta_{\min}}x\right)(x-x_0)^2 dx\right]$$

$$= \frac{2}{A}\left[\int_0^{\eta_{\min}} x^2 dx + \int_{\eta_{\min}}^{\eta_{\max}} \left(\left(1 + \frac{\eta_{\min}}{\eta_{\max}-\eta_{\min}}\right)x^2 - \frac{1}{\eta_{\max}-\eta_{\min}}x^3\right) dx\right]$$

$$= \frac{1}{\eta_{\min} + \frac{1}{2}(\eta_{\max}-\eta_{\min})}\left[\frac{1}{3}\eta^3_{\min} + \left[\left(\frac{1}{3} + \frac{\eta_{\min}}{3(\eta_{\max}-\eta_{\min})}\right)x^3 - \frac{1}{4(\eta_{\max}-\eta_{\min})}x^4 + k\right]_{\eta_{\min}}^{\eta_{\max}}\right]$$

$$= \frac{2}{\eta_{\min}+\eta_{\max}}\left[\frac{1}{3}\eta^3_{\min} + \left(\frac{1}{3} + \frac{\eta_{\min}}{3(\eta_{\max}-\eta_{\min})}\right)(\eta^3_{\max} - \eta^3_{\min}) - \frac{\eta^4_{\max}-\eta^4_{\min}}{4(\eta_{\max}-\eta_{\min})}\right]$$

$$= \frac{2}{\eta_{\min}+\eta_{\max}}\left(\frac{\eta^3_{\max}}{3} + \frac{\eta_{\min}(\eta^2_{\max}+\eta^2_{\min}+\eta_{\min}\eta_{\max})}{3} - \frac{(\eta^2_{\max}+\eta^2_{\min})(\eta_{\min}+\eta_{\max})}{4}\right)$$

$$= \frac{1}{6(\eta_{\min}+\eta_{\max})}\left(\eta^3_{\max} + \eta^3_{\min} + \eta^2_{\max}\eta_{\min} + \eta_{\max}\eta^2_{\min}\right)$$

$$= \frac{\eta^3_{\max}+\eta^3_{\min}}{6(\eta_{\min}+\eta_{\max})} + \frac{\eta^2_{\max}\eta_{\min}+\eta_{\max}\eta^2_{\min}}{6(\eta_{\min}+\eta_{\max})}$$

$$\sigma^2_{2\theta_f} = \frac{1}{6}(\eta^2_{\max} + \eta^2_{\min} - \eta_{\min}\eta_{\max}) + \frac{1}{6}\eta_{\max}\eta_{\min}$$

$$= \frac{\eta^2_{\max}}{6} + \frac{\eta^2_{\min}}{6} \tag{B.1}$$